12-1-2017

Understanding the Long-Term Changes in Hydrologic Processes on a Watershed Scale Due to Climate Variability and Change

Chao Chen
University of Nevada, Las Vegas, lilc1987@hotmail.com

UNDERSTANDING THE LONG-TERM CHANGES IN HYDROLOGIC PROCESSES ON A WATERSHED SCALE DUE TO CLIMATE VARIABILITY AND CHANGE

By

Chao Chen

Bachelor of Science – Water Conservancy and Hydropower Engineering
Zhejiang University of Technology
2009

Master of Science – Hydrology and Water Resources
Hohai University
2012

A dissertation submitted in partial fulfillment
of the requirements for the

Doctor of Philosophy – Civil and Environmental Engineering

Department of Civil and Environmental Engineering and Construction
Howard R. Hughes College of Engineering
The Graduate College

University of Nevada, Las Vegas
December 2017

UNLV | GRADUATE COLLEGE

Dissertation Approval

The Graduate College
The University of Nevada, Las Vegas

September 7, 2017

This dissertation prepared by

Chao Chen

entitled

Understanding the Long-Term Changes in Hydrologic Processes on a Watershed Scale Due to Climate Variability and Change

is approved in partial fulfillment of the requirements for the degree of

Doctor of Philosophy – Civil and Environmental Engineering
Department of Civil and Environmental Engineering and Construction

Sajjad Ahmad, Ph.D.
Examination Committee Chair

Kathryn Hausbeck Korgan, Ph.D.
Graduate College Interim Dean

Alexander Paz, Ph.D.
Examination Committee Member

Haroon Stephen, Ph.D.
Examination Committee Member

Lynn Fenstermaker, Ph.D.
Examination Committee Member

Ashok Singh, Ph.D.
Graduate College Faculty Representative

Abstract

In the past century, the population explosion and economic development have resulted in global warming, which has raised a series of concerns, such as sea-level rise, food security, and water resources management. The water flow patterns and features experience both short-term and long-term changes in responses to the changes in the hydrologic processes and meteorologic conditions. On a watershed scale, it is crucial to understand, quantify, and attribute the influences of climate change on the local water resources system. Such understanding can be of great help to undertake local water management tasks, such as flood control, reservoir operation, ecosystem services, and water quality analysis.

The typical General Circulation Model (GCM) simulation products are too coarse for a local meteorologic study and local hydrologic responses to climate change, such as in the Lehman Creek watershed. Additionally, the Lehman Creek recharge the groundwater system that is a potential source of future water supply to Las Vegas Valley. An evaluation of the influences of groundwater pumping on the local water system is necessary for the purpose of environmental conservation.

To bridge these study gaps, three tasks were proposed. First, the Quantile-Quantile Mapping method was employed to further bias correct the downscaled GCM data from a 12-km resolution to a local resolution, and long-term changes were evaluated. Next, a physically-based parameter-distributed hydrologic model was developed and calibrated using the Precipitation-Runoff Modeling System (PRMS). By driving the developed PRMS with the bias-corrected GCM data, and the streamflow changes over the 21st century were analyzed in terms of rates and timings. Finally, a groundwater flow system model was developed using the three-dimensional finite-difference groundwater-flow system (MODFLOW). By coupling the

developed PRMS model with MODFLOW model, the streamflow variation under climate change and groundwater-withdrawal influences were evaluated from the integrated physical perspective.

The results indicated that, in the study area, there was an increase of 2.3 °C, 2.2 °C, and 35.1 mm in maximum temperature, minimum temperature, and precipitation, respectively, which were mean annual differences from period of 2011-2099 when compared to the mean annual average of 1980-2010 in the study area (Great Basin NP station), by considering all potential climate scenarios. These meteorologic alternations would result in uncertain annual streamflow changes but featured monthly variations regarding timing and rates in both PRMS and GSFLOW model simulations. The integrated GSFLOW model showed a similar but mitigated features in streamflow simulation results, compared to the PRMS model simulation results. There were earlier time-shift in streamflow up to 30 days and 26.3 days by the end of this century, resulting from the PRMS and GSFLOW simulations, respectively. These finding were also supported by the monthly streamflow change pattern found in both models' simulation results, as the streamflow tend to increase during the period of later-spring to early-summer (December to May) and tend to decrease during the summer-to-winter period (June to November). Additionally, the groundwater-pumping influence study showed 11.7 meters drawdown at a rate of 510 m^3/d after 50-year water withdrawals, based on the hydraulic conductivity estimations in this study.

The long-term estimates of climate change and the variations observed in the hydrologic responses found in this research can help local water managers to better understand changes in the water resources in responses to future climate variability and groundwater pumping within the Lehman Creek watershed.

Acknowledgements

There are so many people I would like to thank at this point of my life. Without them, I would not have become who I am right now.

With my deepest appreciation and gratitude, I would like thank my advisor, Dr. Sajjad Ahmad, for all the guidance and support during the last four years. I sincerely appreciate all of his great advice, assistance and opportunities he provided to me. I have learnt from him not only about research, but also precious life experiences and how to be a professional and kind person. He is the person who always backs me up financially and mentally. Whenever I have difficulties and struggles that stressed me out and want to pull all my hairs off, he was always there with guidance and supports, making my life beautiful again. I cannot thank him enough for being my advisor, and I cannot express more how lucky I am to have him in my life.

I would like to thank all my committee for their attention and efforts: Dr. Lynn Fenstermaker, who not only influenced me with her great passion and optimism, but also helped me with useful data and data source to complete my model development; Dr. Haroon Stephen, his critical thinking and rigorous science attitude always enlightened me; Dr. Ashok Singh, a great man with a great heart, who taught me statistical programming and made all my research analysis possible; Dr. Alexander Paz, who provided valuable comments and suggestions for the completion of my research and dissertation.

I would also like to show my deep appreciation to Dr. Ajay Kalra, who always visit or call from wherever he was, sharing his working experiences and providing technical help and ideas. His great passion for life and science always influence me. I would like to acknowledge and thank John Volk for sharing his PRMS model he developed for Lehman and Baker Creek and thank Dr. David Prudic for providing valuable data, guidance, comments, and suggestions

about the PRMS model and the hydrogeologic information in the Lehman Creek watershed. I really appreciate the help from Dr. John Mejia, Dr. Tracy Jackson, Dr. Chang Liao, and Dr. Gina Sully, who spent their own time, shared their precious research experiences, and providing me great help that made contribution to my research. I appreciate the National Science Foundation, grant IIA-1329469, which fund me through the entire four years and let me complete my Ph.D. study.

I would give a great amount of appreciation to my friends and my family for their patience, understanding, and supports for what I am pursuing. Thank you to my friends Qi Shen, Soumya Sagarika, and Kazi Tamaddun for reminding me the beauty of life and the importance of balancing every perspective of it. Thank you to Yu Gao, my boyfriend, who is always there for me and helps me through the difficulties and upsets. My greatest appreciation goes to my parents and my two elder brothers. With their unconditional love and support, I had the opportunity and strength to complete this great endeavor.

Last, but not least, I would like to thank all the people I may not have mentioned here, who shed lights on my life. You all make a better me.

Table of Contents

List of Tables

List of Figures

Chapter 1 Introduction

1.1 Climate Change and Influences

1.1.1 Climate change background

The greenhouse effect is a natural mechanism that is essential to life on Earth. The radiant energy, emitted from the sun, passes through the earth's atmosphere and reaches the earth's surface; some radiant energy gets reflected back to the atmosphere and gets absorbed by gasses. Since the pre-industrial era, anthropogenic greenhouse gas emissions have been increasing and currently at their highest level. This has resulted in the amplification of the greenhouse effect and an increase in the atmosphere temperature. Studies based on instrumental observations showed that the surface temperatures have increased globally with great variations among regions. With an increasing rate, the average global warming was found to be 0.35 °C from the 1910s to the 1940s and 0.55 °C after 1970s (IPCC, 2007). There is impelling evidence that the population growth and economic development alter the energy balance of the atmosphere and are the dominant causes of the observed warming since the 1950s (IPCC, 2014).

1.1.2 Climate change observations

Changes in climate have been observed to have widespread impacts on human society and environmental systems across the oceans and the continents (Thakali et al., 2016). The impact on environmental systems is the strongest and most comprehensive with the evidence from observations (IPCC, 2014). The changing precipitation, increasing temperature extremes, and melting snow and ice are observed in many regions and are altering the hydrologic system and influencing water resources in terms of quantity and quality (Tamaddun et al., 2017a, 2017b, 2017c; Kalra et al., 2017). Several studies covering large regions found shifting in seasonal activity patterns, migration patterns, and biological interactions among many species attributed

to the ongoing climate change (Dullinger et al., 2012; Urban et al., 2012 Settele et al., 2014; Tamaddun et al., 2015). An overall negative impact of warming climate on agriculture was demonstrated, which affects the growth of crops and yields of staple cereals with variations in regions and latitudes (Porter et al., 2014). The increased carbon dioxide also causes acidification of the ocean, and hence influences the marine organisms by lowering oxygen level (Millero, 1995; Brewer & Peltzer, 2009).

1.1.3 **Future climate changes, risks, and impacts**

Under future climate change predictions, the surface temperature will likely rise ranging between 0.3°C to 4.8 °C by the end of the 21st century (2081-2100) when compared to the period of 1986-2005, depending on different emission scenarios (Collins et al., 2013). Along with the global mean temperature increases, higher frequency of hot temperature extremes will occur over most land areas daily and seasonally. Uniform changes in precipitation will occur with a likely increase in the high latitudes and the equatorial Pacific areas and decrease in the mid-latitudes and the subtropical dry areas. In the mid-latitude wet regions, average precipitation will likely increase under the highest emission scenario (IPCC 2014).

Studies indicate that the risks of climate change will be amplified in the future and new challenges will arise (Kalra & Ahmad 2009; Pathak et al., 2017). A variety of risks results from social and environmental interactions of climate-related hazard with the vulnerability of exposure to human and natural systems (IPCC, 2014). The raised risk rates and magnitudes differ by regions (IPCC, 2014).

Through the interaction with climate stressors, a large fraction of species faces an increasing extinction risk due to the insufficiency of keeping up with the ecosystem shift brought by the changing climate (Dullinger et al., 2012; Urban et al., 2012; Settele et al., 2014; Kalra et

al., 2013a). Food security is projected to be undermined with both crop yields, especially in tropical and temperate regions (Baldocchi & Wong, 2008; Farag et al., 2010; Settele et al., 2014), and fishery productivities that are accompanied with the marine biodiversity reduction (Bell et al. 2011; Pratchett et al. 2011). With combined factors including feeding forage, living temperature, water availability, and indirect factors related to diseases, livestock is likely to have mixed influences, differing in regions (Porter et al., 2014). The global temperature increase of ~4 °C or more in the late 20th century levels, combined with increasing food demand, will pose large risks to food security globally (IPCC, 2014). Some studies show that with increasing temperatures, the aggregated economic losses accelerate (Hsiang, 2010; Dell et al., 2012; Porter et al., 2014). These climate change impacts are projected to slow down economic growth and make it difficult for poverty reduction (IPCC, 2014).

Water, through its movement in the hydrological cycle, determines the effects on water-related hazards such as floods and droughts with its high vulnerabilities to the climate. Furthermore, it delivers the impacts of climate change to human society with diverse influences and risks through the interactions with non-climatic drivers such as population, economic growth, and urbanization (Dawadi & Ahmad, 2013). In this context, the study of water availability under climate change can contribute to improving the human adaptation strategies (Jiménez Cisneros et al., 2014).

1.1.4 **Climate change influences on hydrologic processes**

Global water circulation makes atmosphere and hydrology closely interact with fluxes of water and energy, which has immediate and long-term effects on water systems, both on the surface and subsurface. The global influences of increasing temperature directly change the atmospheric moisture, precipitation, and the whole hydrologic system, e.g., the accumulation and

ablation of snow, and evapotranspiration (IPCC, 2007 & 2014). Additionally, the changes in precipitation primarily determine the total water received from the atmospheric system and also results in changes in spatiotemporal flow patterns (Nijssen et al., 2008).

While the global trends in precipitation showed insignificance during 1901-2005 (Bates et al., 2008; Trenberth et al., 2007), regional observations showed more severe extreme events occurred during the 1990s and 2000s compared to the 1950s (Arndt et al., 2010) with certain trends in total volumes and extreme measurements (Trenberth et al., 2007). Along with the warming observations, the snowfall seasons became shorter with an earlier start of snowmelt in north Hemisphere (Takala et al., 2009) and a reduction of Snow Water Equivalent in Norway (Skaugen et al., 2012). Through the study of regional soil moisture, a prolongation of dry periods was concluded, which shows the presence of more severe and frequent droughts (Gemmer et al., 2011; Fischer et al., 2011; Fischer et al., 2013).

In streamflow, the trend detections show its consistency with regional observations in precipitations and temperature since the mid-century (Jiménez Cisneros et al., 2014) with significant differences among regions (Sagarika, Kalra, & Ahmad, 2014, 2015, 2016). In North America, decreases were observed in the southern Atlantic-Gulf regions and U.S. Pacific Northwest during the period of 1951-2002, whereas in Mississippi basin, increases were observed (Kalra et al., 2008; Jiménez Cisneros et al., 2014). In China, there was a small increase in annual streamflow in Yangtze River and a decrease in the Yellow River during 1960-2000 due to the great seasonal changes, especially in summer (Piao et al., 2010). A study by Dai et al. (2009) shows decreasing trends in 45 rivers and increasing trends in 19 rivers among one-third of the top 200 rivers in a global analysis of streamflow simulations (1948-2004).

At short time scales, from days to months, changes in weather patterns can result in changes in the incidences of floods. On longer time scales, from seasons to years, changes in climate can lead to the time shift and trend change of water availability. At annual to decadal time scales, teleconnections in global atmospheric circulation patterns, caused primarily by the dynamic interaction between ocean and atmosphere, strongly affect the hydrology in certain regions of continents. For example, the Pacific decadal oscillation (PDO), North Atlantic oscillation (NAO), Atlantic multi-decadal oscillation (AMO), and El Niño–southern oscillation (ENSO) have been linked to the changes in streamflow (Kalra et al., 2013b), and to the annual precipitation in the southwest of US (Kalra & Ahmad, 2011, 2012).

Direct attributions of climate change to groundwater systems is uncertain, while as an important water recharge, in some regions, the precipitation decreases were attributed to the decreases in the discharge of groundwater-fed springs (Jeelani, 2008; Aguilera & Murillo, 2009) and to a progressive decline in a fraction of precipitation to groundwater recharge, indicating an increasing trend in evapotranspiration process (Aguilera & Murillo, 2009).

1.1.5 **Future climate changes - on a watershed scale**

In 1998, the Intergovernmental Panel on Climate Change (IPCC) was set up by the United Nations and brought the world's leading experts to assess the condition of the Earth's climate system. Thereafter, Global Climate Models (GCMs) were outlined, which try to simulate the functional interactions between atmosphere and oceans and to predict the anticipated climate patterns under likely future emission scenarios, and a series of meteorological model simulations were produced.

However, the spatial scales of meteorological model simulations, resolved from GCMs, are usually around 10 to 100 km or beyond. With high spatial heterogeneities in geology,

ecology, and topography, the meteorological conditions have profound impacts on regional water systems with great interactions among each other and with other parallel systems (Maxwell et al., 2007; Weigel et al., 2007). For example, the increased intensity and variability as predicted in precipitation will likely increase the frequencies and risks of droughts and floods in many regions (Bates et al., 2008). During the seasons with above-average precipitation, the water demand, especially for agricultural irrigation, will decline due to the combined factors of lower solar radiation and temperature and higher humidity (Rosenberg et al., 1999).

It is crucial to understand, quantify, and attribute the impacts of extreme weather and climate change at a finer scale where general meteorological climate data is too coarse for regional water resources studies, such as in flood control, reservoir operation, ecosystem services, and water quality analysis, especially in the estimation of streamflow for water resources management.

1.1.6 **Future hydrologic responses - on a watershed scale**

The global climate change is generally known as global warming, to which the phenomenon is normally identified as the changes in the energy balance and the increased temperature in the atmosphere (Hashmi et al., 2012). The alternations and variations in meteorological condition are scientifically acknowledged to alter the water balance in the hydrologic cycle (Eslamian, 2014). Due to the determinant correlation between meteorological conditions and water resources availability through the hydrologic cycle, the impacts of alternations in the precipitation patterns and other climatic variables are considered to impose significant impacts on a regional water cycle and particularly watershed hydrology (Lambert & Boer, 2001).

Studies showed warmer weather tends to affect the precipitation as more days of temperature above zero degree Celsius results in more rainfall events in winters. The following consequences are not only concerning to the snow season length, but also to runoff formation with related snowmelt features such as snow accumulations, heat exchanges between atmosphere and ground, and soil freezing depth (Whitfield et al., 2003; Zhang, 2005; Lawrence & Slater, 2010; Bailey et al., 2015). Even the modest increases in air temperature, especially in snow-dominant areas, will alter the hydrologic cycle through shifts in streamflow because of the role snowpack plays as a water-storage reservoir (Mote et al., 2005; Barnett et al., 2008; Tague et al., 2008; Zhang et al., 2014). In a study of mountainous regions in central Europe by Eckhardt and Ulbrich (2003), a small ratio of precipitation was predicted falling as rain instead of snow due to warming trends, and it resulted in a reduction in the spring-snowmelt peak with an increase in flood risk in the winter. Thus, to regulate the earlier snowmelt runoff and the lower streamflow in upcoming seasons, corresponding reservoir regulation rules should be justified to fulfill the consequences as brought by the climate change.

For the purposes of water resources planning, and management, reliable estimation of streamflow from a watershed, which is the main water source for local users, is required. Streamflow characteristics such as rate, volume, peak flow, peak time, flow duration, spatiotemporal distributions, and probability distributions are critical parameters in the decision making for water and especially irrigation management (Eslamian, 2014).

1.1.7 **Surface water and groundwater interaction - on a watershed scale**

Due to the more direct visibility, easier accessibility, and more obvious recognition of surface water being affected by global climate, researches have focused more on surface hydrology compared to groundwater systems. Nevertheless, studies of groundwater systems,

compared to the effect of climate change on surface water, have increased in past decades recognizing the importance of the interaction with surface water and water-supply withdrawals (Green et al., 2011).

The global warming and precipitation changes are expected to alter the subsurface-water processes that result from the interactions between surface water and groundwater. The concepts of groundwater discussed in this study are adopted from Green et al. (2011), which considers subsurface water that includes soil water, vadose-zone water, and water within unconfined and confined aquifers (saturated-zone water).

The features of soil water include components of infiltration, evapotranspiration, and soil water capacity (SWC) (Van Dijck et al., 2006). Infiltration and evapotranspiration have more obvious influences from the changes in precipitation and air temperature, which are the two main factors in the interaction and feedbacks between climate and SWC (Seneviratne et al., 2010). For example, under higher air temperature, the evapotranspiration is likely to increase and may result in a reduction in SWC along with the decreases in runoff (Chiew & McMahon, 2002).

The vadose zone is the soil region between the land surface and the saturated zone, where the groundwater recharge occurs. Both water quality and quantity could be affected by the changes in climate that slowly propagate through the vadose zone (Glassley et al., 2003). Studies in some semiarid and arid regions found a great importance in understanding the effects of climate change and variability in the vadose zone and its consequent effects on groundwater (Phillips, 1994; Glassley et al., 2003).

Groundwater in the saturated zone is an important component in the hydrological cycle and contributes an important component to the streamflow as baseflow. Due to the large water storage capacity, baseflow is expected to vary the least (Winter, 2007). It is considered that with

the storage mechanism, groundwater can mitigate the influence brought by global warming and climate change impacts on the water resource availability and the baseflow rate (Ghasemizade & Schirmer, 2013). However, in some semiarid and arid regions, the dry season may be extended, influenced by climate change, which can have substantial effects on the overall water resources if no deep or reliable groundwater resources are available in the region (Giertz et al., 2006).

A study of climatic impacts on the interactions between surface and groundwater requires an understanding of the dynamic interactions between them with local characteristics. Nevertheless, surface water and groundwater systems are usually considered separately and with independent analysis, despite the hydro-geological interconnections. The separation is partially because of the greater time scale due to the slow water movement in the groundwater flow system compared to the free water flow on the land surface, and partially due to the fact that there are difficulties in measuring and modeling the interactions between them. There are numbers of hydrodynamic models for surface flow and groundwater flow simulation independently. However, to capture the dynamics between surface water and groundwater, the integrated models, which couple surface water and groundwater, are becoming increasingly important (Winter et al., 1998; Weill et al., 2011).

1.2 Research Motivations and Questions

Along with the reduction in Colorado River flow in recent years, which Southern Nevada is heavily relying on, and the rapid growth in population and business in the southwestern US, the Colorado River has been threatened to water over-use (Dawadi & Ahmad, 2012). Besides, the droughts since 1999 were further exacerbated under the climate change influences. Serious concerns were raised regarding the heavy reliance of water supply from Colorado River (Dawadi & Ahmad, 2013). Thus, since 2004, the Southern Nevada Water Authority (SNWA) has

proposed a Groundwater Development (GWD) Project that can meet the water demand and ensure the water supply for customers in the Las Vegas Valley and Boulder City, Clark County.

In Snake Valley, SNWA proposed 62.5×10^6 m^3/year (50,679 acre-ft/year) of the groundwater withdrawal, which could be a potential water source supply to Las Vegas, NV (SNWA, 2012; Volk, 2014) to meet the future water need in southern Nevada. The Lehman Creek watershed, the study area in this study, is one of the critical water sources for local irrigation and for water recharge to the basin-fill aquifer in Snake Valley. A better understanding of future climate changes and its mechanisms in hydrologic responses would provide information to help local water resources management and evaluate the GWD for Las Vegas water supply.

This study will focus on three research questions:

Research Question # 1: What are the long-term changes in meteorological conditions on a watershed scale with respect to Global Circulation Models?

Hypothesis: Temperatures and precipitation would change on a watershed scale based on bias-corrected results from the Global Circulation Models, and the results are reliable and can be further applied to a watershed hydrologic study.

Research Question # 2: How do the climatic changes affect the streamflow on a watershed scale?

Hypothesis: Through dynamic interaction between meteorologic variables and hydrologic processes, the streamflow would change in terms of rates and timing, responding to local climate change.

Research Question # 3: How do integrated hydrologic processes respond to external stresses from meteorologic changes and human interference of groundwater pumping?

Hypothesis: The water flux interaction between surface water and groundwater would show varying trend under the climate change and the groundwater would drawdown under the influence of groundwater pumping.

1.3 Importance of This Study

A better understanding of the hydrologic responses to climate change impacts on a watershed scale could better help local water resources managers to make long-term decisions to efficiently utilize limited water resources. The projected meteorological changes and corresponding hydrologic responses in both surface water and groundwater in the Lehman Creek watershed have rarely been studied, especially the mechanisms in a snow-dominant area with high elevation differences.

Due to the coarse resolution of climate change projections, their employment in a small watershed scale, are limited with scaling issues of high heterogeneities, nonlinearities, and non-local transport processes (Gentine et al., 2012). However, as a statistical downscaling and bias-correction method, the Quantile-Quantile Mapping (QM), provides a way to narrow down the data differences between two scales, approaching to a representation of local climate characteristics and assessing the climate changes at a local scale. This could lay groundwork for other studies such as the local ecology, which may be affected as other pine and fir species encroach and outcompete the local species under the local climate change (Volk, 2014).

Studies have shown that climate change impact on water resources may differ from region to region depending on the geographic characteristics and meteorological conditions (Arnell et al., 1992; Huntington & Niswonger, 2012). An integrated hydrologic model can provide a better representation for the study of local hydrologic processes on the land surface and subsurface, as well as the interactions between them. By forcing expected global climate change

projections of meteorological factors, e.g., precipitation, temperature, to watershed scale hydrologic models, the hydrologic processes can be simulated and evaluated with changing trends in water availability for the 21st century. Results can provide scientific insights into future water resources alternations and help water managers to make adaptive water utilization strategies, such as reservoir regulations, irrigation management, and groundwater withdrawal.

Though there has been an earlier study using one GCM (Volk, 2014), it was the first time the climate change evaluation was performed on a watershed scale in the Lehman Creek watershed with all climate change models considered. It provided comprehensive assessments of meteorological trends and variations among different time periods in the 21st century. Based on that, the hydrologic responses were assessed correspondingly, providing a unique evaluation of the surface water changes under the potential climate change. Additionally, it was the first study, in the watershed, of a groundwater flow system model development and coupling with the surface hydrologic model using GSFLOW model. Groundwater pumping influences on the local water resources system were evaluated and more importantly, it provided insights into water resource availability in responses to the potential climate change for the first time.

1.4 Research Goal and Outline

The goal of this research was to evaluate the hydrologic responses to the changing climate at the Lehman Creek on a watershed scale, which would help to develop a better understanding of the long-term meteoro-hydrologic influences. The quantitative assessment of streamflow changes can improve the regional water resources management in the Lehman Creek watershed and the surrounding areas. This study aimed at meeting three research objectives (Figure 1).

Objective 1 was titled "*Long-term Meteorological Changes on a Watershed Scale with Respect to Global Circulation Models*", discussed in Chapter 2. It focused on developing the meteorological data on a watershed scale based on coarse-resolute climate change data obtained from downscaled CMIP5, from which the climate change could be evaluated at a fine resolution. Objective 2 was titled "*Surface Hydrologic Responses to Climatic Changes in the Lehman Creek Watershed*", discussed in Chapter 3. It focused on developing a hydrologic model using the Precipitation-Runoff Modeling System (PRMS) and to drive the model with the climate change data from Objective 1 to simulate and assess the surface hydrologic processes, e.g., streamflow. Objective 3 was titled "*Global Climate Change Influences on the Interactions between Surface and Groundwater in Lehman Creek on a Watershed Scale*", discussed in Chapter 4. It focused on developing a groundwater-flow system using the three-dimension finite-difference groundwater-flow system (MODFLOW) and to couple the developed PRMS model with this MODFLOW model using the coupled groundwater flow and surface-water flow model GSFLOW. This could help to better understand the interactions between surface water and groundwater in snow dominant areas. Chapter 5 summarized the results and conclusions and provided recommendations for future research.

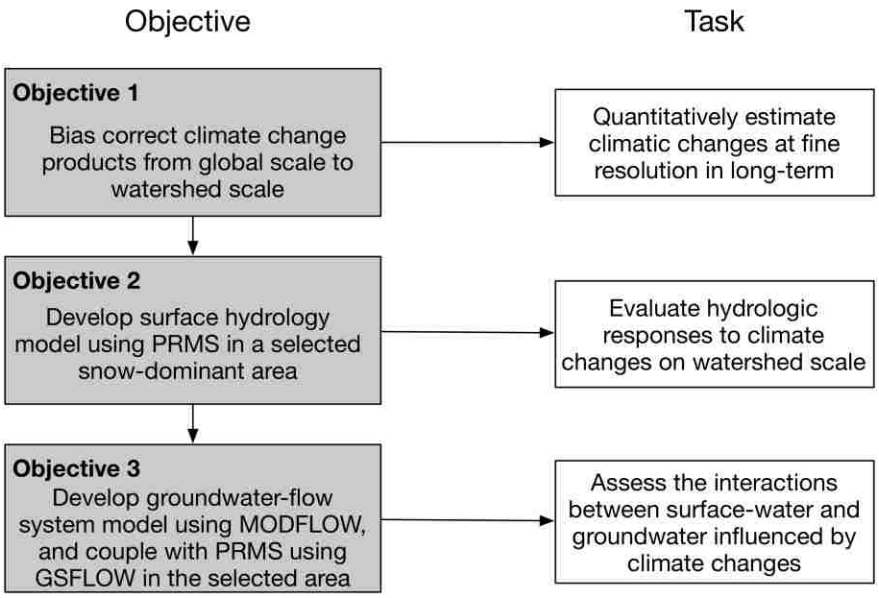

Figure 1. Workflow Diagram of the Study with Three Objectives and the Corresponding Tasks.

Chapter 2 Future Long-Term Meteorological Changes on a Watershed Scale

2.1 Research Objective 1

Research Question # 1: What are the long-term changes in meteorological conditions on a watershed scale with respect to Global Circulation Models?

The climatic variables of precipitation, maximum temperature, and minimum temperature were extracted from the PRISM dataset at the station of Great Basin NP, for the historical period of 1981-2010, and from the CMIP5 dataset at 12 km resolution, for the periods of 1981-2010 and 2011-2099. As PRISM data was considered as historical observations, the CMIP5 data used PRISM data as a reference to identify the bias in historical period of 1981-2010. Assuming these bias were constant in future periods, they were used to correct the CMIP5 data for the period of 2011-2099. The QM bias-correction method was employed to bias correct the climatic variables of precipitation and temperature. The employed technique was intended to resolve the drizzle effect in precipitation and physical unrealistic effect in temperature. Under four likely climate change scenarios, RCP 2.6, 4.5, 6.0, and 8.5, precipitation and temperature data were analyzed at a station scale. The alternations and change trends of the climatic condition at Lehman Creek watershed were evaluated in the 21st century for the three divided periods: 2011-2039 (Period 1), 2040-2069 (Period 2), and 2070-2099 (Period 3), using bias-corrected CMIP5 data.

2.2 Introduction

2.2.1 Climate change influences on the Great Basin

Due to human activity and increasing greenhouse gasses, significant changes in the climate were experienced during the last century and will continue in the future (Chambers, 2008).

In the Great Basin, where the study area is located, the observations in the 20th century show a warming trend of a 0.3 to 0.6° C (0.6° to 1.1 °F) increase region-wide, which has resulted in an increasing probability of warm years and a decreasing probability of cold years. Since the middle of the last century, an increase of annual precipitation, ranging between 6 to 16%, was detected, with specifications in inter-annual variability and extreme events; the snowpack observations on 1 April show an overall decreasing trend with spatial discrimination across the basin. Compared to the 1950s, the timing of the snowmelt in snowmelt dominant regions shows 10-15 days earlier. An increasing streamflow was reflected across the region, especially in winters and springs (Baldwin et al., 2003).

As global warming continues, it is projected with a 2 to 5 °C (3.6 to 9 °F) temperature increase in the west ranges of the US. Due to the large difference in topography, the degree of change will be distinctive (Cubashi et al., 2001). Additionally, snowpack declines and snow water losses are likely to continue and will even be accelerated in a warmer climate (Mote et al., 2005).

2.2.2 **Bias correction techniques**

The meteorological conditions are the most critical input data in the hydrologic models for the determination of volume and timing of the water flow. Before any downscaled data is forced into a model to estimate the specific impact of climate change on small scales, some adjustments should be included to count for the bias within GCMs resulting from resolution differences and model systems, such as systematic bias induced by inadequate terrain resolution (Haerter et al., 2011; Thrasher et al., 2012).

Bias correction, as a concept, was introduced in weather forecasting and later used in climate study (Maraun et al., 2010; Maraun, 2013). It is a variant of Model Output Statistics that

is meant to correct the long-term climate means, variance, and quantile-based biases and to be used to downscale the simulated climate variables averaged in a grid box to point values (Maraun, 2013). This can be done by a variety of downscaling techniques, classified as the dynamic downscaling technique and statistical downscaling technique.

The dynamic technique is a model-based method that tends to increase the resolution of physical models by nesting a finer-scale regional climate model within a global-scale model (Giorgi et al., 1991). It provides a more accurate description of important model components such as cloud physics and terrain height (Hay & Clark, 2003), while demanding copious computational resources (Takle et al., 1999; Hay et al., 2002).

The statistical downscaling technique uses statistical correlations derived from history to describe regional climates (Benestad, 2001; Wood et al., 2004), and encompasses linear and nonlinear methods. Kilsby et al. (1998) and Huth (1999) used Multiple Linear Regression (MLR) models for statistically downscaling GCM data, and based on that, von Storch (1999) proposed Multiple Linear Regression with Randomization (MLRR) to recover the original data variability. Conditioned on atmospheric status, a resampling approach was used to capture the uncertainties in the downscaling process termed the Analogue Method (AM) (Zorita & von Storch, 1999). Brandsma and Buishand (1998), Mehrotra and Sharma (2006) and Moron et al. (2008) extended AM with probability distributions and developed the Nearest Neighbor Analogue Method (NNAM). Schmidli et al. (2006) extended the downscaled procedure from monthly to daily by Local Intensity Scaling (LOCI) approach, and wet-day intensity ratio was applied on the basis of data frequencies. Different from LOCI, Quantile Mapping (QM) method employed the entire empirical cumulative distribution for each day instead of only wet days (Panofsky & Brier, 1968; Dettinger et al., 2004; Wood et al., 2004; Boé et al., 2007).

2.2.3 **Quantile-Quantile Mapping technique**

Not without controversy, the QM technique has been widely used in the bias correction of GCM or RCM products and corrects the bias between model simulations and observations. It assumes a relationship between local scale and large scale predictors being linked to point observations with nearby grid values (Maraun, 2013; Smith et al., 2014; Mishra & Herath, 2015). QM generally adjusts the long-term simulations by adding the difference between observations and simulations that were derived from a same reference period based on the quantile. With various downscaling and error correction methods, Themeßl et al. (2011) showed that the QM method performs best for one of the most critical variables - precipitation; Räisänen and Räty (2013) also demonstrated QM as the best-performing technique in mean temperature for far future evaluation.

The QM technique was initially proposed by Panofsky and Brier (1968), was later modified by Themeßl et al. (2011), and has been employed to climate change studies as a common component (Hay & Clark 2003; Boé et al., 2007; Maraun et al., 2010; Ehret et al., 2012; Maraun, 2013; Sippel et al., 2015). The process combines downscaling aspects with model error correction and is termed as "bias correction." The corrections of implicit differences between GCM simulations and observations are included.

As described by Cannon et al. (2015), QM is based on the Cumulative Distribution Functions (CDFs) $F_{o,h}$ and $F_{m,h}$, respectively, of observed data ($x_{o,h}$) and modeled data ($x_{m,h}$), for the historical period denoted by the subscription h. The bias correction of $x_{m,p}$, which is the modeled data for the projected period denoted by the subscription p, can be expressed by the transfer function as follows:

$$\hat{x}_{m,p}(t) = F_{o,h}^{-1}\{F_{m,h}[x_{m,p}(t)]\} \quad (1)$$

Where $F_{o,h}^{-1}$ is inverse CDFs with observed data in a historical period, t is a time in the projected period. When CDFs (and inverse CDFs) are estimated from empirical data, the algorithm expressed in Eq. (1) can be illustrated via quantile-quantile plots. The QM plots are scatter plots of data values (observed and modeled data) versus corresponding empirical quantiles. With a same data number, the QM plots resulting from observed data and modeled data amount to a lookup table wherein a observed value can be found with an entry of modeled value under the same quantile (Figure 2). The construction of transfer function is based on the historical period exclusively, with no future model projected included.

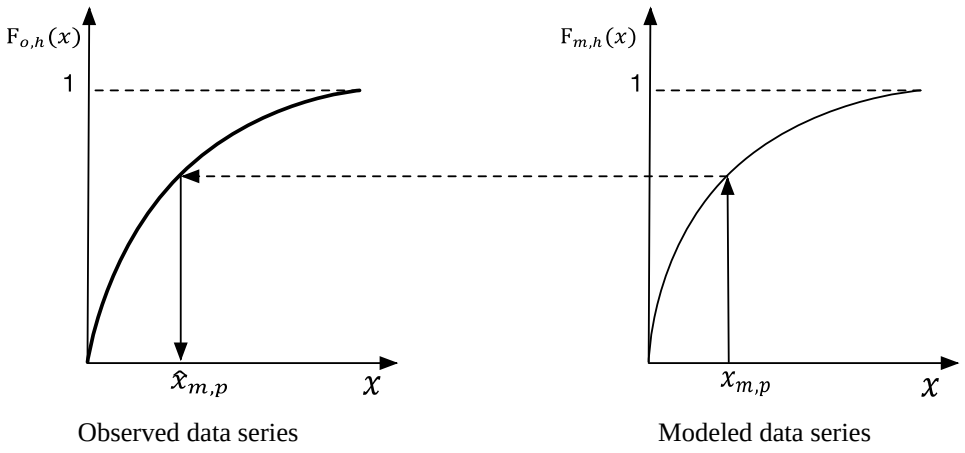

Figure 2. Example Illustration of Quantile Mapping Method. $\hat{x}_{m,p}$ Is the Modeled Value after Bias Correction, Found in the Observed Data Series; $x_{m,h}$ Is the Modeled Value before Bias Correction, Found in the Modeled Data Series; Through Tracing the Same Value in the Cumulative Density Function, the Bias Correction is Performed for Each of the Modeled Data.

The time variable in the equation and the data used for the construction of CDF are both for representations of concepts from data to be bias corrected, which are meteorologic variables in the study. Depending on the specific study interests, the QM method has been used extensively for downscaling in monthly average temperature and precipitation (Wood et al., 2004; Maurer & Duffy, 2005; Hayhoe et al., 2008), and in recent years, it has been employed in daily data (Maurer et al., 2010; Abatzoglou & Brown, 2012). Depending on the research purpose, data availability, and corresponding time scale, the data for each representative time

period can be collected by different means. For example, monthly values are extracted from each continuous year with an annual cycle for a determined month. For a representative day, the time-series can treat each day separately with an annual cycle, or include a moving window (1day $\pm$ 15days) considering seasonal variability.

Much like all statistical downscaling approaches, the biases in GCMs are assumed as constant during the projections relative to historical observations. Thus, the biases can be further employed and corrected for future periods of GCM data, such as in the studies of Hagemann et al. (2011) and Thrasher et al. (2012).

2.3 About Study Area

Lehman Creek is a 23.6 km^2 (5,839 acres) portion of the southern Snake Range of east-central Nevada, on the north side of Wheeler Peak and Jeff Davis Peak, southeast of Bald Mountain (**Error! Reference source not found.**). This is the drainage area above the Lehman Creek Cave stream gauge station (#10243260, LEHMAN CK NR BAKER, NV, from October 1, 1947, to November 4, 2012). The streamflow, mainly consisting of snowmelt originating from a higher-elevated region, coupling with rainfall, flows from west to east across an alluvial fan recharging to the groundwater of Snake Valley (Volk, 2014; Prudic et al., 2015). From December 1947 through September 1955, the mean annual water yield of Lehman Creek was 4.4 $\times 10^6$ m^3 (3,570 ac-ft), with peak runoff occurring in June, and the lowest flows were recorded in January and February. This observation gauge was re-established in the fall of 1992 (Volk, 2014; Prudic et al., 2015).

2.4 Data

2.4.1 Meteoro-hydrologic Data

There are four daily measurement stations within and close to the watershed at different resolutions and with different observation periods (**Error! Reference source not found.**). Two of these stations were parts of the Western Regional Climate Change's Remote Automated Weather Station and have precipitation, temperature, and solar radiation data at one-hour resolutions. The Nevada Climate-ecohydrology Assessment Network (NevCAN) has a new station (built in 2011) for observations of precipitation, temperature, solar radiation, etc. Daily measurements of Great Basin NP (#263340) from the National Weather Service's Cooperative Observer Program are available for precipitation and temperature data (Table 1).

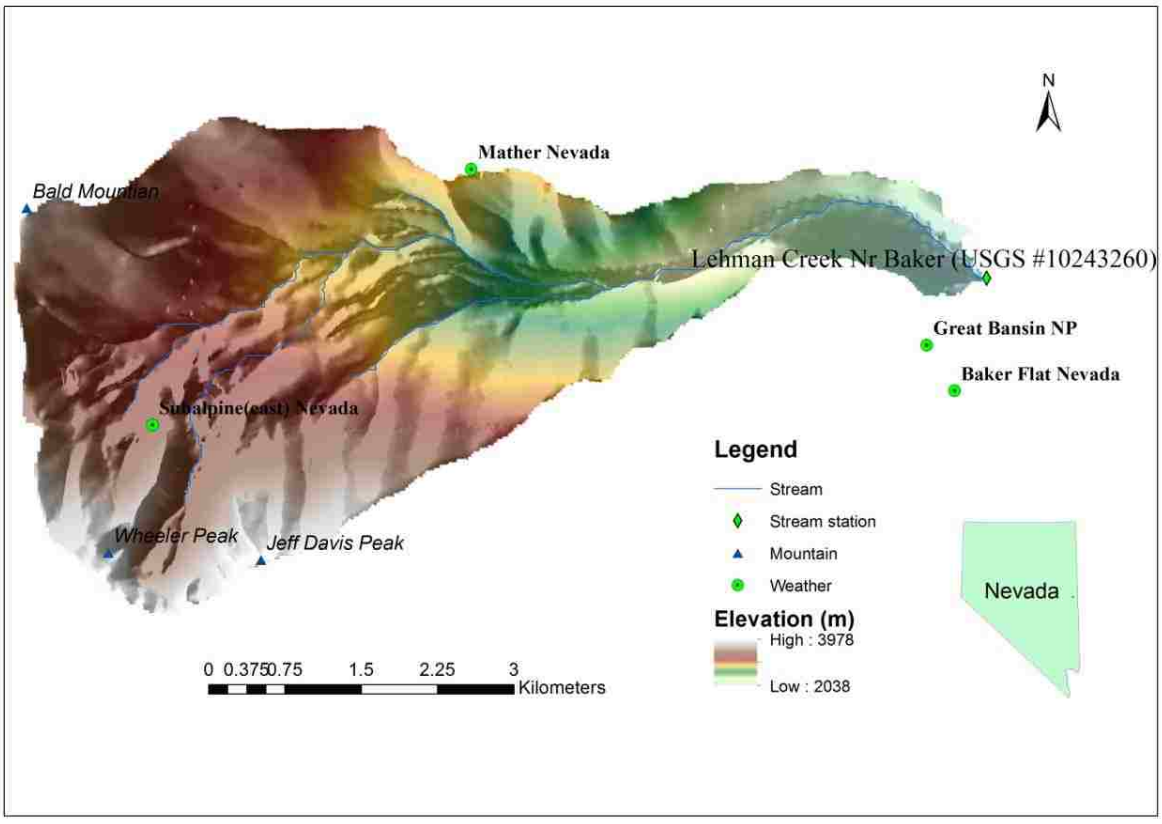

Universal Transverse Mercator projection, Zone 11, NAD 83

Figure 3. The Lehman Creek Watershed and Hydrologic and Meteorological Observation Stations Nearby.

Table 1

Basic Information of the Data Measurement Stations Used in the PRMS Model Developed Calibration and Validation, including Three Meteorological Observation Stations and One Streamflow Gauging Station.

Data Source	Station name	Lat.	Long.	Elev. (m)	Related variables measured	Start time
WRCC RAWS	Baker Flat Nevada	39.0019	-114.218	2085	p,t,sr,w,st,h	4/1/2000
	Mather Nevada	39.0228	-114.272	2825	p,t,w,sr,h	6/1/1998
WRCC NevCAN	Subalpine (east) Nevada	39.0010	-114.309	3081	p,t,w,sr,st,h,sd	8/24/2011
NWS COOP	Great Basin NP	39.0330	-114.221	2088	p,t	7/1/1948
USGS NWIS	Lehman Ck Nr Baker, NV	39.0117	-114.214	2042	discharge	10/1/1947

NevCAN: Nevada Climate-ecohydrology Assessment Network; COOP (COoperative Observer Program); WRCC: Western Regional Climate Center; RAWS: Remote Automated Weather Station; NRCS: National Resources Conservation Service; USGS NWIS: U.S. Geological Survey National Water Information System; DRI: Desert Research Institute. The codes abbreviation: *sr* for solar radiation; *w* for wind speed and direction; *t* for air temperature; *st* for soil temperature; *h* for relative humidity; *p* for precipitation; *sd* for snow depth; *swe* for snow water equivalent.

Based on the observation location, length, resolution, and continuity of the available time series datasets, the meteorology stations of Great Basin NP, Baker Flat Nevada and Mather Nevada, and the streamflow gage of Lehman CK NR were chosen and used. The modeling simulation are for water years from 2003 to 2012. Data of precipitation and temperature from Great Basin NP were used as driving input for the model. Potential evapotranspiration (PET) and solar radiation data from these three meteorological sites, as well as streamflow data from Lehman CK NR Baker (#10243260), were used in the model calibration and validation.

2.4.2 **PRISM Dataset**

Long time-series data were required to capture the climatic features on a local scale. Due to the data shortage in length, instead of using breaking periods of observations, we used the products of Parameter-Elevation Regressions on the Independent Slopes Model (PRISM) to

represent observations (Appendix A-2). It contains a continuous time-series daily dataset at high resolution (AN81D), which resulted from observation networks and showed high reliability and high proximity with observations (Di Luzio et al., 2008; PRISM Climate Group, 2004; PRISM, 2016).

The PRISM Climate Data were developed by the Northwest Alliance for Computational Science and Engineering (NACSE), based at Oregon State University, PRISM Climate Group. For the development of spatial climate datasets that reveal both short-term and long-term climate patterns, climate observations from a variety of monitoring networks were collected and a series of sophisticated quality controls were applied. The product datasets incorporate a variety of modeling techniques and are available at multiple spatial and temporal resolutions, from 1895 to the present. The time series datasets used were modeled using the climatologically-aided interpolation method.

In this study, time series data of daily maximum temperature, minimum temperature, and precipitation at Great Basin NP (#263340) were collected from 1981 to 2010 from PRISM Climate Data (30-Year Normals, PRISM). The data originated from a standard 4km resolution grid cell and was interpolated using the inverse-distance-squared weighting method from surrounding grid cell centers. Gridded data use the climatologically-aided interpolation (CAI) method for point interpolations within a grid, which uses DEM as the predictor to assess the spatial pattern of climatic conditions on specific days over a long-term average pattern (PRISM, 2016). Time-series data at Great Basin NP (#263340, Elev. 2088 m) was interpolated from a 4km resolute grid with an elevation of 2069 m.

2.4.3 **Climate change data - CMIP5**

As the latest global climate projections, the Coupled Model Intercomparison Project (CMIP) released during 2012-2013 was developed by the World Climate Research Program (WCRP). It coupled the Atmospheric Model Intercomparison Project (AMIP), a standard experimental protocol for the global Atmospheric General Circulation Models (AGCMs) with ocean-atmosphere models (coupled GCMs). Products of four Representative Concentration Pathways (RCP 2.6, 4.5, 6.0 and 8.5) simulation from the coupled GCMs were obtained from the Coupled Model Intercomparison Project phase 5 (CMIP5) multi-model ensemble (Taylor et al., 2011; Braconnot et al., 2011; Appendix A-1). It has been widely used in various assessments, research, and educational activities related to climate change processes and outcomes. The selected data are 12 km resolution products of bias-corrected constructed analogs (BCCA) with 67 models: 16 from RCP 2.6, 19 from RCP 4.5, 12 from RCP 6.0, and 20 from RCP 8.5 (Appendix A-1). Full details about climate change models and scenarios were discussed in detail by Taylor et al. (2011) and Brekke et al. (2013). In this study, the gridded climate scenarios data under four RCPs for the historical period of 1981-2010 and the projected period of 2011-2099 were used, which presented the output of various models under four likely future Greenhouse Gas (GHG) emission scenarios over the Lehman Creek watershed.

2.5 Method

The study approach consisted of two steps, as follows:

Step 1. The procedure was validated using PRISM data as observations by means of statistical comparisons with historical records. In this way, the practice of QM in Step 2 was reliable when using PRISM data as the reference data (Section 2.5.1).

Step 2. The QM technique was applied to bias-correct the GCM data onto a station scale, with

three meteorological variables on a daily scale: precipitation, maximum temperature, and minimum temperature (Section 2.5.2).

In Section 2.5.3, methods to assess results were described for validating the use of the PRISM data as observations in the study area (Step 1), evaluating the performance of QM bias correction (Step 2) and long-term meteorological conditions (Step 2).

2.5.1 **PRISM Data Validation**

There was a shortage of meteorological observations in the study area, and the longest continuous data started as late as 1998. This limited the long-term trend capture in the study area and the data implementations in related hydrologic studies, such as the bias correction of the climate-change products. Instead of using short-period observation records, 30 years of PRISM products (AN81D) were used in this study, better representing the fitting of a frequency function and avoiding significant uncertainties (Ford et al., 2008). The PRISM dataset has been widely used for a variety of meteoro-hydrological studies (Leibowitz et al., 2012; Lafontaine et al., 2015).

In order to validate the implication of the PRISM data in the study area, comparisons were performed on the climatic variables between the PRISM data and historical records, and the longest overlapping period of 2003-2012 (water years) was selected. Data were compared for precipitation and temperature with the featured statistics of mean, variance, and standard deviation. While data consistency was usually expected for the temperature (Nijssen et al., 2008; Rahmstorf, 2012), a detailed comparison was also performed on the more uncertain variable of precipitation.

2.5.2 **GCM bias correction and downscaling**

The bias-correction technique that was applied in this study was a merged QM method, which combined the downscaling aspects with error correction of the model (Wilcke et al., 2013). The altitude difference between the GCMs and the observation orography was included implicitly. Similar to all downscaling approaches, this method assumed that the biases relative to historic observations would be consistent in the model projections. It corrected the errors in the shape of the data distribution, and thus was capable of correcting errors in variability. This quantile-based approach originated from the empirical transformation of Panofsky and Brier (1968), and was successfully implemented in studies of hydrologic and biological effects under climate change (Maraun, 2013; Wilcke et al., 2013; Sippel et al., 2015).

In this study, modifications were made on the basis of previous studies (Ines & Hansen, 2006). Instead of being applied to only wet days, QM was applied to daily values to correct the biases and errors in precipitation and temperature (T_{max} and T_{min}). It resulted in a resolution change from a 12-km grid to an individual station (Mejia et al., 2012) for all 67 GCM projections from four climate change scenarios archived in the CMIP5 multiple-model dataset (Maurer, 2007). The QM technique was based on cumulative distribution functions (CDF) that were constructed daily from modeled and observed datasets. The difference between the two quantile maps in the same referenced period were used to bias-correct the simulated projections of climate change for future periods.

For each day of the year, a moving window of ± 15 days was used to select the candidates for the representative day in order to produce the empirical cumulative distribution functions (ECDF) for two datasets, one for PRISM observations and one for CMIP5 GCMs. For this study, the period of 1981-2010 was used as the baseline period from which the bias

correction relationship was derived. Thus, there would be 31 days in the moving window and 30 years in the baseline period, resulting in 930 values to define the ECDF for each day. Future daily bias-corrected data of GCMs were searched through the ECDF of GCMs to determine the quantile with the corresponding value, and then the ECDF observation on the same day from the same quantile was looked up. For example, a 50% value for April.15 in the GCM projections was translated into the same 50% value in observation for April.15; the 50% means that the daily value cannot be exceeded by 50% of the dataset of the 930 days that defined the ECDFs for April 15 (Figure 4). A linear interpolation was applied between two percentiles.

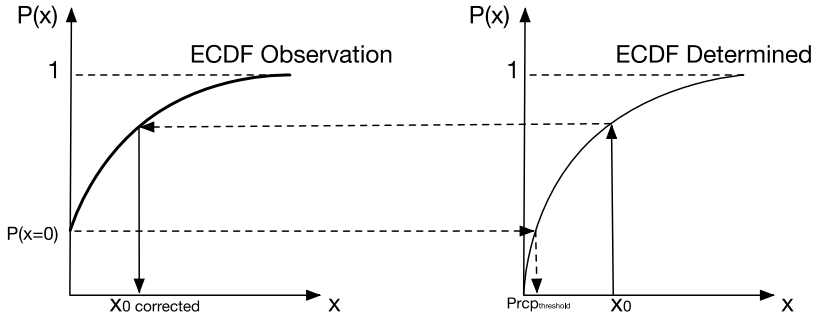

Figure 4. Sample Illustration of the Quantile Mapping Bias Correction Method. Two Empirical Cumulative Density Functions (ECDFs) Resulted from the Observed Data and the Determined Data on April 15th. The Bias-Corrected Value Was Determined by Looking Up the Observation ECDF with the Same Cumulative Density (e.g., 50%) as the Determined Value X0 for the Determined ECDF.

Nevertheless, there were some issues to be dealt with when dealing with the different variables. Regarding precipitation, one fact in the bias correction is that the drizzle effect tends to occur in most models because the probability of little precipitation in the model results is greater than that in the observations (Gutowski et al., 2003). Thus, in this study, precipitation thresholds were defined so that 'zero precipitation' had the same probability in GCMs as in the observations. Values below the thresholds were considered as 'no precipitation'. To determine the extreme values in the GCM projections that exceed the greatest value in the control simulation with the referenced period, the differences between the greatest value in the control

simulation and the corresponding observation were extended and applied to those values outrange of the control simulations (Belprat et al., 2013). Regarding temperature, traditionally, when the maximum temperature (T_{max}) and minimum temperature (T_{min}) are implemented independently, the procedure can change the Diurnal Temperature Range (DTR). In some cases, this can result in a physically unrealistic correlation between T_{max} and T_{min}, which makes $T_{max} < T_{min}$. Therefore, in this study, QM was applied to T_{max} and *DTR*, with T_{min} calculated as $T_{max} - DTR$, in order to improve the performance of bias correction for temperature (Thrasher et al., 2012).

2.5.3 **Validation of Q-Q Bias Correction**

In order to validate the QQ bias-correction method, a validation procedure was performed on a time period of Jan.1 2011- Dec.31 2016, which is beyond the period of 1981-2010 used for bias-correction procedure. Bias-corrected variables of precipitation, maximum temperature, and minimum temperature were compared between bias-correction results and the observations from the PRISM data. The PRISM data were from the same source as the data used for the bias correction, which were point-interpolated values from the 4-km grid where the Great Basin NP station was located.

On a mean monthly scale, the bias-corrected CMIP5 data, i.e., *Prcp*, *Tmax*, and *Tmin*, were compared to the observation to evaluate the performance of the QQ bias-correction method on monthly scale and variation. All climate change models under each potential climate change scenarios were analyzed as an ensemble to evaluate the uncertainties and variances resulting from difference climate models.

2.5.4 **Result assessment**

In order to evaluate the changes among time periods more easily, the entire simulation period was separated into smaller periods. Bias correction and hydrologic simulation were implemented from the past to the end of this century (1981-2099), which was split up into a baseline period of 1981-2010 and a future projected period of 2011- 2099. The future projection period was split into three periods: 2011-2039 (Period 1), 2040-2069 (Period 2), and 2070-2099 (Period 3). In order to assess the results from the two steps, several indices were used.

For the Step 1, the validation of PRISM data was done by comparing PRISM data and historical records during the overlapping period of 2003-2012 (water years). All three climate variables – precipitation, maximum temperature, and minimum temperature – were compared to the mean monthly values. In particular, the daily precipitation values (unit in mm/day) were examined statistically both on a monthly scale and a daily scale.

For the Step 2, the bias correction results were assessed by comparing the datasets of before bias correction and after bias correction with observations for the baseline period of 1981-2010 (Wilcke et al., 2013). Thus, the differences (before bias correction) and fitness (after bias correction) with the observations could be observed. The mean monthly bias and daily data frequencies of time-series data were used. Additionally from Step 2, the results of bias-corrected climate projections were assessed on a mean annual scale. Climate during the three future periods (i.e., 2011-2039, 2040-2069, and 2070-2099) was compared with the baseline period (1981-2010) for the four potential climate change scenarios and multiple models (Appendix A-1). Specifically, this assessment was performed on the mean monthly precipitation to detect the monthly changes.

2.6 Results

Because the study was done in two steps, the results of each step are presented in separate sections as follows:

Section 2.6.1: Validation of using PRISM data as observations

Section 2.6.2: Evaluation of bias-correction performance using results from the baseline period, and assessment of climate change in the study area using results from the projected period.

2.6.1 Validation of PRISM Data

Long time-series data were required for the development of the long-term features, which were used in the procedure of bias correction. Thus, instead of short period observational records, the PRISM data of 1981-2010 were used, which were on a daily scale with point interpolation from the 4-km grid at Great Basin NP (#263340, Elev. 2088 m).

The mean monthly values of maximum temperature, minimum temperature, and precipitation were compared between the PRISM dataset and historical records (Figure 5a,b&c). All three variables showed great consistency especially in temperature, which reached 32.8 °C at the highest (during the summer) and -10.9 °C at the lowest (during the winter). For precipitation, a detailed comparison was made with featured statistics: mean, variance, and standard deviation, on both a monthly scale and daily scale (Table 2). Daily mean precipitation was 1.02 mm/day for both the PRISM dataset and historical records. The variance of precipitation was the same at 0.001 on the monthly scale, while as expected, on the daily scale, historical records showed a higher variance (i.e., 0.020) than the PRISM dataset (i.e., 0.014). The standard deviation was very close at 0.73 and 0.78 mm/day on the monthly scale, and at 3.00 and 3.58 mm/day on the daily scale both corresponding to the PRISM dataset and historical records. Besides, the

distribution of daily and monthly values, examined by box plots (Figure 6), showed great uniformity between those two datasets.

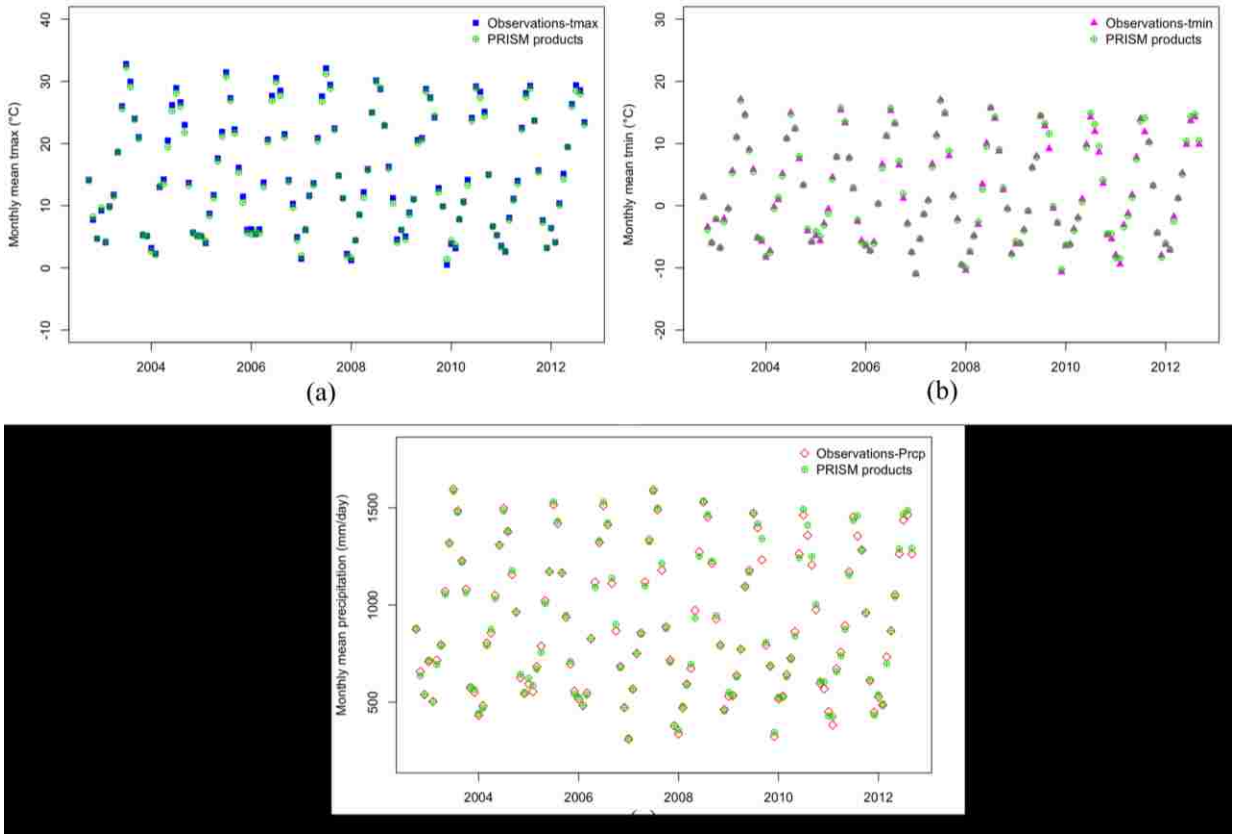

Figure 5. Climatic Variable Comparisons between Point Data Interpolated from PRISM and Meteorological Observations on Monthly Mean Scale during the Same Period of 2003-2012 (Water Years) in: (A) Maximum Temperature , (B) Minimum Temperature, and (C) Precipitation.

Table 2

Mean Daily Statistic Comparisons of Precipitation between Interpolated PRISM Data and Observations at the Great Basin NP (#263340) On Monthly and Daily Scales during the Period of 2003-2012 (Water Years) (Unit: mm/d).

Index	Monthly		Daily	
	PRISM	Observations	PRISM	Observations
Mean	0.96	1.07	0.96	1.06
Maximum	4.10	4.28	42.16	48.26
Standard Deviation	0.73	0.78	3.00	3.57

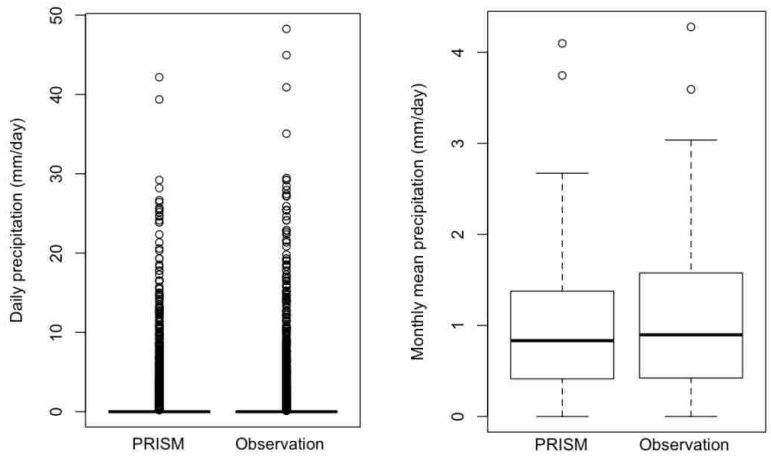

Figure 6. Comparisons of Precipitation between the PRISM Dataset and Observation at Great Basin NP (#263340) on Daily and Monthly Mean Scales, for the Period of 2003-2012 (Water Years).

2.6.2 **Validation of Q-Q Mapping Bias Correction**

While the PRISM data from period of 1981-2010 were used as observations in the bias-correction procedure, the data from the subsequent period of 2011-2016 were used for the validation. The validation results were presented by comparisons between bias-corrected results and observations, as the goodness of fitness between them represents the goodness of performance of the QQ bias-correction procedure. The Value distribution of *Prcp*, *Tmax*, and *Tmin* were analyzed on mean monthly scale as shown in Figure 7 with comparisons with PRISM observations. Specifically for *Prcp*, the basic statistics were performed on both daily and mean monthly scales as shown in Table 3 and Table 4.

Regarding mean monthly temperatures, the results showed narrow distributions, and the PRISM observations were well contained within the bias-corrected CMIP5 data for both maximum temperature and minimum temperature. This indicated a well bias correction procedure – QQ Mapping method - was performed on the temperature.

Regarding the mean monthly precipitation, validation results showed that most PRISM observations were contained within the 5%-95% distributed bias-corrected values; the majority

contained within value ranging between 25% and 75%. Exceptions were mean monthly values at June, RCP 2.6 and December, RCP 8.5. As indicated by the large range of value distribution (Figure 7), the bias-corrected precipitation have high standard deviation ranging between 12.3 and 13.4 with a comparison of 8.8 in PRISM (Table 3).

Regarding the daily precipitation, mean values from the bias-corrected CMIP5 data were all 1.0 mm/d for all climate scenarios, resulting in less than 11% difference from 0.9 mm/d in the PRISM observations. Nevertheless, comparing to 2.9 mm/d in the PRISM observation, the standard deviation reached 3.1-3.4 mm/d in the bias-corrected CMIP5 data with less than 17% of differences between them. This included the days with high precipitation reaching as high as 55.2-66.1 mm/d, while the maximum daily precipitation was 32.8 mm/d in PRISM observation.

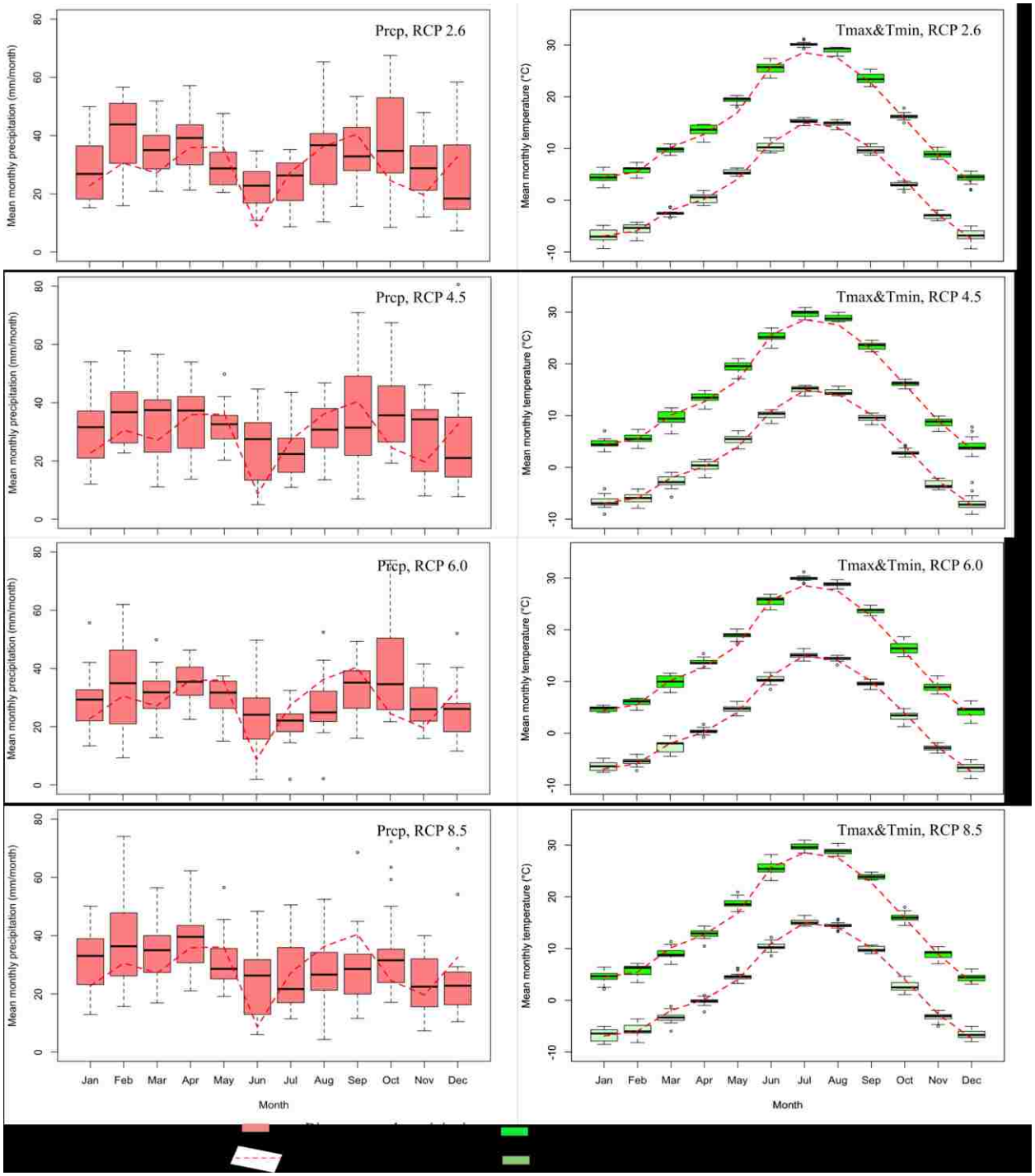

Figure 7. Validation Results of Quantile-Quantile Mapping Method: Comparisons between Bias-Corrected Results and Observations over the Time Period of 2011-2016. Variables of Precipitation (Left) and Maximum & Minimum Temperature (Right) were Analyzed for All Four Potential Climate Change Scenarios: RCP 2.6, RCP 4.5, RCP 6.0, and RCP 8.5. The Box Plot Represents the Result from Different Climate Models.

Table 3

Mean Monthly Statistic Comparisons of Precipitation between Interpolated PRISM Data and Bias-Corrected CMIP5 Data at the Great Basin NP (#263340) during the Period of 2011-2016 (Water Years) (Unit: mm /month).

	PRISM	Bias-corrected Data			
		RCP 2.6	RCP 4.5	RCP 6.0	RCP 8.5
Mean	28.5	31.7	31.1	29.6	30.5
Maximum	40.4	85.2	88.4	77.2	74.1
Minimum	8.7	7.3	5.0	1.9	4.3
Standard Deviation	8.8	13.4	13.2	12.3	13.1

Table 4

Daily Statistic Comparisons of Precipitation between Interpolated PRISM Data and Bias-Corrected CMIP5 Data at the Great Basin NP (#263340) during the Period of 2011-2016 (Water Years) (Unit: mm /day).

	PRISM	Bias-corrected Data			
		RCP 2.6	RCP 4.5	RCP 6.0	RCP 8.5
Mean	0.9	1.0	1.0	1.0	1.0
Maximum	32.8	58.7	55.2	59.7	66.1
Minimum	0.0	0.0	0.0	0.0	0.0
Standard Deviation	2.9	3.4	3.3	3.1	3.2

2.6.3 **Bias Correction**

Baseline Period (1981-2010)

The performance of QM bias correction was evaluated by comparing the mean monthly data distributions and daily data density distributions (Figure 9 &Figure *10*), during the bias correction period of 1981-2010.

Figures 8 &Figure *9* compared the meteorological data among the datasets of before bias correction and after bias correction with observations on a mean monthly scale for all scenarios. Box plots were used for aggregations of the multiple GCMs under each climate change scenario, during the overlapping period of 2003-2012 (water years). Results showed success in correcting the features of temperature (Figure 8) and precipitation (Figures 9), and the observations from PRISM were well contained within the 5% - 95% range of multiple GCMs after bias correction.

Temperature results showed a 0.1°C -3.5°C reduction (median value) on a mean monthly scale. Peak temperature occurred in July, and the lowest values occurred during December and January. For precipitation, an overall increase of 8.3 to 22.0 mm/month resulted from the bias corrections in mean monthly precipitation. In particular, a seasonal pattern was formed of higher precipitation during spring and fall than the rest of the year.

The density distributions of daily meteorological data were compared in Figure 10 during the baseline period of 1981-2010 under each emission scenario. The bias-corrected results of both temperature and precipitation had quite similar shapes in density distribution as those corresponding observations (Gaussian distribution, R 3.3.0) (Läuter, 1988; Sheather & Jones, 1991; Scott, 1992). As shown in Figure 10, a leaning towards higher values than the observations was corrected for temperature, especially minimum temperature. Regarding precipitation, the high density of low values (< 38.1 mm/month) tended to dominate the entire precipitation data, and the corresponding density reached as high as twice of those for the observations. This resulted in lower probabilities of middle to high events (> 38.1 mm/month). After bias correction, the high density of low precipitation was flattened and shifted towards higher values, with extreme events occurring at the tail end of the distribution (Figure 10).

Projected Period (2011-2099)

As suggested in Maurer et al. (2007), a comparison of results over a range of time could better support the conclusions than that of a specific month or day. In this study, the changes were summarized for the three periods: 2011-2039, 2040-2069, and 2070-2099, represented as Period 1, Period 2, and Period 3, respectively, in the 21st century. The bias-corrected climate variables of *Prcp*, T_{max}, and T_{min} were aggregated on a mean annual scale for the three periods, for the four potential climate change scenarios (Figure 11). All scenarios showed general

increasing trends in *Prcp*, T_{max}, and T_{min} from Period 1 to Period 3, at different levels. Specifically, changes in precipitation were aggregated on a mean monthly scale to investigate the monthly variability (Figure 12).

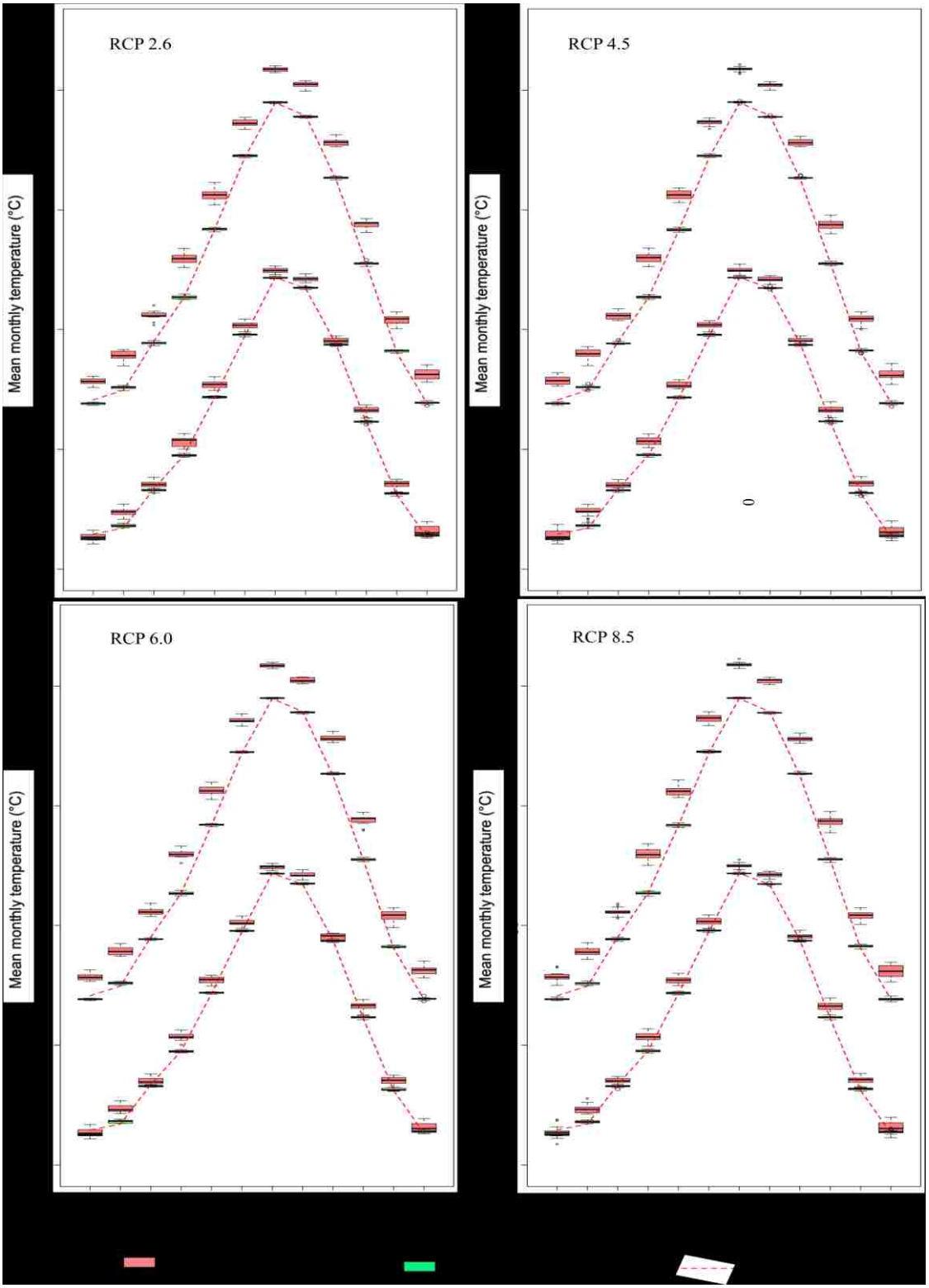

Figure 8. Comparisons of Datasets from Before Bias-Correction, After Bias-Correction, and Observations (PRISM) during the Historical Period of 1981-2010. Each Sub-Figure Shows Two Sets of Variable, i.e., Maximum Temperature and Minimum Temperature. The Boxplot Represents the Variation of Multiple Climate Change Models under Each Scenario: RCP 2.6, RCP 4.5, RCP 6.0, and RCP 8.5.

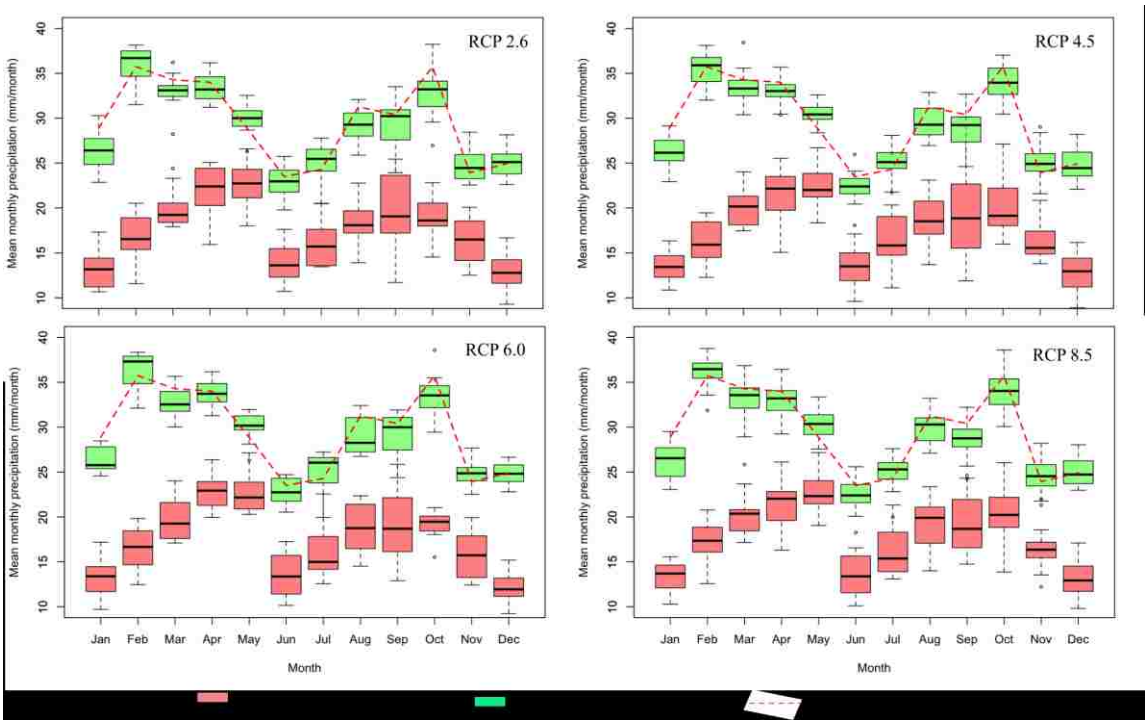

Figure 9. Comparisons of Precipitation Data from Before Bias-Correction, After Bias-Correction, and Observations (PRISM) during the Historical Period of 1981-2010. The Boxplot Represents the Variation of Multiple Climate Change Models under Each Scenario: RCP 2.6, RCP 4.5, RCP 6.0, and RCP 8.5.

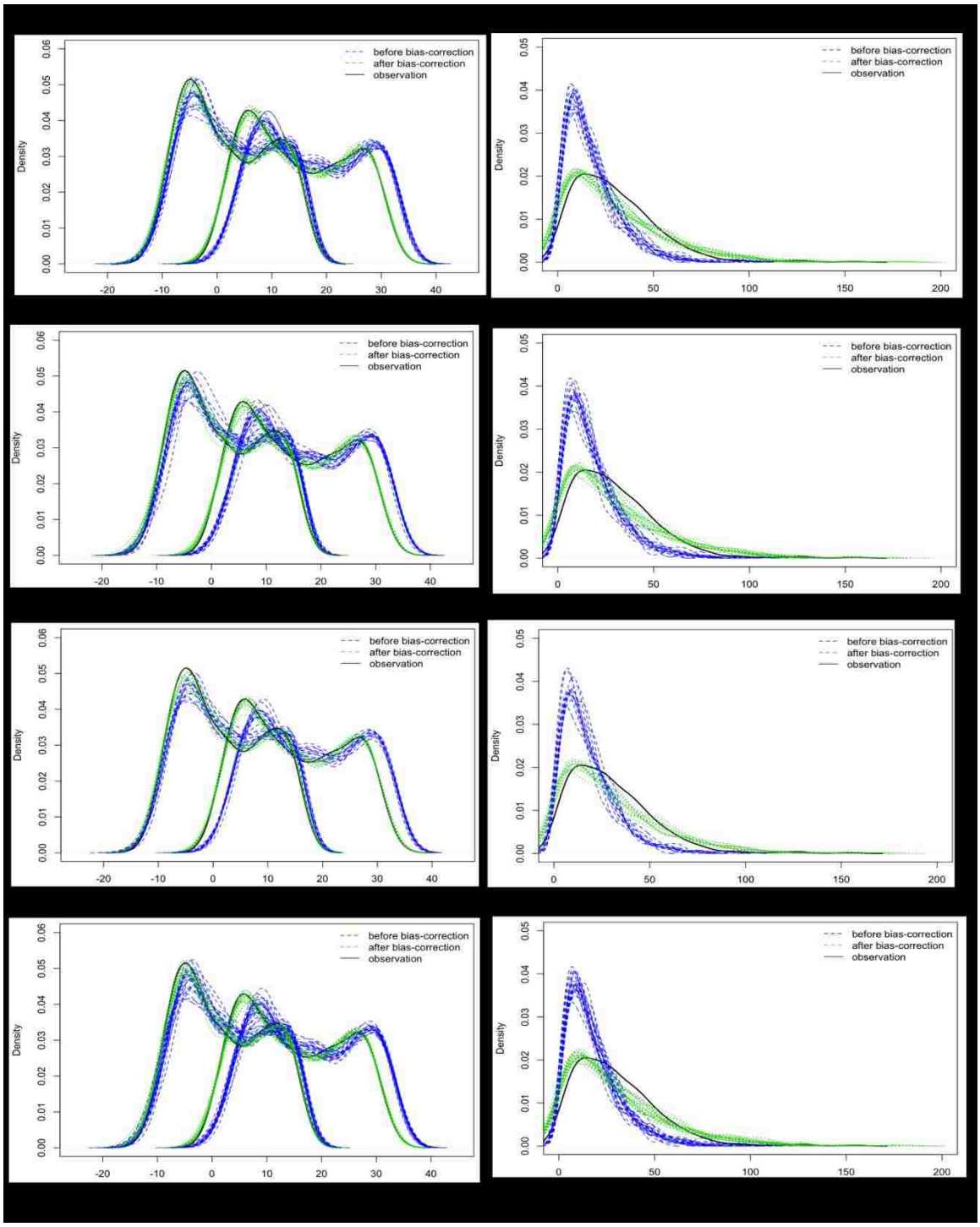

Figure 10. Comparison of the Density Distribution among the Monthly Mean Values for the Dataset Before Bias Correction, After Bias Correction and Observations (PRISM) during the Historical Period of 1981-2010, Using Multiple Projected Models Of RCP 2.6, RCP 4.5, RCP 6.0, and RCP 8.5 for (A) Maximum Temperature and Minimum Temperature And (B) Precipitation.

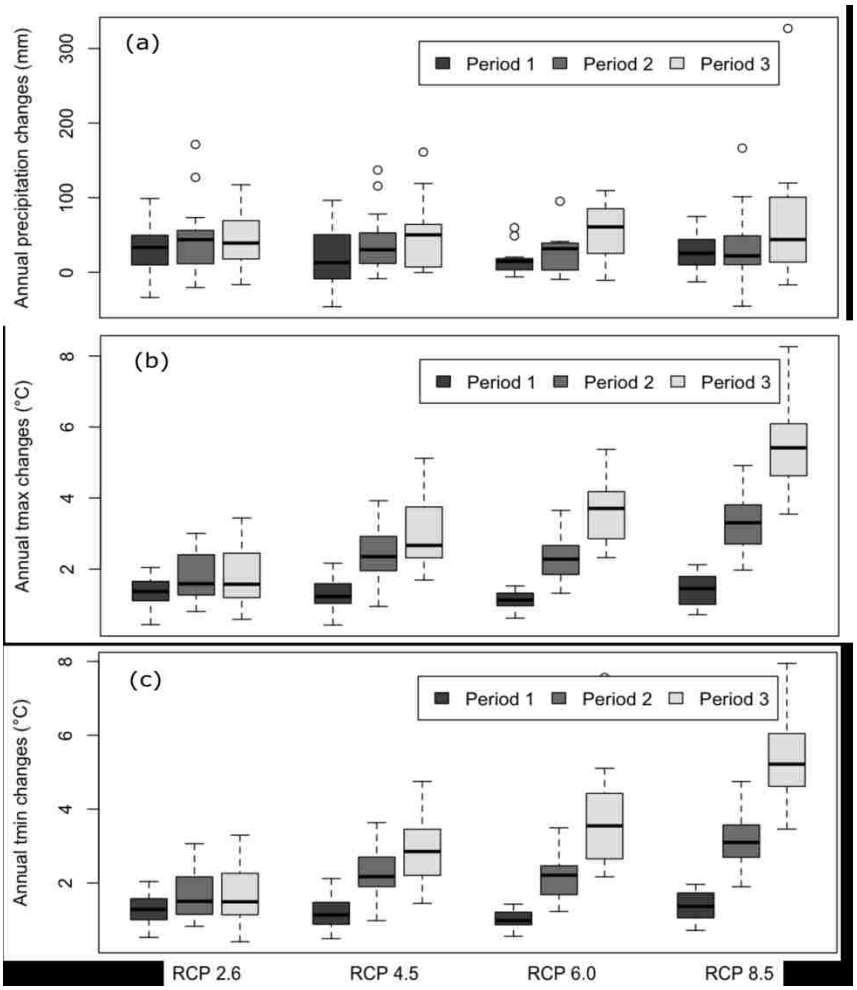

Figure 11. Annual Changes of Climatic Variables: (A) *Prcp*, (B) *Tmax*, and (C) *Tmin* in Three Future Periods: Period 1 (2011-2039), Period 2 (2040-2069), and Period 3 (2070-2099), based on Baseline Period (1981-2010) for Each Climate Change Scenario (i.e., RCP 2.6, RCP 4.5, RCP 6.0, and RCP 8.5).

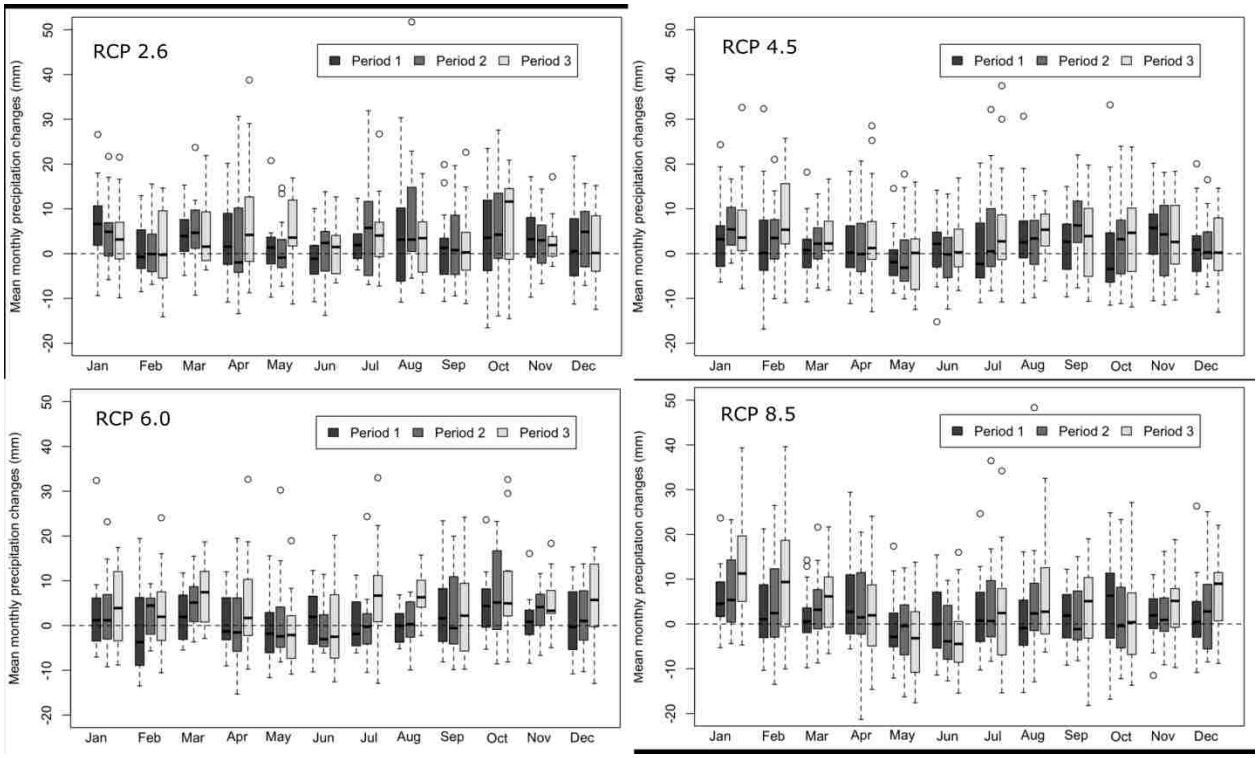

Figure 12. Mean Monthly Precipitaion Changes for Three Future Periods: Period 1 (2011-2039), Period 2 (2040-2069), and Period 3 (2070-2099), based on Baseline Period (1981-2010), for Each Climate Change Scenario (I.E., RCP 2.6, RCP 4.5, RCP 6.0, And RCP 8.5).

On the mean annual scale, T_{max} and T_{min} shared similar patterns in long-term changes, which showed distinctive increases from low-level RCP to high-level RCP and from Period 1 to Period 3. The increase of mean annual T_{max} was at 1.1°C - 1.4°C at the beginning of the century (Period 1), and reached 1.6°C -5.4 °C by the end of the century (Period 3); this increase varied for different climate change scenarios. At the same time, the increase of mean annual T_{min} changed from 1.0°C - 1.4 °C (Period 1) to 1.5°C - 5.2 °C (Period 3) for different climate change scenarios.

Precipitation projections had an overall tendency for an increase, however, trends and uncertainties showed irregularities among periods and scenarios. A mild increase during the three periods was found in RCP 4.5 and RCP 6.0, while uncertain changes were found in RCP 2.6 and RCP 8.5, with an annual *Prcp* in Period 2 either higher or lower than that in Period 3 (Figure 11). Regarding the mean annual *Prcp*, the increases changed from 13.1 mm - 33.2 mm to

39.2 mm - 60.8 mm, corresponding to the increases in Periods 1 and 3 (Figure 11). For mean monthly *Prcp* (Figure 12), there was no evidence of an inter-scenario pattern. However, increasing changes could be observed during winter seasons (i.e., October - April) and decreasing changes during summer seasons (i.e., May – September), with indistinguishable variations in the months in-between. The mean monthly increase in precipitation could reach as high as 14.0 mm (RCP 2.6, Period 3, October), and the decrease could be as low as 5.6 mm (RCP 8.5, Period 3, May).

2.7 Discussion

Prior to applying a bias-correction method or other similar statistical transformations, it is important to understand the limitations or assumptions of the design technique. The differences between GCM products and observations were stationary throughout the bias-correction period, which meant that past correlations were also applicable to the future. The validity of this assumption could not be fully assessed because the observed variables of interest (e.g., precipitation or temperature) may be exceeded under climate change (Gudmundsson et al., 2012). Additionally, some temporal cross-correlation properties may not have been corrected; for example, a duration of wet days that is too short still may exist after correction. In addition, inter-variable dependencies were not considered when using the QM method. For instance, the bias in precipitation may have correlations with a bias in temperature, which might not be corrected independently (Boe et al., 2007). While future climate might never be forecasted accurately, due to the sophisticated dynamic interactions in the large Earth system, an estimation limited by the assumptions could provide an idea of future trends under certain conditions. The bias correction procedure of GCM products is critical in maintaining local climate features and

characteristics, which are important for understanding the trends in alterations under the effects of climate change.

As stated in the description of the data construction, the PRISM dataset resulted from an observation network. When the observation network repository is expanded or reduced due to the addition of new stations or the closing of old stations, it leads to changes in the PRISM data over the time. In this case, the data consistency, long-term trends, and features may not have been well preserved. Therefore, the PRISM dataset typically may not be a good choice for long-term uses, such as bias correction. However, in the study area of the Lehman Creek watershed, the long-term features were well maintained since there was no observation stations added or removed during the period of 1981-2010, the period for which the PRISM data were constructed. Therefore, it was appropriate to implement the PRISM data for observations in the study area, even though this procedure may need further evaluation when used in other areas.

The daily-based bias correction performed on *Prcp*, T_{max}, and T_{min} showed good results with well-maintained features of the density distribution and mean monthly distribution for all emission scenarios and models (Appendix A-1). As the study area was located in a desert, the datasets with coarse resolution, which were averaged over a larger region, tended to have higher temperatures and less precipitation than those on a local scale, especially in mountainous areas. This feature was well observed in the CMIP5 dataset on a 12-km grid, and showed both dry and hot climate conditions with rare precipitation. The QM technique effectively corrected the bias, and resulted in precipitation and temperature congruent with the observations. Therefore, the climate-determinant indexes of elevation and land cover were successfully converted after bias correction, and thus resulted in cooler and wetter weather in the study area.

By comparison, the bias-corrected CMIP5 dataset showed increases in the mean annual precipitation ranging from 13.1 mm to 33.2 mm at the beginning of this century to 39.2 mm - 60.8 mm by the end of this century. At the same time, great increases occurred to the mean annual maximum and minimum temperatures, which changed from 1.1°C -1.4 °C (T_{max}) and 1.0°C - 1.4 °C (T_{min}) in Period 1 to 1.6°C - 5.4 °C (T_{max}) and 1.5°C - 5.2 °C (T_{min}) in Period 3, correspondingly. Among the time periods and four emission scenarios, the increasing temperature differed with certain patterns, with the highest increase occurring in the last period with the highest emission scenario (Period 3, RCP 8.5), and the lowest increase appearing during the first period (Period 1) with a slight difference among emission scenarios. Substantial variations were found when comparing the mean monthly precipitation among periods and emission scenarios; this may be the result of the uncertainties in the QM technique, which relied significantly on the data frequencies.

A previous study indicated considerable discrepancies and varying reliabilities among different GCM products (Mohammed et al., 2015). In comparison to a previous study (Volk, 2014), which only used one GCM product (CCSM4) for the study of warming climate influences on water resources, all GCMs were weighted equally and were used in an ensemble in the current study. Potentially, this approach could be a cause of the uncertainties in the GCM precipitation products, apart from procedures of the bias correction method (Mejia et al., 2014). However, it is reasonable to consider the study results a plausible indication of future changes and which the hydrologic processes over the next century should be capable of responding to. This study laid solid groundwork for future analysis, using the PRISM data as observations on a local scale. Besides, comparisons and evaluations of the future meteorological condition, streamflow alterations, and uncertainties can help to more clearly understand the potential

influences of changing climate on water resources. A further extension of the study might look into the snow process, including annual changes and seasonal patterns.

2.8 Conclusions

This study focused on the quantitative assessment of climate changes on a watershed-scale area, the Lehman Creek watershed in Great Basin National Park, Nevada. Downscaled GCM data from the CMIP5 BCCA dataset were used, which provided the meteorological conditions under four potential climate change scenarios: RCP 2.6, RCP 4.5, RCP 6.0, and RCP 8.5 with resolution at 1/8° (12 km). Instead of 10-year observation records, a 30-year PRISM dataset (1981-2010) was used for the long-term feature capture and the QM bias correction of the CMIP5 dataset in the study area. Evaluation of the results was performed as a relative alteration from the projected period (i.e., 2011-2099) on the basis of a baseline period (i.e., 1981-2010). Three future time periods were defined as 2011-2039, 2040-2069, and 2070-2099.

On the basis of the study results, the following conclusions were made:

1. The PRISM data preserved the value scale, distribution, and long-term features in the observations at Great Basin NP station. This indicates the PRISM data can be applicable, with effective replication of observations in areas that have issues in long-time shortage of data.
2. Results of QM bias correction fit the observations well in monthly distribution and density distribution during a same historical period. This indicates that this approach can be used to correct the combined errors from spatial resolution differences and model systems.
3. Under the influences of climate change, the average value of mean annual ensembles over the entire projected 21st century showed an increase of 2.3 °C, 2.2 °C, and 35.1 mm in

maximum temperature, minimum temperature, and precipitation, respectively, in the study area (Great Basin NP station).

This study could contribute to increase the understanding of water resource alternation with regard to rates and timing by responding to all potential climate change scenarios using downscaled CMIP5 products. During the study, a 30-year PRISM dataset (AN81d) was used to represent observations in order to solve the conflict between the need for observation data to downscale the climate change products and the data shortage that existed at the station. The PRISM data successfully captured the long-time features of local climate statistically, and demonstrated its capability as a valid substitution for missing meteorological observations in the study area. This could provide useful insights if observations are missing in other study areas when needed. The approaches employed in this study provided solid foundation with the implementation of QM for downscaling climate change products.

Chapter 3 Surface Hydrologic Responses to Climatic Changes in Lehman Creek Watershed

3.1 Research Objective 2

Research Question # 2: How do the climatic changes affect the streamflow on a watershed scale?

This study was to develop a hydrologic model for the study area at Lehman Creek watershed using PRMS. The model development includes data collection, watershed delineation, model construction, parameter estimation, and sensitivity analysis. The model calibration and validation were performed through comparisons of the principal hydrologic processes: solar radiation, potential evapotranspiration, and streamflow for the period of 2003-2012 (water years). Especially, the streamflow simulation results were compared to the observations of the annual, mean monthly, monthly mean, and daily scale.

The calibrated model was driven by bias-corrected CMIP5 data for both the baseline period of 1981-2010 and projected three periods during 2011-2099. On the basis of status in the baseline period (1980-2010), the long-term changes, trends, and seasonal variations of streamflow in three projected periods were assessed in both timing and rate.

3.2 Introduction

3.2.1 Hydrologic models

During the last few decades, the study of hydrometeorology has experienced tremendous progress thanks to extensive establishments of observational stations and platforms, the development of new theories and models, and great improvement in computation. As one of the most critical factors in the hydrological cycle, the meteorological system has been studied, extended and coupled with hydrologic processes. Thus, the model predictions of future climatic

conditions can be used as the input to hydrologic models and to investigate the impact of the predicted climate changes to hydrologic processes quantitatively, which helps to identify the potential issues and to support making better management strategies.

Hydrologic models, as widely used tools, provide cost efficient means to study the hydrologic processes and evaluate the water resources within a watershed to support the best water resources management and utilization. While there are so many rainfall-runoff hydrologic models, it is important for the selection of an appropriate model that satisfies both study purposes and data availability.

As classified and described by Beven (2000), one basic classification of model types is by lumped model or distributed model. Lumped models treat the watershed catchment as a single calculation unit, with all variables that represent average levels over the entire catchment area, such as the soil water capacity in the saturated zone. Distributed models make simulations that are distributed in space, with variables that represent a local scale, by spatially discretizing the catchment into a large number of calculation elements. Each of the elements is an average representation of a local space, where equations are solved respectively as parameters are specified for each associated element. Lumped models usually use a number of storages to control the water exchange functionally. Examples are the Hydrological Simulation Program-Fortran (HSPF) model from the USA, the Hydrologiska Byrans Vattenbalansavdelning (HBV) model from Sweden, and the Tank model from Japan, etc. On another hand, distributed models attempt to describe all water flow in the catchment by nonlinear partial differential equations, describing components of interception, evapotranspiration, and snowmelt. A better representation of heterogeneity can be reached through parameters defined for every element. Examples are Système Hydrologique Européen (SHE) model by European organizations,

Institute of Hydrology Distributed Model (IHDM) by the UK, Waterloo Flood Forecasting Model (WFFM) by Canada, and Precipitation-Runoff Modeling System (PRMS) by the USA, etc. Additionally, there is also a range of models that uses a distributed function of catchment characteristics to interpret the surface runoff generation components, such as the Xinanjiang model from China (Ren-Jun, 1992), Variable Infiltration Capacity (VIC) model from the USA (Gao et al., 2010), and the Arno model from Italy (Todini, 1996), which are called semi-distributed models.

Hydrologic models can also be mainly classified by deterministic model or stochastic model, described by Beven (2000), depending on whether or not the model outputs are associated with some variance or uncertainties. The vast majority of models use the deterministic approach, such as physically based models (Ahmad & Simonovic 1999; Mosquera-Machado & Ahmad 2007; Forsee & Ahmad 2011). Additionally, there are many other different ways of hydrologic model classifications, such as empirical models (Ahmad et al., 2009, 2010, Zhang et al., 2014) and data driven models (Ahmad and Simonovic 2005; Ahmad et al., 2010; Stephen et al., 2010a; Stephen et al., 2010b; Puri et al., 2011a and 2011b; Melesse et al., 2011; Carrier et al., 2013; Choubin et al., 2014). More can be found in O'Connell (1991), Wheater et al. (1993), and Singh (1995).

System dynamics approach (Sterman, 2000; Mirchi et al., 2012) has also been used to model streamflow and water resources systems. Some applications include flood management (Ahmad & Simonovic 2000, 2001a, 2001b, 2001c, 2001d, 2005, 2006), river flow changes in response to climate change (Dawadi & Ahmad 2012), urban water system planning and management (Shrestha et al., 2011, 2012; Qaiser et al.,2011, 2013; Dawadi & Ahmad 2013), regional water system planning (Ahmad & Prashar 2010; Wu et al., 2013; Chen et al., 2015a,

2017a) hydrology (Zhang et al., 2017) and water quality management (Venkatesan et al., 2011a, 2011b; Rusuli et al., 2015; Amoueyan et al., 2017).

Eslamian (2014) summarized some climate change studies on regional or watershed scales using different models for various purposes. For an assessment of regional water resources management (Liu et al., 2011; Chen et al., 2011), monthly rainfall-runoff models were generally used for evaluating regional hydrologic consequences to the changes in precipitation, temperature, and other climatic variables (Gleick, 1986; Mimikou et al., 1991; Arnell, 1992; Xu & Singh, 1998). For detail assessment of surface runoff, conceptual models are useful, such as the Sacramento Soil Moisture Accounting model (Burnash et al., 1973), which has been widely used by many studies of climate change impacts (Gleick, 1987; Schaake, 1990; Cooley, 1990; Lettenmaier & Gan, 1990; Nash & Gleick, 1991). For the evaluation of impacts on the potential evapotranspiration in arid and semi-arid regions, the Penman-Monteith Potential Evapotranspiration model was used (Schaake, 1990). For estimations of general annual runoff under different climate scenarios, simple empirical and regression models were chosen in previous studies (Revelle & Waggoner, 1983; Arnell & Reynard, 1989). While, for simulations of spatial patterns of hydrologic responses to climate changes on watershed scales, physical-based distributed-parameter models are required (Arnell & Reynard, 1989; Thomsen, 1990; Running & Nemani, 1991).

3.2.2 **Precipitation-Runoff Modeling System**

The Precipitation-Runoff Modeling System (PRMS) described by Markstrom et.al (2005) is a watershed-scale, physically based, and distributed- parameter model designed for precipitation and snowmelt runoff. As a part of the Modular Modeling System (MMS) (Leavesley et al., 1996), PRMS uses a module library that contains compatible modules of a

variety of process simulations, including water, energy, and biogeochemistry (Leavesley et al., 1996).

The program version under description in this section is PRMS 3.0.5, which was released on April 24, 2013 (PRMS, USGS). A series of mathematical algorithms are used to simulate the hydrologic processes based on physical laws or empirical rules. On daily step, the principle hydrologic processes are simulated ,which include canopy interception; snowmelt and snow accumulation; evapotranspiration; infiltration; and the forming and routing processes of surface flow, subsurface flow, and groundwater flow (Figure 13). The module library provides several options for each hydrologic component with different calculation algorithms. The hydrologic Response Unit (HRU) is a user-defined area unit, in which hydrologic process calculations are performed, on both temporal and spatial scales. The modular deterministic feature enables PRMS to evaluate the effects of meteorological and geographical factors with various combinations on each HRU.

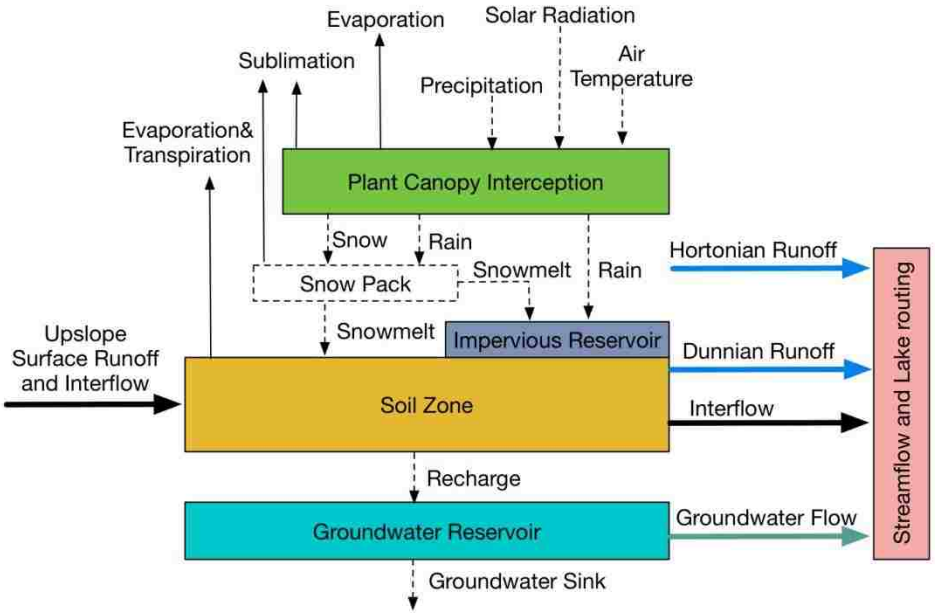

Figure 13. Hydrologic Processes Simulated in the Precipitation-Runoff Modeling System (Modified from Markstrom et al., 2015).

PRMS has been successfully employed in multiple areas of various studies. Through the PRMS simulation of physical processes of surface hydrology and sediment production, Rankl (1987) evaluated the interaction between runoff and sediment load. Dressler et al. (2006) evaluated the experimental, gridded snow cover area (SCA), and snow water equivalent (SWE) products in the upper Rio Grande River basin and the Black River basin through a comparison with PRMS simulations. With a physical-based hydrologic simulation, the streamflow in ungauged areas was assessed with an index comparison in gauged areas with similar hydrologic characteristics in the Lake Tahoe Basin, California, and Nevada (Jeton, 1999). For the development of operating criteria for the interstate allocation of water in the Truckee River and Carson River Basin of western Nevada and eastern California, the precipitation-runoff model helped to estimate three ungauged daily streamflows that were used as inputs to the USGS Truckee River operation model (Jeton, 2000). In 2012, led by the U.S. Department of Interior and U.S. Geological Survey, integrated watershed-scale responses to climate change were studied in 14 regions across the United States: Black Earth Creek, Wisconsin (Hunt et al., 2012); Cathance Stream, Maine (Dudley et al., 2012); Clear Creek, Iowa (Christiansen et al., 2012); East River, Colorado (Battaglin et al., 2012); Feather River, California (Koczot et al., 2005); South Fork Flathead River, Montana (Chase et al., 2012); Flint River, Georgia (Hay & Markstrom, 2012); Naches River, Washington (Maurer et al., 2012); Pomperaug River, Connecticut (Bjerklie et al., 2012); Sagehen Creek, California (Markstrom et al., 2005); Sprague River, Oregon (Risley et al., 2012); Starkweather Coulee, NorthDakota (Vining et al., 2012); Trout Lake, Winsconsin (Walker et al., 2012); and Yampa River, Colorado (Hay et al., 2012)

3.2.3 **Previous studies**

In the study area of the Lehman Creek watershed, Volk (2014) used PRMS for hydrologic simulation in a larger area that included the Lehman Creek watershed. Additionally, a series of studies with different research focuses have been accomplished, which included the Lehman Creek watershed area.

Volk (2014) studied potential effects of a warming climate on water resources within the Lehman and Baker drainages using PRMS. The study area included the Lehman Creek Drainage, Baker Creek Drainage, and Rowland Spring. In his study, the products from one climate change model, Community Climate System Model version 4.0 (CCSM4) from CMIP5 (BCCA) dataset, were used as the PRMS driving forces to simulate the hydrologic responses. In the model simulation, the projected daily temperature products after bias correction were used, while the bias-corrected daily precipitation products came from the archived measurements of 30-year period 1970–1999 (in water years) from BCCA. The archived measurements came from a retrospective period dataset and then were repeated three times into the future (water years 2009-2038, 2039-2068, and 2069-2098) as the precipitation input for this century. Discontinuous periods of data were used for the model calibration and simulation, where the period of 1993-1996 (water years) was used for model calibration and the period of 2003-2010 (water years) was used for model validation. Volk (2014) found temperature sensitivity in the Lehman and Baker drainages, an increased streamflow with an earlier snowmelt timing shift from May to April, temperature increases of 5.5 degrees Fahrenheit by the end of this century, streamflow reduction by 10% with decreases in peak snowpack, and reductions in soil moisture and evapotranspiration in July and August.

A report on the eastern part of the Great Basin National Park and the surrounding areas, where the Lehman Creek watershed is located, summarized the previous studies in the region (Prudic et al., 2015). In Snake Valley, the surface-water and groundwater resources were evaluated by Hood and Rush in 1965; the hydrogeologic conditions were studied by the SNWA, which included water chemistry, characterization of streams and springs, and characterization of geology and hydrogeology (as cited in Prudic et al., 2015). A collaborative study, done by the USGS, the Desert Research Institute, and the State of Utah (Welch et al., 2007), evaluated the aquifer system, aquifer water quality, basin recharge and discharge, inter-basin groundwater flow, regional groundwater flow, and regional water budget in the basin and range carbonate-rock aquifer system in parts of Nevada and Utah. A conceptual model of the Great Basin carbonate and alluvial aquifer system was developed by Heilweil and Brooks (2011), which assessed the regional groundwater availability quantitatively on the basis of a steady-state numerical groundwater flow model (Brook et al., 2014). Prudic and Glancy (2000) investigated the source of the Cave Spring using geochemical assessments. Additionally, a study done between September 2011 and April 2012 to evaluate the connection between the water in Baker Creek and Pole Canyon with the water in caves and at springs in the Baker and Lehman Creek drainage basins using fluorescent dyes (as cited in Prudic et al., 2015). Masbruch et al., (2014) constructed a 3-D groundwater flow model with a transport model in Snake Valley and surrounding areas to predict the impact to the groundwater discharges if well withdrawals increase.

3.3 About Study Area

3.3.1 Geographic Data

The physical geographic and geomorphic conditions of the study area, Lehman Creek watershed, were delineated using elevation, land cover land use, and soil types. These data were obtained from the Digital Elevation Model (DEM) of the National Elevation Dataset portal (DEM, 2013), the National Land Cover Database (Homer et al., 2015; Figure 17a), and the Soil Survey Geographic of the Natural Resources Conservation Service (SSURGO, 2013; Figure 17b) with a 30-m resolution. The Lehman Creek watershed is elevated between 2038 m and 3978 m. The fractured quartzite beneath a thin layer of a coarse glacial deposit dominates the largest portion of the study area. The land cover is dominant by evergreen forests (70%) with deciduous forests, shrubs, and some other mix forests (10%). There are 17% barren area mainly located around Wheeler Peak in southwestern with 2% perennial snow/ice. The only area with relative low permeability is the park roads that are used for visitors' transportation.

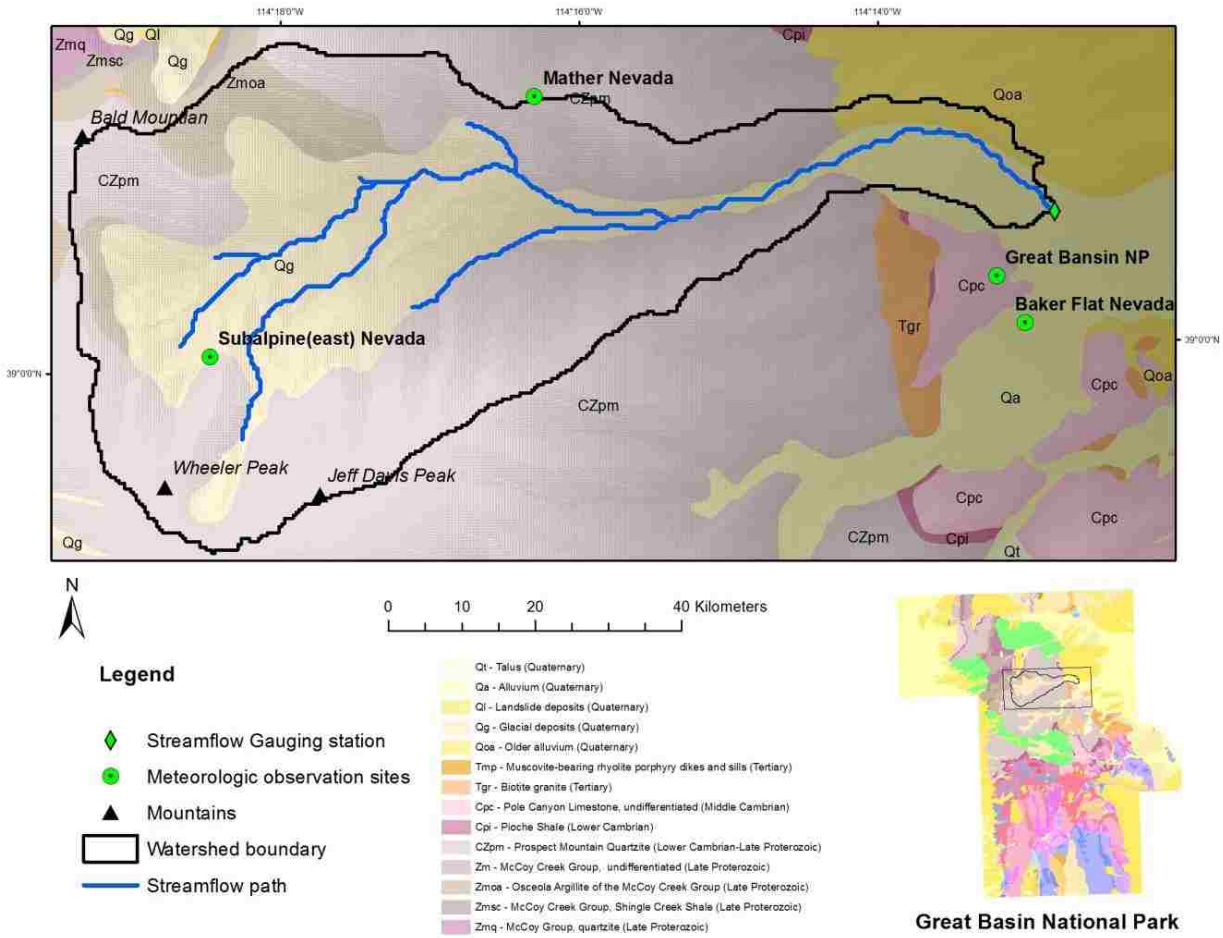

Universal Transverse Mercator projection, Zone 11, NAD 83

Figure 14 Lehman Creek Watershed in the Great Basin National Park, White Pine County Nevada (NPS Geologic Resources Inventory Program, 2014).

3.3.2 **Hydrogeologic Characteristics**

In the Lehman Creek watershed, the large altitude differences, topographic relieves, and geologic condition make the great differentiation in climate, vegetation, and water flow path, which divide the study area into two parts: Mountain-Upland Zone and Karst Limestone Zone (Prudic et al., 2015).

As described by Prudic et al. (2015), the Mountain-Upland Zone was defined as the area where the elevation is greater than 2134 m (7,000 ft) with steep slopes and a thin layer of soil. High-density conifer forest covers the area between the elevation of 2134 - 3353 m (7,000-11,000 ft), with bare land and tundra covering beyond 3353 m (11,000 ft) (Houghton et

al., 1975). As the only water source in the zone, precipitation is mostly lost to evapotranspiration (over 50%) and the rest forms the water flow. Glacial and alluvial deposits, which resulted from the active erosion, overlay the thick layer of granite, quartzite, and shale with low permeability. Therefore, most of the water flow (over 90%) is surface runoff. The groundwater flow passes through the large pores in the glacial deposits and through small pores in the thin layer of alluvial deposits or consolidated rocks, which helps maintain perennial flow downstream.

At the lower part of the mountain and beneath the thin alluvial deposits, karst and limestone formation makes Lehman Creek a losing stream. The dissolution of circulation of shallow groundwater develops the large cave system and more permeable limestone. Consistent water loss occurs in the karst limestone zone (Prudic et al., 2015).

3.4 Method

3.4.1 PRMS

Principal hydrologic processes

The PRMS uses compatible modules to compute the simulation of hydrologic processes. The main components of the simulated hydrologic processes include Solar Radiation Process, Potential Evapotranspiration Process, Canopy Interception Process, Snow Process, Cascading Flow Process, Surface Runoff, Soil-Zone Process, Groundwater Process, and Streamflow Process. The following descriptions of the hydrologic process simulation are from Markstrom et al. (2015), where detail simulation equations can be found.

The Solar Radiation Process calculates 366 values for days of clear-sky solar radiation and daylight length for each of the hydrologic Response Unit (HRU) according to the basic topography information, e.g. latitude, aspect, and slope. Based on the availability of data

observation in the study area, solar radiation can either be direct input by users with pre-distributed data or computed by the PRMS module.

The Potential Evapotranspiration Process is computed for each HRU with user-specified method options. Depending on the requirement of data observations and the sophistication of method algorithms, seven options are available: the modified Jensen-Haise formulation (Jensen & Haise, 1963; Jensen et al., 1969), the empirical Hamon formulation (Hamon, 1961), the Hargreaves-Samani formulation (Hargreaves & Samani, 1985), the Priestley-Taylor formulation (Priestley & Taylor, 1972), the Penman-Monteith formulation (Penman, 1948; Monteith, 1965), pan-evaporation measurement-based method (Markstrom et al., 2015), and user defined input file with pre-distributed data.

The Canopy Interception Process is simulated for calculations of intercepted rainfall and snowfall, evaporation from the intercepted water, and the throughfall reaching to the snowpack or soil. The canopy density by the dominant vegetation in each HRU is a determinant factor.

The Snow Process is computed through two balance processes: energy balance and water balance. Energy is calculated between the atmosphere and snowpack through the conduction, convection, and radiation. With an isothermal condition of 0 degree Celsius, energy budget is calculated as snow pack melts when energy is above the status, and snow pack accumulates when heat deficit exists. Water balances among the throughfall precipitation, snowpack storage, sublimation, and melt.

The Cascading Flow Process is the flow routing simulation for surface water and groundwater. It routes flows from/to contiguous HRU, from upslope to downslope, and terminates in streams, lakes, or swales. The specification of directed, acyclic-flow network is

required to define the flow path in the domain. Complex routing paths with both one-to-one routing (to one downslope neighbor) and many-to-many routing (to many downslope neighbors) are allowed.

The Surface Runoff Process partitions water from net precipitation, snowmelt, and any upslope cascading flow into infiltration and infiltration-excess runoff. On the basis of the fraction of impervious area and depression area for each calculation unit, several components are calculated: retention storage, evaporation, infiltration, water exceeding infiltration capacity from pervious areas, and direct runoff generated from impervious areas.

The Soil-Zone Process computes all the inflows, outflows, and storage changes in the soil zone of each HRU. While taking the same physical space, three reservoirs are conceptualized in the soil zone: preferential-flow reservoir, capillary reservoir, and gravity reservoir. The conceptualizations are meant to simulate the water status and flow direction. In this process, the infiltration is the main inflow, apart from lateral water inflows, and the outflows are evapotranspiration, fast flow, slow flow, and Dunnian runoff (Figure 15). The soil-water processes are calculated in a sequence as illustrated in Table 5.

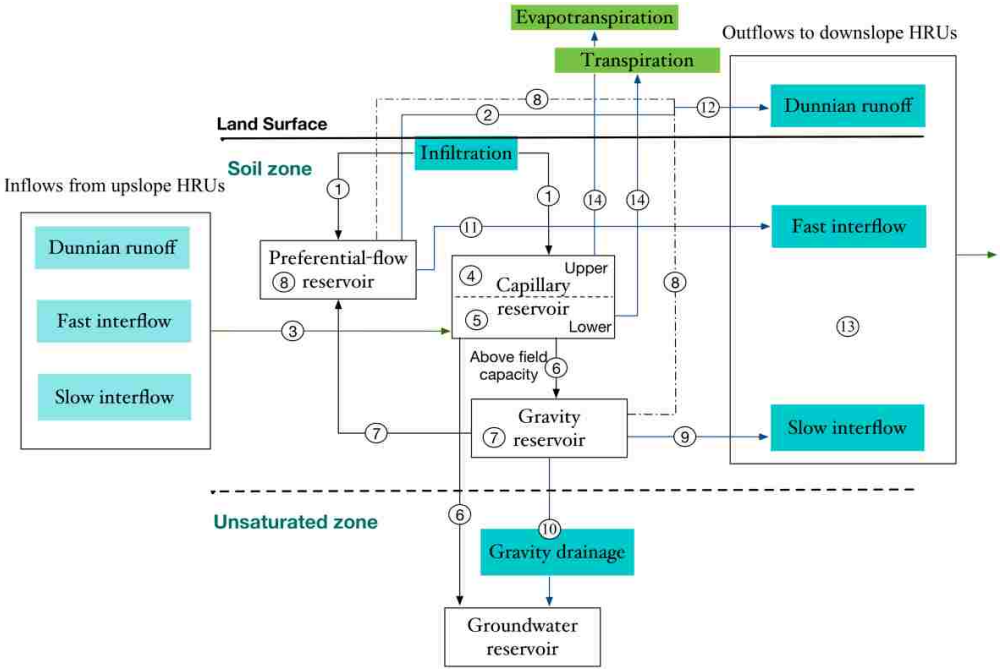

Figure 15. Inflow and Outflow Diagram of Three Conceptualized Reservoirs In Soil-Zone: Capillary, Gravity, and Preferential-Flow Reservoirs in PRMS for a Single HRU.

Table 5

Sequence of Steps Used in the Computation of Flow into and out of the Soil Zone Used in PRMS (Markstrom et al., 2015).

Sequence No.	Description of flow into and out of soil zone
1	Partition infiltration between capillary and Preferential-flow Reservoir.
2	Calculate Dunnian surface runoff (part 1) from preferential-flow reservoir.
3	Add interflow and Dunnian runoff (Dunne & Black, 1970) from upslope to Capillary Reservoir.
4	Add maximum inflow to the recharge zone of the Capillary Reservoir up to the recharge-zone storage capacity.
5	Add excess inflow to the Capillary Reservoir up to the maximum storage capacity.
6	Add excess inflow from the Capillary Reservoir to the Groundwater Reservoir up to a recharging threshold; move the remaining excess inflow to the Gravity Reservoir.
7	Calculate Gravity Reservoir storage up to the preferential-flow threshold; move the rest to the Preferential-flow Reservoir.
8	Calculate storage of Preferential-flow Reservoir up to its maximum storage capacity; set the remaining excess water to Dunnian surface runoff (part 2).
9	Calculate slow interflow from gravity reservoirs.
10	Calculate gravity drainage from the Gravity Reservoir to the Groundwater Reservoir.
11	Calculate fast interflow from Preferential-flow Reservoir.
12	Calculate the total Dunnian runoff as the sum of part 1 from step 2 and part 2 from step 8.
13	Calculate the outflows of current HRU to downslope HRUs
14	Calculate and remove the evapotranspiration from upper zone of Capillary Reservoir up to the recharge-zone storage; calculate and remove the transpiration from lower zone of Capillary Reservoir up to the lower zone storage.

The Groundwater Process in PRMS has been simplified as groundwater storage, receiving water from soil zone and giving water through groundwater flow and baseflow as contributed to streamflow.

The Streamflow Process calculates the total streamflow flowing out of the model domain with components of baseflow, interflow, and surface runoff.

Other task processes are also included to help the realization of simulation algorithms of principle hydrologic processes, such as the Transpiration Period Process, which determine the period of active transpiration during the model simulation.

Model files and executions

As described in the PRMS user manual (Markstrom et al., 2015), PRMS is a stand-alone executable program for a physical-based distributed-parameter hydrologic model. The physical-based hydrologic processes are represented by algorithms that are based on physical laws or empirical studies. The capability of distributed parameters is enabled by the discretization of HRUs in a watershed with physical features.

Prior to PRMS simulation execution, three basic input files are required: the Control File, the Data File, and the Parameter File. The following descriptions are from Markstrom et al. (2015), where detailed explanations can be found.

The Control File specifies the control parameters that control a course of model simulations, regarding the model executions, model input, model output, initial conditions, and the active modules that are in use. Particularly, it defines the file names and paths for model inputs and outputs, the variables chosen to output, simulation time period, and the active modules in use.

The Data File is to specify the measured time-series data that are used in PRMS model simulations. On daily time step, the daily measurements, based on the user-selected modules/algorithms, may contain variables of precipitation, maximum temperature, minimum temperature, solar radiation, pan evaporation, humidity, wind speed, snow water equivalent, and streamflow. Specifically, the precipitation, maximum temperature, and minimum temperature are the minimum input requirements for a running PRMS, and they can also be defined in separate files if needed (see Markstrom et al., 2015).

The Parameter File contains all the parameters that are used in the equations of algorithms for the selected modules, and it is the file where the sensitivity analysis and model adjustments are performed.

Without a user-friendly interface, it is important to acquire the operation sequence of the model execution, which mainly includes 12 steps of reading, assigning, and computing:

1. Read the Control File and assign the specified modules as active modules to the corresponding processes.
2. Declare the parameters and variables used in the selected module simulation and allocate arrays.
3. Read parameters from the Parameter File as required for each selected module.
4. Set up model initialization.
5. Run time-step loop.
6. Read data input from the Data File.
7. Execute model simulation for each active module, starting with the spatial distribution modules for climate and energy information, such as precipitation, maximum temperature, and minimum temperature.
8. Compute states and fluxes on HRU from land surface processes to subsurface; from the Canopy Interception Process, Snow Process, and Surface runoff Process to the Soil-zone Process and Groundwater Process.

9. Compute streamflow network and lake related processes if included.
10. Summarize output and export to output files.
11. Execute the next time step and repeat steps 6-10 until the last one is completed.
12. Close all output files.

3.4.2 Model Development in Lehman Creek Study

Watershed delineation

The Lehman Creek watershed was delineated from the DEM) with 30-m resolution of 1 arc-second (2013) from the U.S. Geological Survey (USGS), which defined the elevation of the entire Lehman Creek watershed ranging from 2040 m in the east plain area to 3980 m on the Wheeler Peak in the southwestern point (**Error! Reference source not found.**). The watershed surface boundary, stream flow path, and primary topographic characteristics of the watershed were depicted (Figure 16). The resulted watershed area was 23.7 km^2. Five tributaries along with one main stream were delineated based on the watershed topography with considerations of seasonal streams and potential groundwater flow impacts. The Lehman Creek originates from high-elevated mountain in the west, passing the gauging station Lehman Creek Nr Baker (USGS # 10243260), and flows to the plain area in the east towards the town of Baker.

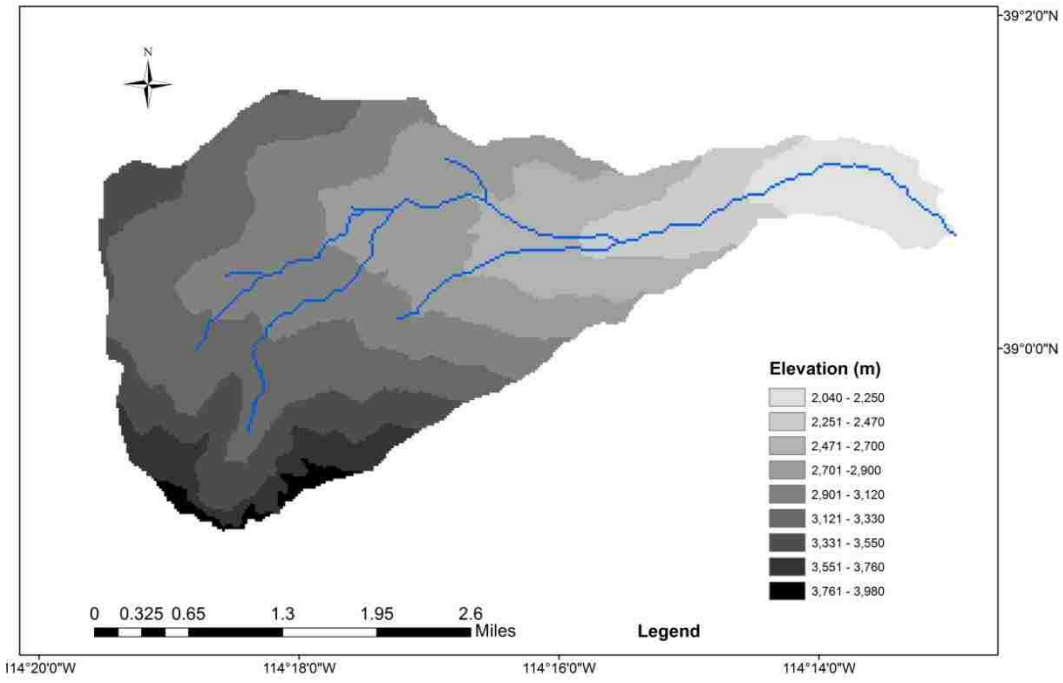

Figure 16. Resulted Watershed Delineation with Watershed Boundary ad Water Flow Path Defined Using the USGS National Elevation Dataset (DEM, 2013).

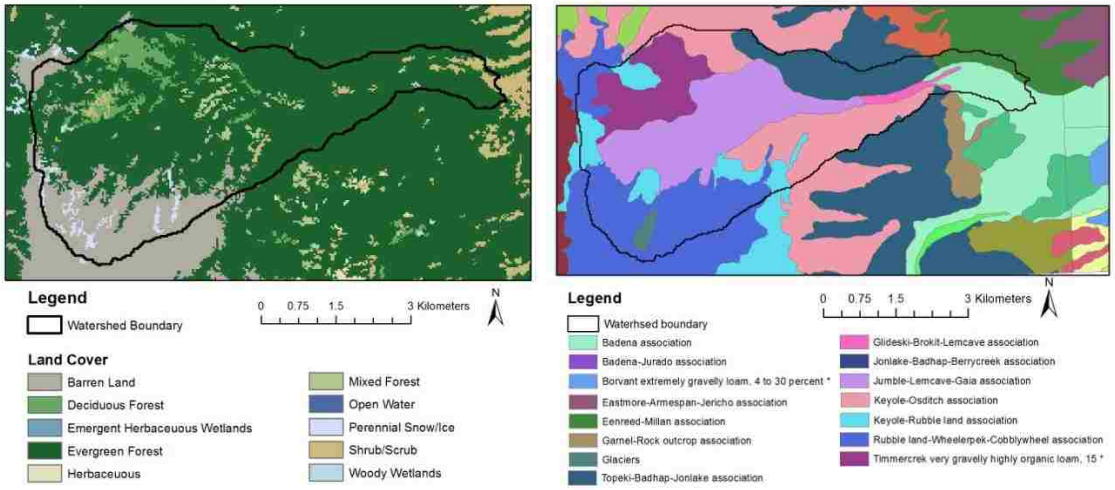

Figure 17. (A) Land Cover of the Study Area, Sourced from National Land Cover Database (2011); (B) Soil Type Of The Study Area, Sourced from Soil Survey Geographic (SSURGO) Database.

Watershed discretization

In order to represent the spatial discrepancies in the hydrologic simulation, the delineated watershed was then discretized into 96 columns and 49 rows using 100 m^2 square-size cells, covering the entire defined watershed. Cells within the watershed were active during model simulation, which were counted to be 2516 out of the total of 4704 cells (Figure 18).

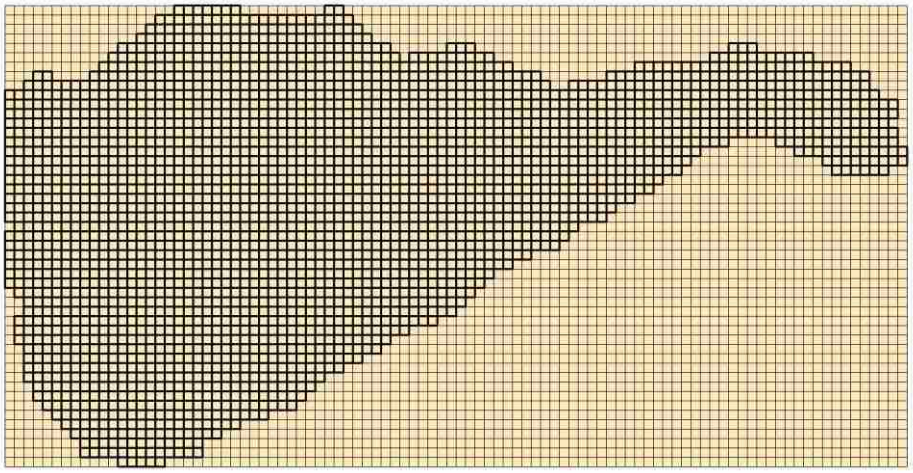

Figure 18. Discretization of the Study Area By 96 Columns and 49 Rows In Cell Sized 100m by 100m.

Hydrologic Process Simulations

Apart from the functional modules for basic definitions of the model along with the summary, the principle hydrologic-process modules used in this model have been discussed in sub-section 3.2.2, which includes: the Cascading Flow, Precipitation Distribution, Solar Radiation, Potential Evapotranspiration (PET), Canopy Interception, Snow Computation, Soil Zone Computation, Surface Runoff, Groundwater Flow, and Streamflow Routing (Table 6).

Table 6

Modules Used in the PRMS Model Development in Lehman Creek Watershed.

Process simulated	Module used
Cascading Flow	cascade
Precipitation Distribution	precip_1sta
Temperature Distribution	temp_1sta
Solar Radiation	soltab, ddsolrad
Potential Evapotranspiration	potet_jh
Canopy Interception	intcp
Snow Computation	snowcomp
Soil Zone Computation	soilzone
Surface Runoff	srunoff_smidx
Groundwater Flow	gwflow
Streamflow Routing	strmflow
Basics and summary	basin, basin_sum

The Cascade Flow process was specified through one-to-one routing between neighbored HRUs. The four directions for each HRU to be routed were determined by the slope of the flow (Figure 19). The modules of Precipitation Distribution and Temperature Distribution were distributing processes based on points of data input that were performed on the entire watershed and on each HRU. In this study, due to the shortage of data availability, one point of meteorological observations was used, which provided the related precipitation and temperature information at one single location. Thus, for each HRU, the value of precipitation or temperature was calculated by the point observation with an adjusted coefficient that considered location differences that differed from the observation point and the calculated HRU. The Solar Radiation process was simulated using a modified degree-day method (Leavesley et al., 1983), which was on the basis of potential solar radiation, a ratio of actual to potential daily solar radiation, and the slope of the calculated HRU. The potential solar radiation was available through the calculation of a solar table with the solar radiation and daylight length for every day of a year considering

the factors of slope, aspect, and latitude. The PET was simulated using the modified Jensen-Haise formulation (Jensen & Haise, 1963; Jensen et al., 1969), which is a function of solar radiation, air temperature, and two coefficients related to the regional air temperature, elevation, and saturation vapor pressure. The Canopy Interception was a result of vegetation density and the water storage, where four types of vegetation were classified: bare land, grass, shrubs, and trees. As to account for the seasonal variations, summer and winter were considered with variability in the vegetation canopy density and the corresponding water storage. The Snow process was combined with balances in water and energy (affected by factors and processes of precipitation, snow-cover area, albedos, energy, melt, and sublimation). For example, the effects of rainfall and snowfall were applied first with heat transference between snow pack and precipitation; then, the snow-cover area was determined from the snow water equivalent by a depletion curve. After this step, the energy balance was computed as a sum of net long-wave radiation, short-wave radiation, convection, and the latent heat during condensation. They were mainly determined by factors of the air temperature, vegetation canopy density, and snow albedo; and by parameters involved with convection and latent heat related. Soil Zone computation relied on the conceptualization of soil-water storage, where subsurface flows were generated (see Chapter 2). In the Surface Runoff module, a non-linear variable-source-area method was used, which considered surface-runoff generation from pervious areas and impervious areas. The estimation of pervious runoff generation used non-linear equations. The streamflow was calculated as the sum of the surface runoff, interflow, and groundwater discharge reaching the streamflow network. The Groundwater Flow was simulated through a conceptualization of a groundwater reservoir for each HRU. Water balance was computed with inflows of gravity drainage, excess soil water, seepage, and cascading flow from upslope

groundwater; with outflows of baseflow and groundwater sink; and with groundwater storage changes.

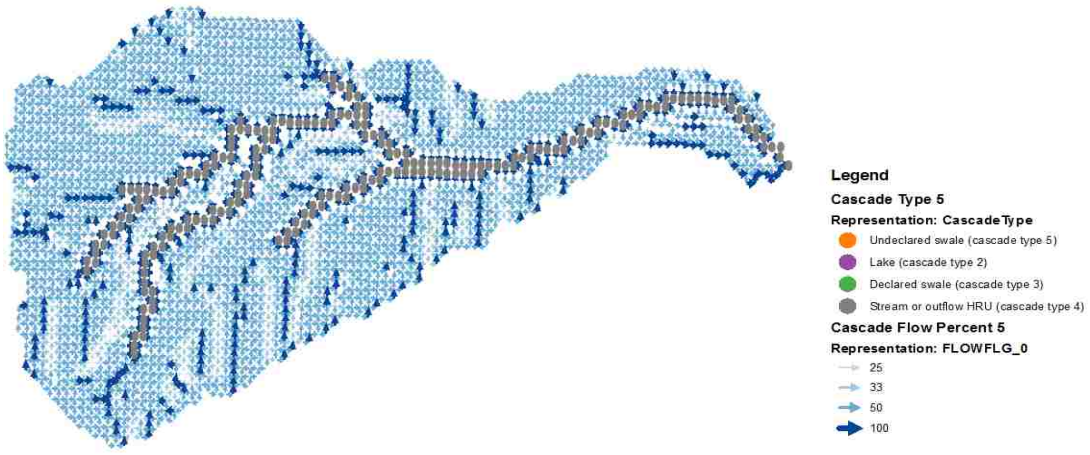

Figure 19. Determination of Cascade Flow Paths for Grid-Based Watershed Models Using Cascade Routing Tool (CRT, USGS).

Parameter initializations

Distributed parameters were defined for each HRU for geographical characteristics such as elevation, aspect, and slope, which were used in algorithms of hydrologic process simulations, such as interception, snowmelt, and infiltration, and for meteorological information distribution. Non-distributed parameters were kept constant throughout the watershed. Both the parameters could be either related to model definitions, such as the number of HRUs, or related to model algorithms, such as the Julian date. Nevertheless, there were some determinant parameters, which were directly used in the simulation algorithms, and they were initialized with their default values or from previous studies (Hay et al., 2007; Volk, 2014; Martkstrom et al., 2015). Model calibrations were performed to finalize these parameters.

3.4.3 Sensitivity Analysis of Model Parameters

The sensitivity analysis was performed on the parameters from the selected modules for the simulation of each hydrologic component. The initial estimations of parameters were based

on previous studies (Hay et al., 2007; Volk, 2014; Martkstrom et al., 2015). Only process-determinant parameters were selected and tested in this study, while keeping watershed-delineated parameters unchanged, such as elevation, soil type, and land cover land use. The simulations to determine the sensitivity of parameters were performed through multiplying the initial parameter estimations by a 10% increase.

The sensitivity analysis was performed on the model for the period from October 1, 2002 to September 30, 2007 to evaluate the fitness between the streamflow simulations and observations, identifying the most influential parameters that influence the characteristics in the basin hydrograph. Evaluations were made by comparing two streamflow simulations, resulted from different setups: the initial parameter and the adjusted parameter with a 10% increment. Absolute changes of Sum of Square Error (SSE) was used to describe the parameter sensitivities affecting the hydrograph, measuring the differences between daily simulations and observations. A higher value indicates greater sensitiveness for the determined parameter.

3.4.4 **Model Calibration**

On the basis of the longest continuing streamflow observation records for the period of 2003 to 2012 (water years), the interpolated daily PRISM dataset (see Chapter 2.5.1) was split into two parts: data from 2003 to 2007 (water years) were used for model calibration, and data from 2007 to 2012 (water years) were used for model validation. The principle hydrological processes of solar radiation (SR), potential evapotranspiration (PET), and streamflow were compared and calibrated with mean monthly observation values where records are available.

A step-wise multi-objective calibration procedure was applied to the model calibration, which uses the Shuffled Complex Evolution technique as the optimization algorithm (Hay & Umemoto, 2006; Hay et al., 2007). The optimization algorithms were performed for each step

until the convergence criteria were met, and the next step would be executed, as in order of SR, PET, streamflow volume, and streamflow timing, similar to the study of Hay et al. (2007) (Figure 20). The number of rounds/iterations was set to 4, and when one round ended at step 4, the calibration would continue and start from step 1 again.

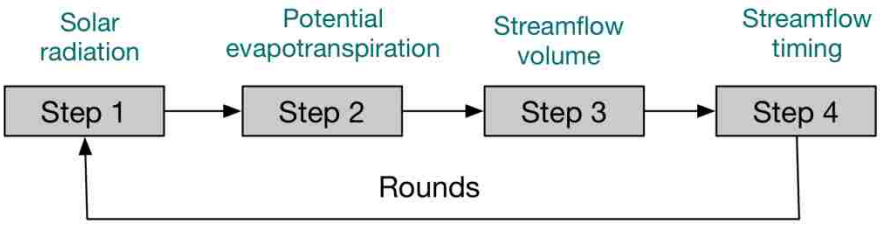

Figure 20. A Step-Wise Multi-Objective PRMS Model Calibration Scheme Performed for the Lehman Creek Watershed Using Luca, for the Calibration Period of 2003-2007 (Water Years).

As listed in Table 7, corresponding to each calibration step in Figure 20, sensitive parameters were selected with defined value ranges and objective functions. For each calibration step, the model simulation results were compared with measured data for (1) mean monthly solar radiation, (2) mean monthly potential evapotranspiration, (3) streamflow volumes on annual, monthly mean, and mean monthly scales, and (4) streamflow timing on monthly mean and daily scales.

Table 7

Parameters Calibrated in Step-Wise Multi-Objective Procedure for the PRMS Model Developed in the Lehman Creek Watershed (Adapted From Lauren E Hay et al., 2007).

Calibration dataset	Objective function	PRMS parameter	Value range	Calibrated values	Parameters Description
1. Solar Radiation •Mean monthly	Sum of absolute difference in observed and simulated values	dday_intcp	-70 to 10	individual	Intercept in temperature degree-day equation for determining the ratio of actual to potential daily solar radiation
		dday_slope	0.2 to 0.9	mean	Slope in temperature degree-day equation for determining the ratio of actual to potential daily solar radiation
		tmax_index	50 to 90	mean	Index temperature used to determine precipitation adjustments to solar radiation
2. Potential evapotranspiration •Mean monthly	Sum of absolute difference in observed and simulated values	jh_coef	0.001 to 0.09	individual	Coefficient in Jensen-Haise PET computation
3. Streamflow (volume) •Annual Mean •Mean Monthly •Monthly Mean	Normalized Root Mean Square Error	rain_adj	0 to 2	mean	Adjustment factor for rain days
		snow_adj	0 to 2	mean	Adjustment factor for snow days
		rad_trncf	0 to 1	mean	Transmission coefficient for short-wave radiation through the winter vegetation canopy
		tmax_lapse	-10 to 10	individual	Maximum air temperature change per 1,000 elev_units of elevation change
		tmin_lapse	-10 to 10	individual	Minimum air temperature change per 1,000 elev_units of elevation change

Table 7

Parameters Calibrated in Step-Wise Multi-Objective Procedure for the PRMS Model Developed in the Lehman Creek Watershed (continued).

Calibration dataset	Objective function	PRMS parameter	Value range	Calibrated values	Parameters Description
4. Streamflow (timing) •Daily •Monthly Mean	Normalized Root Mean Square Error	adjmix_rain	0.6 to 1.4	mean	Factor to adjust the rain proportion in a mix rainfall and snowfall event
		cecn_coef	0 to 20	mean	Convection condensation energy coefficient
		emis_noppt	0.757 to 1	individual	Emissivity of air on days without precipitation
		freeh2o_cap	0.01 to 0.2	mean	Free water holding capacity of snowpack
		gwflow_coef	0 to 0.3	mean	Groundwater routing coefficient
		potet_sublim	0.1 to 0.75	mean	Proportion of PET that is sublimated from snow surface
		smidx_coef	0.0001 to 1	mean	Coefficient in nonlinear surface runoff contributing area algorithm
		smidx_exp	0.2 to 0.8	mean	Exponent in nonlinear surface runoff contribution area algorithm
		soil_moist_max	0 to 20	mean	Maximum available water-holding capacity in soil
		soil_rechr_max	0 to 20	mean	Maximum available water holding capacity for soil recharge zone
		soil2gw_max	0 to 0.5	mean	Maximum rate of soil water excess moving to ground water
		tmax_allrain	50 to 75	mean	Rainfall occurs when maximum temperature exceeds this value
		tmax_allsnow	30 to 40	mean	Snowfall occurs when maximum temperature is under this value

3.4.5 **CMIP5-Driven PRMS Simulation**

The bias-corrected CMIP5 data resulting from Research Objective 1 (Chapter 2) represents both the retrospective and projected meteorologic condition in the study area. They were used to drive the calibrated hydrologic PRMS model in order to evaluate the corresponding streamflow changes (Chen et al., 2016). As both retrospective and projected meteorologic data were from the same data source CMIP5, the system errors/bias that were generated during climate model simulations can be avoided when relative changes, differentiation between these two datasets, were used. Through comparing the streamflow simulations, driven by retrospective and projected CMIP5 data (bias-corrected), the corresponding differences between these two periods of datasets were evaluated as the results of meteorologic alternation from climate change.

3.4.6 **Assessment of Model Results**

First, the hydrologic model was calibrated and validated by comparing model simulations with streamflow gauging observations during the available period of 2003-2012 (water years). Indicators of the square of correlation (R^2), percent bias (PBIAS), and Nash-Sutcliffe efficiency (NSE), following Santhi et al. (2001) and Moriasi et al. (2007 & 2015), were used to assess the daily streamflow simulation during calibration and validation (Shi et al., 2011, 2013; Guo et al., 2012).

The PBIAS measures the average data trend of the model simulations to be smaller or larger than the observations. A positive value indicates an overestimation of model simulations while a negative value means underestimations (Gupta et al., 1999). It was calculated as:

$$PBIAS = (\sum_{t=1}^{T}(Q_{s,t} - Q_{o,t}) / \sum_{t=1}^{T} Q_{o,t}) * 100 \quad (1)$$

where, $Q_{s,t}$ and $Q_{o,t}$ are simulated values and observed values at time *t* (from 1 to T), respectively.

The NSE describes the fitness between the plot of model simulations versus observations and the linear line of y equals x, which ranges from -∞ to 1. The larger the NSE the better the model performance is (Nash & Sutcliffe, 1970). It was calculated as:

$$NSE = 1 - \sum_{t=1}^{T}(Q_{o,t} - Q_{m,t})^2 / \sum_{t=1}^{T}(Q_{o,t} - \overline{Q_o})^2 \quad (2)$$

where, $\overline{Q_o}$ is the average observation over the entire time period T.

The R^2 is the square of correlation between modeled data and observed data. R^2 ranges between 0 and 1, and higher values indicate better performance. It was calculated as:

$$R^2 = \left\{ \sum_{t=1}^{T}\left(Q_{o,t} - \overline{Q_o}\right)\left(Q_{m,t} - \overline{Q_m}\right) \Big/ \left[\sum_{t=1}^{T}\left(Q_{o,t} - \overline{Q_o}\right)^2\right]^{0.5}\left[\sum_{t=1}^{T}\left(Q_{m,t} - \overline{Q_m}\right)^2\right]^{0.5} \right\}^2 \quad (3)$$

where, $\overline{Q_m}$ is the average model simulation over the entire time period T.

Changes in streamflow simulation regarding the baseline period were assessed. Comparisons were performed on both mean annual and mean monthly scales for multiple scenarios and models. An important feature of global climate change in a snow-dominant region, the timing shift of peak flow occurrences, was assessed quantitatively using a winter-spring center of volume (WSCV) (Hodgkins & Dudley, 2006). This was improved on the basis of a study by Court (1962) for a robust measure of streamflow timing: the center of volume (CV) date was calculated as the time when the cumulative streamflow volume reached half of the year's total streamflow volume, starting from the beginning to the end of the year. In this study, seasonal WSCV (from January 1 – June 30) were used to evaluate the changes in snowmelt streamflow, with no disturbances from fall precipitation.

3.5 Results

3.5.1 Sensitivity Analysis

Among 58 tested parameters, the top 20 were selected based on the values of the absolute change of SSE in responses of 10% of parameter value increase (Figure 21). The results show the selected parameters had an absolute SSE change value greater than 0.58%, against which the developed PRMS model was most sensitive. However, during the analysis, the sensitive parameters might have some differences based on the selected model initial condition.

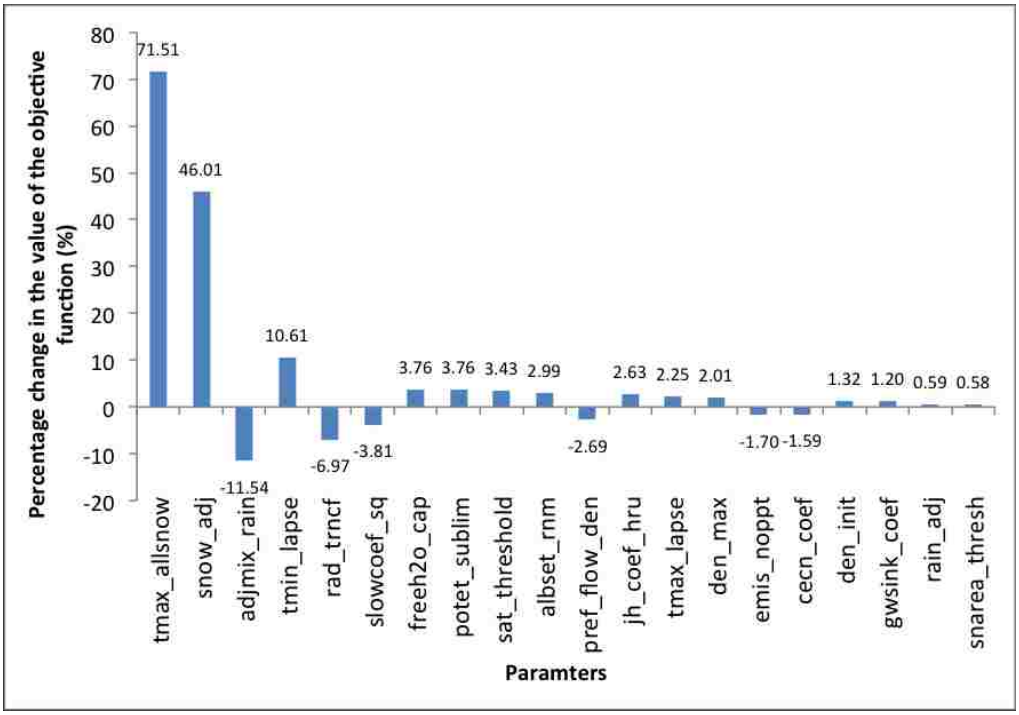

Figure 21. Results of Sensitivity Analysis for the PRMS Model Parameters in terms of the Percentage Variation in Absolute Value of Objective Function SSE.

3.5.2 Model Calibration

Solar radiation and potential evapotranspiration

As the two main components calibrated in the model, the model simulation results of Solar Radiation (SR) and Potential Evapotranspiration (PET) were compared with the observations to investigate the performance of the developed model. At the station Subalpine

(east) where the corresponding HRU was HRU 1934, the values were compared between observations and model simulations on mean monthly scale. As shown in Figure 22 and Figure 23, the SR and PET processes were well simulated as the simulations matched with observations on mean monthly scales at HRU 1934.

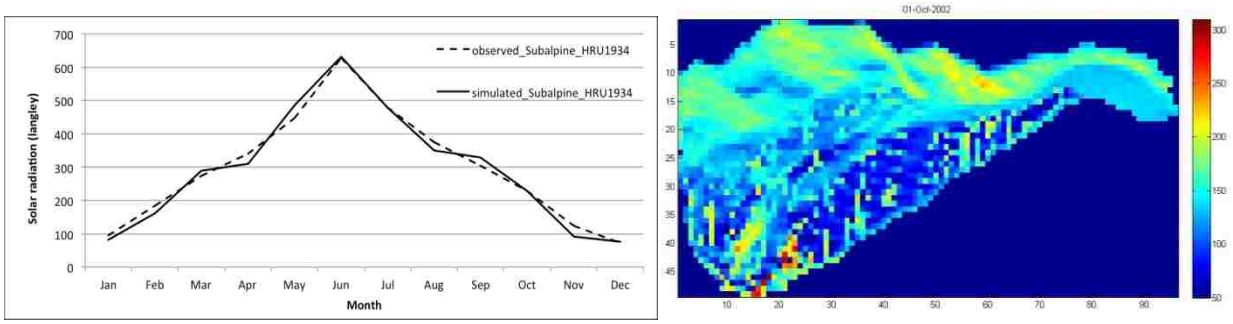

(a) (b)

Figure 22. Model Results of Solar Radiation where the Subalpine (East) Station is Located: (A) Mean Monthly Comparison Between Station Records and Simulated Values at Corresponding HRU 1934, (B) Exemplary Spatial Distribution on October 1, 2002.

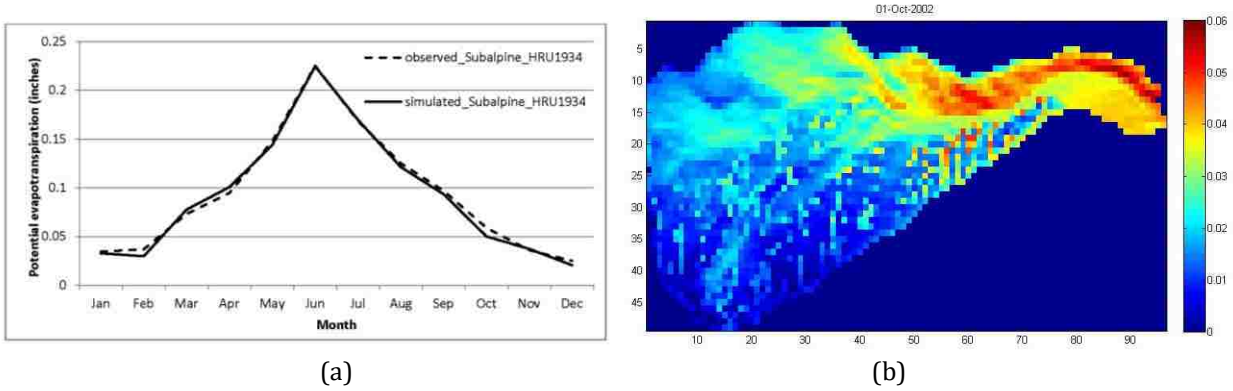

(a) (b)

Figure 23. Model Results of Potential Evapotranspiration where the Subalpine (East) Station is Located: (A) Mean Monthly Comparison Between Station Records and Simulated Values at Corresponding HRU 1934, (B) Exemplary Spatial Distribution on October 1, 2002.

Annual water balance

The annual water balance for the study area is shown in Table 8. Relative error was computed between model simulations and observations for each water year. During the model calibration period (2003-2007, water years), relative errors in streamflow were between 0.02 to

0.19, and during the validation period (2008-2012, water years), relative errors ranged from -0.36 to 0.31.

Figure 24 shows an annual comparison between simulated runoff and measured runoff. Model results showed a good model performance from 2003 to 2012 (water years). However, in 2011, the overestimated model simulation was not able to reproduce the peak flow in the observation (Prudic et al., 2015; Chen et al., 2015), which resulted in the high relative error of -0.31.

Table 8

The Annual Water Balance Among Precipitation, Evapotranspiration, Water Storage, and Runoff, during 2003 to 2012 (Water Years) in the Study Area of the Lehman Creek Watershed. (Unit: inches, 1 inch= 25.4 mm).

Year	Prcp.	ET	Storage	S-Runoff	O-Runoff	Relative Error
2003	23.1	19.4	3.8	5.8	5.6	0.02
2004	24.3	17.2	4.9	6.0	4.9	0.19
2005	42.4	19.4	8.4	19.6	19.1	0.02
2006	22.6	16.9	4.4	9.6	8.0	0.17
2007	20.7	15.1	5.8	4.2	3.9	0.07
2008	16.0	14.6	4.2	3.1	4.2	-0.36
2009	25.7	17.1	4.4	8.4	7.1	0.15
2010	20.7	15.1	4.2	5.9	5.7	0.04
2011	40.3	19.0	8.1	17.4	11.9	0.31
2012	21.9	17.2	6.6	6.2	4.6	0.26

Prcp.: precipitation; ET: evapotranspiration; Storage: water storage; S-Runoff: simulated runoff; O-Runoff: observed runoff.

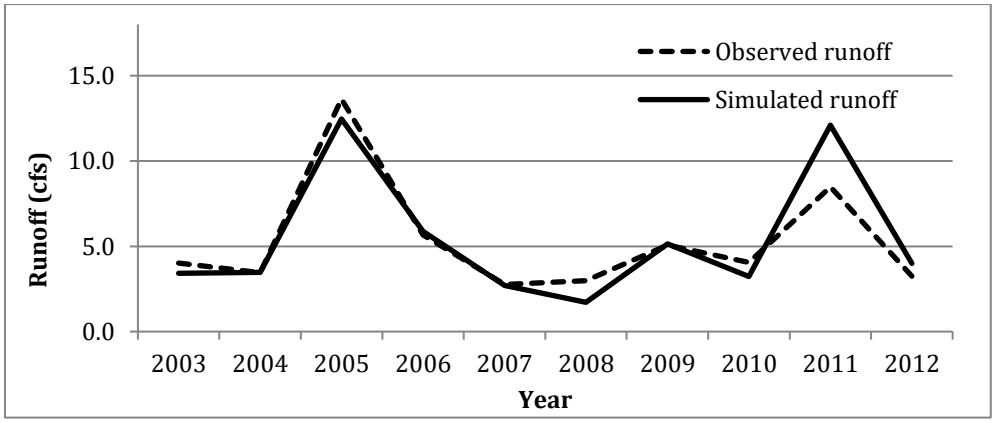

Figure 24. Annual Runoff Comparisons between Observations and Model Simulations for the Period of 2003-2012, Water Years.

Mean monthly streamflow

Combined with both model calibration and validation periods, the mean monthly streamflow were compared between model simulations and observations (Figure 25). The model was able to replicate the shape and magnitude of runoff at Lehman Creek and capture the peak flow during summer in June and low flows from late fall to early spring, which is consistent with the features in a snow-dominated area.

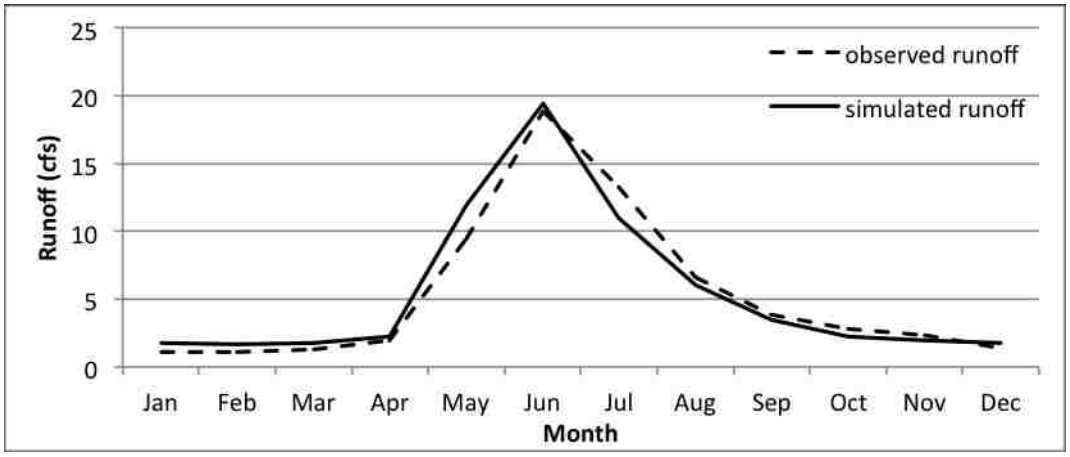

Figure 25. Comparison of Model Simulations and Observations with Mean Monthly Runoff over the Simulation Period of 2003-2012 (Water Years) at Lehman Creek Gauging Station.

3.5.3 **Model Calibration and Validation for PRISM Driven Model**

A comparison of the monthly hydrograph was performed between the PRMS simulations, driven by PRISM data and the observation records, for the period of 2003-2012 water years (Table 9). The results indicated a good match, as was evident by the statistical performance during both the periods of calibration and validation. Indicators of PBIAS, R^2, and NSE were used to examine the daily streamflow simulations. During the calibration and validation periods, results showed that both R^2 and NSE were above 0.64, and PBIAS was -9.8% and 2% for these two evaluation periods. Previous studies (Santhi et al., 2001; Moriasi et al., 2007 & 2015) suggested model simulations were beyond satisfactory when NSE was higher than 0.5, R^2 greater

was than 0.6, and PBIAS was below ±10%. For detailed model calibration procedures, refer to Chen et al. (2015).

Table 9

Statistical Comparison of Observed and Simulated Daily Streamflow at Lehman Creek for Calibration (2003-2007, Water Years) and Validation Period (2008-2012, Water Years).

Index	Calibration Period	Validation Period
PBIAS (%)	-9.8	2.0
R^2	0.85	0.69
NSE	0.82	0.64

3.5.4 **Hydrologic Simulation – Long-term Changes in Streamflow**

Periodic variation

The streamflow simulations, driven by bias-corrected CMIP5, were analyzed using the simulation differences in the future periods (Period 1, Period 2, and Period 3) based on the baseline period, for each of the emission scenarios. As shown in Figure 26, the changes in annual streamflow varied from -14.3% to 32.8% (1st quarter to 3rd quarter), depending on the emission scenarios and time periods. The highest range (from the first quartile to the third quartile) was found in RCP 8.5, Period 3, and the lowest range was found in RCP 6.0, Period 1.

Similar patterns were found between precipitation and streamflow. A gradually increasing trend was seen along multi-decadal periods in emission scenarios RCP 4.5 and RCP 6.0. In RCP 2.6 and RCP 8.5, a decrease occurred from Period 1 to Period 2, and an increase from Period 2 to Period 3. RCP 2.6 had the highest median value of 13.3%, 12.6%, and 16.3% for the three corresponding time periods, respectively, and RCP4.5, RCP 8.5, and RCP 6.0 had the lowest median values during these time periods.

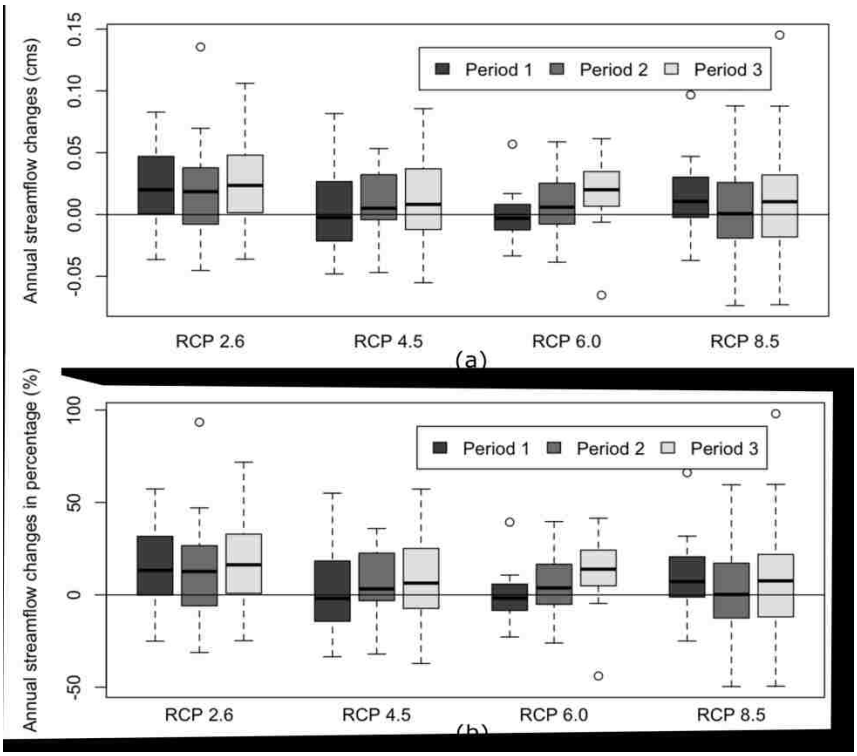

Figure 26. Comparisons of the Annual Streamflow Change Simulated by PRMS Model, Assessed at: (A) Absolute and (B) Ratio/Percentage among Four Climate Change Scenarios: RCP 2.6, RCP 4.5, RCP 6.0, and RCP 8.5, during Three Future Periods of 2011-2039, 2040-2069, and 2070-2099.

Monthly pattern

Changes in the simulated mean monthly streamflow, with regard to the baseline period, were compared with different scenarios among the three future periods (Figures 27 & 28). Variations among the multiple projections are presented by means of box plots. Positive values indicate streamflow increases and negative values signify decreases. In a calendar year, a distinguishing time point was found between May and June that showed an increase of mean monthly streamflow during the winter (December to May) and a decrease during the summer (June to November).

As shown in Table 10, changes in the mean monthly streamflow (in percentage), during the increasing trend before May and decreasing trend after June, gradually became obvious from Period 1 to Period 3 (Figures 27 & 28). Additionally, an increasing variation in the value of changes was found among the time periods. The largest discrepancy ranged from 0.01 m^3/s to 0.25 m^3/s in May for RCP 2.6 during Period 3. When comparing the results among the emission scenarios, the differentiation might not be evident during the first two periods. Nevertheless, great increases in streamflow changes, especially during January to April, were observed (Figures 27 & 28).

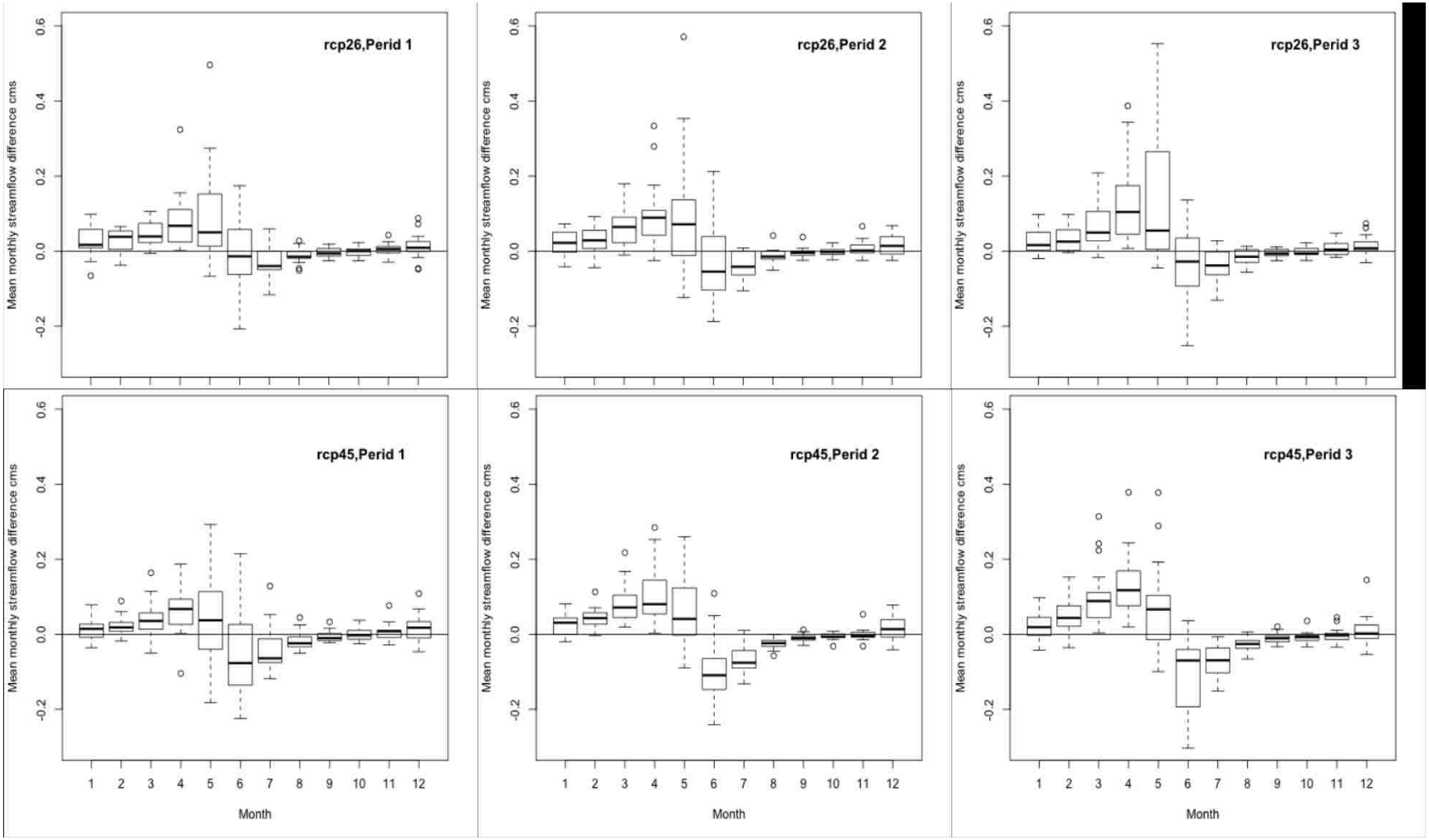

Figure 27. Mean Monthly Streamflow Changes on the basis of Baseline Period (1981-2010), Resulting from the PRMS Model Simulation. Three Periods were Compared: Period 1 (2011-2039), Period 2 (2040-2069), and Period 3 (2070-2099), under all Climate Change Scenarios of RCP 2.6 and RCP 4.5.

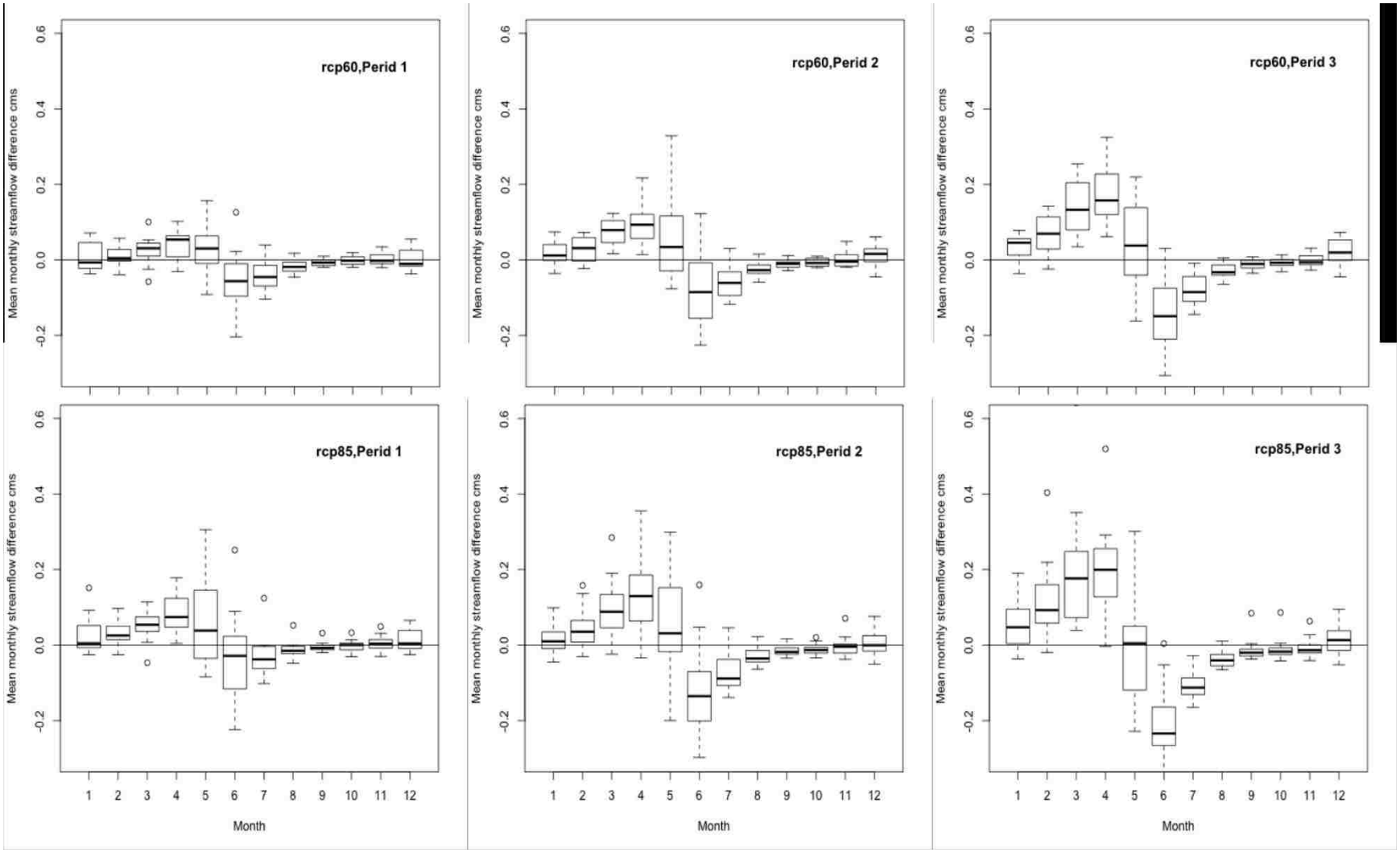

Figure 28. Mean Monthly Streamflow Changes on the Basis of Baseline Period (1981-2010), resulting from the PRMS Model Simulation. Three Periods were Compared: Period 1 (2011-2039), Period 2 (2040-2069), and Period 3 (2070-2099), under All Climate Change Scenarios of RCP 6.0 and RCP 8.5.

Table 10.

The PRMS Model Results from the CMIP5-Driven Simulation: Median Values of Mean Monthly Streamflow Changes based on the Baseline Period for Each RCP, in Percentage (%).

Emission scenario	Time period	Jan.	Feb.	Mar.	Apr.	May	Jun.	Jul.	Aug.	Sep.	Oct.	Nov.	Dec.
RCP 2.6	Period 1	22.6	45.4	31.3	32.7	13.2	-3.9	-18.8	-17.8	-9.3	0.3	7.6	10.9
	Period 2	28.0	34.0	46.7	50.3	19.0	-14.7	-28.1	-16.5	-6.3	-4.0	2.7	17.2
	Period 3	20.3	36.3	33.2	48.2	13.4	-7.5	-18.0	-15.2	-10.9	-10.5	6.5	9.9
RCP 4.5	Period 1	13.7	18.2	37.4	39.9	9.7	-22.3	-34.3	-25.2	-16.6	-4.5	12.7	22.4
	Period 2	34.4	53.2	63.5	50.0	10.9	-27.2	-38.6	-27.9	-16.9	-10.4	-5.7	19.1
	Period 3	27.6	51.6	72.3	69.7	16.2	-19.3	-38.1	-27.0	-16.5	-12.5	-4.4	3.2
RCP 6.0	Period 1	-8.7	5.7	27.8	26.4	8.0	-15.1	-24.8	-20.9	-11.9	-3.4	-3.4	-13.7
	Period 2	13.8	39.5	63.0	52.6	9.4	-23.2	-35.1	-28.9	-15.3	-13.0	-6.6	18.4
	Period 3	53.7	81.4	94.0	90.8	10.3	-38.7	-48.1	-32.8	-18.3	-12.6	-9.5	24.7
RCP 8.5	Period 1	7.1	32.5	51.6	44.7	9.9	-7.7	-20.0	-16.1	-11.0	0.4	5.7	5.7
	Period 2	12.1	46.2	75.2	68.9	8.7	-34.4	-46.7	-38.7	-28.1	-22.1	-6.5	-0.5
	Period 3	58.0	105.5	145.0	114.6	1.2	-58.2	-58.1	-43.6	-32.0	-28.0	-19.6	18.4

Timing shift

The date changes for WSCV were analyzed among the various projections and scenarios on the basis of the baseline period (Figure 29). Positive values indicate a time lag when the WSCV date was late relative to the WSCV in the baseline period. Negative values mean earlier occurrences of the WSCV date relative to that in the baseline period. The results showed negative values, overall, in the changes during all the periods and emission scenarios, which meant that the WSCV date tended to shift earlier than in the baseline period.

Furthermore, early shifts of the WSCV date were intensified with increased variances along the time periods. Median values for the WSCV date shifts over four climate change scenarios showed a range from 2.9 to -9.1 days for the different scenarios during Period 1, -10.1 to -16.1 days during Period 2, and -10.1 to -30 days during Period 3. Comparisons of the results from the different emission scenarios showed an increase trend in the date shift, in an order of

RCP 2.6, RCP 4.5, RCP 6.0, and RCP 8.5 in Period 3. No certain pattern was found during the first two periods.

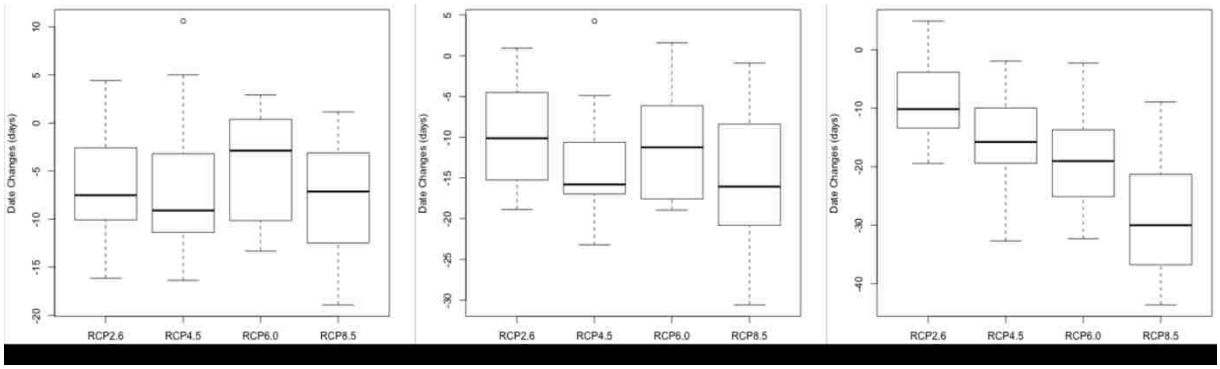

Figure 29. Comparisons of Winter-Spring Center Of Volume (WSCV) Date-Shifting among Four Climate Change Scenarios: RCP 2.6, RCP 4.5, RCP 6.0, and RCP 8.5, during Three Future Periods: 2011 to 2039 (Period 1), 2040 to 2069 (Period 2), and 2070 to 2099 (Period 2). The WSCV Values Calculated using PRMS Streamflow Simulations, and the Box Plot Represents Results from Multiple Climate Models of Each Scenario.

3.6 Discussion

The PRMS model was used to simulate the physical processes and to represent combination effects from distributed land cover land use (Wu et al., 2016), soil information, and climatic information. One important assumption is that the geomorphic condition maintains consistent and with no changes in land cover land use throughout the model simulation from 1981 to 2099. This limitation could be out of the study region in this paper, and further studies could be extended into modeling the dynamic changes in the geomorphic status of the study area along with a modification in PRMS modules. Additionally, the current practice of hydrologic modeling uses PRMS, and selecting an alternative hydrologic model may lead to different uncertainties due to the different algorithms that each model employs (Najafi et al., 2011).

Volk (2014) studied potential effects of a warming climate on water resources within the Lehman and Baker drainages using PRMS. The study area included the Lehman Creek drainage, Baker Creek Drainage, and Rowland Spring. In his study, the products from one climate change model, Community Climate System Model version 4.0 (CCSM4) from CMIP5 (BCCA) dataset,

were used as the PRMS driving forces to simulate the hydrologic responses. In the model simulation, the projected daily temperature products were directly used after bias correction, while the daily precipitation products came from the archived measurements from BCCA after bias correction. The archived measurements came from a retrospective period dataset and used as a reference dataset and then were repeated three times into the future as the precipitations for this century. Discontinuous periods of data were used for the model simulation, where the period of 1993-1996 (water years) was used for model calibration and the period of 2003-2010 (water years) was used for model validation. Volk (2014) found temperature sensitivity in the Lehman and Baker drainages, an increased streamflow with an earlier snowmelt timing shift from May to April, and temperature increases of 5.5 degrees Fahrenheit by the end of this century, streamflow reduction by 10% with decreases in peak snowpack, and reductions in soil moisture and evapotranspiration in July and August.

Comparing to Volk's study, this study differs in multiple ways. In this study only a portion of study area was considered compared to Volk's study, because NevCAN observations were only available for the Lehman Creek watershed and were used for model calibration procedure. Regarding the climate change evaluation, instead of only using CCSM4 model data, the current study used data from 67 GCM models under 4 emission scenarios to consider uncertainties from different climate models. Moreover, while Volk used historical precipitation of CMIP5 as future projections for climate change evaluations, which excluded the factor of potential future precipitation change due to climate change influences; the current study included this factor by using projected precipitation data of CMIP5. This resulted subsequent differences in streamflow during the 21st century: 1) the annual streamflow increased resulting from current study and decreased resulting from Volk's study; 2) by using different indicators, the timing of

streamflow showed different results. Additionally, the current study focused on streamflow in terms of rates and timing, and Volk focused on water components in terms of evapotranspiration, snowmelt, and streamflow, as well as future trend detection.

Finally, as the PRMS model is a physically based, parameter distributed hydrologic model, a large set of parameters was required to represent the non-linearity, spatial and temporal dependencies, and heterogeneity in the hydrologic processes (Fatichi et al., 2016). This brings the challenges in study areas where limited observation records are available, such as the study area of Lehman Creek watershed. Thus, with improved observation datasets in both quantity and quality, the model performance can always further be enhanced.

3.7 Conclusions

The data for bias-corrected climate change were forced to drive the hydrologic model, PRMS, which was calibrated using PRISM data. The changes in annual streamflow responses resulted in an increasing trend from -2.0% — 13.3% during Period 1 to 6.3% — 16.3% in Period 3 for the various emission scenarios. The variation among the emission scenarios was not consistent with the emission levels, which showed a decrease in RCP 4.5 and RCP 6.0 and an increase in RCP 2.6 and RCP 8.5 during the first study period. This pattern also could be found for precipitation, and could be a potential cause for the streamflow changes. As climate change continued during the three time periods, the signals of a warming climate were so strong that, by the end of the 21st century, they would offset the signal differences in Period 1. The greatest streamflow decreases occurred in June (-3.9 to -58.2%), July (-18.0 to -58.1%), and August (-15.2 to -43.6%). During late winter, the greatest increase in streamflow could be greater than 100% due to an early snowmelt resulting from the increased temperature. An overall increase in precipitation was derived from the bias-corrected CMIP5 data with seasonal patterns (higher

during spring and fall, and lower during summer and winter). This pattern was compared with the streamflow changes. The streamflow changes had very different responses, showing a decrease from the summer until mid-winter. As a result of the temporal distribution changes in streamflow volume, an earlier shift of the WSCV date could be found that ranged from 10 to 30 days by the end of this century, depending on emission levels.

On the basis of the study results, the following conclusions were made:

- With the combined effects of precipitation and temperature, a distinguishing point could be identified between May and June: before May, the streamflow increased and after June, the streamflow decreased. This conclusion is supported by an earlier WSCV date, which showed an intensifying trend during the 21st century.
- A wide range of variance was found in both precipitation and streamflow. This variance became larger during the three time periods in the 21st century, indicating increasing uncertainties in the estimation results.

By using a physically based parameter-distributed hydrologic model, the snow process was simulated with a two-layer simulation of energy and water balance. Consequently, the modeling results were more reliable, especially in a snow-dominant area. Finally, simulation of the streamflow responses to climate change, with regard to rates and timing, provided useful information. There have been several attempts on this topic at regional scale, but fewer efforts have focused on watershed hydrology.

As the temperature keeps rising during the 21st century (as projected), the results showed an increasing streamflow was expected from the Lehman Creek. This was primarily due to earlier snowmelt driven by the increasing temperature and secondarily due to the increasing precipitation. Additionally, decreases in the late-spring and summer flows were expected, along

with an earlier arrival time for peak flow and less water storage in the snowpack by the end of the winter season. The degree of these changes varied with the emission scenarios, and was highly correlated with the GCMs that were used. The quantitative evaluations of the ensemble changes under each emission scenario in this study, provided insight regarding the effects of climate change on a watershed scale that has known and unknown uncertainties. By providing a better understanding and assessment of the changing trends of the local streamflow under the long-term climate change in this century, this study could help local water resource management to devise more adaptive water strategies.

Chapter 4 Global Climate Change Influences on the Integrated Water System of Lehman Creek on a Watershed Scale

4.1 Research Objective 3

Research Question # 3: How do integrated hydrologic processes respond to external stresses from meteorologic changes and human interference of groundwater pumping?

The proposed Research Question 3 included two studies. The first study was on the basis of MODFLOW model development, and the groundwater flow system in the study area was evaluated. This study provided detailed procedures of groundwater model development and calibration, with an emphasis on future coupling processes with the surface hydrologic model (PRMS), in terms of data linkages in soil percolation, unsaturated water, and streamflow. The second study was to couple the developed PRMS model with MODFLOW model to build up the GSFLOW model. Through GSFLOW model simulation, the integrated water responses to the groundwater pumping and potential climate change were evaluated, in terms of groundwater-level drawdowns and hydrologic components variations.

In the following sections, the contents are organized as follows:

4.2 Introduction of integrated modeling - the development of the groundwater model and the coupling process in an integrated modeling;

4.3 Geologic condition in the study area - additional background information for the model development;

4.4 Integrated modeling of GSFLOW – groundwater modeling using MODFLOW and the coupling processes between PRMS model and MODFLOW;

4.5 Study 1: MODFLOW modeling to evaluate the groundwater flow system in the study area;

4.6 Study 2: GSFLOW modeling to evaluate the potential climate change effects on the water system.

4.2 Introduction

Interactions between surface water and subsurface water occur in most rivers. Depending on the hydraulic connectivity and geologic features, the water interaction usually is complex (Scanlon et al., 2007) and affects variations in baseflow and streamflow (Ghasemizade & Schirmer, 2013; Kalra et al., 2013c; Sagarika et al., 2016). This interaction may be influenced by climate, environmental factors, and human activities, resulting in spatial and temporal changes in water resources (Sophocleous, 2002; Furman et al., 2007; Pathak et al., 2016a, 2016b; Tamaddun et al., 2016a, 2016b).

Integrated hydrologic models usually are used to better understand the exchange of water between surface and subsurface sources, interpret the water flow path, and predict water-system behavior (Kim et al., 2008; Xu et al., 2012). These types of models result from the integration of a surface water system and a groundwater flow system (Prudic et al., 2015), and the coupling between surface water and subsurface flow is the core of the model (Carrier et al., 2016; Ghasemizade & Schirmer, 2013).

4.2.1 Groundwater Modeling

There are several types of models that have been used in the simulation of groundwater flow systems. They can be categorized into three types (Prickett, 1975; Wang & Anderson, 1982): sand tank models, analog models, and mathematical models.

As described by Wang and Anderson (1982), a tank model is a physical model that is based on a laboratory experiment, which consists of a tank filled with an unconsolidated porous medium with induced water to pass through it. However, due to the scaling difference between a

field situation and a laboratory dimension, the phenomena measured in the laboratory model are usually different from the field observations. The difficulties lie in the instrumentation of a small time scale for a small vertical depth, the enlarged capillarity measurement in the capillary rise, and the artificial homogeneous and isotropic medium creation (Prickett, 1975). These are the major drawbacks of this model, from which the conclusions made should always be qualified when used as of a field representation.

Analog models mainly include two types: viscous fluid models and electrical models. The viscous fluid models are also known as Hele-Shaw or parallel-plate models. The model uses a viscous fluid, such as oil, to flow between two parallel plates in a narrow space to analog the water flow in porous medium. One big disadvantage concerns the complexities of the model construction and operational procedures. The electrical models are expressed in mathematical forms to simulate the similarities between Ohm's law for the flow of electricity and Darcy's law for the groundwater flow. It uses voltage changes to analog the changes in groundwater heads. As a drawback in both of these analog models, an analog model is designed for a unique aquifer system; thus, when the studied aquifer changes, the entire electrical model must be rebuilt (Prickett, 1975; Wang & Anderson, 1982).

The mathematical models consist of a set of differential equations to govern the groundwater flow in the system. While simplified assumptions should always be made, the reliability of a groundwater model performance depends on how closely the assumptions can be made to represent the real groundwater flow system. With fairly restricted assumptions, such as homogeneity and isotropy, analytical solutions are not widely used in practical applications (Anderson & Woessner, 1991). To deal with more realistic and relatively flexible assumptions, such as heterogeneity and anisotropy, numerical solutions are usually preferred, especially since

high-speed digital computers have become available. With differences in mathematical-handling methods, finite difference models and finite element models are the principal types currently used, depending on the study purpose and personal preference.

Considered as the international standard for the groundwater system simulation, the MODFLOW is the most popular and well-known program for a three-dimensional (3D) finite-difference groundwater model simulation (McDonald & Harbaugh, 1984). Developed by the USGS in 1984, MODFLOW has been updated since then, and the latest version is MODFLOW-2005, written in standard FORTRAN language (Harbaugh, 2005). The robust framework the model was constructed in provides a great flexibility for model improvement and integration of additional model capability. This leads to an extensive development of groundwater-related programs with capabilities in broader areas, such as solving techniques, study focuses, and processing utilities. Examples include: MODFLOW-NWT, developed by the USGS, which uses Newton formulation to calculate unconfined groundwater flow; MODFLOW-USG, which uses unconstructed-grid method for the discretization of groundwater flow; MODFLOW-LGR, which uses grid refinement in a local domain of interests; MODFLOW-OWHM, which analyzes interactive correlations between human and groundwater systems; and Groundwater Management (GWM) Process, which supports groundwater management with decision-making variables (MODFLOW and related Programs, USGS). There are a variety of commercial programs available that are based on the open-sourced MODFLOW codes. Examples include MODFLOW-SURFACT Flow and Visual MODFLOW Flex developed by Waterloo Hydrogeologic, Groundwater Modeling System (GMS) developed by Aquaveo, MODHMS developed by HydroGeoLogic, and the Processing MODFLOW for Windows (PMWIN) released by Simcore Software.

Besides MODFLOW, other groundwater simulation models in different spatial dimensions include: the Prickett-Lonnquist Aquifer Simulation (PLASM) (Prickett & Lonnquist, 1971), originally developed by the Illinois State Water Survey, is a two-dimensional (2D) finite differences groundwater flow model, and the Multi-Layered Finite-Element Aquifer Flow Model (AQUIFEM-N) (Townley, 1990), which can additionally simulate 2D contaminant transport, is a quasi-three-dimensional groundwater flow model evolved from one finite element model AQUIFEM-1 (Townley & Wilson, 1980).

Since the water quality is not considered in this study, groundwater models for particle tracking and solute transportation simulations are not discussed here.

4.2.2 **Integrated Models**

As integrated hydrologic models examine and simulate the dynamic water interaction between surface and groundwater they have been widely used in the studies of hydrologic mechanisms (Gilbert & Maxwell, 2017; Huntington & Niswonger, 2012; Hwang et al., 2015) and water system responses to external stresses by natural or human interferences, e.g., climate change (Gamvroudis et al., 2017; Huntington & Niswonger, 2012) and water policies (Brookfield et al., 2017; Hwang et al., 2015).

Various algorithms and techniques are used to describe the groundwater-surface water interactions (Furman, 2008), ranging from conceptual models (Arnold et al., 1993; Ponce et al., 1999; Osman & Bruen, 2002) to physical-based models of varying complexity (Abbott et al., 1986; Moussa et al., 2002). In recent years, more rigorous physically-based integrated models have been developed, which couple one-dimensional or two-dimensional surface flow with a three-dimensional subsurface flow (Kollet & Maxwell, 2006; Moussa et al., 2002; Weill et al., 2009). MODFLOW, has been widely used in such integrated models as SWAT-MODFLOW

(Kim et al., 2008), HSPF-MODFLOW (Davis, 2001), SWAP-MODFLOW (Xu et al., 2012), TOPNET-MODFLOW (Guzha, 2008), MODHMS (Tang et al., 2014), and GSFLOW (Markstrom et al., 2005).

The Coupled Groundwater and Surface-Water Flow (GSFLOW) model integrates the Precipitation-Runoff Modeling System (PRMS) with MODFLOW (Harbaugh, 2005; Markstrom et al., 2005; Regan et al., 2016), simulating both the surface hydrology and groundwater flow systems. It has been widely used in a variety of studies, such as water management alternatives, surface hydrologic responses to climate change, and the surface and subsurface water interactions (Ely & Kahle, 2012; Huntington & Niswonger, 2012; Volk, 2014). Depending on the study objectives, an integrated model can operate at various temporal scales (e.g., hours, days, or months) and spatial scales (e.g., hillslope or watershed) (Goderniaux et al., 2011). This adds the complexity to the model development, calibration, and especially integration. Due to the mathematical difficulties during the model simulation for coupled processes, it is common to simplify the model development processes by starting with a decoupled surface model and groundwater model. However, developing separate models without considering future coupling could result in several integration challenges in the following procedures. Extensive research efforts have focused on the coupling processes (Panday & Huyakorn, 2004), such as linking the channel flow regime with groundwater domains (Prudic, 1989; Swain & Wexler, 1996; Walton et al., 1999), linking the overland flow with the unsaturated and saturated subsurface flow (Akan & Yen, 1981; Pinder & Sauer, 1971), and linking overland flow, channel flow, and subsurface flow to examine interactions between them (Govindaraju & Kavvas, 1991; Refsgaard & Storm, 1995). Fewer studies are available in the literature on the coupling procedure, especially regarding the MODFLOW component in the GSFLOW model.

4.3 About Study Area

4.3.1 Geology

The Great Basin National Park is located in the southern Snake Range, which is part of a metamorphic core complex that was uplifted and exposed by erosion during extensional faulting from the Tertiary period (Miller et al., 1999; Elliott et al., 2006). It resulted in the east tilting of the southern Snake Range: a mild slope on the east side, and a steep slope on the west side (Orndorff et al., 2001; Elliott et al., 2006). The uplifting is much greater on the north side of the park, where the core complex is exposed with Lehman Creek formed, than on the south. As the processes of erosion and fill continue, the detritus eroded from the uplifted mountains partially fill the adjacent valleys, such as in the Lehman Creek watershed (Figure 30).

The surface geology of the Lehman Creek watershed shown in Figure 30 is sourced from the Data Store of the National Park Service (NPS, 2014). The bedrock geology of the study area consists of metamorphic, sedimentary, and igneous rocks aged from the Late Proterozoic to the Quaternary periods (Elliott et al., 2006). Quartzite, argillite, and shale are most of the undifferentiated rocks from the Late Proterozoic and the Lower Cambrian periods with correspondence to McCoy Creek Group, Prospect Mountain Quartzite, and Pioche Shale (Misch & Hazzard, 1962; Whitebread, 1969; Hose & Blake, 1976; McGrew et al., 1995; Miller et al., 1995a & 1995b; Elliott et al., 2006). The McCoy Creek Group generally combines metamorphosed quartzite, argillite, and siltstone with about 1097 m (3,600 ft) thickness (Misch & Hazzard, 1962; Miller et al., 1995a). The Prospect Mountain Quartzite is grained from fine to coarse with crossbeddings and fine joints, thickening around 1524 m (5,000 ft) at most (Misch & Hazzard, 1962; McGrew et al., 1995). The Pioche Shale is fine-grained calcareous quartzite with

lenses of sandy limestone, siltstone, and sandy siltstone with 137 m (450 ft) in thickness at most (Whitebread, 1969; Hose & Blake, 1976; McGrew et al., 1995; Miller et al., 1995a).

Limited by the geologic properties of older undifferentiated rocks of the Late Proterozoic and the Lower Cambrian, the groundwater flow is impeded and restricted as little water is stored and transmitted unless the rock is highly fractured (Harrill & Prudic, 1998).

The highly fractured Pole Canyon Limestone, where serious dissolution along the fracture resulted in high porosity and allows a large quantity of water passing through, forms the Lehman Cave system as one of the largest cave systems in Nevada (Halladay & Peacock, 1972).

The alluvial and glacial deposits consist of unconsolidated gravel, sand, silt, and clay that eroded from the adjacent mountains (Elliott et al., 2006). The glacial deposits mostly come from two stages of ground moraine (Whitebread, 1969; Miller et al., 1995a). Depending on the age of the alluvium deposits, the soil status can range between unconsolidated and consolidated. As stated by Thornbury (1969) and Elliott (2006), alluvium and glacial deposits can be at a status from poorly sorted to well sorted. Thus, the hydrogeologic properties of water storativity, hydrologic conductivity, and transmissivity can be largely various depending on the material size, sorting, and the status of cementation (Elliott et al., 2006).

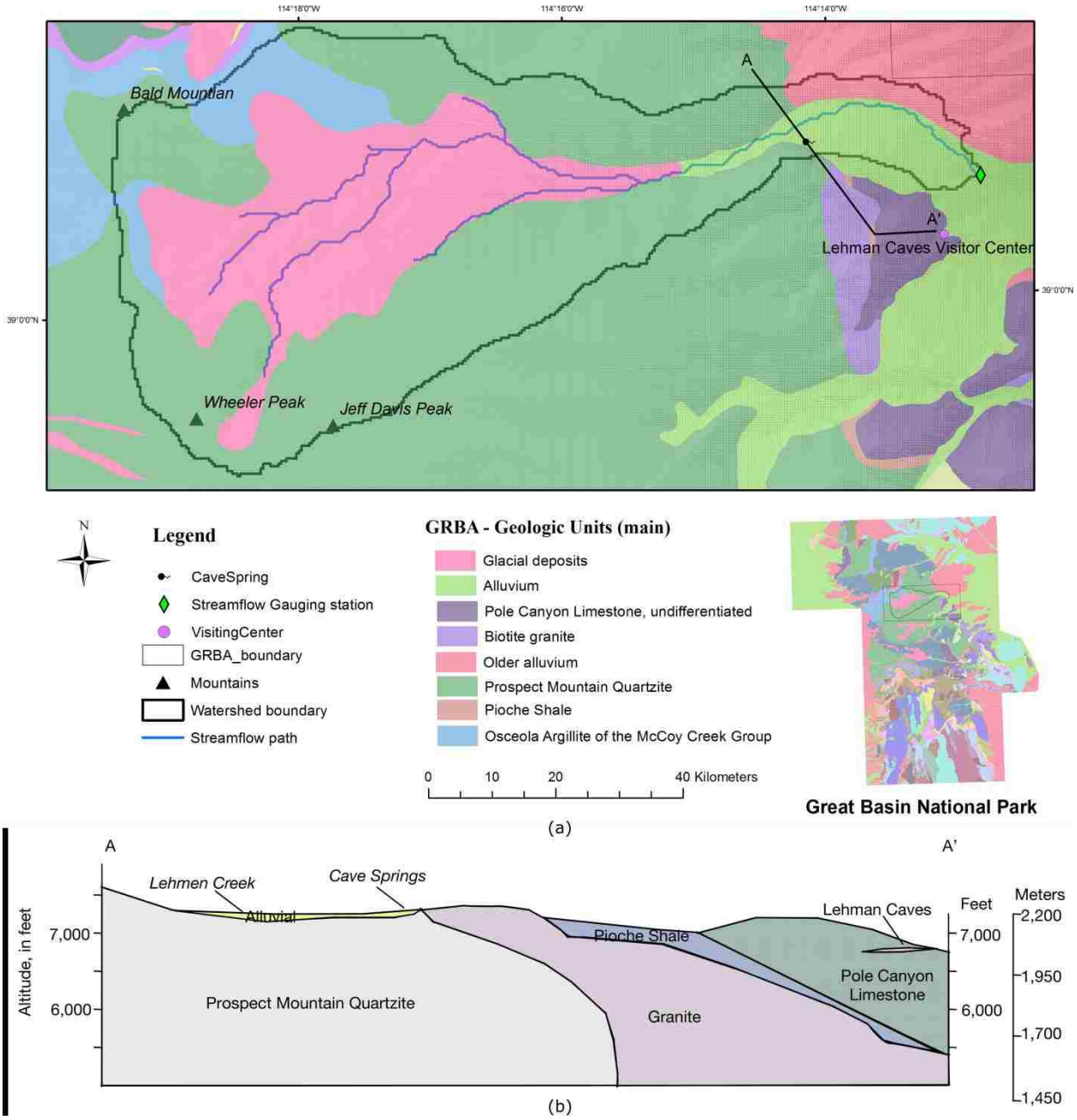

Figure 30. (A) The Surface Geology Map in the Lehman Creek Watershed, Great Basin National Park, Nevada and (B) an Interpretive Geologic Cross-Section with Location Indications for Cave Springs and Lehman Caves (Adapted from Prudic et al., 2015).

4.4 GSFLOW Model

4.4.1 Modular three-dimensional (3D) finite-difference ground-water flow model-MODFLOW

The modular ground-water model - MODFLOW- was developed by the U.S. Geological Survey in 1984 (McDonald & Harbaugh, 1984), which is a consolidation of all previously developed capabilities of computer simulation of ground-water flow. It has been improved and revised 4 times, i.e., MODFLOW-88, 96, 2000 and 2005, and it is widely used and considered the standard code for ground-water simulation as well as the best tool to meet the challenge of its prediction.

Different from surface hydrology, MODFLOW simulates the subsurface hydrologic processes with potential ground-water interferences both naturally, such as lakes, seawater intrusion, geological formation, and artificially, such as wells and reservoirs. It is a mathematical model that simulates the groundwater flow by means of a governing equation to represent the physical processes that occur in the system. In order to help decision-making or geologic judgment, ground-water models intend to describe spatial variability and temporal trends in hydrologic stresses and past and future trends in water levels.

By using a modular structure of grouped functions, the specified computational and hydrologic processes are described independently, which enables MODFLOW to have the option of different combinations of modules, and thus makes it easier for a connection with further extensions of functionalities. With a definition of ‘package’, the model is divided into several aspects of simulations, which include Basic package, Groundwater Flow package, Multiplier, Zone arrays, Boundary Condition package, Solvers, Output Control, and Subsidence packages. Under each of the functional packages, subroutines are further divided: the Well Package, for

example, simulating the effect of wells, and the River Package simulating the influence of rivers, are options in Boundary Condition packages; the Strongly Implicit Procedure Package, solving the system of simultaneous finite-difference equations, is one option in Solvers. The main program calls the various subroutines of the packages in a proper sequence to simulate ground-water flow. The descriptions of Mathematical Model, Discretization Convention, and Finite-different Equation from Harbaugh et al. (2005) were summarized in Appendix.

4.4.2 **Coupled Groundwater and Surface-water Flow Model - GSFLOW**

GSFLOW is a coupled Groundwater and Surface-water FLOW model based on the integration of the U.S. Geological Survey (USGS) Precipitation-Runoff Modeling System (PRMS) and the USGS Modular Groundwater Flow Model (MODFLOW). Due to the excessive complexity of problems with water resources faced by society, an integrated hydrologic model is more useful for considering and analyzing the dynamic interactions between surface water and subsurface water that affect the timing and rates of such processes as surface runoff, evapotranspiration, soil-zone flow, and groundwater flow (Markstrom et al., 2005).

GSFLOW was developed to simultaneously model water flow both underground and on the surface through simulations of overflow crossing the land surface; interflow within subsurface, saturated or unsaturated media; and water flow in rivers and lakes. As such, it is used to evaluate the influences and effects of such factors as climate variability, land-surface change, and groundwater withdrawals on the spatial and temporal distribution of water resources for regions ranging from a few square kilometers to thousands of square kilometers, for time periods ranging from months to decades. For example, to better understand the groundwater system in Chamokane Creek basin, Ely and Kahle (2012) constructed a numerical model for a surface-water flow and groundwater-flow system in three dimensions and with transient

processes, which tend to help water-management agencies and stakeholders with a quantitative understanding of the effects resulting from the potential increase of groundwater pumping on the regional water resources. Others developed transient, integrated hydrologic models to provide an understanding of dynamic interactions between surface water and groundwater in seasonal changes at montane meadows (Essaid & Hill, 2014) and in a complex hard rock system (Hassan et al., 2014). Considering climate change influences, quantitative assessments were made for the evaluation of hydrologic responses (Mejia et al., 2012; Huntington & Niswonger, 2012; Hunt et al., 2013) , which would help water resources policy makers, natural resources managers, stakeholders and the public to better understand the corresponding alternations in the water resources availabilities and the increasing risks of extreme events (e.g. winter storm and flood). It could further improve the regional water resources management with better policies (Woolfenden & Nishikawa, 2014; Allander et al., 2014; Niswonger et al., 2014; Fulton et al., 2015; Albano et al., 2016). An integrated hydrologic model could be a better representation for the study of regional hydrologic processes on the land surface and subsurface, especially the interactions between them. In Huntington and Niswonger's paper (2012), a GSFLOW model was used to study the causality of observed decreasing summer flow. Through the interactive investigation of the groundwater recharge and discharge to the streamflow, the role the groundwater plays in the formation of a snow-dominated runoff was clarified (Huntington & Niswonger, 2012).

Coupling of PRMS and MODFLOW

The typical hydrologic processes in land surface and subsurface is shown in Figure 31, where the interactive water flows occur between surface and subsurface through soil, streams, and lakes. The vadose zone connects surface water and groundwater, which simulates the water

flow from infiltration to the formation of subsurface flow until it reaches the saturated zone (groundwater system). The vadose zone simulated in GSFLOW is split into two parts: Soil Zone and Unsaturated Zone.

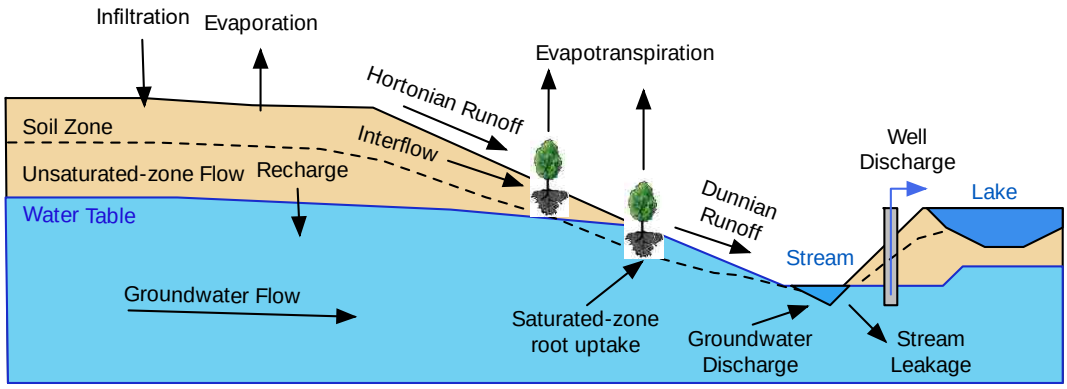

Figure 31. Hydrologic Cycle For Surface-Water and Groundwater Integration (Modified from Markstrom et al., 2005).

Soil zone is simulated in PRMS. It is the area where horizontal flow and evapotranspiration occur, based on soil properties and water content status. Excess water in the form of gravity drainage goes into the Unsaturated Zone, simulated in MODFLOW, where water penetrates vertically in the form of a water wave until it reaches the saturated zone. The schematic diagram of the exchange of flow between PRMS and MODFLOW in GSFLOW is shown in Figure 32. Detailed calculation algorithms of water flux between two models are from Marstrm et al. (2005), which were summarized in Appendix.

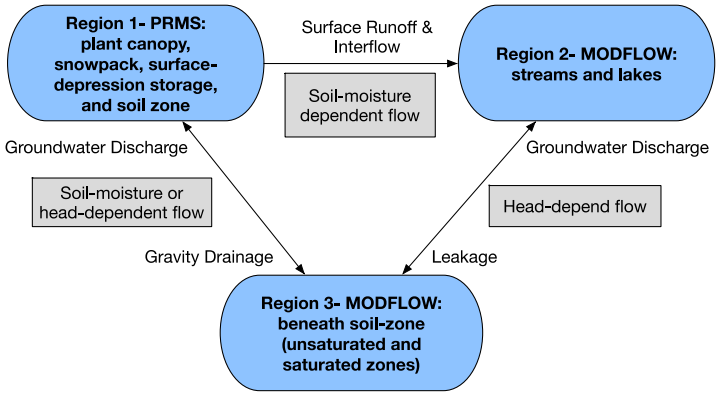

Figure 32. The Schematic Diagram of the Exchange of Flow between PRMS and MODFLOW in GSFLOW (Adapted from Markstrom et al., 2005).

4.4.3 **Steady State and Transient State**

Steady state and transient state are two important status of a system. In a hydrologic system, the steady state describes an unvarying status that the system behavior does not change with time and so do the water flow magnitude and direction. On the other hand, the transient state describes a varying status, under which the system behavior changes with time. Different from surface hydrology, the groundwater usually has a hindrance feature as it flows through the porous media. This hindrance feature can be represented as the hydraulic conductivity and storativity, which describes the easiness of fluid passes through porous media, and the porous media's storage feature, respectively. These are important parameters to describe the hydrogeologic features.

The steady state represents the condition in a regimented system, in which inflows balance with outflows. In MODFLOW, this equilibrium indicates water head is independent of time. It is usually used to determine the initial condition for the transient-state model. Assuming water is incompressible and with no sources or sinks, the water head distribution is determined by hydraulic gradient and hydraulic conductivity (Eq.(4).

$$Q_i = SS\frac{\Delta h}{\Delta t}\Delta V \tag{4}$$

The transient state represents a condition, under which variable is time dependent, which means the water head changes with time. In the derivation of the governing equation (Anderson et al., 2015; Eq. 19), an expression for the water release rate from the aquifer storage is introduced, which is described as aquifer storativity: the water volumes released from aquifer storage per unit area of aquifer per unit head decline (Wang & Anderson, 1995). It is another important geologic feature describing the aquifer ability of storing and releasing water.

4.5 MODFLOW Model Development

The model development of GSFLOW model includes two components: surface hydrologic model (PRMS) and the groundwater flow model (MODFLOW), which simulates the surface hydrologic processes on physical bases and the groundwater flow system in three dimensions. As the surface hydrologic modeling using PRMS was introduced in Chapter 3, in this chapter, the focuses were on a steady-state groundwater flow system development (Chen et al., 2017b). Before that, the concept of model state was introduced, which are steady state and transient state.

4.5.1 Groundwater Flow System Modeling – Steady State

The steady-state MODFLOW simulation includes: (1) building a conceptual model – defining hydrostrategraphic units, preparing the water budget, and defining the flow system (Anderson et al., 2015; Kuzara, 2011); (2) classifying the groundwater flow model as well as spatial and temporal discretization; (3) using the trial-and-error method to calibrate model parameters with hydrogeologic features and water budget components.

Hydrogeology Conceptualization

Hydrostrategraphic Units

In order to couple with the surface hydrologic model PRMS, the realm of the groundwater system simulation was kept consistent with the realm of the PRMS model. The boundary of the realm was defined by topographic divides by using a digital elevation model (Anderson et al., 2015). This boundary definition usually is used in surface hydrologic studies; most of the time, the boundary of groundwater flow system is not the same as the surface hydrology. Nevertheless, it was important to define a realm with an overlapping area in which surface and subsurface water interacted.

Within the simulation realm, the geologic units of similar hydrogeologic properties were broken into hydrostrategraphic units (Maxey, 1964; Seaber, 1988) to simplify the modeling system while still retaining the hydrologic features. Thus, a two-layer groundwater flow system was defined. Layer 1 consisted of glacial and alluvial deposits and Layer 2 consisted of fractured quartzite in the upper stream, limestone downstream, and granite and shale intrusions in between (Figure 33).

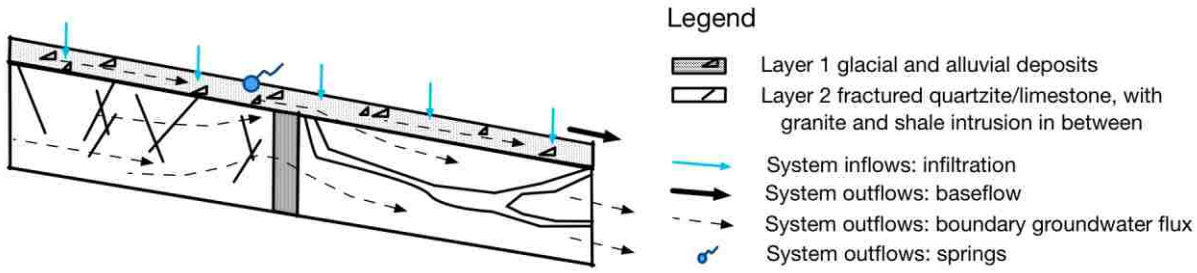

Figure 33. Geological Conceptualization of the Study Area in Hydrogeologic Profile. Layer 1 Represents Glacial and Alluvial Deposits; and Layer 2 Includes Fractured Quartzite, Limestone, and the Granite and Shale Intrusion in between. (The Diagram is not to the Scale, and is modified from Prudic et al., 2015).

Water Budget

Taking into consideration accommodating the PRMS model in the integrated GSFLOW, the water balance of the simulated groundwater flow system consisted of one inflow and three outflows. The model inflow was initiated using the results from the surface hydrologic model PRMS, which was the vertical water recharge to the groundwater flow system. The vertical water recharge was the excess water after the fast interflow and slow interflow were generated, and entered the unsaturated zone in the simulated groundwater system (Figure 33). The three outflows leaving the simulated groundwater system consisted of spring discharges (Cave Springs), stream baseflow (Lehman Creek), and the groundwater outflows through the limestone formation to adjacent areas. Evapotranspiration was not considered in the groundwater system but was considered in the integrated GSFLOW model. The three outflows that left the

groundwater system were Cave Springs, the Lehman Creek baseflow, and the groundwater flows.

Flow System

According to Prudic et al. (2015), in the area where the geology is dominated by quartzite and glacial deposits (Figure 30 & Figure 33), most of precipitation forms into surface runoff, with minor groundwater flow occurring. Groundwater flow receives a recharge from macrofractures as well as coarse sediment in the glacial deposits and alluvium with small storativities. Impervious quartzite and granite impede the groundwater flow and force it into the spring discharge (Figure 33). In the area between the intrusion and the watershed boundary, the losing-stream recharges the groundwater by means of both glacial and alluvial deposits as well as the underlying karst limestone.

Model Setup

Modular Modeling

To model the groundwater system in this study, MODFLOW-NWT was used. This model uses the Newton-Raphson formulation for MODFLOW-2005 to improve the solution of unconfined groundwater-flow problems (Niswonger, Panday, & Ibaraki, 2011). The selected modules are summarized in Table 11. The Discretization File (DIS) was used to specify temporal and spatial discretization. Basic model settings related to each cell, such as active simulation cells and initial heads, were set up in the Basic Package (BAS6). Layer properties were specified in the Upstream Weighting Package (UPW), which controlled the flow between cells. By defining data and parameters related to the hydraulic properties of the unsaturated zone, evapotranspiration, and infiltration, the Unsaturated-Zone Flow Package (UZF) was used to

simulate the vertical flow from the unsaturated zone to the saturated zone. The Stream-Routing Package (SFR) was used to simulate the streamflow routing process with a kinematic wave equation. Regarding the groundwater outflows from the study area, the General-Head Boundary package (GHB) was used to calculate the water flux, depending on head differences. The Well Package (WEL) was used to simulate the influences of groundwater pumping on the groundwater system.

Table 11

Summary of Lehman Creek Watershed MODFLOW Model Designed as a Coupling Component in the Integrated GSFLOW Model.

Category	**Content**	**Details**
Model description	MODFLOW version	MODFLOW-NWT
Model setup	Groundwater flow process	Basic Package (BAS6) Discretization File (DIS)
	Groundwater flow package	Upstream Weighting Package (UPW) Unsaturated-Zone Flow Package (UZF)
	Boundary condition package	Streamflow-Routing Package (SFR) General-Head Boundary (GHB) Well Package (WEL)
	Solver	Newton Solver (NWT)

Since the MODFLOW developed in this study was a groundwater component in the GSFLOW model, the development required not only a basic understanding of the groundwater flow system in the study area, but also needed to take into consideration the coupling processes regarding the water interaction with the surface water system. As represented in the selected modeling packages, the main data linkages between the two single-regime components included:

- Water infiltration from the surface water components, recharging to the groundwater component;
- Storage changes in the unsaturated zone that affect vertical infiltration to the saturated zone, evapotranspiration, corresponding consequences in the runoff; and

- Groundwater discharges to and recharges from streams, which influence water-flow paths and hydrogeologic features.

For water percolation, as horizontal flows, i.e., fast flow and slow flow, were simulated in the soil zone of the surface hydrologic model PRMS, only the vertical flow left the surface hydrologic system and percolated into the deeper unsaturated zone, as simulated in the groundwater flow system (Figure 34). This water percolation was computed as the gravity drainage that exceeded the fulfillment of the horizontal flow in the soil layer by PRMS; it was used as the input for water recharge to the groundwater model, MODFLOW. Thus, during this process, this water percolation as an intermediate variable was not required in the integrated model. However, in the independent MODFLOW model developed in this study, this vertical recharge input, which was the water percolation derived from the PRMS model, was required.

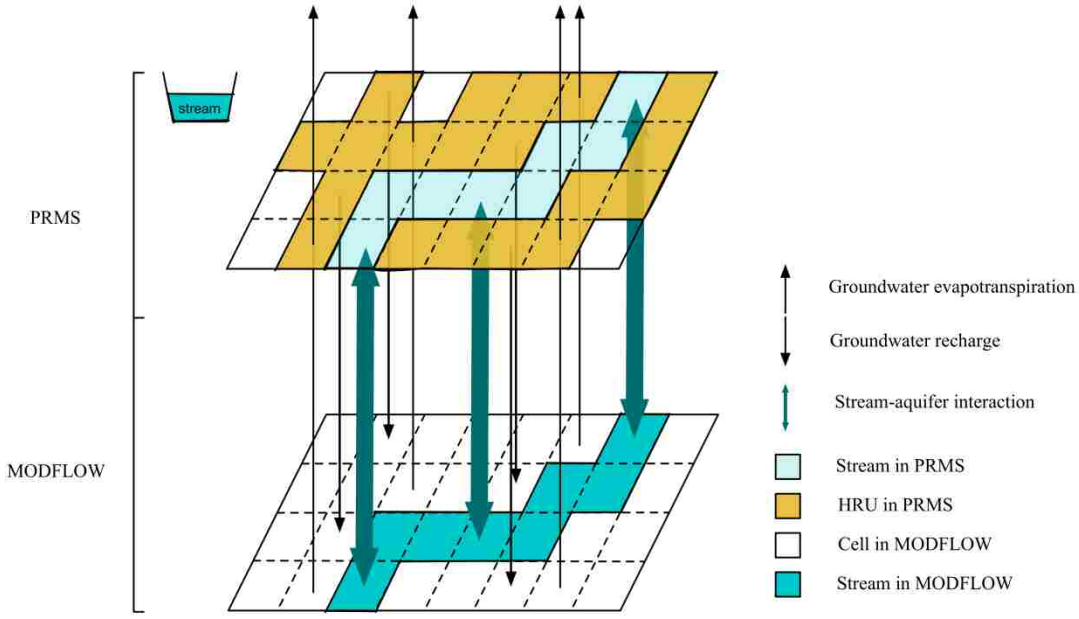

Figure 34. Schematic Diagram of Water Interactions between a Surface Hydrologic Model (PRMS) and a Groundwater Flow Model (MODFLOW).

Also simulated by the UZF package, the unsaturated water was assumed only to flow vertically with the homogeneous unsaturated zone (Niswonger et al., 2006). The diffusive gradients and capillary pressure gradient were negligible, and the capillary fringe was not simulated. On the basis of these assumptions, a one-dimension finite-difference form of Richards' equation was used with a kinematic-wave approximation, taking into consideration evapotranspiration (ET) losses (Niswonger et al., 2006). Additionally, ET in the unsaturated zone could be set up and calculated as a function of three factors: the potential evapotranspiration (PET) that could not be satisfied from the soil zone, the water content in the unsaturated zone within the reach of root depth, and the water table of the saturated zone. In this study, the results of percolation, subtracting ET, was used as vertical recharge; therefore, the ET process was not considered separately.

In streamflow simulation, the recharges and discharge through the streambed facilitated streams, both gaining and losing features (Figure 34). Regarding the relative relationship between stream head at the midpoint of the stream reach and the groundwater head at the center of grid (higher or lower), the SFR package calculated the water flow rate (losing or gaining) by using Darcy's Law (Prudic et al., 2004). In this study, the streamflow routing process was set to the sum of all the inflows, as it is a small watershed. While, this algorithm required input of precipitation, ET, and surface runoff computed by PRMS (Prudic et al., 2004), no value was initiated in this steady state model, as the conceptualized model assuming all outflows were balanced with vertical recharges. Furthermore, the precipitation and ET could be ignored in both steady state and transient state model.

Spatial and Temporal Discretization

A major difference that exists in the development of a surface water and groundwater model is the spatial and temporal discretization. In the surface hydrological model, PRMS, the entire model domain can be differentiated into either sub-basins or grids; however, the groundwater model, MODFLOW uses only a finite-difference grid to describe the model domain. A different computation unit requires extra transformation to smooth the water connections between the two systems; for further details, refer to Markstrom et al. (2015).

Thus, before developing an integrated model, model conceptualizations for both the surface water system and the groundwater flow system are important. In this study, the same-sized grid was employed that was used to delineate the PRMS model also was used to represent the finite-difference grid. The horizontal spatial discretization was kept consistent with the PRMS model in order to facilitate the coupling process. The study area was delineated using 100-m by 100-m cells, which resulted in 96 columns and 49 rows (Figure 35). Out of a total of 4704 cells, 2516 cells were within the study area, and were active. Vertically, the top surface and the first layer was lined with topographic reliefs, using the digital elevation model (DEM). For a convenient coupling process in future GSFLOW modeling, where the top layer is the soil zone base contacting with the PRMS model, the layers were defined considering the thickness of the soil zone. In this study, 4-m soil zone was defined. Layer 1 was defined as a 10-m-deep layer beneath the soil zone. The formula used for defining Layer 1 was:

$$\text{model\_upper\_aquifer\_top} = \text{land\_elevation} - \text{soil\_zone\_thickness} \quad (5)$$

$$\text{model\_upper\_aquifer\_bottom} = \text{land\_elevation} - \text{soil\_zone\_thickness} - 10\ \text{m} \quad (6)$$

Layer 2 was defined as a 350-m-deep layer underlying Layer 1, using the formula of:

$$\text{model\_lower\_aquifer\_top} = \text{model\_upper\_\_aquifer bottom} \quad (7)$$

$$\text{model\_lower\_aquifer\_bottom} = \text{model\_upper\_aquifer\_bottom} - 350\ \text{m} \quad (8)$$

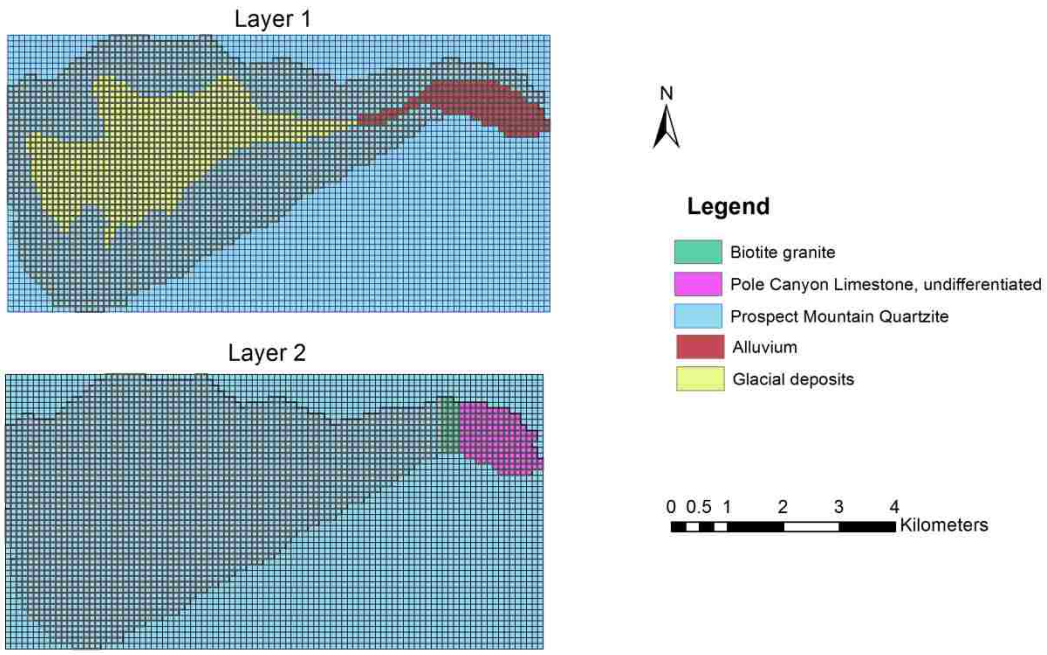

*Figure 35***.** The Spatial Discretization of the Study Area with a 100-m by 100-m Grid, with Conceptualized Hydrostrategraphic Units.

The granite and shale that underlie the quartzite only was represented in the intrusion at the contact where the quartzite meets the limestone formation. They were not simulated as a defined layer due to their low permeability and storativity. These geologic formations were considered as no-flow boundaries for purposes of model simplification (Figure 33; Table 12).

Time steps of interest for surface water and groundwater may have differences that could be in terms of hours, days, or months. Nevertheless, since the PRMS model only supports the daily time step for a PRMS-IV simulation (Markstrom et al., 2015), the daily step was used for both surface and groundwater modeling systems in order to keep the temporal consistency in this study.

Table 12

Aquifer Units and Corresponding Hydrogeologic Characteristics as Simulated in Groundwater Model Layers.

Layer	Hydrogeologic Unit	Thickness (m)	Hydrogeologic Characteristics
1	The glacial and young alluvial deposits	10	Most groundwater passes through these layers where the glacial deposits sit in the mountain upland zone and alluvial deposits are located in the karst limestone.
2	The mountain quartzite and karst limestone, with the biotite granite intrusion	350	The thick mountain quartzite dominates the upper watershed, with karst limestone simulated within the same layer. The granite intrudes between the mountain upland zone and the karst limestone zone, and introduces the groundwater flow to the surface.

Model Calibration

The calibration procedure for a component of an integrated hydrologic model requires a different approach than the more traditional single-regime model. The dynamic interactions between surface water and groundwater indicate that the parameters and variables in both systems should be adjusted for integration. Simplifying assumptions were made that took into consideration the potential interactions with water levels, flows, and water budgets (Davis, 2001). In this study, the model was calibrated using a trial-and-error technique, using water balance and hydrogeologic features as the two main indices to estimate the hydraulic conductivity for each hydrostrategraphic unit.

First, the developed MODFLOW model was set up and calibrated under steady-state conditions, which meant that during the entire simulation period, the water flow rate, path, and scale did not change. The total water inflow, i.e., vertical water recharge, equaled the total water outflows, i.e., springs, baseflow, and groundwater outflows; no storage changed, and the storage term equaled to 0. The water balance for each component was estimated from the literature review ("Aquifer tests at Baker," 2016; Elliott et al., 2006; Prudic et al., 2015; Scanlon et al., 2002). As the model inputs were derived from the surface hydrologic model, PRMS – and were scaled to match with the inflow of the groundwater flow system – the model was calibrated

against the outflows of the groundwater flow system. For a groundwater model, the aquifer hydraulic conductivity and storativity are the primary calibration parameters (Kim et al., 2008). Under the current steady-state simulation, only the hydraulic conductivity values were estimated. For each hydrostrategraphic units and streambeds, the hydraulic conductivity values were adjusted until water budget results matched with the estimated flow rates within a ±10% range.

The calibration technique performed in this study was a manual calibration process, which involved iterative parameter changes according to the evaluation of model responses. The value scale, spatial distribution, and value scale correlations among parameters were the principal concerns when iterative adjustments were performed. The gravity drainage resulting from the PRMS simulation was used as the infiltration inflow in the MODFLOW model. By scaling its spatial distribution and the hydraulic conductivity distribution, a balance with estimated water budgets was sought, while maintaining a reasonable groundwater level distribution that fits the hydrogeologic features in the study area.

It was important that the spatial distribution of hydrogeologic features were reasonably approximated. This occurs at Cave Springs at the contact where the quartzite meets the granite intrusion 1 mi east of the Lehman Caves Visitor Center. The baseflow, mainly maintained by groundwater recharge, leaves the watershed through the outlet. The groundwater outflows through the alluvial deposits and limestone, leaving the simulated area. Additionally, the water head distribution generally should be consistent with topographical reliefs, especially in mountainous areas underlain with low permeable rock.

Sensitivity Analysis

The sensitivity analysis was carried out for the estimated hydraulic conductivity of each hydrostrategraphic unit in order to assess the effects on the water-balance estimation. The model

simulations were conducted for 14 different values of hydraulic conductivity, ranging from 0.2 to 10 times the estimated value. For each run, the Root Mean Square Error (RMSE) was calculated (9), which measures the error of the fit of the estimation to the data (Kenney, 2013). The lower value of RMSE meant a better model simulation with fewer errors. Accordingly, the sensitivity of the hydraulic conductivity values could be estimated by corresponding changes in the model errors. RMSE for each tested run was expressed as:

$$RMSE = \sqrt{\frac{\sum_{i=1}^{n}(h_{c,i} - h_{t,i})^2}{n}} \quad (9)$$

where, h_c and h_t represented the calibrated and tested results of the water-balance components (i). The value n was 4 under this study as there are 4 water-balance components.

4.5.2 **Results**

Water balance simulation

One important target for the development of a groundwater flow system is to establish a good estimation of water budgets, as this is fundamental for water management plans. The water budget quantitatively describes the hydrogeologic water balance, which reflects the equality between the total inflows and the total outflows in the groundwater system. Table 13 summarizes the water balance in the study area, using data obtained from previous studies; these data were used in the model development as boundary conditions. The estimation of vertical infiltration, derived from the PRMS model, was 1010 m^3/d. Driven by input of this inflow, the outflows were simulated, and components were described as follows.

Table 13

Water Budget Estimations of the Conceptualized Groundwater Flow System in the Lehman Creek Watershed under Steady-State Simulation.

	Water Budget Component	Flow Rate (m^3/d)	Estimation Source
Inflow	Vertical infiltration	1010	Water balance estimation
Outflow	Streamflow baseflow	450	Between 3% of 5.3 cfs and 415 m^3/d estimated from Prudic et al. (2015)
	Spring discharge	245	(David E. Prudic & Glancy, 2009)
	Groundwater flow	315	Estimation according to Prudic et al. (2015)

Stream baseflow

For the water balance estimation, studies have indicated that the base flow is recharged by the groundwater (Hall, 1968; Smakhtin, 2001; Hamel et al., 2013). On the basis of a hydrogeologic study from Prudic and Sweetland (2011), the groundwater flow takes about 2% - 3% of the total precipitation, while the streamflow takes 45% of the precipitation. The historical streamflow records showed an average daily flow rate of 5.3 cfs during 2003 to 2012 water years, and so the baseflow was estimated to be 538 m^3/d (0.22 cfs). The baseflow from Prudic et al. (2015),was used to estimate the baseflow of 415 m^3/d in Lehman Creek. Thus, the estimation of 450 m^3/d, which is between 415 m^3/d and 538 m^3/d was used as the baseflow rate in the current study.

Spring discharge

According to previous studies at Cave Springs (Halladay & Peacock, 1972; Prudic & Glancy, 2009), four springs emerge at the contact area where the quartzite meets granite at the downstream side of Lehman Creek. Spring water is collected at a rate of around 245 m^3/d (0.1 cfs).

Groundwater outflow

The groundwater flux from the southeast side of the Lehman Creek watershed to the adjacent area was difficult to estimate due to its complex geologic formation of caves. In this model, constant heads at specific location cells were specified to simulate the water outflows' variation with the water heads' change. An estimation of 315 m^3/d of groundwater flux was simulated through the boundary cells for the steady-state simulation in this study. Figure 36 shows the position where the boundary flow occurred.

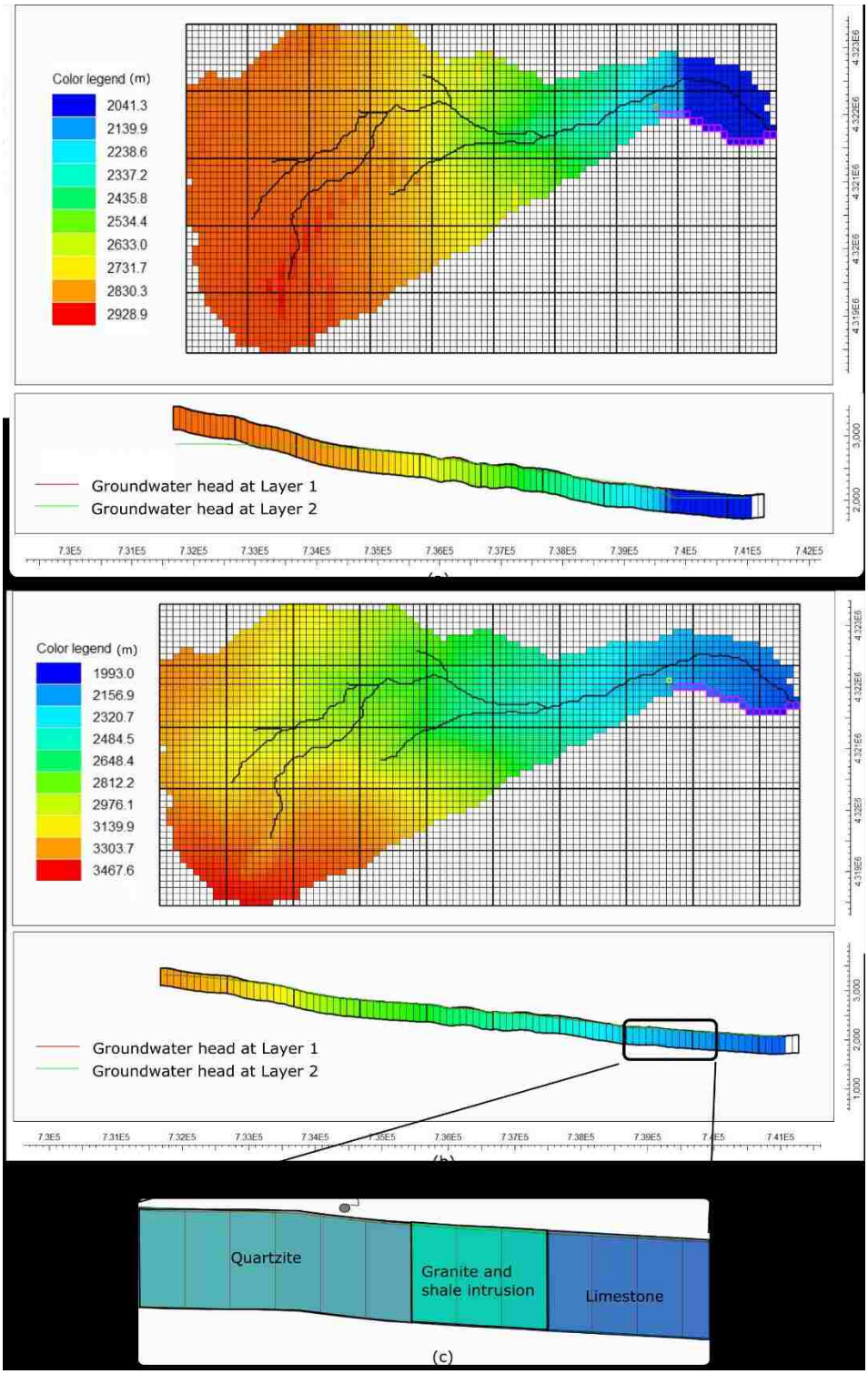

Figure 36. Water-Level Distribution of the Top View (Layer 1) and the Front-View Cross-Section of Cave Springs (Layers 1 and 2), using the Modelmuse Tool: (A) with Initialized Hydraulic Conductivity Values before Model Calibration; (B) with Hydraulic Conductivity Values after Model Calibration; (C) Detailed Cross-Section of Cave Springs.

Model calibration

The groundwater model calibration involved determining the magnitude and spatial distribution of the model parameters. These parameters reproduced the observed system state with hydraulic heads and groundwater flows (Kim et al., 2008). Within the region of the study area, there were no drill holes or well observations; therefore, the traditional method for parameter identification could not be used. Instead, hydrogeologic features and components in water balance were used to calibrate the hydraulic conductivity.

Hydrogeologic features

In order to compare the effects of hydraulic conductivity on the simulated groundwater-flow model, water head distribution was compared between the initial condition and simulated steady-state condition, by using estimated parameters and calibrated parameters, respectively. As shown in Figure 36a, the overall water level ranged between 2041.3 m at low elevations and 2928.9 m at high elevations. However, in the western region, where the land surface elevation was higher than 2805 m, results for the water level were within a relatively narrow range of 2810 m to 2900 m. This was in a contrast to the high variation in land surface, which ranged between 2805 m and 3980 m. This indicated a deep water level with low spatial variability in the mountainous area, which did not capture the features of high topographic reliefs. This also could be observed from the front view of the water level (Figure 36a), as both water levels from Layer 1 and Layer 2 were deep below the land surface. However, with calibrated parameters, the water level was adjusted (Figure 36b), resulting in the water levels being a subdued replica of the topography. The front view of the cross section at Cave Springs shows the groundwater flow was impeded by low permeable granite (and shale) intrusion, where

the water level was raised, resulting in the groundwater being discharged to the land surface. Additionally, the groundwater outflows at the defined boundary cells.

Hydraulic conductivity

As summarized in Table 14, hydraulic properties for each hydrostrategraphic unit were initialized, estimated from a groundwater study at Baker Creek ("Aquifer tests at Baker," 2016; Haitjema & Mitchell-Bruker, 2005). By trial and error, the hydrologic conductivity was adjusted to minimize the error within 10% (Table 14). During this process, the hydrogeologic features were maintained because the direction of groundwater flow was a crucial indication to groundwater levels. Results showed that in Layer 1, the coarse glacial deposits sitting in the center of the valley and along the streams has a relative higher horizontal hydraulic conductivity (5E-2 m/d) than the vertical value (3E-2 m/d), and around the downstream side, the alluvial deposits had a higher vertical hydraulic conductivity (2 m/d) than horizontal value (5E-2 m/d). Underneath this, in Layer 2, the fractured Prospect mountain quartzite formation had a low hydraulic conductivity of 5E-7 m/d; meanwhile, the granite (and Pioche shale) intrusion had an even lower value of 1E-7 m/d. The limestone were with 1E-2 m/d and 4E-4 m/d for the horizontal and vertical hydraulic conductivities, respectively. In the model, the Brooks-Corey exponent and horizontal anisotropy were 3.5 and 1, respectively.

Table 14

Hydraulic Conductivity of Each Hydrostrategraphic Unit in the MODFLOW Model (Unit: m/d)

	Horizontal	Vertical	Value Ranges of selected rocks (Heath 1983)	
Glacial deposits	5E-02	3E-02	Value range for Glacial Till	1E-7 to 0.3
Alluvial deposits	5E-02	2	Value range for Silty, Loess, Silty Sand, Clean Sand, Gravel	1E-3 to 5E3
Quartzite	5E-7	5E-7	Value range for Igneous and Metamorphic Rock	1E-8 to 5
Limestone	1E-02	4E-04	Value range for Carbonate Rocks	1E-4 to 5E3
Granite and Pioche shale	1E-7	1E-7	Value range for Shale	1E-8 to 1E-4

Sensitivity analysis

The sensitivity analysis was carried out to analyze the influences of tested parameters on the model-simulated water balance. Both horizontal and vertical hydraulic conductivities for each hydrostrategraphic unit – i.e., glacial deposits, alluvial deposits, granite, and limestone – were selected. Hydraulic conductivities were changed by using a coefficient that ranged between 0.2 to 10, and the error indicator RMSE was used to evaluate the model performance regarding the water balance calibration.

As shown in Figure 37, among all the hydrostrategraphic units, the hydraulic conductivity in glacial deposits had the greatest influence on the model results, as the greatest increase was found in the RMSE values for glacial deposits. This was followed by horizontal hydraulic conductivity in alluvial deposits, horizontal hydraulic conductivity in limestone, and vertical hydraulic conductivity in limestone. While the model was most sensitive to these mentioned parameters, the current steady-state model was not sensitive to hydraulic conductivities of granite and quartzite formations, as the RMSEs did not change much when the parameters changed.

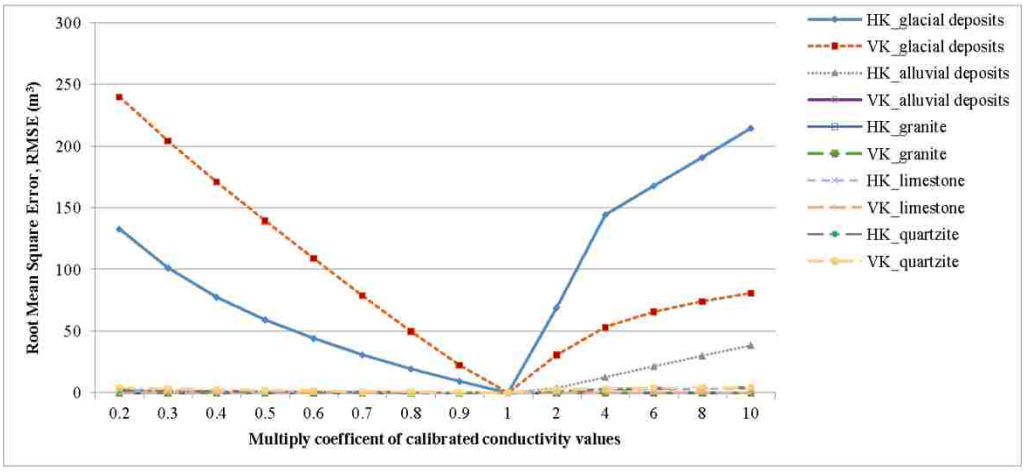

Figure 37. Results of a Sensitivity Analysis for the Hydraulic Conductivity of Each Hydrostrategraphic Unit Influencing the Model Results. Root Mean Square Error (RMSE) (HK = Horizontal Hydraulic Conductivity; VK= Vertical Hydraulic Conductivity).

As RMSE is an absolute measure of fitness, the value '0' indicates the best fit, and had the same unit as the response variable, which was m^3/d or m^3 as model ran on daily basis. The RMSE plot (Figure 37) showed a range of 0 to 240 m^3/d for all 10 parameters that were tested, using different coefficients. The point where the multiplying coefficient was 1 represents the calibrated model, and other points represent SA tested models.

4.5.3 **Discussion**

The primary objective of the current study was to better understand the role MODFLOW plays in integrated GSFLOW modeling from the perspective of model development. When developing GSFLOW model, there were some assumptions, limitations, and uncertainties related to the groundwater flow system in the Lehman Creek watershed study area. For example, it was assumed that the vegetation roots were within the soil layer overlaying the MODFLOW simulation region, the evapotranspiration process was considered in the surface hydrologic PRMS model and thus was not considered in the MODFLOW model developed in this study. Additionally, an evenly distributed thickness of every defined layer was assumed, using a unique value among all the hydrostrategraphic units. For example, the thickness of alluvial deposits downstream was 3 m (10 ft) (Prudic et al., 2015); however, it was assumed to be 10 m in the model because of the uniform thickness of Layer 1. This simplification may result in an underestimation of hydraulic conductivity. Nevertheless, on the basis of current available hydrogeographic conditions, this assumption was reasonable for a conceptual simulation of the groundwater flow system.

The groundwater contours portrayed the integrated nature of the geography, lithology, and effects of weathering and fracturing on rocks. In the modeling results, the highest groundwater levels were at Wheeler Peak, where land elevations are the highest; the lowest

groundwater level was at the eastern watershed, close to the stream outlet. This steady-state results are consistent with the commonly accepted premise in hydrogeology that a water table in unconfined aquifers often is a subdued replica of the topography or land surface (Haitjema & Mitchell-Bruker, 2005). Nevertheless, the groundwater recharges not only the streamflow, but also recharges the springs and groundwater outflows at the southeastern boundary of the study area. With a steady-state calibration, the MODFLOW model could not be used because a transient-state model calibration also was required to further estimate the storativity of the hydrostrategraphic unit and refine the corresponding hydraulic properties. The process used in this study illustrates the use of a preliminary model in an interpretive sense and demonstrates the strength of a groundwater-flow model as a framework for organizing the available hydrogeologic information.

Regarding the sensitivity analysis with all 10 tested parameters, the vertical and horizontal hydraulic conductivity of glacial deposits and horizontal alluvial deposits are the most sensitive parameters because the RMSE showed the largest variation with the parameter changes. This is reasonable as glacial and alluvial deposits are beneath the streams, where the hydraulic conductivities substantially influence the water exchange between streams and groundwater. However, the vertical hydraulic conductivity of alluvial deposits is not a sensitive parameter. This is because, the vertical hydraulic conductivity is high enough that all the water infiltration was able to be passing through the groundwater system. The local value variation would not change this fact or the resulting water balance simulation.

The model simulation performance could be improved further by aquifer pumping tests and improved configurations of the boundary groundwater flux. The complex cave system at the east side of the watershed results in complex groundwater flow, with nonlinearity and uncertain

groundwater outflows to the adjacent region. In this study, the groundwater outflow, as a boundary condition, was simulated by using the GHB package, which treated the water flux as linearly correlated with the head differences between the defined values and model simulations. This simplification could not represent well the complexity and nonlinearity of the groundwater flow in this diluted limestone formation. Moreover, according to two piezometers tests of the streambed at karst-limestone zone (2009 and 2010) in a nearby watershed, the hydraulic conductivity tremendously varied from one to the other, as did the ratio of vertical value *versus* horizontal (Prudic et al., 2015). In this study, the spatial variation was represented by defined hydrostrategraphic units instead of grids, thus an averaged value was calibrated which was able to capture the water-losing features at downstream and the boundaries with the best knowledge currently available.

4.5.4 **Conclusions**

In this study, a MODFLOW model was developed for the Lehman Creek watershed, to be coupled with the PRMS model in an integrated surface and groundwater flow system. With the available data from adjacent areas and water balance estimations from available literatures, the groundwater system was conceptualized. The MODFLOW model was calibrated under a steady state using boundary conditions of streams, springs, and groundwater outflows.

The main conclusions drawn from the study are:

- There are three data linkages between the surface hydrologic model PRMS and the groundwater flow model MODFLOW, i.e., direct vertical recharges, unsaturated-zone features, and streamflow-aquifer interactions, as they were the critical water-flow features in the coupling processes where the two subsystems interacted.

- The water budget estimation with a consideration from the PRMS modeling results plays a critical role in the coupling process with the surface hydrologic processes in the GSFLOW model, such as vertical infiltration and stream baseflow.
- The hydraulic conductivity of glacial deposits, and alluvial deposits sitting in the central valley and having frequent interactions with the streamflow, have the greatest influences on the groundwater flow system simulation.

Based on the documented literature and the author's knowledge, this research sets up the fundamentals of MODFLOW development and its integration with surface water modeling in the study area of Lehman Creek watershed. The current study produced a model that can provide understanding of existing hydrogeologic conditions within the watershed. More importantly, the model development process presented in the current study highlights the compatibility consideration with the PRMS model, serving the future integration of the MODFLOW and PRMS models. This will enhance the capability of addressing the climatic variability effects on the hydrologic system of Lehman Creek and provide useful information to other similar model coupling attempts.

4.6 Meteorologic Change Influences on an Integrated Hydrologic System

In this section, the integrated model GSFLOW (v. 1.1.6; GSFLOW Release Note, 2016), which coupled the surface hydrologic model PRMS and groundwater flow system MODFLOW, was introduced. It includes two parts: model calibration and model implementation.

The purpose of this study was to evaluate the influences on the local water resources system by potential external stresses from groundwater pumping and climate change. These two cases capture the impacts of typical human interferences and natural variations, which have implication for groundwater management and hydrologic process research.

4.6.1 Integrated Hydrologic Modeling –Transient State

Groundwater flow system modeling – transient state

The model integration includes two parts: first, the simulation role changes, i.e., the streamflow simulation changes from PRMS model to MODFLOW model; second, water exchanges, i.e., the one-way water flow in the PRMS model into the two-way interactive water exchanges between surface and subsurface within PRMS model and MODFLOW model. Such changes could result in substantial differences in the model simulation results; thus, further model calibration is required for a successful integration of two sub-systems.

Furthermore, the transient-state model simulation is necessary to capture system variations when external stresses change, i.e., to analyze the time-dependent problems. It is more complicated and requires additional parameters related to hydraulic information. As suggested by Anderson and Woessner (2002), a transient model simulation requires specifications of storage parameters, initial conditions, i.e., heads and boundaries, and time discretization.

Storage parameters

During a transient-state simulation, the storage feature in the porous medium allows water to be taken in or released. As a result of the water transfer, the water heads change over time. In order to specify the capability of an aquifer to transfer water from the storage or to the storage, parameters that are usually used include: specific storage (S_s), specific yield (S_y), or storage coefficient (S) (Anderson & Woessner, 2002).

The storage coefficient (S), also termed *storativity*, is the volume of water that a permeable unit will absorb or expel from storage per unit surface area per unit change in head. In a confined aquifer, owing to the compressibility of the mineral skeleton, the water volume stored or expelled from the storage in a unit volume of porous material per unit change in head is

defined as *specific storage* (S_s). Thus, the storativity of a confined aquifer is defined as the product of the specific storage (S_s) and the aquifer thickness (b) (Eq. (10). In an unconfined aquifer, the water level rises and falls with water-storage changes in the porous medium, and this water storage change includes two components. One is caused by gravity, termed *specific yield* (S_y). The other one is the specific storage of the unit. Thus, the storativity in an unconfined aquifer is found by the formula in Eq. (11.

$$S = bS_s \tag{10}$$

$$S = S_y + bS_s \tag{11}$$

where, S is the storativity, dimensionless;

S_s is the specific storage, (1/L);

b is the thickness of the saturated zone (L);

S_y is the specific yield, dimensionless.

For an unconfined aquifer, the value of S_y is several orders of magnitude greater than bS_s, thus the estimation of S_y is more important as it is the predominant weight in the storativity.

Initial conditions

The phrase *initial conditions* refer to the initial head distribution over the entire simulation region, which means there is a head value for each grid cell, including boundaries. It is standard procedure to use the water-head results from a calibrated steady-state model simulation as the initial condition in a transient-state simulation. As explained by Franke et al. (1987), this ensures the consistency between model inputs and the initial head during the beginning of the model simulation.

In this study, water heads from steady state were used, which were constant values over time with spatial variations that include the boundary cells.

Time discretization

The model simulation time period was the same as in the PRMS model, which was from October 1, 2002 to September 30, 2012 (2003-2012, water years). The calibration period was from 2003 to 2007 (water years), and the validation period was from 2008 to 2012 (water years).

One steady-state stress period and one transient-state stress period were included. The one-day steady-state model simulation was used to initialize conditions for the model. The following transient-state model simulation had 1825 one-day time steps. The time period is the same as in the PRMS model.

Coupling procedures of surface-water and groundwater systems

With the developed PRMS model for the surface hydrology simulation and steady-state MODFLOW model, the development of the transient-state GSFLOW model required two additional steps: 1) modifications in the parameters of the MODFLOW model to transition from the steady state to a transient state, and 2) the modification in the PRMS model to facilitate the coupling processes.

Transient-state Model Modifications in MODFLOW

The first step was to change the steady-state simulation to a transient-state simulation in MODFLOW. The steady-state MODFLOW simulation could help to determine the hydraulic conductivities by means of the equilibrium between inflows and outflows of the system. However, most of the time, this equilibrium is disturbed by external stresses, such as water recharge variations. Such stresses affect the groundwater-flow system through the hydrogeologic features, especially aquifer storativity and stream conductance. In GSFLOW, a transient-state model simulation was required to improve the reliability of the model simulation.

As documented in the MODFLOW-NWT guide ("Online Guide to MODFLOW-NWT," 2016), several modifications were required to the four packages used in the current steady-state MODFLOW model.

For the Discretization File (DIS) package:

- The number of stress periods (*NPER*) was updated from 1, which was only a steady-state simulation, to 2 for one steady-state and one transient-state simulation.
- The length of a stress period (*PERLEN*) and the number of time steps in a stress period (*NSTP*) was changed. For first stress period, the setup of *PERLEN* and *NSTP*, which were both defined as "1", maintained as the steady-state simulation. For the second stress period, the *NSTP* was the same as PRMS running step, which was the daily step; therefore, the *PERLEN* was pertained the same length of simulation days.
- Variable (*Ss/tr*) was coded as a transient state (*tr*) for the second stress period, and steady state (*Ss*) simulation was kept the same for the first stress period.

For the UPW package:

- The specific storage (*Ss*) and specific yield (*Sy*) were initiated with estimations for each layer in defined grids, which represented the storage capability of aquifers.

For the UZF Package:

- For the steady-state period, the integer values – indicating reusing or reading the infiltration rates (*NUZF1*) – and corresponding infiltration rate input (*FINF*) remained the same.
- For the transient-state period, *NUZF1*, *NUZF2*, *NUZF3*, and *NUZF4* were specified as negative values (< 0), which meant that the infiltration-related parameters (i.e., *FINF, PET, EXTDP,* and *EXTWC*) were the same as previous stress period (i.e., steady-state stress period).

For the SFR package:

- Basic stream parameters were required to be defined for each stress period; thus, no changes were needed for the first period, as that already was defined in the previous steady-state simulation.
- During the steady-state simulation, the streamflow, initiated at the beginning of each tributary by variable FLOW, was set to zero, as it would be simulated by PRMS model.
- During the transient-state simulation, the parameter ITMP was used and defined as a negative value (< 0), indicating that the stream-segment data were defined as the same as for the previous stress period, which was the steady-state period.

Hydrologic-process Modifications in PRMS

As mentioned in previous sections, there were changes in the roles played by the hydrologic processes in the PRMS-only simulation and the GSFLOW integrated simulation. Two critical components which link the data across the two systems, the streamflow routing process and the groundwater flow beneath the soil zone, change substantially. The streamflow routing process was included in the PRMS simulation when focusing only on the surface hydrologic model. Nevertheless, in the integrated GSFLOW, this process simulation was performed instead by a MODFLOW package (SFR in this study); thus, it was removed from the PRMS simulation. In addition, the groundwater flow simulated in the PRMS simulation, which used a concept of stock and flow, was replaced by the MODFLOW simulation, which simulated detailed unsaturated flow, saturated flow, and additional ET. Therefore, in the previous PRMS model, some modules and related parameters were no longer required (Table 15).

To perform the integration functionality of directing data results from the PRMS model as the data input to the MODFLOW model, additional modules were used. The integration

process was determined primarily by two modules in GSFLOW (Markstrom et al., 2005; Regan et al., 2016): gsflow_prms2mf and gsflow_mf2prms. The gsflow_modflow2 module was used to direct the PRMS results to the MODFLOW model, which included distributing the gravity drainage and unsatisfied ET to the MODFLOW UZF package as well as allocating the surface runoff, i.e., overland flow, Dunnian runoff, and Hortonian runoff, and subsurface interflow from Hydrologic Response Units (HRUs) to stream segments ("GSFLOW Input Instructions", 2015). The gsflow_mf2prms module was used to distribute the groundwater discharges from the MODFLOW cells to PRMS HRUs as the soil-zone input. Additional parameters, which were required for these two modules, were summarized in Table 16.

Additionally, in the Control File, where the parameters related to each run were defined as a model input file for PRMS, the module definition for the streamflow simulation was removed, and the model mode was changed from ‘PRMS’ to ‘GSFLOW’.

Table 15

Modules and Related Parameters Removed for Model Transformation from a PRMS Model Run to a GSFLOW Model Run, as Defined in the Parameter File (Cited from Table 1, GSFLOW Input Instruction 2015; Table 1-3, PRMS Manual (Markstrom et al., 2015)).

Module Name	Module Description	Related Parameter	Parameter Description
gwflow	Sums inflow to and outflow from PRMS groundwater reservoirs. Outflow can be routed to downslope groundwater reservoirs and stream segments.	hru_gwres	Identifier of groundwater reservoir associated with an HRU.
		gwflow_coef	Linear coefficient in the equation to compute groundwater discharge for each GWR.
		gwsink_coef	Linear coefficient in the equation to compute outflow to the groundwater sink for each GWR.
		gwstor_init	Storage in each GWR at the beginning of a simulation.
		gwstor_min	Minimum storage in each GWR to ensure that storage is greater than the specified value in order to account for inflow from deep aquifers or injection wells with the water source outside the basin.
		ssr_gwres	Index of the GWR that receives flow from each associated subsurface or gravity reservoir.
		gw_pct_up	Fraction of GWR area used to compute flow contributed to a downslope GWR or stream segment for the cascade area.
		gw_strmseg_down_id	Index number of the stream segment to which the cascade area contributes flow.
		gw_up_id	Index of GWR containing the cascade area.
		gw_down_id	Index number of the downslope GWR to which the upslope GWR contributes flow.
strmflow	Computes daily streamflow as the sum of surface runoff, shallow-subsurface flow (interflow), detention reservoir flow, and groundwater flow	-	No related parameters removed since they are used in other modules as well.

Table 16

Modules and Related Parameters Required for Model Transformation from a PRMS Model Run to GSFLOW Model Run, as Defined in Parameter File (Cited From Table 1, GSFLOW Input Instruction 2015; GSFLOW Manual *(Markstrom et al., 2005)*).

Module Name	Module Description	Related Parameter	Parameter Description
gsflow_mf2prms	Distributes computed groundwater discharge from MODFLOW cells to HRUs for input to the PRMS soil-zone module at the end of each time step.	gvr_cell_id	Index of the grid cell associated with each gravity reservoir.
gsflow_prms2mf	At the end of each time step, distributes:	gvr_cell_pct	Proportion of the grid-cell area associated with each gravity reservoir.
	The gravity drainage and unsatisfied potential evaporation from HRUs to MODFLOW cells, computed from the PRMS soil-zone module for input to the UZF Package, and	gvr_hru_id	Index of the HRU associated with each gravity reservoir.
	The Hortonian and Dunnian surface runoff and interflow from HRUs to stream segments and lakes and precipitation and evaporation to lakes, computed by the PRMS surface- runoff and soil-zone module for input to the SFR and LAK Packages.	gvr_hru_pct	Proportion of the HRU area associated with each gravity reservoir.
		id_obsrunoff	Index of measured streamflow station corresponding to the basin outlet.
		mnsziter	Minimum number of iterations for which soil-zone states are computed.
		mxsziter	Maximum number of iterations for which soil-zone states are computed.
		Szconverge	Significant difference for checking soil-zone states.

Model calibration

After composing the GSFLOW model with PRMS and MODFLOW models, the calibrated parameters from the PRMS were used as initial values for the parameters in the GSFLOW model. Most parameters can remain unchanged in the GSFLOW model, while focusing on a few parameters that determine the amount and timing of water flux exchanges between surface and subsurface. Through GSFLOW model calibration, these parameters were adjusted and calibrated from perspectives of water balance and water transference through porous medium. The objective of the integrated model calibration is to match the observed and simulated hydrographs both in flow rates and timing.

Regarding the water balance, two principal factors were considered in the calibration of the integrated hydrologic system: 1) the evapotranspiration within the soil zone where water loses from capillary reservoir of the surface hydrologic system and 2) gravity drainage recharging the groundwater system. Firstly, adjustment to the evapotranspiration was performed, which was overestimated in the PRMS model to compensate the missing representation of groundwater outflow losses. During this process, the parameter (*jh_coef*) determining the potential evapotranspiration was adjusted. Secondly, as the groundwater discharges, either to the surface or out of the water system, the gravity drainage was increased to remain the groundwater level and in balance with the groundwater level from steady state. In this process, the adjusted parameters (*ssr2gw_rate*, *ssr2gw_exp*) were coefficients that determine the gravity drainage rate from the gravity reservoir in soil zone simulated in PRMS model.

Regarding the water transference through porous medium, secondary model calibrations were performed to further improve the hydraulic conductivity values to improve the integrated model's performance. Seasonal features of groundwater discharge and recharge were calibrated

by adjusting the hydraulic conductivity, storage property for hydrostrategraphic units and streambeds.

Sensitivity analysis

A sensitivity analysis was performed to determine the effects of changes in the determinant parameters on the streamflow rates and timing. There are several methods for sensitivity analysis, such as Morris screening method and Sobol's method, which are widely used in global sensitivity analysis (Morris, 1991; Campolongo et al., 2007; Song et al., 2015). Compared to their relative high computation size and costs, the sensitivity analysis method used in this study employed the one-at-a time sampling design and analyzed the sensitiveness of parameters to the modeling results, which qualitatively captured the sensitivity characteristics with high reliability and low computation costs.

The storativity and the streambed conductivity were the two principal parameters analyzed in this transient model. In the study area, the only hydrological observations available are the streamflow gauging records. Thus, by varying the selected parameter estimates of specific yield, specific storage, and streambed hydraulic conductivity, the uncertainty in the calibrated GSFLOW model were quantified.

Based on one-at-time (OAT) method, local sensitivity analysis was performed with estimated initial values, which could substantially reduce the computation cost while retaining high reliability (Song et al., 2015). In this study, a sequence of perturbation in forms of coefficients was selected. For each hydrostrategraphic unit, the model simulations were conducted for 14 different values of pre-determined parameters, ranging from 0.2 to 10 times the estimated value. Relative to calibrated model results, the root mean square error (RMSE) (Eq. (9)

and Mean Absolute Error (MAE) (Eq. (12) were calculated and measure the error of the fit of the estimation to the data (Kenney John, 1939). MAE was calculated for each tested run as:

$$MAE = \frac{\sum_{i=1}^{n} |Q_{c,i} - Q_{t,i}|}{n} \quad (12)$$

Different from previous steady-state sensitivity analysis, *i* indicates the number of sample size, which is the number of streamflow days since the streamflow calibration results were used for evaluation (n=1826).

For each hydrostrategraphic unit, by multiplying 14 coefficients, the model simulations were conducted for 14 different values of each selected parameter of specific yield, specific storage, and streambed hydraulic conductivity. Specific yield, specific, horizontal hydraulic conductivity, and vertical hydraulic conductivity were tested for 5 hydrostrategraphic units, and whereas, streambed hydraulic conductivity was tested for 11 stream segments. One set of parameter took 13.35 minutes for 1,826 days/steps of model simulation, resulting in 96.565 hours of total running time (Duo CPU E7600, 4 GB RAM, and 64-bit Operation System).

Model result evaluation

Same as the evaluation methods used in the PRMS model, the developed integrated hydrologic model was calibrated and validated by comparing model simulations with streamflow gauging observations during the available period of 2003-2012 (water years). The indicators of the square of correlation (R^2), percent bias (PBIAS), and Nash-Sutcliffe efficiency (NSE), were used to assess the daily streamflow simulation during calibration and validation, which are the same as used in the PRMS model.

More importantly, the integrated model results were compared to the results of PRMS model to evaluate the model performance. In addition to comparisons of model evaluation

indexes, i.e., R^2, PBIAS, NSE, the hydrographs were compared on mean monthly and monthly mean scales.

GSFLOW simulation

Well pumping

Because the Lehman Creek study area is in southern Snake Valley, where the groundwater could be a potential water supply source to support Las Vegas for future social and economic development, it is important to understand the potential influences on the local water resources system. Although groundwater withdrawal from Lehman Creek is not a realistic scenario, it was introduced as a what-if scenario to better understand groundwater responses to pumping. The location of the pumping well was selected at the downstream of Lehman Creek close to the stream. Vertically, it extends to the second layer of the geological formation, where complex limestone hydrostrategraphic unit is located. The total water application from Snake Valley is 1.7×10^5 m^3 per day (50,679 afy) (SNWA, 2012). The Lehman Creek watershed is 23.6 km^2 (5,839 acres) in area, which takes 0.3% of the total 9013.2 km^2 (3,480 mi^2) area of the Snake Valley (Hood & Rush, 1965; Masbruch & Gardner, 2014). Based on the share of the area, the groundwater potentially to be pumped from the study area is 510 m^3 per day. Therefore, in this study, water pumping rates of 50% (255 m^3 per day), 100% (510 m^3 per day), and 200% (1020 m^3 per day) of the share of Lehman Creek watershed in total application were evaluated.

A 70-year period of the GSFLOW model, starting from 1980- 2049, ran prior to the start of the designed groundwater withdrawals; thus, the groundwater flow system was brought to a stable condition before the water was pumped. Starting from 2050, a 50-year groundwater withdrawal was introduced until year 2099. The consequent effects on the groundwater-flow system were assessed regarding the water-level changes.

Hydrologic modeling

In this study, instead of using the surface hydrologic PRMS model, the integrated hydrologic GSFLOW model was used to evaluate the hydrologic processes. Further assessments were performed on the water alternation in hydrologic components, regarding the water flux exchange between land surface and subsurface, and corresponding variations in the related storage.

The main water balance components in the entire integrated hydrologic system included the inflow of precipitation, and the outflows of evapotranspiration, streamflow, and groundwater boundary flow. The precipitation occurred as rainfall, snowfall, and a mix of the two forms. Evapotranspiration occurred throughout the year, reaching the highest rates during the summer especially when sufficient water was available in the soil zone. The streamflow was composed of surface runoff, soil interflow, and groundwater discharge. The surface runoff in the study area of Lehman Creek watershed was mostly Dunnian runoff, which occurs when soil is saturated. The soil interflow continually contributing to the streamflow, whether or not the soil was saturated or unsaturated. While it was the predominant water component of Lehman Creek, surface runoff could become significant and surpass the maximum soil interflow when great precipitation occurs The groundwater flow both contributed to the streamflow as baseflow and flows leave the system through the watershed boundary.

Several factors affect the water flux between surface water and groundwater: 1) the storage in soil zone, 2) the groundwater level relative to the soil-zone base, and 3) the vertical hydraulic conductivity. The determinant influence on the water flux varies with climate, topography, and subsurface properties (Markstrom et al., 2005). In this model, there were two places where water exchanges between surface and underground: 1) areal water-flux exchange

and 2) streamflow water exchange. The areal water exchange occurs through two forms. The first is gravity drainage, which is the water exceeds from the soil- zone and recharges the groundwater system through unsaturated or saturated zone. The second is the groundwater discharge, which is groundwater replenishes the soil-zone when groundwater level is higher than the soil-zone base. The streamflow water exchange occurs when there is a water level difference between the streamflow level and the groundwater level. Streamflow loses water when its water level is physically higher than the groundwater level and gains when it is lower.

The bias-corrected CMIP5 data resulting from the Research Question 1 (Chapter 2) represent both the retrospective and projected meteorologic conditions in the study area. They were used to drive the calibrated integrated model to evaluate the corresponding changes. Regarding the four climate change scenarios (i.e., RCP 2.6, 4.5, 6.0, and 8.5), there are results from 16, 19, 12, and 20 models corresponding to each scenario (Appendix A-1). As the total model run number was 67, and each model run from 2010 to 2099 on a daily basis took 4.095 hours, total running time for all 67 climate model results was 274.365 hours (11.43 days) using Windows 10 64-bit Operating System, Intel ® Core™ i7-4785T CPU @ 2.20 GHz, and 8.0 GB RAM.

4.6.2 **Results**

Integrated model calibration and validation

The GSFLOW model-calibration period was from 2003 to 2007 (water years), and the model calibration period was from 2008 to 2012 (water years). Because these are the longest continuous data available for streamflow, they were used to assess the hydraulic properties and model-simulation performance. The storativity, basedflow, and streamflow were evaluated in the following sections.

Storativity

Regarding aquifer storage properties, specific yield (S_y) and specific storage (S_s) are two parameters that determine the water storage feature in the unconfined aquifer and confined aquifer, respectively, as they were defined in the developed groundwater model. As summarized in Table 17 of each hydrostrategraphic unit, the specific yield for glacial deposits and alluvial deposits are 4E-2 and 3E-2, which are the principal formations of the unconfined aquifer; the specific storage for limestone and granite are 1.8E-1 and 1E-6, respectively, which were defined in the confined aquifer. The quartzite formation dominates the mountain upland from the deep level to land surface. Both specific yield and specific storage of the quartzite formation were defined and read by the MODFLOW program as this formation was defined both in unconfined aquifer in Layer 1 and confined aquifer in Layer 2, which are 2E-6 and 5E-7, respectively. Compared to values of selected rocks suggested by Heath (1983), the calibrated values of storage-related parameters are reasonable as they fell into the value ranges of each suggested rock.

Table 17

Comparisons of Storage-Related Parameters Between Model Calibration Estimations and Reference Values Selected for Each Hydrostrategraphic Unit in the MODFLOW Model (S_s = Specific Storage; S_y = Specific Yield, Dimensionless).

Hydrostrategraphic unit	S_s	S_y	Value Ranges of selected rocks (Heath 1983)	
Glacial deposits	NA(1E-5)	4E-2	Value range for Glacial Till	1E-7 to 0.3
Alluvial deposits	NA(1E-5)	3E-2	Value range for Silty, Loess, Silty Sand, Clean Sand, Gravel	1E-3 to 5E3
Quartzite	2E-6	5E-7	Value range for Igneous and Metamorphic Rock	1E-8 to 5
Limestone	1.8E-1	NA(1.8E-1)	Value range for Carbonate Rocks	1E-4 to 5E3
Granite (and shale)	1E-6	NA(1E-3)	Value range for Shale	1E-8 to 1E-4

Baseflow

The baseflow, which was estimated as the annual minimum daily streamflow in this study, was compared between observations and simulations (Figure 38). The calibrated model

simulation was able to capture the variation in wet years and dry years caused by above-average and below-average precipitation. In the comparison of the estimated baseflow between observation and model simulation, the high precipitation in water year 2005 resulted in high baseflow. This high baseflow receded annually until year 2011 when another wet year occurred. The 2011 flow recorded by the Lehman Creek gauging station was underestimated due to the high overland runoff, and some flow bypassed the gauging station (Prudic, 2012). Because the precipitation in 2011 was similar to the precipitation in 2005, the baseflow in 2011 is expected to be close to the baseflow value in 2005. Additionally, at the first year of model simulation, the baseflow estimation from the model simulation was underestimated compared to the estimation from observation records. This underestimation suggested the initial model condition was not well captured and simulated by the current model.

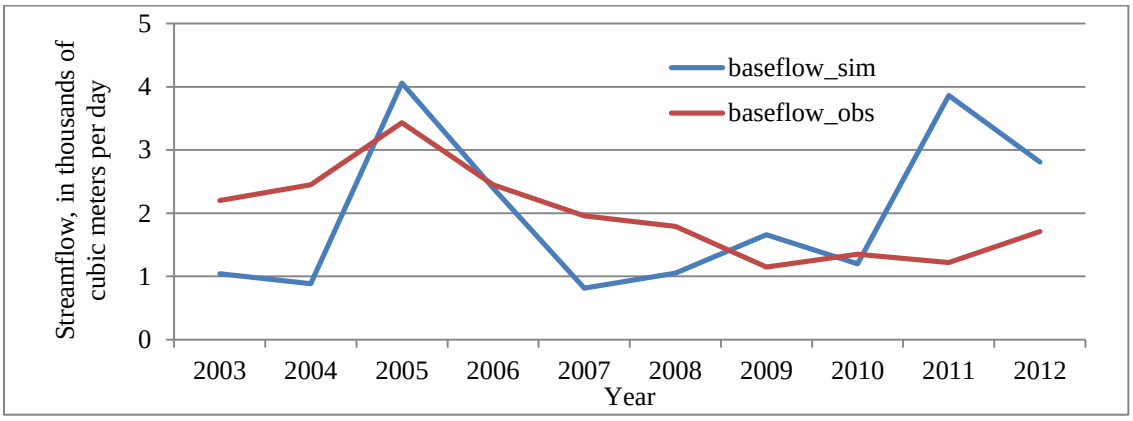

Figure 38. Baseflow Comparisons Between GSFLOW Model Simulations and Observations for Water Years 2003-2012, Estimated from the Annual Minimum Streamflow at the Gauging State of Lehman Creek.

Streamflow

Streamflow, as the critical evaluation variable available are in observation records of the study area, was used to evaluate the performance of the integrated model. The hydrographs resulted from the PRMS model and the GSFLOW model were compared with observations for both calibration and validation periods (Figure 39 a, b & c). On all evaluated annual, mean

monthly, and monthly mean scales, the streamflow simulation results from PRMS model and GSFLOW model are quite similar with slight differences in temporal distribution of mean monthly values. Compared to the PRMS model simulation results, the mean monthly streamflow resulting from the GSFLOW model tend to fit more closely with observations during months before peak and after streamflow peaks (Figure 39b).

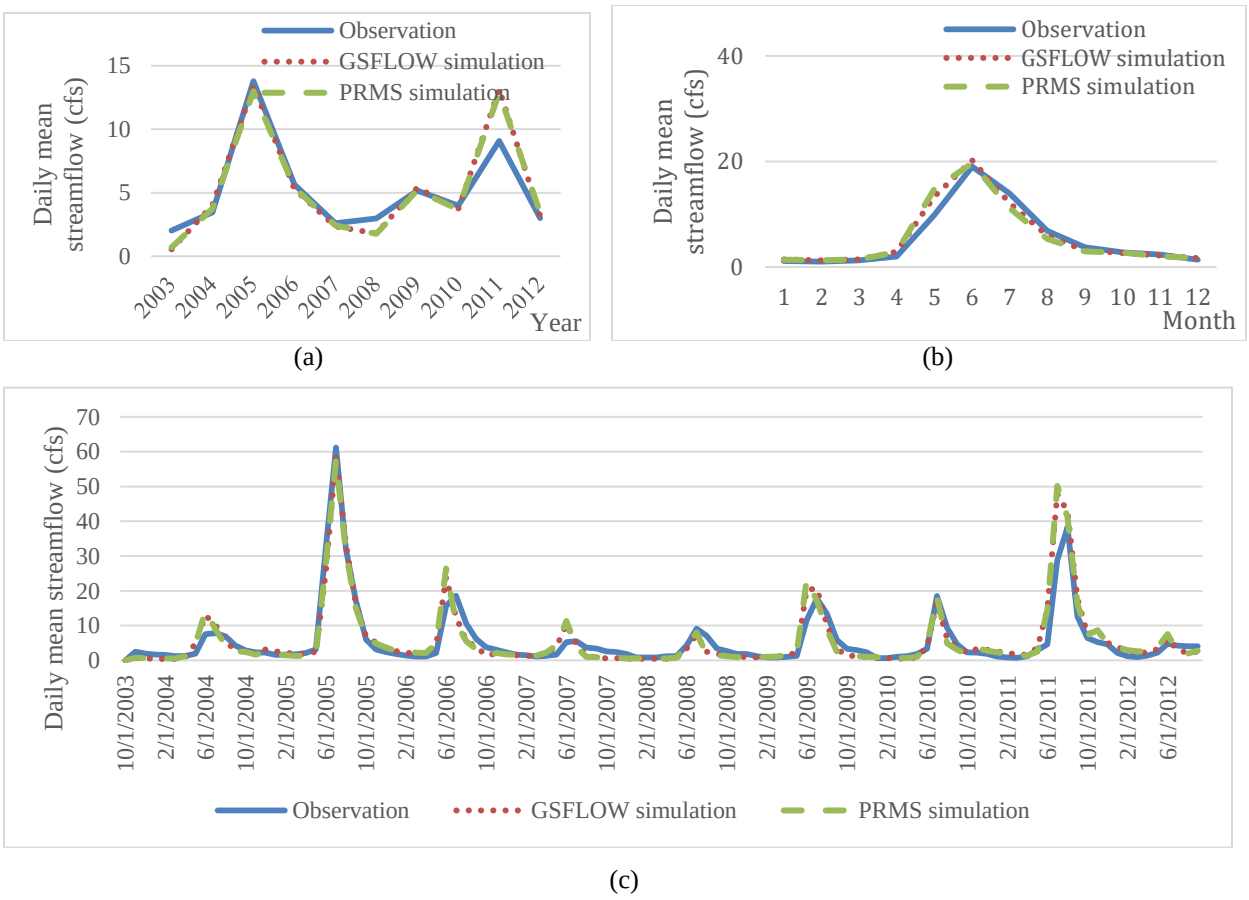

Figure 39. Streamflow Results Comparisons of GSFLOW Model Simulations, PRMS Simulations, and Observations on: A) Annual Scale, B) Mean Monthly Scale, and C) Monthly Mean Scale.

In addition to the hydrograph comparisons, the model evaluation indexes were calculated and compared to provide a quantitative evaluation of the performances of these two models (Table 18). For calibration period, the performance of the PRMS model was evaluated as good based on PBIAS, good based on R^2, and very good based on NSE, suggested by Moriasi et al.'s

(2015) watershed-scale model evaluation criteria. Similarly, for the validation period, the performance of the PRMS model was evaluate as *very good* based on PBIAS, *satisfactory* based on R^2, and *satisfactory* based on NSE. Regarding the GSFLOW model performance, for the calibration period, it was evaluated as *very good* based on PBIAS, *good* based on R^2, and *good* based on NSE; for the validation period, it was evaluated as *very good* based on PBIAS, *good* based on R^2, and *good* based on NSE.

Table 18

Statistical Comparisons between PRMS Model Simulation and GSFLOW Model Simulation Regarding the Observed and Simulated Daily Streamflow at Lehman Creek for Calibration (2003-2007, Water Years) and Validation Period (2008-2012, Water Years).

Index	Calibration Period		Validation Period	
	PRMS	GSFLOW	PRMS	GSFLOW
PBIAS (%)	-9.8	-0.19	2.0	-0.09
R^2	0.85	0.76	0.69	0.81
NSE	0.82	0.74	0.64	0.75

Sensitivity analysis

Sensitivity analysis was performed on the parameters determining the hydraulic properties. The parameters include horizontal and vertical hydraulic conductivity, specific yield and specific storage for each hydrostrategraphic unit, and streambed conductivity for each stream segment. The evaluation indexes of RMSE, NSE, R^2, and PBIAS were calculated by comparing observations and model simulations resulting from varying parameters. Results showed that, by multiplying the parameters with values ranging from 0.2 to 10, the calculated values of RMSE, NSE, R^2, and PBIAS varied between 6.21 to 6.31, 0.73 to 0.74, 0.75 to 0.76, and -20.4% to -17.3%, respectively (Appendix A-3).

The sensitivity analysis results show the streambed conductivity for each stream segment is not sensitive to the GSFLOW streamflow simulations, as indicated by lack of substantial variation anywhere except the last stream segment, i.e., segment 11, right before the watershed

outlet, overlaying the alluvial deposits and karst-limestone (Appendix A-3). By multiplying a coefficient of 10, the calculated indicator values for this streamflow segment have -40% (NSE), -13% (PBIAS), -34% (R^2), and 45% (RMSE) differences from the values resulting from the calibrated parameters, which indicates substantial reduction in the model's performance.

The SA results of the indicators for specific yield, specific storage, horizontal hydraulic conductivity, and vertical hydraulic conductivity in each defined hydrostrategraphic unit, are shown in the Figure 40. As the figure shows, in all indicator results, the specific yield of glacial deposits, the horizontal hydraulic conductivity of glacial deposits, and the vertical hydraulic conductivity of karst-limestone were the most sensitive parameters, as the results changed when these parameters changed. Variations of more than 5% were found in resulting outcomes when comparing to the calibrated model results.

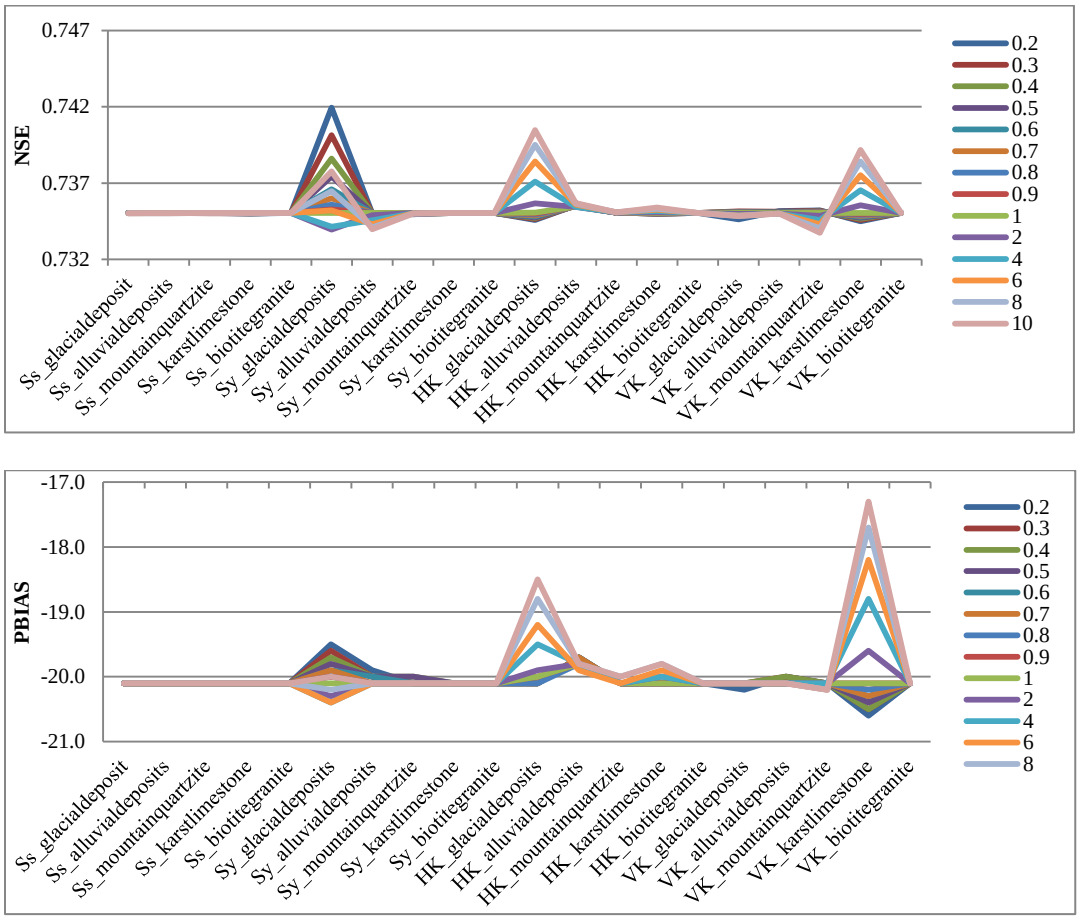

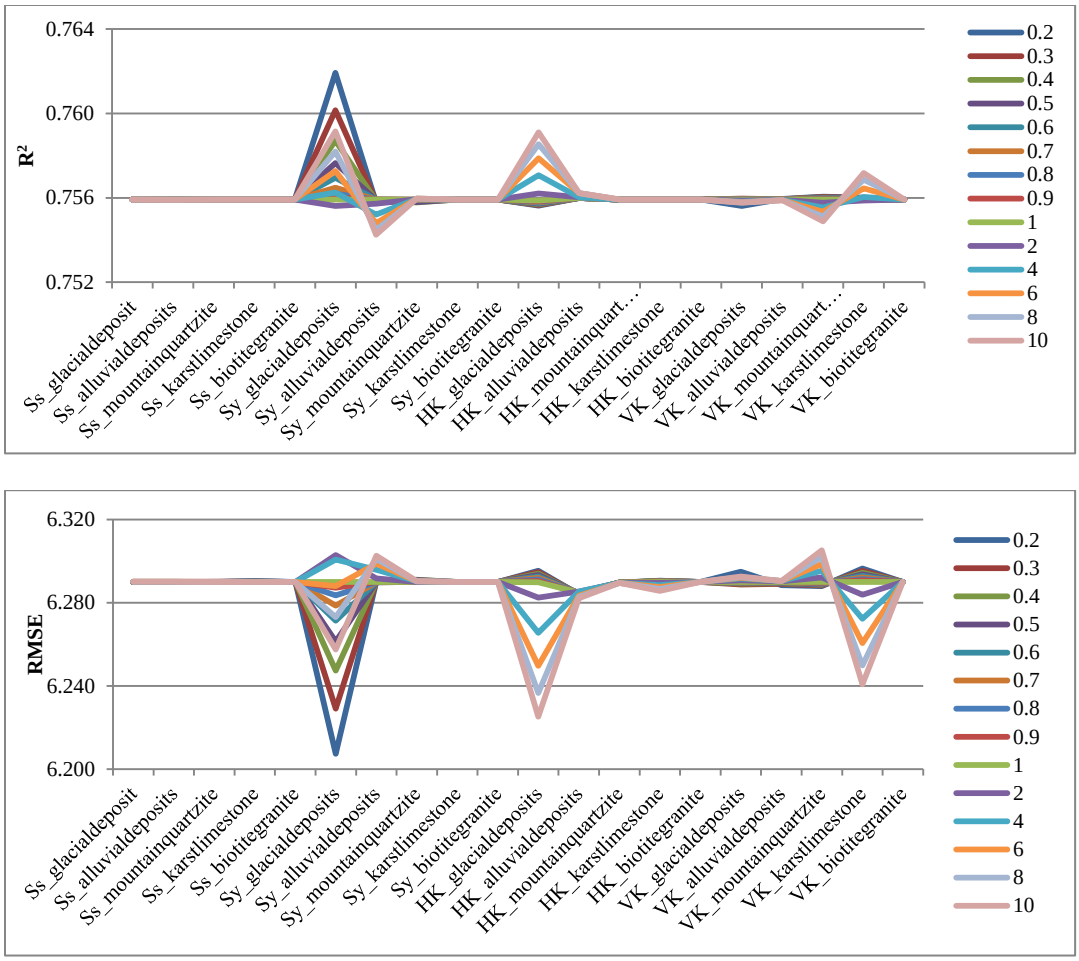

Figure 40. Results of a Sensitivity Analysis for the Hydraulic Conductivity of Each Hydrostrategraphic Unit Influencing the Transient-State Model Results, by Nash-Sutcliff Coefficient (NSE), Percentage of Bias (PBIAS), Square of Correlation (R^2), and Root Mean Square Error (RMSE) (HK = Horizontal Hydraulic Conductivity; VK= Vertical Hydraulic Conductivity).

GSFLOW simulation

Well pumping influences on the local water system

In order to evaluate the responses of the water resource system to the water pumping, a designed pumping rate proportional to the total water application in the Snake Valley was applied to the groundwater-flow system. On the basis of area ratio taken in the entire Snake Valley, different water pumping rates of 50% (255 m^3/d), 100% (510 m^3/d), and 100% (1020 m^3/d) were used as the external stresses to the groundwater system. Water level responses at the

pumping location and adjacent areas were evaluated by the groundwater-level changes, which were the water-level differences comparing to groundwater-level at the water-pumping starting time, especially at the location of the assumptive pumping location (column 86, row 11). As the Figure 41 indicated, the water-level drawdown increases tremendously with the water pumping increases as the water drawdown get to 5.3 m by the 50% of the designed withdrawal, 11.7 m by the 100% of the designed withdrawal, and 24.0 m by the 200% of the designed withdrawal by the end of 50-year continuous groundwater withdrawal.

Comparing the water-level drawdown among the neighboring grids, the water-level drawdown increased over the pumping time and showed non-linear increases with the increase in the water withdrawal (Table 19). The largest water drawdown occurred for the largest pumping rate (i.e., 200% of designed pumping rate), reaching to 0.46 m by the end of the 50-year simulation period. Additionally, the results showed that at the lower groundwater withdrawal (50% of designed pumping rate, 255 m^3/s), the groundwater drawdown is negligible (i.e., 7E-5 meter).

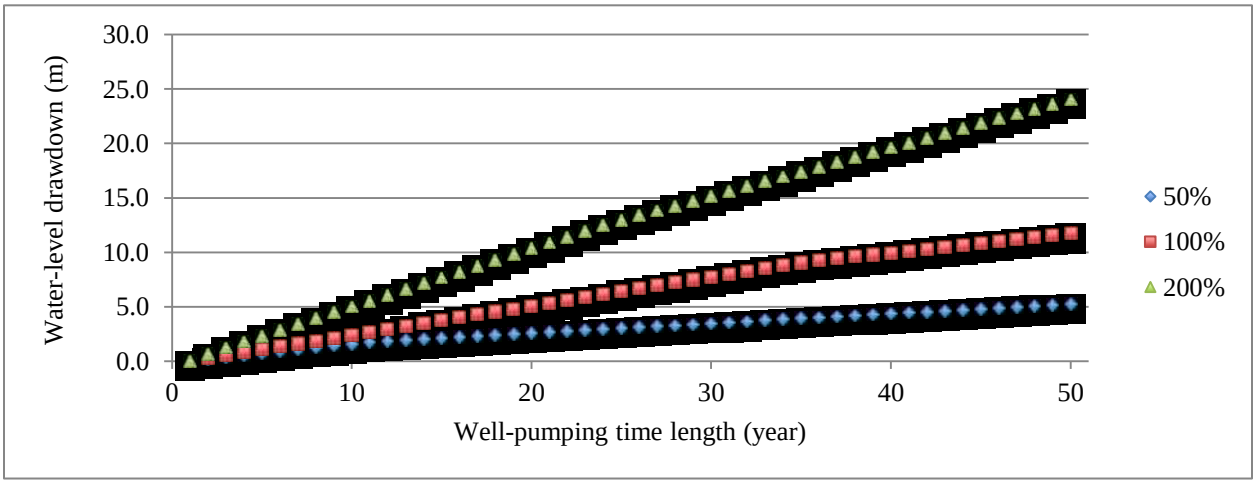

Figure 41. Results of Water-Level Drawdown with Different Pumping Rates, I.E., 50%, 100%, and 200% at the Pumping Location – South of Downstream Lehman Creek Watershed (Column 86, Row 11, Layer 2), Reported Annually with 50-Year Withdrawal.

Table 19

Results of Water-Level Drawdown at Simulation Cells Surround the Assumptive Pumping Location at Different Pumping Rates, i.e., 50%, 100% , and 200% of the Design Rate, Reported Annually with 50-Year Withdrawal.

	Left (85,11,2)			Right (87,11,2)		
	50%	100%	200%	50%	100%	200%
1	0	0	0	0	0	0
2	0	0	1E-05	0	0	1E-05
3	0	1E-05	1E-05	1E-05	1E-05	1E-05
4	1E-05	1E-05	1E-05	1E-05	1E-05	1E-05
5	1E-05	1E-05	2E-05	1E-05	1E-05	2E-05
6	1E-05	1E-05	2E-05	1E-05	1E-05	2E-05
7	1E-05	1E-05	2E-05	1E-05	1E-05	2E-05
8	1E-05	1E-05	2E-05	1E-05	1E-05	3E-05
9	1E-05	1E-05	3E-05	1E-05	2E-05	3E-05
10	1E-05	2E-05	3E-05	1E-05	2E-05	3E-05
11	1E-05	2E-05	3E-05	1E-05	2E-05	3E-05
12	1E-05	2E-05	4E-05	1E-05	2E-05	4E-05
13	1E-05	2E-05	4E-05	1E-05	2E-05	4E-05
14	1E-05	2E-05	4E-05	1E-05	2E-05	4E-05
15	1E-05	2E-05	5E-05	2E-05	2E-05	5E-05
16	1E-05	2E-05	5E-05	2E-05	3E-05	5E-05
17	1E-05	3E-05	5E-05	2E-05	3E-05	5E-05
18	2E-05	3E-05	5E-05	2E-05	3E-05	6E-05
19	2E-05	3E-05	6E-05	2E-05	3E-05	6E-05
20	2E-05	3E-05	6E-05	2E-05	3E-05	6E-05
21	2E-05	3E-05	6E-05	2E-05	3E-05	6E-05
22	2E-05	3E-05	7E-05	2E-05	3E-05	7E-05
23	2E-05	4E-05	7E-05	2E-05	4E-05	7E-05
24	2E-05	4E-05	7E-05	2E-05	4E-05	7E-05
25	2E-05	4E-05	7E-05	2E-05	4E-05	8E-05
26	2E-05	4E-05	8E-05	2E-05	4E-05	8E-05
27	2E-05	4E-05	8E-05	2E-05	4E-05	8E-05
28	2E-05	4E-05	8E-05	2E-05	4E-05	8E-05
29	2E-05	4E-05	8E-05	2E-05	4E-05	9E-05
30	2E-05	5E-05	9E-05	2E-05	5E-05	9E-05
31	2E-05	5E-05	9E-05	2E-05	5E-05	9E-05
32	2E-05	5E-05	9E-05	2E-05	5E-05	9E-05
33	2E-05	5E-05	9E-05	2E-05	5E-05	1E-04
34	2E-05	5E-05	1E-04	2E-05	5E-05	1E-04
35	2E-05	5E-05	1E-04	3E-05	5E-05	1E-04
36	2E-05	5E-05	1E-04	3E-05	5E-05	1E-04
37	3E-05	5E-05	1E-04	3E-05	6E-05	1E-04
38	3E-05	6E-05	1.10E-04	3E-05	6E-05	1.10E-04
39	3E-05	6E-05	1.10E-04	3E-05	6E-05	1.10E-04
40	3E-05	6E-05	1.10E-04	3E-05	6E-05	1.10E-04
41	3E-05	6E-05	1.10E-04	3E-05	6E-05	1.10E-04
42	3E-05	6E-05	1.20E-04	3E-05	6E-05	1.20E-04
43	3E-05	6E-05	1.20E-04	3E-05	6E-05	1.20E-04
44	3E-05	6E-05	1.20E-04	3E-05	6E-05	1.20E-04
45	3E-05	6E-05	1.92E-02	3E-05	6E-05	1.20E-04
46	3E-05	6E-05	1.08E-01	3E-05	6E-05	8.65E-02
47	3E-05	6E-05	1.97E-01	3E-05	7E-05	1.76E-01
48	3E-05	7E-05	2.87E-01	3E-05	7E-05	2.65E-01
49	3E-05	7E-05	3.76E-01	3E-05	7E-05	3.54E-01

50	3E-05	7E-05	4.65E-01	3E-05	7E-05	4.43E-01
	Front (86,10,2)			Back (86,12,2)		
	50%	100%	200%	50%	100%	200%
1	0	0	0	0	0	0
2	0	0	0	0	0	1E-05
3	0	0	1E-05	0	1E-05	1E-05
4	0	1E-05	1E-05	1E-05	1E-05	1E-05
5	0	1E-05	1E-05	1E-05	1E-05	2E-05
6	1E-05	1E-05	2E-05	1E-05	1E-05	2E-05
7	1E-05	1E-05	2E-05	1E-05	1E-05	2E-05
8	1E-05	1E-05	2E-05	1E-05	1E-05	2E-05
9	1E-05	1E-05	3E-05	1E-05	1E-05	3E-05
10	1E-05	1E-05	3E-05	1E-05	2E-05	3E-05
11	1E-05	2E-05	3E-05	1E-05	2E-05	3E-05
12	1E-05	2E-05	3E-05	1E-05	2E-05	4E-05
13	1E-05	2E-05	4E-05	1E-05	2E-05	4E-05
14	1E-05	2E-05	4E-05	1E-05	2E-05	4E-05
15	1E-05	2E-05	4E-05	1E-05	2E-05	5E-05
16	1E-05	2E-05	5E-05	2E-05	3E-05	5E-05
17	1E-05	2E-05	5E-05	2E-05	3E-05	5E-05
18	1E-05	3E-05	5E-05	2E-05	3E-05	5E-05
19	1E-05	3E-05	6E-05	2E-05	3E-05	6E-05
20	2E-05	3E-05	6E-05	2E-05	3E-05	6E-05
21	2E-05	3E-05	6E-05	2E-05	3E-05	6E-05
22	2E-05	3E-05	6E-05	2E-05	3E-05	7E-05
23	2E-05	3E-05	7E-05	2E-05	4E-05	7E-05
24	2E-05	4E-05	7E-05	2E-05	4E-05	7E-05
25	2E-05	4E-05	7E-05	2E-05	4E-05	7E-05
26	2E-05	4E-05	8E-05	2E-05	4E-05	8E-05
27	2E-05	4E-05	8E-05	2E-05	4E-05	8E-05
28	2E-05	4E-05	8E-05	2E-05	4E-05	8E-05
29	2E-05	4E-05	8E-05	2E-05	4E-05	8E-05
30	2E-05	4E-05	9E-05	2E-05	5E-05	9E-05
31	2E-05	5E-05	9E-05	2E-05	5E-05	9E-05
32	2E-05	5E-05	9E-05	2E-05	5E-05	9E-05
33	2E-05	5E-05	9E-05	2E-05	5E-05	9E-05
34	2E-05	5E-05	1E-04	2E-05	5E-05	1E-04
35	2E-05	5E-05	1E-04	2E-05	5E-05	1E-04
36	2E-05	5E-05	1E-04	3E-05	5E-05	1E-04
37	2E-05	5E-05	1E-04	3E-05	6E-05	1E-04
38	2E-05	5E-05	1.10E-04	3E-05	6E-05	1.10E-04
39	2E-05	6E-05	1.10E-04	3E-05	6E-05	1.10E-04
40	3E-05	6E-05	1.10E-04	3E-05	6E-05	1.10E-04
41	3E-05	6E-05	1.10E-04	3E-05	6E-05	1.10E-04
42	3E-05	6E-05	1.10E-04	3E-05	6E-05	1.20E-04
43	3E-05	6E-05	1.20E-04	3E-05	6E-05	1.20E-04
44	3E-05	6E-05	1.20E-04	3E-05	6E-05	1.20E-04
45	3E-05	6E-05	1.20E-04	3E-05	6E-05	1.11E-02
46	3E-05	6E-05	8.70E-02	3E-05	6E-05	1.00E-01
47	3E-05	6E-05	1.76E-01	3E-05	6E-05	1.89E-01
48	3E-05	6E-05	2.65E-01	3E-05	7E-05	2.78E-01
49	3E-05	7E-05	3.54E-01	3E-05	7E-05	3.68E-01
50	3E-05	7E-05	4.43E-01	3E-05	7E-05	4.57E-01

CMIP5-driven GSFLOW model simulation

Streamflow – mean annual changes

The streamflow simulations, driven by bias-corrected CMIP5 data, were analyzed using the simulation differences in the future periods (Period 1, Period 2, and Period 3) based on the baseline period, for each of the emission scenarios. It used the same methods and scales that were used for the PRMS model simulations for easier comparisons with the PRMS simulation results (Figure 42). On the basis of baseline period, the absolute changes and percentage changes of mean annual streamflow simulations over three future time periods were compared. Results showed substantial uncertainties regarding the changing trends over time periods and among the four potential climate change scenarios. From Periods 1, 2, and 3, the mean annual streamflow

- under RCP 2.6, increases 5.4%, increases 2.5%, and increases 1.0%, respectively;
- under RCP 4.5, decreases 8.7%, decreases 5.2%, and decreases 6.8%, respectively;
- under RCP 6.0, it decrease 7.8%, decrease 3.9%, and increase 5.9%, respectively;
- under RCP 8.5, it increases 0.7%, decreases 7.0%, and decreases 8.3%, respectively.

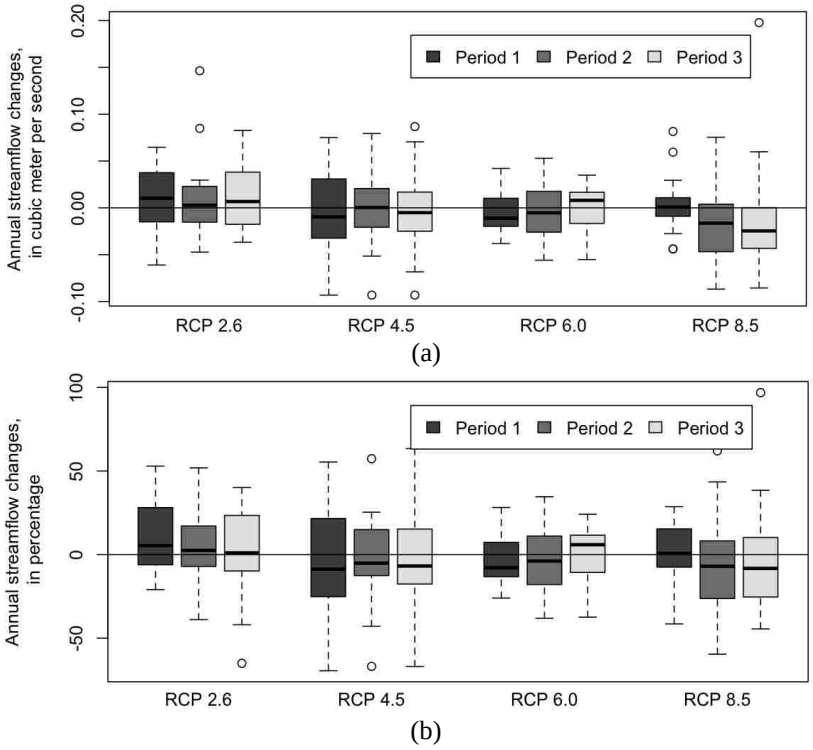

Figure 42. Comparisons of the Annual Streamflow Change Simulated by GSFLOW Model, Assessed at: (A) Absolute and (B) Percentage among Four Climate Change Scenarios: RCP 2.6, RCP 4.5, RCP 6.0, and RCP 8.5, during Three Future Periods of 2011-2039, 2040-2069, and 2070-2099.

Streamflow – mean monthly changes

Changes in the simulated mean monthly streamflow, with regard to the baseline period, were compared for different scenarios during the three future periods (Figure 43& Figure 44). Variations among the multiple projections are presented by means of box plots. Positive values indicate streamflow increases, and negative values signify decreases. Results similar to the results from the PRMS simulation were found: There was a distinguishing time point between May and June that showed an increase of mean monthly streamflow during the winter (December to May) and a decrease during the summer (June to November).

The changes in percentage were calculated, based on the absolute difference with baseline scenarios (Figure 45 & Figure 46). Evaluated by median values (Table 20), the largest increases occurred were during April and May, which reached to 27.5% - 129.4% and 26.6% -

117.2 %, respectively; the largest decreases occurred during July and August, which reached 23.1% - 85% and 221.% - 85 %, respectively. Different from the simulation results of the CMIP5-driven PRMS modeling, the median increases in April and May were 27.8%-145.0% and 26.4%-114.6%; the median decreases in July and August were 18.0% - 58.1% and 15.2 % and 43.6%. This means the results from the GSFLOW model simulation have larger changes in mean monthly flow than the results from the PRMS model simulations. Additionally, during September and October, immediately after the largest mean monthly streamflow decreases occurred in July and August, the changes in streamflow are still higher than results from the PRMS model simulations. The streamflow change decreases during September and October are 23.5% - 74.4% and 7.1% - 35.5%, respectively, resulting from the GSFLOW model simulations; they were 6.3% - 32% and 0.4% - 28.0%, resulting from the PRMS model simulations. (Table 10).

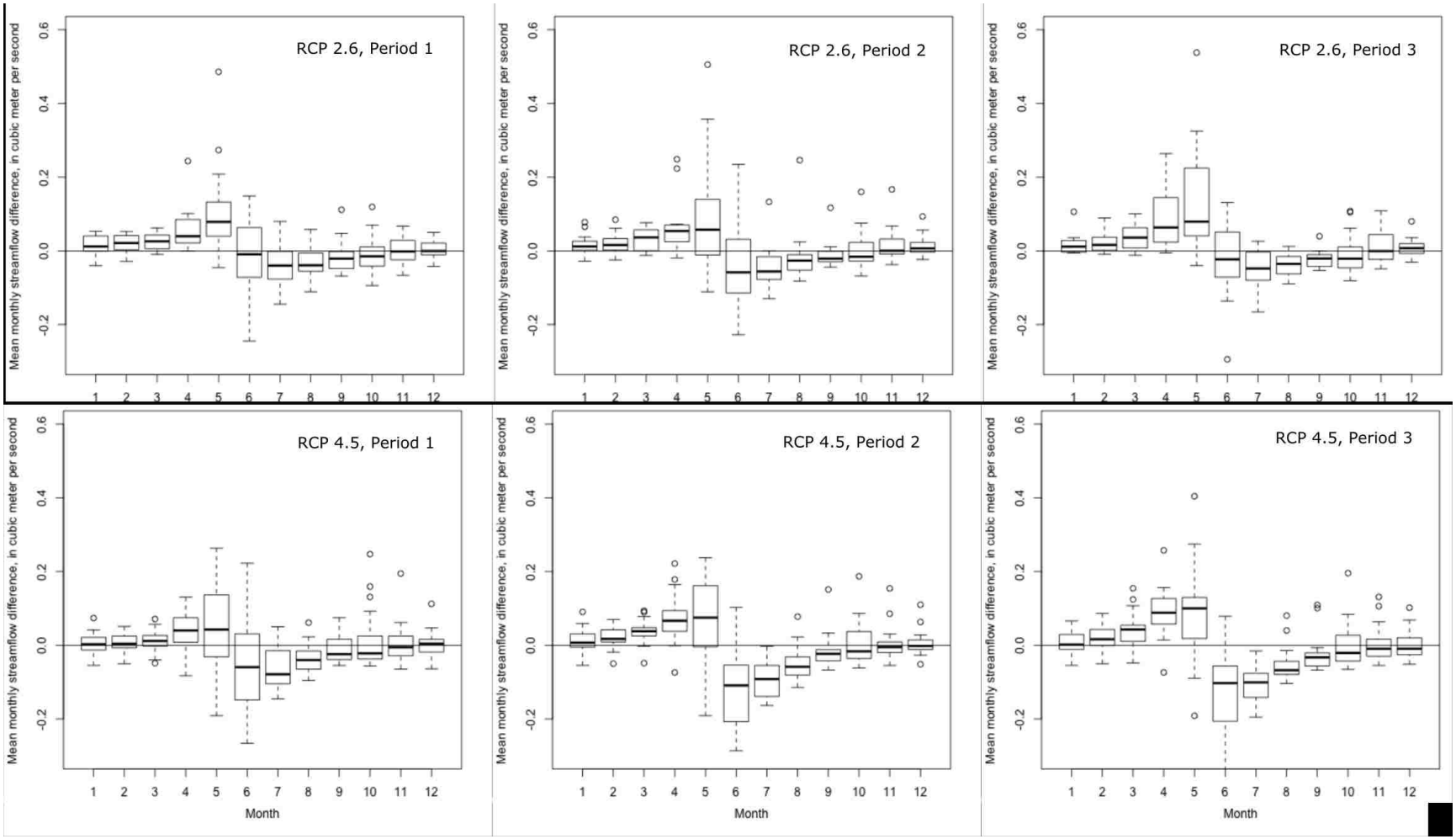

Figure 43. Mean Monthly Streamflow Changes on the Basis of Baseline Period (1981-2010), Resulting fromthe GSFLOW Model Simulation. Three Periods were Compared: Period 1 (2011-2039), Period 2 (2040-2069), and Period 3 (2070-2099), under All Climate Change Scenarios of RCP 2.6 and RCP 4.5.

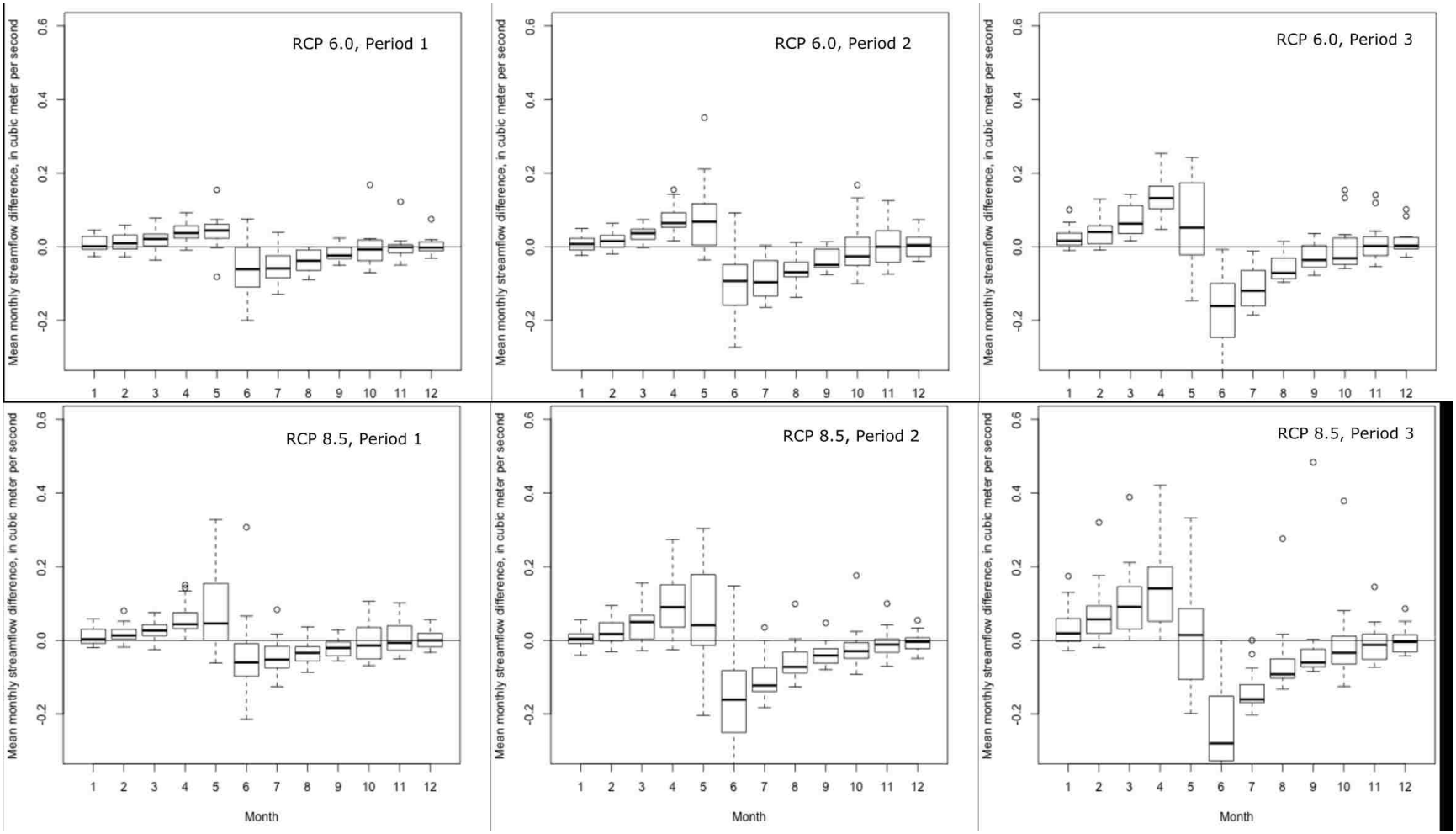

Figure 44. Mean Monthly Streamflow Changes on the Basis of Baseline Period (1981-2010), Resulting from the GSFLOW Model Simulation. Three Periods were Compared: Period 1 (2011-2039), Period 2 (2040-2069), and Period 3 (2070-2099), under All Climate Change Scenarios of RCP 6.0 and RCP 8.5.

.

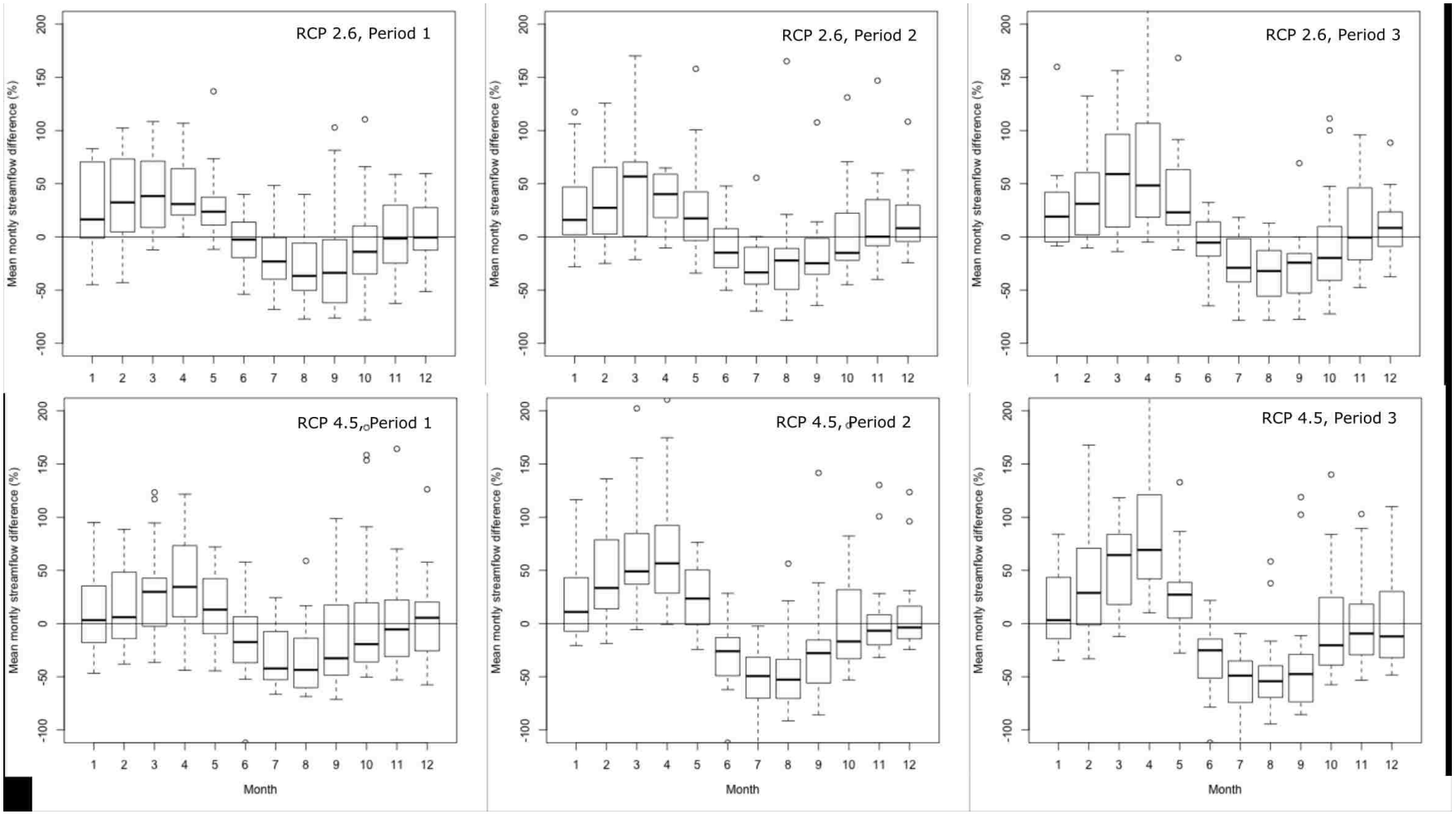

Figure 45. Mean Monthly Streamflow Percentage Changes on the Basis of Baseline Period (1981-2010), Resulting from the GSFLOW Model Simulation. Three Periods were Compared: Period 1 (2011-2039), Period 2 (2040-2069), and Period 3 (2070-2099), under All Climate Change Scenarios of RCP 2.6 and RCP 4.5.

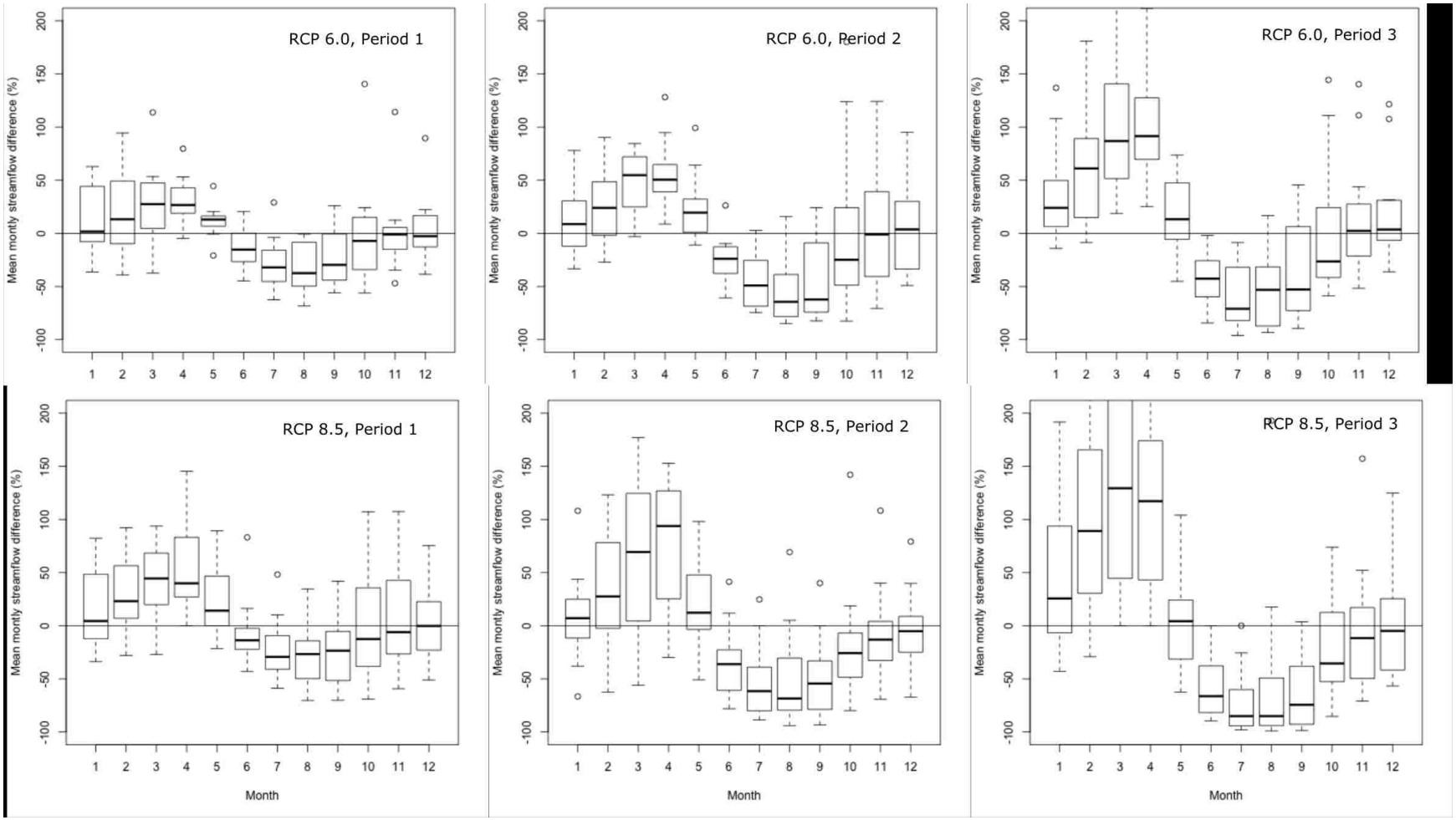

Figure 46. Mean Monthly Streamflow Percentage Changes on the Basis of Baseline Period (1981-2010), Resulting from the GSFLOW Model Simulation. Three Periods were compared: Period 1 (2011-2039), Period 2 (2040-2069), and Period 3 (2070-2099), under All Climate Change Scenarios of RCP 6.0 and RCP 8.5.

Table 20.

The GSFLOWS Model Results from the CMIP5-Driven Simulation: Median Values of Mean Monthly Streamflow Changes based on the Baseline Period for Each RCP, in Percentage (%).

Emission scenario	Time period	Jan.	Feb.	Mar.	Apr.	May.	Jun.	Jul.	Aug.	Sep.	Oct.	Nov.	Dec.
RCP 2.6	Period 1	16.5	32.4	38.4	30.9	23.7	-2.5	-23.1	-36.6	-33.8	-14.0	-1.5	-0.5
	Period 2	16.0	27.3	56.8	40.2	17.4	-14.8	-33.4	-22.1	-24.8	-15.0	0.3	8.2
	Period 3	19.1	31.2	59.1	48.4	23.1	-5.4	-29.0	-32.1	-24.2	-19.8	-0.6	8.5
RCP 4.5	Period 1	3.2	6.0	29.8	34.5	13.1	-17.3	-42.2	-43.5	-32.6	-19.3	-5.4	5.5
	Period 2	11.0	33.5	49.1	56.6	23.5	-26.0	-49.3	-52.7	-27.8	-16.8	-6.7	-3.7
	Period 3	3.2	28.9	64.4	69.2	27.2	-25.1	-48.9	-54.2	-47.5	-20.4	-9.3	-12.0
RCP 6.0	Period 1	1.7	13.2	27.5	26.6	13.0	-15.3	-32.1	-37.4	-29.7	-7.1	-1.0	-2.7
	Period 2	8.7	24.0	54.7	50.5	19.5	-23.9	-49.1	-64.4	-62.3	-24.9	-1.0	3.7
	Period 3	24.0	61.1	86.8	91.5	13.3	-42.6	-71.0	-53.2	-52.8	-26.4	2.3	3.6
RCP 8.5	Period 1	4.5	23.1	44.5	39.9	14.1	-13.7	-29.3	-26.7	-23.5	-12.5	-6.0	-0.2
	Period 2	7.1	27.5	69.4	93.8	12.2	-36.2	-61.6	-68.5	-54.4	-25.8	-13.1	-5.1
	Period 3	25.7	89.1	129.4	117.2	4.3	-66.3	-85.0	-85.0	-74.4	-35.5	-11.7	-4.9

Streamflow – Winter-Spring Center of Volume (WSCV) dates

The date changes for WSCV were analyzed among the various projections and scenarios on the basis of the baseline period (Figure 47). Positive values indicate a time lag when the WSCV date was late relative to the WSCV in the baseline period. Negative values mean earlier occurrences of the WSCV date relative to that in the baseline period. Similar to the results from the CMIP5-driven PRMS model simulation, the WSCV date change results showed negative values generally during all the periods and emission scenarios, indicating an earlier occurrence of snowmelt.

The same as results from the PRMS model simulation, the streamflow shifted earlier. Median changes for the WSCV date shifts over four climate change scenarios showed a range from -3.7 to -8.1 days, -9.6 to -13.4 days, and -9.3 to -26.3 days during Period 1, 2, and 3, respectively, comparing to 2.9 to -9.1 days, -10.1 to -16.1 days, and -10.1 to -30 days during the corresponding period resulting from the PRMS model simulation. This means the GSFLOW

model simulation show milder changes regarding the WSCV date, compared to the PRMS model. Moreover, among all three time periods, the increasing tendency over the potential climate change scenarios in Period 3 was more apparent than in Period 1 and 2.

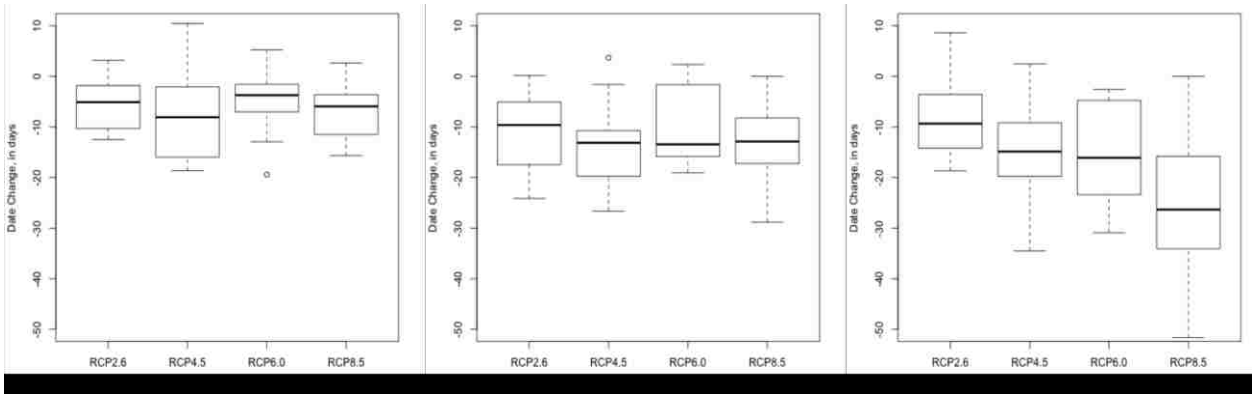

Figure 47. Comparisons of Winter-Spring Center of Volume (WSCV) Date-Shifting among Four Climate Change Scenarios: RCP 2.6, RCP 4.5, RCP 6.0, and RCP 8.5, during Three Future Periods: 2011 to 2039 (Period 1), 2040 to 2069 (Period 2), and 2070 to 2099 (Period 2). The WSCV Values Calculated using GSFLOW Streamflow Simulations, and the Box Plot Represents Results from Multiple Climate Models of Each Scenario.

Water balance

The main water balance components in the entire integrated hydrologic system included the inflow of precipitation, and the outflows of evapotranspiration, streamflow, and groundwater boundary flow. By comparisons of three periods, the future variations of the principal water balance components over the time period of 2011-2099 were plotted using box plots in Figure 48. For each period, the mean annual value was calculated over the 29/30 years for each climate change model, and the box plot represented the value distribution of different climate change models under each potential climate change scenario (Figure 48).

The results showed gradual increases in annual precipitation and annual evapotranspiration over three future periods (Figure 48). The increasing precipitation results were consistent with the climate change evaluation from the Research Objective 1. The increasing evapotranspiration results were reasonable as the temperatures keep rising as the results from Research Objective 1 indicated.

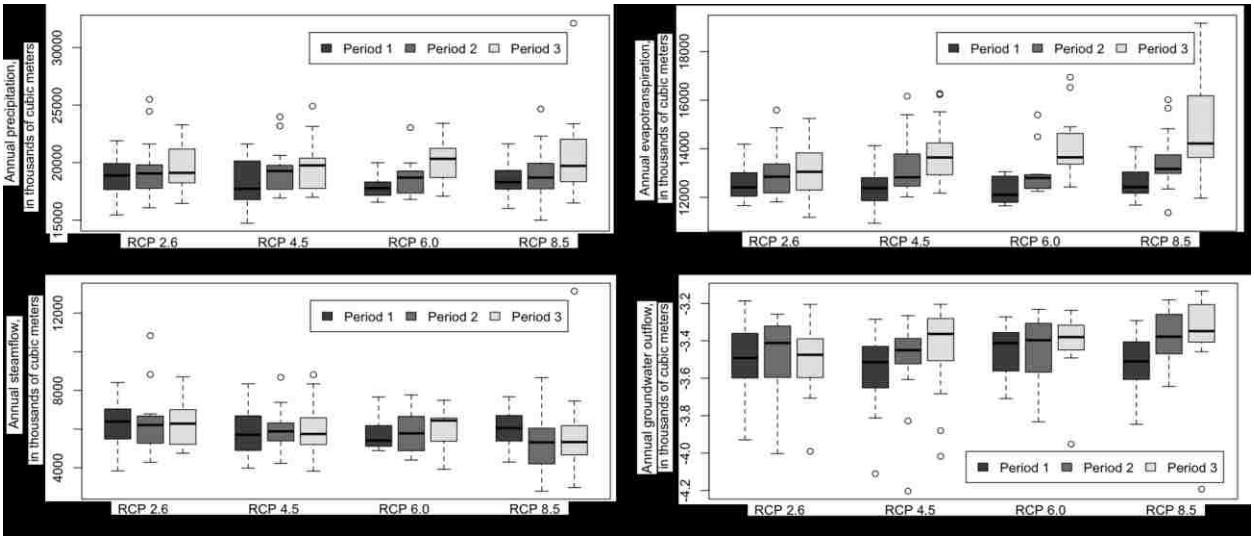

Figure 48. Comparisons of: (A) Annual Precipitation, (B) Evapotranspiration, (C) Streamflow, and (D) Groundwater Outflow over the Three Future Periods of 2011-2039, 2040-2069, and 2070-2099 for Four Climate Change Scenarios: RCP 2.6, RCP 4.5, RCP 6.0, and RCP 8.5.

Water exchange

In this study, two forms of surface-subsurface water interactions were evaluated: 1) areal water flux between the soil zone and groundwater-flow system, which used variables of *net_sz2gw* and *basingw2sz*; the streamflow water interaction with the groundwater-flow system, which were *stream_leakage* and *gwflow2strms* (Markstrom et al., 2005). The *net_sz2gw* is the gravity drainage from the soil zone to the unsaturated/saturated zone, indicating the actual water volume leaves the soil zone of the surface hydrology and enters the groundwater-flow system. The *basin_gw2sz* is the groundwater discharge from saturated zone to the soil zone, representing the areal water recharge to the soil zone of the surface hydrology. The *stream_leakage* is the streamflow leakage to the groundwater-flow system, and the *gwflow2strms* is the streamflow recharge from the groundwater-flow system. The results of the changes in water exchange were presented on annual scale, which were the mean annual water volume averaged over each analysis time period, e.g., Period 1, 2, and 3 (Figure 48 & Figure 49). Multiple climate change models were considered and represented by box plots under each potential climate change

scenario. As the figures showed, positive values in changes mean increase and negative values in changes mean decrease, while the negative values in *stream_leakage* stream water gaining.

As shown in Figure 49, the areal water interaction increased comparing to the baseline period in both groundwater recharge from the soil zone (Figure 49a) and groundwater discharge to soil zone (Figure 49b), as the resulting water-change values were positive. However, these increasing changes showed a declining trend over three time periods in a long term, which was especially noticeable under climate change scenario RCP 8.5. Apart from the changing trend over the time periods, the results showed that the groundwater recharge from the soil zone (Figure 49a) were higher than and groundwater discharge to soil zone (Figure 49b), which means in the long-term future, more water would enter the groundwater-flow system from soil zone than the water leave to soil zone.

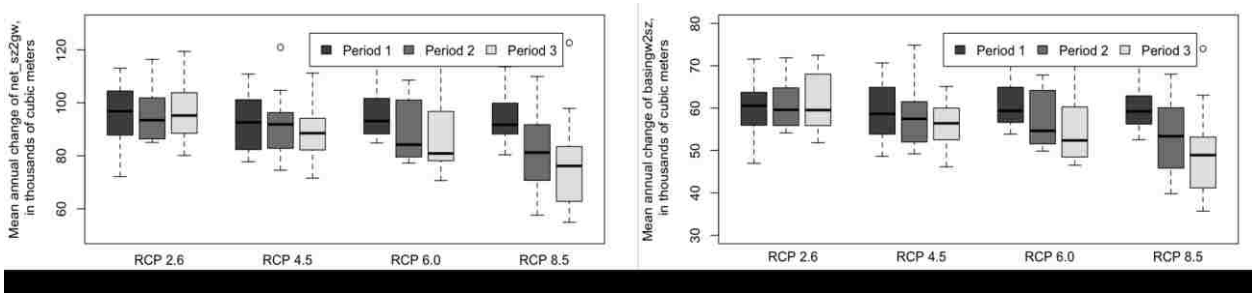

Figure 49. Comparisons of Changes in Areal Water Interactions using Variables of Net_Sz2gw and Basingw2sz, over the Three Future Periods of 2011-2039 (Period 1), 2040-2069 (Period 2), and 2070-2099 (Period 3) for Four Climate Change Scenarios: RCP 2.6, RCP 4.5, RCP 6.0, and RCP 8.5. (A) net_Sz2gw, Water Volume from Soil Zone to Groundwater System; (B) basingw2sz, Water Volume from Groundwater System to Soil Zone.

The stream-water interactions were shown in Figure 50. While the negative values shown in changes of stream_leakage mean water gaining, both groundwater recharge from the streams (Figure 50a) and groundwater discharge to the streams (Figure 50b) increased, comparing to the baseline period. Similar to the results from the area water-interaction change, there was a declining trend in the increases in the water flux between streams and the groundwater.

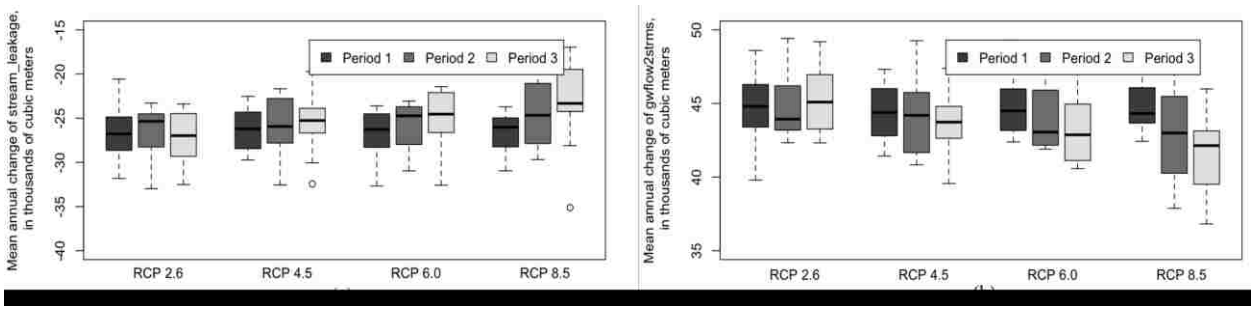

Figure 50. Comparisons of Changes in Stream Water Interactions Using Variables of *stream_leakage* and *gwflow2strms*, over the Three Future Periods of 2011-2039 (Period 1), 2040-2069 (Period 2), and 2070-2099 (Period 3) for Four Climate Change Scenarios: RCP 2.6, RCP 4.5, RCP 6.0, and RCP 8.5. (A) *stream_leakage*, Water Volume from Streams to Groundwater System; (B) gwflow2strms, Water Volume from Groundwater System to Streams. Negative Sign in *stream_leakage* Means Stream Water Gaining.

4.6.3 **Conclusions and Discussion**

In this study, a GSFLOW model was developed for the Lehman Creek study area. The GSFLOW model coupled the developed surface hydrologic PRMS model and groundwater-flow MODFLOW model. Detailed coupling procedures were implemented regarding the module changes in the streamflow routing process, MODFLOW package change, and related parameter modifications. Furthermore, the GSFLOW model was further implemented in groundwater-withdrawal and climate-change studies.

The results of groundwater withdrawal indicate a groundwater-level drawdown of 11.7 m was found with a 50-year water-withdrawal at the designed rate of 510 m^3/d. The withdrawal rate was estimated using the SNWA water application and the share of study area in the Snake Valley

The major findings from the CMIP5-driven GSFLOW model during the 3 time periods of the 21st century (2011-2039, 2040-2069, and 2070-2099) include:

- The projected annual streamflow during the 21st century showed no certain trends under conditions of increasing precipitation and evapotranspiration, which are the major components in the water-balance budget.
- Similar to the CMIP5-driven PRMS model simulation results, the changes in mean monthly

streamflow, a distinguishing point was identified where the increasing and decreasing trend occurred before May and after June, respectively. However, the streamflow results from GSFLOW model show larger decreases than the results from the PRMS model, especially during months of July, August, September, and October.

- The peak of the streamflow shifted earlier for 3.7 to 26.3 days during the 21st century, and it is less than the days shifted resulting from the CMIP5-driven PRMS model simulation, i.e., -2.9 to 30 days.
- The water exchange between the surface water and groundwater in the future projections were found to be higher compared to the baseline scenario, and this increasing water exchange became less as the time progressed in the future (from Period 1 to Period 3).

The hydrologic responses to the climate change resulting from the GSFLOW modeling were similar overall to the results from the PRMS modeling. The GSFLOW modeling results show lesser changes compared to the PRMS modeling results. Additionally, the GSFLOW model simulation provided results regarding the dynamic water exchange between systems of surface hydrology and groundwater hydrology, even though the value was relatively small in the overall water budget.

The development of an integrated hydrologic model can better represent the dynamic surface-and-subsurface water interaction. Since the groundwater-flow system was conceptualized as a water storage in the surface hydrologic PRMS model (section 3.4.), the resulting one-way vertical water flow from surface and underground may be unrealistic. However, by considering a detailed groundwater-level fluctuation using MODFLOW model, the GSFLOW model can simulate the two-way water flux interactions between surface water and groundwater from a physical hydrogeologic perspective. In this way, the integrated GSFLOW

model can better capture and represent hydrologic processes, and thus it can be performed reliably for future hydrologic studies.

However, there were several limitations in the current study. First, the sensitivity analysis results may be limited by the data availability for streamflow used in the objective function and the use of local sensitivity analysis approach. Second, the amount of water exchanged between surface water and groundwater was small comparing to the total water budget, thus they were not further analyzed in terms of seasonal variations. Third, the grid used in the MODFLOW simulation needs further refinement to capture the detail drawdown propagation around the pumping well.

Chapter 5 Contribution of Current Research

5.1 Summary

Water, one of the most critical components of life on Earth, limits the social-environmental development. With the increasing water demand, Las Vegas Valley (LVV) is close to suing its allocation from the Colorado River. Southern Nevada Water Authority (SNWA) is responsible for water supply in the LVV, meeting water needs for residents, businesses, and tourists. SNWA hold an application for 50,679 afy in Snake Valley, where the groundwater could potentially support LVV for future development (SNWA, 2012). Variables of precipitation, temperature, streamflow, and groundwater are critical indicators to evaluate regional climate and water resources. Thus, to evaluate water resources, it is important to understand the meteorological conditions, hydrologic processes, and corresponding influences by natural changes and human disturbances, especially in the areas that can potentially supply water to LVV.

Climate change is an important fact that was, is, and will continue to be studied. Results from climate change, spatially and temporally distributed meteorological variations, corresponding hydrologic alternations, and complex interactions between surface water and groundwater, make physically based modeling a very data intensive and demanding task, especially in snow-dominant areas.

In this study, an integrated hydrologic model was developed and used as a tool to evaluate the impacts of climate change on water resources. The area of interest in this study was the Lehman Creek watershed in the Great Basin National Park, Nevada. In order to help provide scientific support for local water resources management, the hydrologic evaluation of climate change influences was performed. Three research questions were addressed towards this goal.

Research Question # 1: What are the long-term changes in meteorological conditions on a watershed scale with respect to Global Circulation Models?

Research Question # 2: How do the climatic changes affect the streamflow on a watershed scale?

Research Question # 3: How do integrated hydrologic processes respond to external stresses from meteorologic changes and human interference of groundwater pumping?

To address the first question, the hypothesis tested was that the Quantile-Quantile Mapping method, used to bias correct the meteorological data from a coarse scale to a watershed scale, can keep the statistical characteristics of the data consistent with regional observations and result in reliable meteorological data that can be used for further watershed hydrologic study. The biases were identified from a statistical comparison between tested dataset and observed dataset during the same historical period, and then the biases were removed from the future-test dataset. In this way, the future-test dataset can be bias corrected and used for further hydrologic study. The downscaled GCM data from the CMIP5 BCCA dataset were used as a tested dataset, which provided the meteorological variables, i.e., daily precipitation (*Prcp*), maximum temperature (T_{max}), and minimum temperature (T_{min}), under four potential climate change scenarios: RCP 2.6, RCP 4.5, RCP 6.0, and RCP 8.5 at the resolution of 1/8° (12 km). Instead of 10-year observation records, a 30-year PRISM dataset (1981-2010) was used to represent the observed dataset.

Before the PRISM data was used for bias correction procedure, the data validation procedure was performed using mean monthly comparisons with observations for all three variables, i.e., *Prcp*, T_{max}, and T_{min}, during the overlapping period of 2003-2012 (water years). Then, after verifying the PRISM dataset as a reliable replication of observations, it was used to

capture the statistical long-term features and to bias correct the CMIP5 dataset in this study. Evaluation of the results was performed as a relative difference between the projected period, i.e., 2011-2099 and the baseline period, i.e., 1981-2010. Three future time periods were defined as 2011-2039, 2040-2069, and 2070-2099. Results showed that the PRISM data well preserved the meteorological features both in terms of values and distributions; thus, it was an effective replication of the meteorological observations in the study area. It helps resolving the issue of long-time data shortage. Additionally, the results of QM bias correction fit the observations well in terms of monthly distribution and density distribution during the same historical period. It indicates that this approach can be used to correct the combined errors from spatial resolution differences and model systems. Lastly, under the influences of climate change, the average value of mean annual ensembles over the entire projected 21st century showed an increase of 2.3 °C, 2.2 °C, and 35.1 mm in maximum temperature, minimum temperature, and precipitation, respectively, in the study area (Great Basin NP station).

To address the second question, the hypothesis tested was that through dynamic interaction between meteorologic variables and hydrologic processes, the streamflow would change in terms of rates and timing, responding to local climate change. In the study area of Lehman Creek watershed, snow-dominant runoff was simulated using the physically based parameter distributed hydrologic model PRMS. In order to retain data consistency when comparing the climate change results, the same PRISM dataset used for CMIP5 bias correction in the Research Question 1, was used as the driving force for the hydrologic model PRMS simulation for model calibration and validation. After the development of a valid hydrologic PRMS model, the bias-corrected CMIP5 climate-change data drove the model to simulate the corresponding streamflow. The model simulation results indicated that, as the temperature keeps

rising during the 21st century (projected results from Research Question 1), an increase in streamflow was expected from Lehman Creek. This was primarily due to the earlier snowmelt driven by increasing temperatures and secondarily due to the increasing precipitation. Additionally, decreases in the late-spring and summer flows were expected, along with an earlier arrival time for peak flow and less water storage in the snowpack by the end of the winter season. The degree of these changes varied with emission scenarios, and was highly correlated with the GCMs that produced the meteorological projections. The quantitative evaluations of the ensemble changes under each emission scenario provided insights regarding the effects of climate change on a watershed scale that has both known and unknown uncertainties. By providing a better understanding based on the assessment of the changing trends in the local streamflow under the long-term climate change in this century, this study could help local water resources management to devise more adaptive water strategies.

The hypothesis tested to address the third question was that the water flux interaction between surface water and groundwater would show varying trend under the climate change and the groundwater would drawdown under the influence of groundwater pumping. To simulate the dynamic water interactions between the surface water and groundwater, a groundwater flow system model was developed using the three-dimensional finite-difference groundwater flow system (MODFLOW). Next, the MODFLOW model was coupled with the surface hydrologic model PRMS to develop the integrated hydrologic model GSFLOW. However, there were no hydraulic measurements within and around the study area of the Lehman Creek watershed. Due to an observation data shortage, the hydraulic properties, including hydraulic conductivity, specific yield, specific storage, and streambed hydraulic conductivity were estimated using a steady-state MODLFOW model and further improved using a transient GSFLOW model. By

using the developed GSFLOW model, two model implementations were made: 1) groundwater pumping influences and 2) evaluation of hydrologic responses to potential climate change. Different from PRMS-only modeling, the climate change evaluation using the GSFLOW model provided an integrated hydrologic view toward the water flow system, which includes surface and subsurface water systems, rather than the surface water system only. GSFLOW model results were assessed using the same approach used for the PRMS model. Comparisons were made between these two model evaluation results.

Furthermore, with consideration of groundwater flow system in the GSFLOW model, evaluation of groundwater pumping effects on the local groundwater system becomes possible. On the basis of share of Lehman Creek watershed area in the entire Snake Valley, different water pumping rates of 50% (255 m^3/d), 100% (510 m^3/d), and 200% (1020 m^3/d) were used as the external stresses to the groundwater system. They were simulated by 50-year groundwater pumping simulations at the cell at column 86, row 11, and layer 2. A 70-year period of the GSFLOW model ran prior to the start of the groundwater withdrawals to stabilize the groundwater condition before the water was pumped. Results showed that the water-level drawdown increased significantly with the water pumping increases; water drawdown was 5.3 m for the 50% withdrawal, 11.7 m for the 100% withdrawal, and 24.0 m for the 200% withdrawal by the end of 50 year of continuous groundwater pumping. Regarding the climate change influences on hydrologic processes, the projected annual streamflow during the 21st century showed no clear trends under conditions of increasing precipitation and evapotranspiration, which are the major components in the water balance. For the changes in mean monthly streamflow, similar to the CMIP5-driven PRMS model simulation results, a distinguishing point was identified where the increasing and decreasing trend occurred before May and after June,

respectively. However, the streamflow results from GSFLOW model show larger decreases than the results from the PRMS model, especially during July, August, September, and October. Moreover, the peak of the streamflow shifted earlier from 3.7 to 26.3 days during the period of 2011-2099, and it is less than the days shifted resulting from the CMIP5-driven PRMS model simulation, i.e., -2.9 to 30 days, where the negative value means a delayed shift. Overall, the GSFLOW modeling results show lesser changes than the PRMS modeling results. However, GSFLOW provided results regarding the dynamic water exchange between surface and groundwater systems, even though the value of this exchange was relatively small in the entire water budget. The study results can provide integrated assessment of water resource changes regarding potential climate change and potential groundwater pumping in the study area.

5.2 Contribution

There are two main contributions from the Research Question 1. Firstly, this is the first time in the Lehman Creek that all 67 GCM models and scenarios (Appendix A - 1) were considered as an ensemble to evaluate climate change trends and variations among different time periods in the 21st century. Results showed increases in both precipitation and temperatures in the study area of Lehman Creek watershed, which lays solid groundwork that can help to provide a clearer understanding of the potential influences of changing climate on water resources and other disciplines. Secondly, the PRISM dataset was validated as a representation of observations in the study area, which indicates it can help resolve the data-shortage issue in areas where limited observation stations are available.

The results from Research Question 2 could contribute to a better understanding of streamflow change in response to the climate change in Lehman Creek. Through the model simulation of meteor-hydrologic correlation in the study area, a platform was built to assess the

hydrologic processes, especially snow processes which are important in snow-dominant Lehman Creek watershed. Secondly, by using the bias-corrected CMIP5 datasets, it was the first time in the study area to consider all GCMs in the evaluation of corresponding streamflow changes under different climate change scenarios. The results of earlier-shift in streamflow peak-time and uncertainty in annual streamflow rates provide useful information for evaluation of future water resources. Based on this information different options can be considered for better water resources management.

The results from question 3 could contribute to an improvement in the hydrologic evaluation in the study area responding to the external stresses: potential climate change and potential groundwater pumping. Considering three-dimensional groundwater-flow system, the GSFLOW model completes the water flow system by coupling the groundwater-flow system model with the surface hydrologic model PRMS. It fills a gap because the PRMS model only considers the groundwater flow system as a one-way water storage with no groundwater discharging to or influencing the surface water, such as the deeper root transpiration, groundwater outflow, and well pumping. As the dynamic water interactions between the unsaturated zone and streamflow, and soil zone and groundwater were simulated, the GSFLOW modeling improves the hydrologic simulation with a better representation. This is the first study in the Lehman Creek watershed that uses GSFLOW to evaluate climate change influences. Moreover, it was the first time that groundwater-pumping influences within the study area of Lehman Creek watershed were evaluated as a what-if scenario. The GSFLOW model developed built a valuable platform for groundwater studies, such as the influences by groundwater pumping/recharging with varied rates and locations.

Furthermore, in this study, through the development and calibrations of a steady-state MODFLOW model and a transient-state GSFLOW model, the hydraulic conductivity and specific storage of each hydrostrategraphic unit were estimated. This estimation of hydraulic properties in this area is useful, because there are no or limited groundwater observation sites around the study area. Last, but not the least, the groundwater pumping influences on the local groundwater system was assessed with the evaluated groundwater-head drawdown. This study is the first to explore how groundwater-head responses at different pumping rates in a simulated well that sits within the study area. These study results could help local water resources managers to better comprehend the water resources alternations under conditions of climate change and groundwater pumping.

5.3 Limitations

Like most statistical downscaling techniques, the Quantile-Quantile Mapping method kept the differences between GCM products and observations stationary throughout the bias-correction period and did not consider future variation. Additionally, the cross-correlation within each variable and between variables may not have been corrected. As the local climate change study heavily relies on the global climate change products, the uncertainties resulting from these limitations may add to the uncertainties within climate change forecast products, which users should be aware of when implementing in the future.

An important assumption during PRMS model simulation is that the geomorphic condition remains consistent, as no changes in land-cover and land use are considered throughout the model simulation. Furthermore, in PRMS, the vertical flows in the soil go only one way. This could limit the simulation of water interactions between surface and sub surface, such as springs

and groundwater outflows, and thus influence the model simulation results. However, the MODFLOW model improved upon the PRMS model simulation.

In the MODFLOW model simulation, there was no groundwater observation information available within the study area. This caused the greatest uncertainties in the hydraulic property estimation and groundwater flow evaluation. Furthermore, in the model set up, an evenly distributed thickness of every defined layer was assumed, which was a simplification of the geologic formation with similar hydraulic features. This further increases the uncertainties in the estimation of hydraulic properties and their spatial distribution in the study area. When the groundwater component is small relative to the surface flow and soil-zone flow, the estimation of the hydraulic properties becomes more challenging and uncertain when using streamflow for model calibration.

In the GSFLOW model simulation, the interactive water-flux exchanges water between soil zone and unsaturated zone/saturated zone, and between streamflow and the groundwater. As the water exchange is highly correlated with the hydraulic properties and its spatial distribution, the uncertainties in the hydraulic property estimation will further disseminate to the GSFLOW model simulation. This uncertainty may not be detectable in the streamflow simulation because the groundwater component is small.

Overall, this study - ‘Understanding the Long-term Changes in Hydrologic Processes on a Watershed Scale due to Meteorological Influences under Climate Change’ relied heavily on numerical model simulations. There are uncertainties when modeling physical processes, including uncertainties in input data, model calibration, and post-processing. Considering that two models were combined in this study, the resulting uncertainties may be significant, which will require additional attention when interpreting the results.

5.4 Recommendations

In the study area of Lehman Creek watershed, the observation data are very limited. It is a typical snow-dominant area that plays an important role in the recharge of the local groundwater system, the Lehman Creek watershed is such a small area that it is typically called *Lehman Creek drainage*. The number of observation stations within the watershed, is not enough to represent the spatial distribution of the meteoro-hydrologic conditions. Courtesy of the NevCAN stations built in recent years, in the future, new measurements taken at these stations can substantially improve the hydrologic model performance with a long-term observation records used in the model development.

The current study was based on the performance of hydrologic models, which directly determine the study results. The conceptualization of hydrologic procedures, one of the most important steps in the model development, has substantial effects on the model simulation. For example, while the evapotranspiration process was conceptualized within the soil zone simulated by the PRMS model, the deep root transpiration was not considered separately. In future, this can be further improved with the consideration of potential evapotranspiration in the unsaturated zone simulated by the MODFLOW model. The hydrogeological properties were conceptualized into 5 hydrostrategraphic units in this study, the spatial heterogeneity can be further improved by a more detailed classification of hydrostrategraphic units. In that case, the global optimization method, by using tools such as Parameter EStimation Tool (PEST), could be employed to explore the best parameter values and distributions instead of manual trial-and-error method used in this study.

Appendix

A - 1 Coupled Model Intercomparison Project (CMIP5) Groups and Models.[1,2]

No.	Modeling Center (or Group)	Institute ID	Model Name	Available Scenarios
1	Commonwealth Scientific and Industrial Research Organization (CSIRO) and Bureau of Meteorology (BOM), Australia	CSIRO-BOM	ACCESS1.0	rcp4.5,rcp8.5
2	Beijing Climate Center, China Meteorological Administration	BCC	BCC-CSM1.1	rcp2.6, rcp4.5, rcp6.0, rcp8.5
3	Canadian Centre for Climate Modelling and Analysis	CCCMA	CanESM2	rcp2.6, rcp4.5, rcp8.5
4	National Center for Atmospheric Research	NCAR	CCSM4	rcp2.6, rcp4.5, rcp6.0, rcp8.5
5	Community Earth System Model Contributors	NSF-DOE-NCAR	CESM1(BGC)	rcp4.5, rcp8.5
6	Centre National de Recherches Météorologiques /Centre Européen de Recherche et Formation Avancée en Calcul Scientifique	CNRM-CERFACS	CNRM-CM5	rcp4.5, rcp8.5
7	Commonwealth Scientific and Industrial Research Organization in collaboration with Queensland Climate Change Centre of Excellence	CSIRO-QCCCE	CSIRO-Mk3.6.0	rcp2.6, rcp4.5, rcp8.5
8	NOAA Geophysical Fluid Dynamics Laboratory	NOAA GFDL	GFDL-CM3	rcp2.6,rcp6.0, rcp8.5
9			GFDL-ESM2G	rcp2.6, rcp4.5, rcp6.0, rcp8.5
10			GFDL-ESM2M	rcp2.6, rcp4.5, rcp6.0, rcp8.5
11	Institute for Numerical Mathematics	INM	INM-CM4	rcp4.5,rcp8.5
12	Institut Pierre-Simon Laplace	IPSL	IPSL-CM5A-LR	rcp2.6, rcp4.5, rcp6.0, rcp8.5
13			IPSL-CM5A-MR	rcp2.6, rcp4.5, rcp6.0, rcp8.5
14	Japan Agency for Marine-Earth Science and Technology, Atmosphere and Ocean Research Institute (The University of Tokyo), and National Institute for Environmental Studies	MIROC	MIROC-ESM	rcp2.6, rcp4.5, rcp6.0, rcp8.5
15			MIROC-ESM-CHEM	rcp2.6, rcp4.5, rcp6.0, rcp8.5
16	Atmosphere and Ocean Research Institute (The University of Tokyo), National Institute for Environmental Studies, and Japan Agency for Marine-Earth Science and Technology	MIROC	MIROC5	rcp2.6, rcp4.5, rcp6.0, rcp8.5
17	Max-Planck-Institut für Meteorologie (Max Planck Institute for Meteorology)	MPI-M	MPI-ESM-LR	rcp2.6, rcp4.5, rcp8.5
18			MPI-ESM-MR	rcp2.6, rcp4.5, rcp8.5
19	Meteorological Research Institute	MRI	MRI-CGCM3	rcp2.6, rcp4.5, rcp6.0, rcp8.5
20	Norwegian Climate Centre	NCC	NorESM1-M	rcp2.6, rcp4.5, rcp6.0, rcp8.5

[1] http://cmip-pcmdi.llnl.gov/cmip5/docs/CMIP5_modeling_groups.pdf.

[2] The products used in this study were resulted from the first initial condition (run) for each model.

A - 2 Descriptions of Station Networks Used In PRISM Spatial Climate Datasets.[3] [4]

Stations	Descriptions	Focus
AGRIMET	Bureau of Reclamation Agricultural Weather Network	Prcp, Temp
AGWXNET	Washington State University's Agricultural Weather Network	Prcp, Temp
ASOS/ISH	Automated Surface Observing System and related networks (e.g., AWOS), and Integrated Surface Hourly network Notes: ASOS network began installation in 1996, with poor instrumentation for measuring snowfall.	Prcp, Temp
CIMIS	California Irrigation Management Information System	Temp
COAGMET	Colorado Agricultural Meteorological Network	Prcp, Temp
COCORAHS	Community Collaborative Rain, Hail and Snow Network. Notes: Currently the largest ppt observing network in the US.	Prcp
COOP	National Weather Service Cooperative Observer Program. Notes: These stations are part of the GHCN-D database. COOP is the longest-running climate network (US).	Prcp, Temp
EC	Environment Canada	Prcp, Temp
FAWN	Florida Agricultural Weather Network	Prcp, Temp
HDSC	NOAA Hydrometeorological Design Studies Center. Notes: A collection of ppt stations in California used by HDSC and PRISM to produce the NOAA Atlas 14 ppt frequency maps. Period of record ends in 2010.	Prcp
HJA	HJ Andrews Experimental Forest, Oregon, NSF Long Term Ecological Research Site (LTER); benchmark sites, reference stands, cold air transects Notes: Data lag time is currently longer than 6 months, which is our cutoff for operational inclusion; this means that at present, HJA data can be included only when new versions of the datasets are created.	Prcp, Temp
HYD	Advanced Hydrologic Prediction Service River Forecast Centers Notes: Selected stations from a combination of many different networks. Stations available from networks for which we have direct feeds are excluded (difficulties identifying the source networks in HYD produce occasional duplications).	Prcp
LUKEAFB	Luke Air Force Base network, SW Arizona	Prcp, Temp
MEXICO	Global Historical Climate Network – Mexico. Notes: These stations are part of the GHCN-D database	Prcp, Temp
MN	Minnesota Climatology Working Group, previously called Minnesota HiDen, now called MNGage	Prcp
NEVCAN	Nevada Climate-Ecohydrological Assessment Network	Prcp, Temp
NDAWN	North Dakota Agricultural Weather Network	Prcp, Temp
NDSWC	North Dakota State Water Commission	Prcp
NDBC	National Data Buoy Center. Notes: Used to characterize near-coastal air temperature and humidity	Temp
RAWS	U.S. Forest Service and Bureau of Land Management Remote Automated Weather Stations	Prcp, Temp
SCAN	USDA NRCS Soil Climate Analysis Network	Prcp, Temp
SFWMD	South Florida Water Management District	Prcp
SNOTEL	Natural Resources Conservation Service Snowpack Telemetry Notes: The main high elevation network in western mountains.	Prcp, Temp
WBAN	Weather Bureau, Army, Navy. Notes: These stations are part of the GHCN-D database. In 1996, many WBAN stations converted to ASOS instrumentation.	Prcp, Temp
WRCC	Western Regional Climate Center	Prcp, Temp
OKMESONET	Oklahoma Mesonet	Temp
AHPS RADAR	Advanced Hydrometeorological Prediction System (Stage 2 and 4 grids)	Prcp

[3] AN81d data, from 1 Jan, 1981-ongoing, daily step, at 2.5 min (4 km) resolution. http://prism.oregonstate.edu

[4] Data station used in AN81d varied due to the station equipment and location changes, opening and closing.

A - 3 Sensitivity Analysis Results of NSE for Specific Storage, Specific Yield, Horizontal and Vertical Hydraulic Conductivity in Each Hydrostrategegraphic Unit (i.e., GD - Glacial Deposit; AD – Alluvial Deposits; MQ - Mountain Quartzite; KL – Karst Limestone; BG – Biotite Granite).

multiply coefficient	Ss					Sy					HK					VK				
	GD	AD	MQ	KL	BG	GD	AD	MQ	KL	BG	GD	AD	MQ	KL	BG	GD	AD	MQ	KL	BG
0.2	0.749	0.749	0.746	0.745	0.749	0.750	0.749	0.749	0.749	0.749	0.749	0.740	0.749	0.749	0.749	0.749	0.749	0.749	0.743	0.749
0.3	0.749	0.749	0.749	0.746	0.749	0.751	0.749	0.749	0.749	0.749	0.749	0.740	0.749	0.749	0.749	0.749	0.749	0.749	0.744	0.749
0.4	0.749	0.749	0.749	0.748	0.749	0.751	0.749	0.749	0.749	0.749	0.749	0.740	0.749	0.749	0.749	0.749	0.749	0.749	0.746	0.749
0.5	0.749	0.749	0.749	0.748	0.749	0.751	0.749	0.749	0.749	0.749	0.749	0.740	0.749	0.749	0.749	0.749	0.749	0.749	0.747	0.749
0.6	0.749	0.749	0.749	0.749	0.749	0.750	0.749	0.749	0.749	0.749	0.749	0.741	0.749	0.749	0.749	0.749	0.749	0.749	0.747	0.749
0.7	0.749	0.749	0.749	0.749	0.749	0.750	0.749	0.749	0.749	0.749	0.749	0.741	0.749	0.749	0.749	0.749	0.749	0.749	0.748	0.749
0.8	0.749	0.749	0.749	0.749	0.749	0.750	0.749	0.749	0.749	0.749	0.749	0.741	0.749	0.749	0.749	0.749	0.749	0.749	0.748	0.749
0.9	0.749	0.749	0.749	0.749	0.749	0.749	0.749	0.749	0.749	0.749	0.749	0.741	0.749	0.749	0.749	0.749	0.749	0.749	0.749	0.749
1	0.749	0.749	0.749	0.749	0.749	0.749	0.749	0.749	0.749	0.749	0.749	0.741	0.749	0.749	0.749	0.749	0.749	0.749	0.749	0.749
2	0.749	0.749	0.749	0.749	0.749	0.746	0.749	0.749	0.749	0.749	0.749	0.741	0.749	0.749	0.749	0.749	0.748	0.749	0.746	0.749
4	0.749	0.749	0.749	0.749	0.749	0.743	0.749	0.749	0.749	0.749	0.749	0.741	0.749	0.749	0.749	0.749	0.747	0.748	0.741	0.749
6	0.749	0.749	0.749	0.749	0.749	0.742	0.749	0.749	0.749	0.749	0.749	0.741	0.749	0.749	0.749	0.749	0.747	0.748	0.741	0.749
8	0.749	0.749	0.749	0.749	0.749	0.742	0.748	0.749	0.749	0.749	0.749	0.742	0.749	0.749	0.749	0.749	0.746	0.749	0.741	0.749
10	0.749	0.749	0.749	0.749	0.749	0.742	0.748	0.749	0.749	0.749	0.749	0.742	0.749	0.749	0.749	0.749	0.746	0.748	0.741	0.749

A - 4 Sensitivity Analysis Results of PBIAS For Specific Storage, Specific Yield, Horizontal and Vertical Hydraulic Conductivity in Each Hydrostrategegraphic Unit (i.e., GD - Glacial Deposit; AD – Alluvial Deposits; MQ - Mountain Quartzite; KL – Karst Limestone; BG – Biotite Granite).

multiply coefficient	Ss					Sy					HK					VK				
	GD	AD	MQ	KL	BG	GD	AD	MQ	KL	BG	GD	AD	MQ	KL	BG	GD	AD	MQ	KL	BG
0.2	-11.4	-11.4	-11.2	-17.1	-11.4	-11.1	-11.3	-11.4	-11.4	-11.4	-11.4	8	-11.4	-11.4	-11.4	-11.4	-10	-11.4	-18.5	-11.4
0.3	-11.4	-11.4	-11.3	-16.3	-11.4	-11.1	-11.3	-11.4	-11.4	-11.4	-11.4	8	-11.4	-11.4	-11.4	-11.4	-9.5	-11.4	-17.8	-11.4
0.4	-11.4	-11.4	-11.4	-14.6	-11.4	-11.2	-11.3	-11.4	-11.4	-11.4	-11.4	8	-11.4	-11.4	-11.4	-11.4	-9.5	-11.4	-17.2	-11.4
0.5	-11.4	-11.4	-11.4	-12.5	-11.4	-11.2	-11.4	-11.4	-11.4	-11.4	-11.4	7.9	-11.4	-11.4	-11.4	-11.4	-9.8	-11.4	-16.5	-11.4
0.6	-11.4	-11.4	-11.4	-12.1	-11.4	-11.3	-11.4	-11.4	-11.4	-11.4	-11.4	7.9	-11.4	-11.4	-11.4	-11.4	-10.1	-11.4	-15.6	-11.4
0.7	-11.4	-11.4	-11.4	-11.8	-11.4	-11.3	-11.4	-11.4	-11.4	-11.4	-11.4	7.9	-11.4	-11.4	-11.4	-11.4	-10.4	-11.4	-14.6	-11.4
0.8	-11.4	-11.4	-11.4	-11.6	-11.4	-11.3	-11.4	-11.4	-11.4	-11.4	-11.4	7.9	-11.4	-11.4	-11.4	-11.4	-10.8	-11.4	-13.5	-11.4
0.9	-11.4	-11.4	-11.4	-11.5	-11.4	-11.4	-11.4	-11.4	-11.4	-11.4	-11.4	7.9	-11.4	-11.4	-11.4	-11.4	-11.1	-11.4	-12.5	-11.4
1	-11.4	-11.4	-11.4	-11.4	-11.4	-11.4	-11.4	-11.4	-11.4	-11.4	-11.4	7.9	-11.4	-11.4	-11.4	-11.4	-11.4	-11.4	-11.4	-11.4
2	-11.4	-11.4	-11.4	-11.3	-11.4	-11.6	-11.4	-11.4	-11.4	-11.4	-11.4	7.7	-11.4	-11.4	-11.4	-11.4	-13.5	-11.4	-1.5	-11.4
4	-11.4	-11.4	-11.4	-11.2	-11.4	-12	-11.4	-11.4	-11.4	-11.4	-11.4	7.5	-11.4	-11.4	-11.4	-11.4	-15.3	-11.4	6.8	-11.4
6	-11.4	-11.4	-11.4	-11.2	-11.4	-12.1	-11.4	-11.4	-11.4	-11.4	-11.3	7.3	-11.4	-11.4	-11.4	-11.4	-16	-11.5	7	-11.4
8	-11.4	-11.4	-11.4	-11.2	-11.4	-12.3	-11.4	-11.4	-11.4	-11.4	-11.3	7.2	-11.4	-11.4	-11.4	-11.4	-16.3	-11.4	7.2	-11.4
10	-11.4	-11.4	-11.4	-11.2	-11.4	-12.3	-11.4	-11.4	-11.4	-11.4	-11.3	7.1	-11.4	-11.3	-11.4	-11.4	-16.5	-11.4	7.5	-11.4

A - 5 Sensitivity Analysis Results of R^2 for Specific Storage, Specific Yield, Horizontal and Vertical Hydraulic Conductivity in Each Hydrostrategegraphic Unit (i.e., GD - Glacial Deposit; AD – Alluvial Deposits; MQ - Mountain Quartzite; KL – Karst Limestone; BG – Biotite Granite).

multiply coefficient	Ss					Sy					HK					VK				
	GD	AD	MQ	KL	BG	GD	AD	MQ	KL	BG	GD	AD	MQ	KL	BG	GD	AD	MQ	KL	BG
0.2	0.762	0.762	0.758	0.763	0.762	0.763	0.762	0.762	0.762	0.762	0.762	0.752	0.762	0.762	0.762	0.762	0.761	0.762	0.762	0.762
0.3	0.762	0.762	0.762	0.763	0.762	0.764	0.762	0.762	0.762	0.762	0.762	0.752	0.762	0.762	0.762	0.762	0.761	0.762	0.763	0.762
0.4	0.762	0.762	0.762	0.763	0.762	0.764	0.762	0.762	0.762	0.762	0.762	0.752	0.762	0.762	0.762	0.762	0.761	0.762	0.763	0.762
0.5	0.762	0.762	0.762	0.762	0.762	0.764	0.762	0.762	0.762	0.762	0.762	0.752	0.762	0.762	0.762	0.762	0.761	0.762	0.763	0.762
0.6	0.762	0.762	0.762	0.762	0.762	0.763	0.762	0.762	0.762	0.762	0.762	0.752	0.762	0.762	0.762	0.762	0.761	0.762	0.763	0.762
0.7	0.762	0.762	0.762	0.762	0.762	0.763	0.762	0.762	0.762	0.762	0.762	0.752	0.762	0.762	0.762	0.762	0.761	0.762	0.763	0.762
0.8	0.762	0.762	0.762	0.762	0.762	0.763	0.762	0.762	0.762	0.762	0.762	0.752	0.762	0.762	0.762	0.762	0.762	0.762	0.763	0.762
0.9	0.762	0.762	0.762	0.762	0.762	0.762	0.762	0.762	0.762	0.762	0.762	0.752	0.762	0.762	0.762	0.762	0.762	0.762	0.763	0.762
1	0.762	0.762	0.762	0.762	0.762	0.762	0.762	0.762	0.762	0.762	0.762	0.752	0.762	0.762	0.762	0.762	0.762	0.762	0.762	0.762
2	0.762	0.762	0.762	0.762	0.762	0.759	0.762	0.762	0.762	0.762	0.762	0.752	0.762	0.762	0.762	0.762	0.763	0.762	0.756	0.762
4	0.762	0.762	0.762	0.762	0.762	0.756	0.762	0.762	0.762	0.762	0.762	0.752	0.762	0.762	0.762	0.762	0.763	0.762	0.752	0.762
6	0.762	0.762	0.762	0.762	0.762	0.756	0.761	0.762	0.762	0.762	0.762	0.752	0.762	0.762	0.762	0.762	0.763	0.761	0.753	0.762
8	0.762	0.762	0.762	0.762	0.762	0.756	0.761	0.762	0.762	0.762	0.762	0.753	0.762	0.762	0.762	0.762	0.763	0.762	0.753	0.762
10	0.762	0.762	0.762	0.762	0.762	0.757	0.761	0.762	0.762	0.762	0.762	0.753	0.762	0.762	0.762	0.762	0.763	0.762	0.753	0.762

A - 6 Sensitivity Analysis Results of RMSE for Specific Storage, Specific Yield, Horizontal and Vertical Hydraulic Conductivity in Each Hydrostrategegraphic Unit (i.e., GD - Glacial Deposit; AD – Alluvial Deposits; MQ - Mountain Quartzite; KL – Karst Limestone; BG – Biotite Granite).

multiply coefficient	Ss					Sy					HK					VK				
	GD	AD	MQ	KL	BG	GD	AD	MQ	KL	BG	GD	AD	MQ	KL	BG	GD	AD	MQ	KL	BG
0.2	6.123	6.122	6.161	6.169	6.122	6.104	6.124	6.122	6.122	6.122	6.123	6.226	6.122	6.123	6.122	6.121	6.121	6.120	6.192	6.122
0.3	6.122	6.122	6.127	6.152	6.122	6.103	6.124	6.122	6.122	6.122	6.123	6.225	6.122	6.123	6.122	6.122	6.122	6.120	6.177	6.122
0.4	6.122	6.122	6.125	6.138	6.122	6.103	6.123	6.123	6.122	6.122	6.123	6.225	6.122	6.123	6.122	6.122	6.123	6.121	6.163	6.122
0.5	6.122	6.122	6.123	6.130	6.122	6.103	6.123	6.123	6.122	6.122	6.123	6.225	6.122	6.123	6.122	6.122	6.123	6.121	6.152	6.122
0.6	6.122	6.122	6.122	6.127	6.122	6.105	6.123	6.123	6.122	6.122	6.123	6.225	6.122	6.123	6.122	6.122	6.122	6.121	6.143	6.122
0.7	6.122	6.122	6.122	6.125	6.122	6.108	6.123	6.123	6.122	6.122	6.123	6.225	6.122	6.123	6.122	6.122	6.122	6.122	6.135	6.122
0.8	6.122	6.122	6.122	6.124	6.122	6.112	6.123	6.123	6.122	6.122	6.123	6.224	6.122	6.123	6.122	6.122	6.122	6.122	6.129	6.122
0.9	6.122	6.122	6.122	6.123	6.122	6.117	6.122	6.122	6.122	6.122	6.123	6.224	6.122	6.122	6.122	6.122	6.122	6.122	6.124	6.122
1	6.122	6.122	6.122	6.122	6.122	6.122	6.122	6.122	6.122	6.122	6.123	6.224	6.122	6.122	6.122	6.122	6.122	6.122	6.122	6.122
2	6.123	6.122	6.123	6.121	6.122	6.164	6.123	6.123	6.122	6.122	6.122	6.222	6.122	6.122	6.122	6.123	6.129	6.124	6.153	6.122
4	6.124	6.122	6.123	6.121	6.122	6.198	6.125	6.123	6.122	6.122	6.121	6.218	6.122	6.122	6.122	6.123	6.140	6.128	6.214	6.122
6	6.124	6.122	6.123	6.121	6.122	6.206	6.127	6.123	6.122	6.122	6.121	6.214	6.122	6.121	6.122	6.123	6.148	6.131	6.215	6.122
8	6.124	6.122	6.123	6.121	6.122	6.207	6.128	6.123	6.122	6.122	6.120	6.211	6.122	6.121	6.122	6.124	6.153	6.128	6.216	6.122
10	6.125	6.122	6.123	6.121	6.122	6.208	6.129	6.123	6.122	6.122	6.119	6.208	6.122	6.120	6.122	6.124	6.157	6.130	6.220	6.122

A - 7 Sensitivity Analysis Results of PBIAS For Streambed Hydraulic Conductivity in Each Stream Segment.

multiply coefficient	strmseg1	strmseg2	strmseg3	strmseg4	strmseg5	strmseg6	strmseg7	strmseg8	strmseg9	strmseg10	strmseg11
0.2	-11.4	-11.4	-11.3	-11.4	-11.4	-11.3	-11.1	-11.4	-11	-10.7	-11
0.3	-11.4	-11.4	-11.3	-11.4	-11.4	-11.4	-11.2	-11.4	-11.1	-11	-11.4
0.4	-11.4	-11.4	-11.3	-11.4	-11.4	-11.4	-11.3	-11.4	-11.2	-11.1	-11.6
0.5	-11.4	-11.4	-11.4	-11.4	-11.4	-11.4	-11.3	-11.4	-11.2	-11.2	-11.6
0.6	-11.4	-11.4	-11.4	-11.4	-11.4	-11.4	-11.3	-11.4	-11.3	-11.3	-11.6
0.7	-11.4	-11.4	-11.4	-11.4	-11.4	-11.4	-11.3	-11.4	-11.3	-11.3	-11.6
0.8	-11.4	-11.4	-11.4	-11.4	-11.4	-11.4	-11.4	-11.4	-11.3	-11.3	-11.5
0.9	-11.4	-11.4	-11.4	-11.4	-11.4	-11.4	-11.4	-11.4	-11.4	-11.4	-11.5
1	-11.4	-11.4	-11.4	-11.4	-11.4	-11.4	-11.4	-11.4	-11.4	-11.4	-11.4
2	-11.4	-11.4	-11.4	-11.4	-11.4	-11.4	-11.4	-11.4	-11.5	-11.5	-10.9
4	-11.4	-11.4	-11.4	-11.4	-11.4	-11.4	-11.5	-11.4	-11.5	-11.6	-10.7
6	-11.4	-11.4	-11.4	-11.4	-11.4	-11.4	-11.5	-11.4	-11.6	-11.6	-10.7
8	-11.4	-11.4	-11.4	-11.4	-11.4	-11.4	-11.5	-11.4	-11.6	-11.6	-10.9
10	-11.4	-11.4	-11.4	-11.4	-11.4	-11.4	-11.5	-11.4	-11.6	-11.6	-11.1

A - 8 Sensitivity Analysis Results of R^2 For Streambed Hydraulic Conductivity in Each Stream Segment.

multiply coefficient	strmseg1	strmseg2	strmseg3	strmseg4	strmseg5	strmseg6	strmseg7	strmseg8	strmseg9	strmseg10	strmseg11
0.2	0.762	0.762	0.762	0.762	0.762	0.762	0.762	0.762	0.762	0.763	0.762
0.3	0.762	0.762	0.762	0.762	0.762	0.762	0.762	0.762	0.762	0.763	0.762
0.4	0.762	0.762	0.762	0.762	0.762	0.762	0.762	0.762	0.762	0.762	0.762
0.5	0.762	0.762	0.762	0.762	0.762	0.762	0.762	0.762	0.762	0.762	0.762
0.6	0.762	0.762	0.762	0.762	0.762	0.762	0.762	0.762	0.762	0.762	0.762
0.7	0.762	0.762	0.762	0.762	0.762	0.762	0.762	0.762	0.762	0.762	0.762
0.8	0.762	0.762	0.762	0.762	0.762	0.762	0.762	0.762	0.762	0.762	0.762
0.9	0.762	0.762	0.762	0.762	0.762	0.762	0.762	0.762	0.762	0.762	0.762
1	0.762	0.762	0.762	0.762	0.762	0.762	0.762	0.762	0.762	0.762	0.762
2	0.762	0.762	0.762	0.762	0.762	0.762	0.762	0.762	0.762	0.762	0.762
4	0.762	0.762	0.762	0.762	0.762	0.762	0.762	0.762	0.762	0.762	0.762
6	0.762	0.762	0.762	0.762	0.762	0.762	0.762	0.762	0.762	0.762	0.761
8	0.762	0.762	0.762	0.762	0.762	0.762	0.762	0.762	0.762	0.762	0.761
10	0.762	0.762	0.762	0.762	0.762	0.762	0.762	0.762	0.762	0.762	0.761

A - 9 Sensitivity Analysis Results of RMSE For Streambed Hydraulic Conductivity in Each Stream Segment.

multiply coefficient	strmseg1	strmseg2	strmseg3	strmseg4	strmseg5	strmseg6	strmseg7	strmseg8	strmseg9	strmseg10	strmseg11
0.2	6.123	6.122	6.122	6.122	6.122	6.119	6.116	6.123	6.116	6.106	6.108
0.3	6.123	6.122	6.122	6.122	6.122	6.121	6.118	6.123	6.118	6.112	6.113
0.4	6.123	6.122	6.122	6.122	6.122	6.120	6.120	6.123	6.119	6.115	6.117
0.5	6.123	6.122	6.122	6.122	6.122	6.120	6.120	6.123	6.120	6.118	6.119
0.6	6.123	6.122	6.122	6.122	6.122	6.121	6.121	6.123	6.121	6.119	6.120
0.7	6.123	6.122	6.122	6.122	6.122	6.121	6.121	6.123	6.121	6.120	6.121
0.8	6.122	6.122	6.122	6.122	6.122	6.122	6.122	6.122	6.122	6.121	6.122
0.9	6.122	6.122	6.122	6.122	6.122	6.122	6.122	6.122	6.122	6.122	6.122
1	6.122	6.122	6.122	6.122	6.122	6.122	6.122	6.122	6.122	6.122	6.122
2	6.122	6.122	6.122	6.123	6.122	6.123	6.124	6.122	6.124	6.125	6.124
4	6.122	6.122	6.122	6.123	6.122	6.123	6.125	6.122	6.125	6.127	6.127
6	6.122	6.123	6.122	6.123	6.122	6.123	6.126	6.122	6.126	6.127	6.130
8	6.122	6.123	6.122	6.123	6.122	6.124	6.126	6.122	6.126	6.128	6.132
10	6.122	6.123	6.123	6.123	6.122	6.124	6.126	6.122	6.126	6.128	6.135

A - 10 Sensitivity Analysis Results of NSE For Streambed Hydraulic Conductivity in Each Stream Segment.

multiply coefficient	strmseg1	strmseg2	strmseg3	strmseg4	strmseg5	strmseg6	strmseg7	strmseg8	strmseg9	strmseg10	strmseg11
0.2	0.749	0.749	0.749	0.749	0.749	0.749	0.749	0.749	0.750	0.750	0.750
0.3	0.749	0.749	0.749	0.749	0.749	0.749	0.749	0.749	0.749	0.750	0.750
0.4	0.749	0.749	0.749	0.749	0.749	0.749	0.749	0.749	0.749	0.750	0.749
0.5	0.749	0.749	0.749	0.749	0.749	0.749	0.749	0.749	0.749	0.749	0.749
0.6	0.749	0.749	0.749	0.749	0.749	0.749	0.749	0.749	0.749	0.749	0.749
0.7	0.749	0.749	0.749	0.749	0.749	0.749	0.749	0.749	0.749	0.749	0.749
0.8	0.749	0.749	0.749	0.749	0.749	0.749	0.749	0.749	0.749	0.749	0.749
0.9	0.749	0.749	0.749	0.749	0.749	0.749	0.749	0.749	0.749	0.749	0.749
1	0.749	0.749	0.749	0.749	0.749	0.749	0.749	0.749	0.749	0.749	0.749
2	0.749	0.749	0.749	0.749	0.749	0.749	0.749	0.749	0.749	0.749	0.749
4	0.749	0.749	0.749	0.749	0.749	0.749	0.749	0.749	0.749	0.749	0.749
6	0.749	0.749	0.749	0.749	0.749	0.749	0.749	0.749	0.749	0.749	0.748
8	0.749	0.749	0.749	0.749	0.749	0.749	0.749	0.749	0.749	0.749	0.748
10	0.749	0.749	0.749	0.749	0.749	0.749	0.749	0.749	0.749	0.749	0.748

6.1 Model simulation algorithms in MODLFOW

The following descriptions of Mathematical Model, Discretization Convention, and Finite-different Equation are from Harbaugh et al. (2005).

6.1.1 Mathematical Model

The three-dimensional movement of groundwater with constant density through porous media is described using a partial-differential equation:

$$\frac{\partial}{\partial x}\left(K_{xx}\frac{\partial h}{\partial x}\right)+\frac{\partial}{\partial y}\left(K_{yy}\frac{\partial h}{\partial y}\right)+\frac{\partial}{\partial z}\left(K_{zz}\frac{\partial h}{\partial z}\right)+W=S_s\frac{\partial h}{\partial t} \quad (13)$$

Where,

K_{xx}, K_{yy}, and K_{zz} are hydraulic conductivity along the x, y, and z coordinate axes, in unit of length per time (L/T);
h is the potentiometric head, in unit of length (L);
W is a volumetric flux per unit volume, representing sources and/or sinks, with W<0 for flow out of the groundwater system, and W>0 for flow into the groundwater system (T^{-1});
S_s is the specific storage of the porous material (L^{-1});
t is time (T).

The equation above describes the groundwater flow under non-equilibrium conditions in a heterogeneous and anisotropic medium, with which the principal axes of hydraulic conductivity are aligned with the coordinate direction. A mathematical representation of a groundwater flow system includes the general governing equation above with the specifications of flow and/or head conditions at the boundaries of an aquifer system and specification of initial-head conditions. See Rushton and Redshaw (1979) for the derivation of the equation.

6.1.2 Discretization Convention

An analytical solution for the equation above is rarely possible, so numerical methods are employed to gain an approximated solution. *Figure 51*shows the spatial discretization of an aquifer system in three dimensions with a block gridded into cells. The aquifer block is described in terms of rows, columns, and layers, with i, j, k indexes representing the locations in three directions (*Figure 51*).

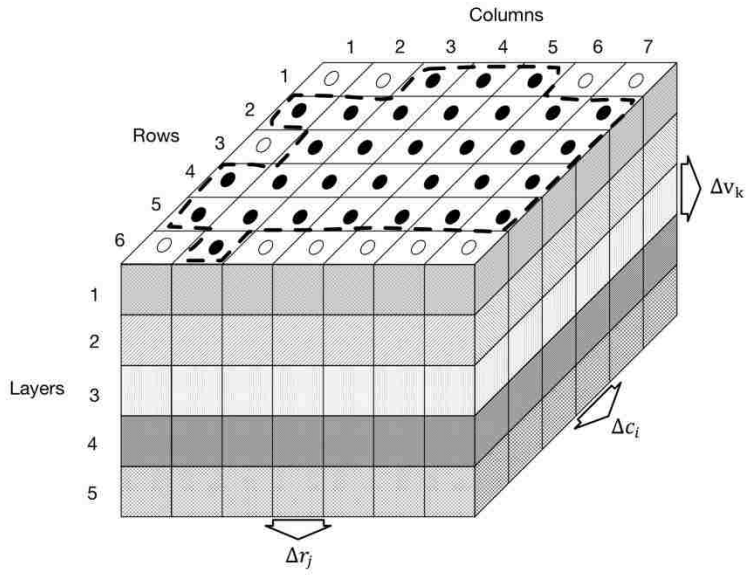

--- Aquifer boundary
• Active cell
Δc_i Width of cell in column direction, i indicates the number of the row
Δr_j Width of cell in row direction, j indicates the number of the column
Δv_k Width of cell in vertical direction, k indicates the number of the layer

Figure 51. Discretization of Hypothetical Aquifer (Adapted from Mcdonald & Harbaugh, 1988; Harbaugh et al., 2005).

Each grid is defined to be rectangular both horizontally and vertically. In the column direction, the width of cells at a given row i is designated Δc_i; in the row direction, the width of cells at a given column j is designated Δr_j; in the layer direction, the thickness of cells at a given layer k is designated Δv_k.

6.1.3 **Finite-Difference Equation**

The finite- difference equation of groundwater flow is following the law of continuity: The sum of the inflow and outflow of a cell must be equal to the rate of the storage change within the cell. With an assumption of constant water density, the continuity equation of a single cell is:

$$\sum Q_i = SS\frac{\Delta h}{\Delta t}\Delta V \quad (14)$$

Where,

Q_i is a flow rate into the cell (L^3T^{-1});
SS is specific storage, which is the volume of water that can be injected per unit volume of aquifer per unit change in head (L^{-1});
ΔV is the volume of the cell (L^3);
Δh is the head change over the time interval of Δt.

Figure 52 shows the indices of cells that are used for the calculation of flow between adjacent cells.

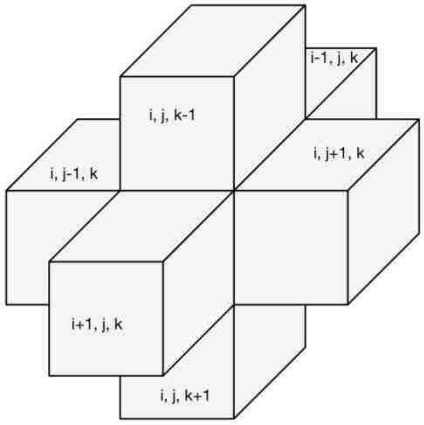

Figure 52. Indices of the Hypothetic Cell (i,j,k) and Its Surrounding Cells (Adapted from Mcdonald & Harbaugh, 1988; Harbaugh et al., 2005).

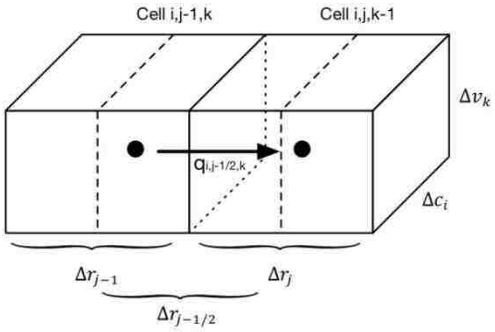

Figure 53. Flow from Cell i,j-1,k To Cell i,j,k (Adapted from Mcdonald & Harbaugh, 1988; Harbaugh et al., 2005).

According to Darcy's law, a one-dimensional stead-state flow passes through a block of aquifer from cell i, j-1, k to cell i, j, k with the cross section area of $\Delta c_i \Delta v_k$ is shown below (*Figure 53):*

$$q_{i,j-1/2,k} = KR_{i,j-1/2,k}\Delta c_i \Delta v_k \frac{(h_{i,j-1,k}-h_{i,j,k})}{\Delta r_{j-1/2}} \quad (15)$$

Where,

$q_{i,j-1/2,k}$ is the volumetric flow rate passing from cell i,j,k to cell i,j-1,k (L^3T^{-1});
$h_{i,j-1,k}$ is the head at the node i,j-1,k;
$\Delta c_i \Delta v_k$ is the cross section area that the flow passes through the row direction;
$\Delta r_{j-1/2}$ is the distance between node i,j,k and node i,j-1,k (L).

Taking into account the flows from the six adjacent cells, the continuity equation with consideration of external rate yields:

$$q_{i,j-1/2,k} + q_{i,j+\frac{1}{2},k} + q_{i-\frac{1}{2},j,k} + q_{i+\frac{1}{2},j,k} + q_{i,j,k-1/2} + q_{i,j,k+1/2} + P_{i,j,k}h_{i,j,k} + Q_{i,j,k} = SS_{i,j,k}(\Delta r_j \Delta c_i \Delta v_k)\frac{\Delta h_{i,j,k}}{\Delta t} \quad (16)$$

Where,

$SS_{i,j,k}$ is the specific storage at cell i,j,k (LT^{-1});
$\Delta r_j \Delta c_i \Delta v_k$ is the volume of cell i,j,k (L^3);
$\frac{\Delta h_{i,j,k}}{\Delta t}$ is the finite-difference approximation of head change with respect to time (LT^{-1});

Thus, the approximation of finite-differences for cell i, j, k is:

$$CR_{i,j-\frac{1}{2},k}(h_{i,j-1,k} - h_{i,j,k}) + CR_{i,j+\frac{1}{2},k}(h_{i,j+1,k} - h_{i,j,k}) + CC_{i-\frac{1}{2},j,k}(h_{i-1,j,k} - h_{i,j,k}) + CC_{i+\frac{1}{2},j,k}(h_{i+1,j,k} - h_{i,j,k}) + CV_{i,j,k-\frac{1}{2}}(h_{i,j,k-1} - h_{i,j,k}) + CV_{i,j,k+\frac{1}{2}}(h_{i,j,k+1} - h_{i,j,k}) + P_{i,j,k}h_{i,j,k} + Q_{i,j,k} = SS_{i,j,k}(\Delta r_j \Delta c_i \Delta v_k)\frac{\Delta h_{i,j,k}}{\Delta t}\ \frac{\Delta h_{i,j,k}}{\Delta t} \quad (17)$$

Where,

$$q_{i,j-1/2,k} = CR_{i,j-\frac{1}{2},k}(h_{i,j-1,k} - h_{i,j,k})$$
$$q_{i,j+1/2,k} = CR_{i,j+\frac{1}{2},k}(h_{i,j+1,k} - h_{i,j,k})$$
$$q_{i-1/2,j,k} = CC_{i-\frac{1}{2},j,k}(h_{i-1,j,k} - h_{i,j,k})$$
$$q_{i+1/2,j,k} = CC_{i+\frac{1}{2},j,k}(h_{i+1,j,k} - h_{i,j,k})$$
$$q_{i,j,k-1/2} = CV_{i,j,k-\frac{1}{2}}(h_{i,j,k-1} - h_{i,j,k})$$
$$q_{i,j,k+1/2} = CV_{i,j,k+\frac{1}{2}}(h_{i,j,k+1} - h_{i,j,k})$$

In order to predict groundwater level at successive times, the transient simulation is considered with a reformulation of the finite-difference equation:

$$CR_{i,j-\frac{1}{2},k}\left(h^m_{i,j-1,k}-h^m_{i,j,k}\right)+CR_{i,j+\frac{1}{2},k}\left(h^m_{i,j+1,k}-h^m_{i,j,k}\right)+CC_{i-\frac{1}{2},j,k}\left(h^m_{i-1,j,k}-h^m_{i,j,k}\right)+CC_{i+\frac{1}{2},j,k}\left(h^m_{i+1,j,k}-h^m_{i,j,k}\right)+CV_{i,j,k-\frac{1}{2}}\left(h^m_{i,j,k-1}-h^m_{i,j,k}\right)+CV_{i,j,k+\frac{1}{2}}(h^m_{i,j,k+1}-h^m_{i,j,k})+P_{i,j,k}h^m_{i,j,k}+Q_{i,j,k}=SS_{i,j,k}(\Delta r_j\Delta c_i\Delta v_k)\frac{h^m_{i,j,k}-h^{m-1}_{i,j,k}}{t^m-t^{m-1}} \quad (18)$$

Where,

t^m refers to the end of the interval at time step m.

This is the backward-difference equation used as the basis for a simulation of the partial differential equation of groundwater flow. The seven head in the equation is unknown, and thus cannot be solved independently; however, the equation can be written for each cell, which will make only one unknown in one cell. In the system there are “n” equations with “n” unknowns, therefore, the system can be solved simultaneously, given the initial head distribution, the boundary condition, the hydraulic parameters, and external stresses.

6.2 Coupling algorithms in GSFLOW

6.2.1 Soil Zone

The Soil Zone in PRMS is defined as the area between land surface and vegetation root depth, and the vegetation root depth is termed soil-zone base. Soil Zone is the region where evapotranspiration and horizontal subsurface flow occur. On the basis of physical mechanisms, it is conceptualized into three reservoirs to represent pore-space volumes for a given volume of soil: the capillary, gravity, and preferential reservoirs. All three reservoirs are contained within the same physical space, but they represent different soil-water processes with different soil-water content thresholds.

As shown in Figure 54a, the capillary reservoir is defined by the water content between wilting point to field capacity threshold. The gravity reservoir is defined by the water content between field capacity and soil saturation. The preferential-flow reservoir is that part of the gravity reservoir from which fast interflow occurs, and it is defined by the preferential-flow threshold. Preferential flow refers to the uneven and often rapid water movement through porous media, such as wormholes, root holes, and racks (Markstrom et al., 2005).

Through defying the water-content thresholds, which are determined by soil types combined with wilting point, field capacity, preferential-flow threshold, and saturation threshold, water storage and water flow features can be determined for each reservoir (Figure 54b).

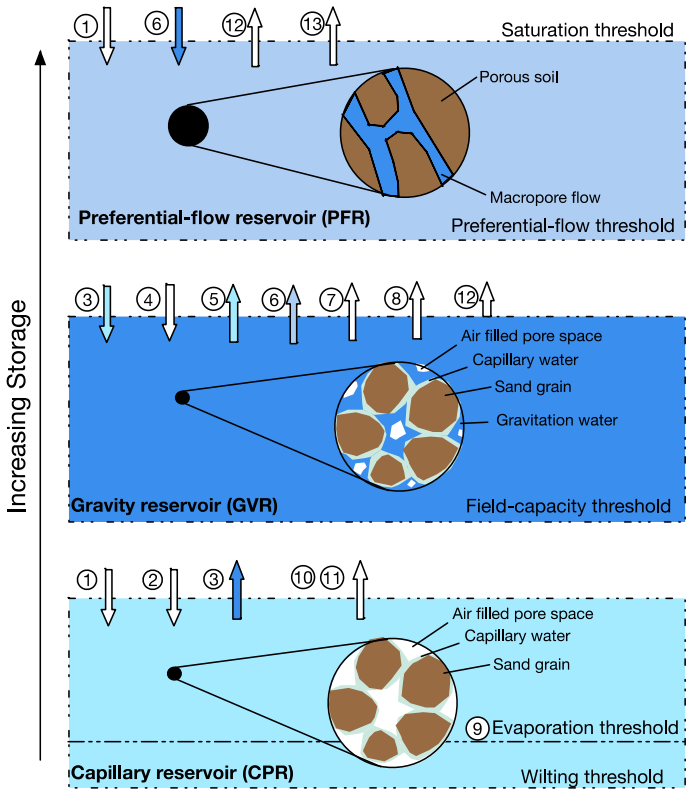

(a)

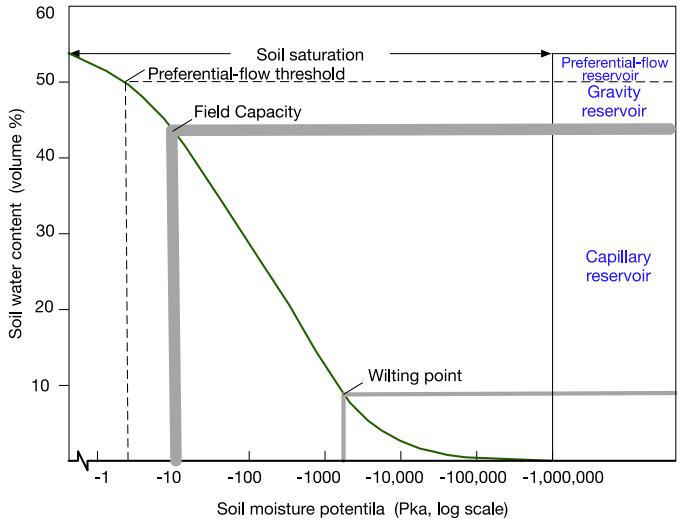

(b)

Figure 54. The Conceptualization in Soil Zone Consists of Three Reservoirs: Capillary, Gravity, and Preferential-Flow. They Represent the Pore-Space Volumes for a Given Volume of Soil, Which Can Be Defined by: (A) Physical And Mathematical Definition Of Each Reservoir (Markstrom et al., 2005), and (B) Soil Content Definition for Each Reservoir Using Soil Moisture Retention Curve (Modified based on Soil Science, Lajos, 2008).

Different from the PRMS model (Figure 15 & Table 5), the soil zone simulation in GSFLOW model has considerable changes. The procedure of 1st part Dunnian runoff generation from the Preferential-flow Reservoir was removed. Regarding the interactive flows of recharges and discharges between surface water and groundwater, the GSFLOW model uses two-way water flows instead of one-way water flow in the PRMS model. The two-way water flow not only allows water flowing downward from soil zone to unsaturated zone, but also allows the groundwater replenish upward from unsaturated zone to soil zone. It includes, as shown in Table 21 & Figure 54, the computation of groundwater replenishment from groundwater to Gravity reservoir (step 4) and the computation of Capillary Reservoir replenishment from Gravity Reservoir (step 5).

Table 21

Sequence of Steps Used in the Computation of Flow into and out of the Soil Zone Used in GSFLOW (Markstrom et al., 2005).

Sequence No.	Description of flow into and out of soil zone
1	Partition infiltration between capillary and Preferential-flow Reservoir.
2	Add interflow and Dunnian runoff (Dunne & Black, 1970) from upslope to Capillary Reservoir.
3	Add excess inflow from the Capillary Reservoir to the Groundwater Reservoir up to a recharging threshold; move the remaining excess inflow to the Gravity Reservoir.
4	Add groundwater from MODFLOW discharge to the Gravity Reservoir
5	Replenish Capillary Reservoir from Gravity Reservoir when Capillary Reservoir storage is below field capacity
6	Move a fraction of water in the Gravity Reservoir to the Preferential-flow Reservoir
7	Calculate slow interflow from gravity reservoirs.
8	Calculate gravity drainage from the Gravity Reservoir to the Groundwater Reservoir.
9	Partition Capillary Reservoir into two zones: upper zone and lower zone, where occurs evapotranspiration and transpiration, respectively.
10	Calculate the transpiration from the lower zone of the Capillary Reservoir.
11	Calculate the evapotranspiration from the upper zone of the Capillary Reservoir.
12	Calculate Dunnian runoff from Preferential-flow Reservoir when its storage is none zero, or directly from Gravity Reservoir when the storage is zero
13	Compute fast interflow from Preferential-flow Reservoir.

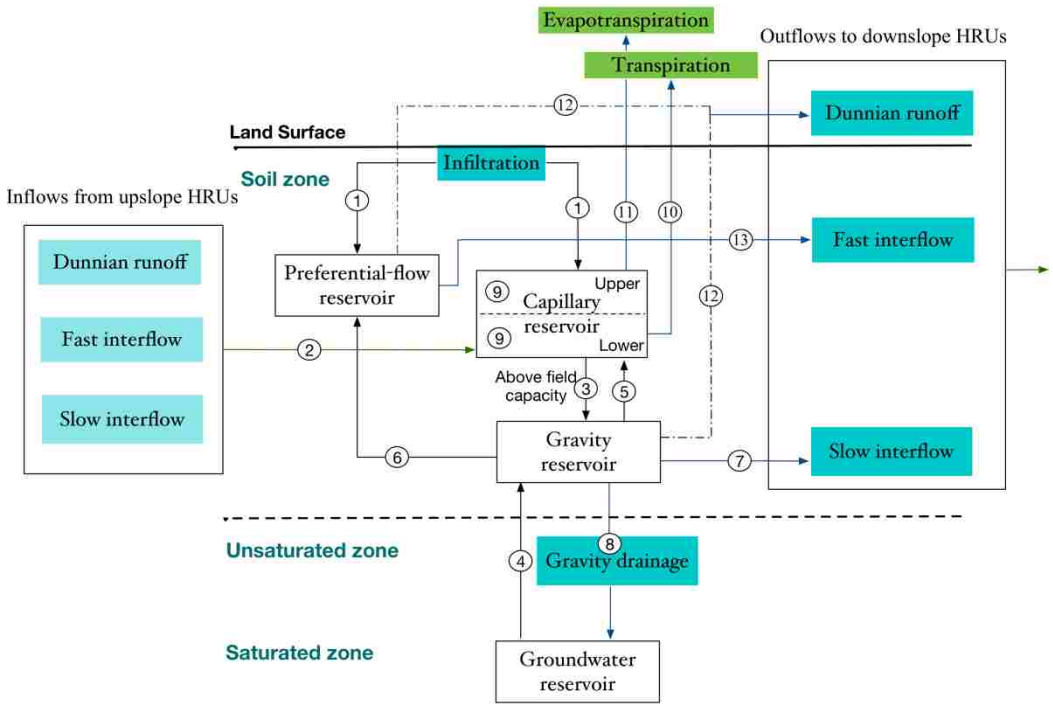

Figure 55. Inflow and Outflow Diagram of Three Conceptualized Reservoirs in Soil-Zone: Capillary, Gravity, and Preferential-Flow Reservoirs in PRMS for a Single HRU.

A main assumption in the soil zone is that the soil type is uniformly simulated in the calculation unit –Hydrologic Response Unit (HRU) - throughout the simulation period, which means the parameters that define the flow and storage are constant for each of the HRU during a simulation. Other important assumptions include: the soil parameters, due to the processes of temperature change, e.g. freezing and thawing, are not affected during a simulation; the water-flow features in the capillary reservoir, which are defined by a constant value of root depth, is not affected by the changes in vegetation, e.g., growing and dying; the soil perturbation results in preferential flow remaining constant during a model simulation.

6.2.2 **Unsaturated Zone**[5]

The Unsaturated Zone is simulated using the Unsaturated-Zone Flow (UZF1) package in MODFLOW, which simulates water flow and storage in the unsaturated zone and is partitioned into evapotranspiration and groundwater recharge. The water flow in the unsaturated zone, on a larger scale, such as a watershed scale, is dominated by vertical flow. Thus, one assumption is that the unsaturated zone is homogeneous in the vertical direction. Besides, the diffusive gradients and capillary pressure gradients are negligible, and capillary fringe is not simulated.

On the basis of these assumptions, a one dimension finite-difference form of Richards' equation is used with kinematic-wave approximation, considering evapotranspiration losses:

$$\frac{\partial \theta}{\partial t} + \frac{\partial K(\theta)}{\partial z} + i = 0 \tag{19}$$

where,

θ is the volumetric water content, in volume of water per volume of rock (L^3/L^3);
z is the altitude in the vertical direction in length (L);
$K(\theta)$ is the unsaturated hydraulic conductivity as a function of water content and is equal to the vertical flux in length per time (L/T);
i is the evapotranspiration rate beneath the soil-zone base per unit depth in length per time per length (LT^{-1}/L) and;
t is time (T).

The resulted characteristic equations are:

$$\frac{dz}{dt} = \frac{\partial K(\theta)}{\partial z} = v(\theta) \tag{20}$$

$$\frac{d\theta}{dz} = \frac{-i}{v(\theta)} \tag{21}$$

$$\frac{d\theta}{dt} = -i \tag{22}$$

where,

[5] The descriptions and equations in this subsection are sourced from Niswonger et al. (2006), where details can be found.

$v(\theta)$ is the characteristic velocity restricted to the downward (positive z) direction, in length per time (L/T).

The wetting front velocity can be derived by the following equation with a control volume integrated that contains the wetting front, and details of derivation can be found in Niswonger et al. (2006):

$$\frac{dz_f}{dt} = u_s\left(\theta_{z_1}, \theta_{z_2}\right) = \frac{K\left(\theta_{z_1}\right) - K\left(\theta_{z_2}\right)}{\theta_{z_1} - \theta_{z_2}} \tag{23}$$

where,

u_s is the velocity of the wetting front, in length per time (L/T);
z_1 and z_2 are the points before and after the wetting front at a distance far enough that $\frac{\partial_\theta}{dz} \approx 0$, in length (L).

In order to estimate the unsaturated hydraulic conductivity, the Brooks-Corey method is used (Brooks & Corey, 1966):

$$K(\theta) = K_s\left[\frac{\theta - \theta_r}{\theta_s - \theta_r}\right]^{\varepsilon} \tag{24}$$

where,

K_s is the saturated hydraulic conductivity (L/T);
θ_r is the residual water content, in volume of water per volume of rock (L^3/L^3);
θ_s is the saturated water content, in volume of water per volume of rock (L^3/L^3); and
ε is the Brooks-Corey exponent, dimensionless.

6.2.3 **Interactions between Soil Zone and Unsaturated Zone[6]**

The gravity drainage from Soil Zone to Unsaturated Zone is calculated on the basis of the storage of gravity reservoir and the hydraulic conductivity (K_s) of the unsaturated zone.

First, potential gravity drainage is defined based on the groundwater head and the vertical hydraulic conductivity of the connecting face:

$$q_{gd,pot}^{m,n} = coeflin\left[\frac{D_{GVR}^{m,n}}{Dmx}\right]^{coefex} \tag{25}$$

[6] Descriptions and equations are sourced in this subsection are from Markstrom et al. (2008), where details can be found.

where,

$q_{gd,pot}^{m,n}$ is the potential gravity drainage for time step m, iteration n, per unit area, in inches per day;
$coeflin$ is the linear coefficient used to compute gravity drainage from the gravity reservoir, in inches per day;
$coefex$ is the exponent coefficient used to compute gravity drainage from the gravity reservoir, dimensionless;
Dmx is the maximum gravity drainage from the gravity reservoir, in inches.

Second, the actual gravity drainage to the unsaturated zone depends on the conditions in the unsaturated zone. That means the actual gravity drainage equals to potential gravity drainage, or equals to the hydraulic conductivity when the potential gravity drainage exceeds the hydraulic conductivity in the unsaturated zone.

The volumetric water content at the top of the unsaturated zone is calculated from potential gravity drainage and the Brooks-Corey equation (1966):

$$\theta^{m,n} = \left(\frac{q_{gd,pot}^{m,n}}{K_s}\right)^{1/\varepsilon}(S_y) + \theta_r \qquad 0 < q_{gd,pot}^{m,n} < K_s \tag{26}$$

$$\theta^{m,n} = \theta_s \qquad K_s < q_{gd,pot}^{m,n} \tag{27}$$

Where,

$\theta^{m,n}$ is the water content at the top of the unsaturated zone for time step m, iteration n, dimensionless;
S_y is the specific yield, approximated by $\theta_s - \theta_r$, dimensionless;
θ_r is the residual water content, in volume of water per volume of rock (L^3/L^3); and
θ_s is the saturated water content, in volume of water per volume of rock (L^3/L^3).

References

Abatzoglou, J. T., & Brown, T. J. (2012) A comparison of statistical downscaling methods suited for wildfire applications. *International Journal of Climatology, 32,* 772-780. http://doi.org/10.1002/joc.2312.

Abbott, M. B., Bathurst, J. C., Cunge, J. A., O'Connell, P. E., & Rasmussen, J. (1986). An introduction to the European Hydrological System - Systeme Hydrologique Europeen, "SHE", 1: History and philosophy of a physically-based, distributed modelling system. *Journal of Hydrology*, *87*(1–2), 45–59. http://doi.org/10.1016/0022-1694(86)90114-9

Aguilera, H., & Murillo, J.M. (2009). The effect of possible climate change on natural groundwater recharge based on a simple model: a study of four karstic aquifers in SE Spain. *Environmental Geology*, 57(5), 963-974. http://doi.org/10.1007/s00254-008-1381-2

Ahmad, M. M., Ghumman, A. R., & Ahmad, S. (2009). Estimation of Clark's instantaneous unit hydrograph parameters and development of direct surface runoff hydrograph. *Water resources management*, *23*(12), 2417-2435. https://doi.org/10.1007/s11269-008-9388-8

Ahmad, M. M., Ghumman, A. R., Ahmad, S., & Hashmi, H. N. (2010). Estimation of a unique pair of Nash model parameters: an optimization approach. *Water resources management*, *24*(12), 2971-2989. https://doi.org/10.1007/s11269-010-9590-3

Ahmad, S., & Prashar, D. (2010). Evaluating municipal water conservation policies using a dynamic simulation model. *Water Resources Management*, *24*(13), 3371-3395. https://doi.org/10.1007/s11269-010-9611-2

Ahmad, S., & Simonovic, S. P. (1999). Comparison of one-dimensional and two-dimensional hydrodynamic modeling approaches for Red river basin. *Report to the International Joint Commission-Red River Basin Task Force, Ottawa, Washington* 1-51.

Ahmad, S., & Simonovic, S. P. (2000). System dynamics modeling of reservoir operations for flood management. *Journal of Computing in Civil Engineering*, *14*(3), 190-198. https://doi.org/10.1061/(ASCE)0887-3801(2000)14:3(190)

Ahmad, S., & Simonovic, S. P. (2001a). Integration of heuristic knowledge with analytical tools for the selection of flood damage reduction measures. *Canadian Journal of Civil Engineering*, *28*(2), 208-221. https://doi.org/10.1139/l00-097

Ahmad, S., & Simonovic, S. P. (2001b). A decision support tool for evaluation of impacts of flood management policies. *Hydrological Science and Technology*, *17*(1-4), 11.

Ahmad, S., & Simonovic, S. P. (2001c). Modeling human behavior for evacuation planning: A system dynamics approach. In *Bridging the Gap: Meeting the World's Water and Environmental Resources Challenges* (pp. 1-10). https://doi.org/10.1061/40569(2001)462

Ahmad, S., & Simonovic, S. P. (2001d). Modeling Dynamic Processes in Space and Time--A Spatial System Dynamics Approach. In *Bridging the Gap: Meeting the World's Water and Environmental Resources Challenges* (pp. 1-20). https://doi.org/10.1061/40569(2001)88

Ahmad, S., & Simonovic, S. P. (2005). An artificial neural network model for generating hydrograph from hydro-meteorological parameters. *Journal of Hydrology*, *315*(1), 236-251. https://doi.org/10.1016/j.jhydrol.2005.03.032

Ahmad, S., & Simonovic, S. P. (2006). An intelligent decision support system for management of floods. *Water Resources Management*, *20*(3), 391-410. https://doi.org/10.1007/s11269-006-0326-3

Ahmad, S., Kalra, A., & Stephen, H. (2010). Estimating soil moisture using remote sensing data: A machine learning approach. *Advances in Water Resources*, *33*(1), 69-80. https://doi.org/10.1016/j.advwatres.2009.10.008

Akan, A. O., & Yen, B. C. (1981). Mathematical model of shallow water flow over porous media. Journal of the hydraulics division, 107(4), 479-494. http://doi.org/10.1061/9780784480113.008

Albano, C. M., Dettinger, M. D., McCarthy, M. I., Schaller, K. D., Welborn, T. L., & Cox, D. A. (2016). Application of an extreme winter storm scenario to identify vulnerabilities, mitigation options, and science needs in the Sierra Nevada mountains, USA. *Natural Hazards*, *80*(2), 879-900. http://doi.org/10.1007/s11069-015-2003-4

Allander, K. K., Niswonger, R. G., & Jeton, A. E. (2014). Simulation of the Lower Walker River Basin Hydrologic System , West-Central Nevada , Using PRMS and MODFLOW Models Scientific Investigations Report 2014 - 5190.

Amoueyan, E., Ahmad, S., Eisenberg, J. N., Pecson, B., & Gerrity, D. (2017). Quantifying pathogen risks associated with potable reuse: A risk assessment case study for Cryptosporidium. *Water Research*, *119*, 252-266. http://doi.org/10.1016/j.watres.2017.04.048

Anderson, M. P., Woessner, W. W., & Hunt, R. J. (2015). *Applied groundwater modeling: simulation of flow and advective transport*. Academic Press.

Anderson, M.P., & Woessner, W.W. (1991). Applied Groundwater Modeling: simulation of flow and advective transport. San Diego, Academic Press.

Aquifer tests at Baker. (n.d.). Retrieved December 1, 2016, from http://nevada.usgs.gov/water/AquiferTests/snake_val-ley_baker.cfm?studyname=snake_valley_baker

Arndt, D.S., Baringer, M.O., & Johnson, M.R. (Eds.). (2010). State of the climate in 2009. *Bulletin of the American Meteorological Society*, 91(7), S1-S224.

Arnell, N.W. (1992). Factors controlling the effects of climate change on river flow regimes in a humid temperate environment. *Journal of Hydrology*, *132*,321-342. http://doi.org/10.1016/0022-1694(92)90184-W

Arnell, N.W., & Reynard, N.S. (1989). Estimating the impacts of climatic change on river flows: Some examples from Britain, *Proceedings of the Conference on Climate and Water*, Helsinki, Finland, *1*, 413- 425.

Arnold, J. G., Allen, P. M., & Bernhardt, G. (1993). A comprehensive surface-groundwater flow model. *Journal of Hydrology*, *142*(1–4), 47–69. http://doi.org/10.1016/0022-1694(93)90004-S

Baldocchi, D., & Wong, S. (2008). Accumulated winter chill is decreasing in the fruit growing regions of California. *Climatic Change*, *87*, 153-166. http://doi.org/10.1007/s10584-007-9367-8

Baldwin, C. K., Wagner, F. H., & Lall, U. (2003). Rocky Mountain/Great Basin Regional Climate-Change Assessment. In Wagner, F. H. (Ed.). Report of the U.S. Global Change Research Program. Utah State University, Logan, UT.

Barnett, T.P., Pierce, D.W., Hidalgo, H.G., Bonfils, C., Santer, B.D., Das, T., Bala, G., Wood, A.W., Nozawa, T., Mirin, A.A., Cayan, D.R., & Dettinger, M.D. (2008). Human- induced changes in the hydrology of western United States. *Science*, *319* (5866), 1080-1083. http://doi.org/10.1126/science.1152538

Bates, B., Kundzewicz, Z.W., Wu, S., & Palutikof, J.P. (2008). Climate Change and Water. Technical Paper VI of the Intergovernmental Panel on Climate Change. Intergovernmental Panel on Climate Change Secretariat, Geneva Climate Change and Water. Technical Paper VI of the Intergovernmental Panel on Climate Change.

Battaglin, W. A., Hay, L. E., & Markstrom, S. L. (2012). Watershed Scale Response to Climate Change-East River Basin, Colorado. U.S. Geologic Survey. Fact sheet 2011-3126.

Becker, R. A., Chambers, J. M. and Wilks, A. R. (1988) The New S Language. Wadsworth & Brooks/Cole (for S version).

Bell, J., Andrew,N.L., Batty,M.J., Chapman, L.B., Dambacher, J.M., Dawson, B., Ganachaud, A.S., Gehrke, P.C., Hampton, J., Hobday, A.J., Hoegh-Guldberg, O., Johnson, J.E., Kinch, J.P., Le

Borgne, R., Lehody, P., Lough, J.M., Pickering, T.D., Pratchett, M.S., Vunisea, A. & Waycott. M. (2011). Adapting tropical Pacific fisheries and aquaculture to climate change: management measures, policies and investments. In: Vulnerability of Tropical Pacific Fisheries and Aquaculture to Climate Change [Bell, J.D., J.E. Johnson, and A.J. Hobday (eds.). Secretariat of the Pacific Community, Noumea, New Caledonia.

Benestad, R.E. (2001) A comparison between two empirical downscaling strategies. *International Journal of Climatology, 21,* 1645-1668. http://doi.org/10.1002/joc.703

Beven, K.J. (2000). Rainfall-Runoff Modelling The Primer. John Wiley&Sons, Ltd. Baffins Lane, Chichester, West Sussex PO19 1UD, England.

Bjerklie, D. M., Hay, L. E., & Markstrom, S. L. (2012). Watershed Scale Response to Climate Change-Pomperaug River Watershed, Connecticut. U.S. Geologic Survey. Fact sheet 2011-3122.

Boé, J., Terray, L., Habets, & F., Martin, E. (2007). Statistical and dynamical downscaling of the Seine basin climate for hydro-meteorological studies. *International Journal of Climatology, 27,* 1643-1655. http://doi.org/10.1002/joc

Braconnot, P., Harrison, S. P., Otto-Bliesner, B. L., Abe-Ouchi, A., Jungclaus, J., & Peterschmitt, J.-Y. (2011). The Paleoclimate Modeling Intercomparison Project contribution to CMIP5. *CLIVAR Exchanges*, *16*(56), 15–19.

Brandsma, T., & Buishand, T.A. (1998). Simulation of extreme precipitation in the Rhine basin by nearest-neighbour resampling. *Hydrology and Earth System Sciences*, *2*, 195-209. http://dx.doi.org/10.5194/hess-2-195-1998

Brekke, L. D., Thrasher, B. L., Maurer, E. P., & Pruitt, T. (2013). Downscaled CMIP3 and CMIP5 Climate and Hydrology Projections: Release of Downscaled CMIP5 Climate Projections, Comparison with preceding Information, and Summary of User Needs, (May), 116 p. Retrieved from http://gdo-dcp.ucllnl.org/downscaled_cmip_projections/techmemo/downscaled_climate.pdf

Brewer, P.G., & Peltzer, E.T. (2009). Limits to marine life. *Science*, *324*(5925), 347- 348. http://dx.doi.org/10.1126/science.1170756

Brookfield, A., Gnau, C., & Wilson, B. (2017). Incorporating surface water operations in an integrated hydrologic model: Model development and application to the lower Republican River Basin, United States. *Journal of Hydrologic Engineering*, *22*(4), 4016065. http://doi.org/10.1061/(ASCE)HE.1943-5584.0001486

Brooks, L. E., Masbruch, M. D., Sweetkind, D. S., & Buto, S. G. (2014). Steady-State Numerical Groundwater Flow Model of the Great Basin Carbonate and Alluvial Aquifer System. *USGS Report*.

Brooks, R. H., & Corey, A. T. (1966). Properties of Porous Media Affecting Fluid Flow. *Journal of the Irrigation and Drainage Division*. Retrieved from http://cedb.asce.org/cgi/WWWdisplay.cgi?14175

Burnash, R.J.C., Ferral, R.L., & McGuire, R.A. (1973). A Generalized Streamflow Simulation System, Conceptual Modeling for Digital Computer , U.S. Department of Commerce, National Weather Service and State of California, Department of Water Resources, Sacramento, CA.

Campolongo, F., Cariboni, J., & Saltelli, A. (2007). An effective screening design for sensitivity analysis of large models. *Environmental Modelling and Software*, *22*(10), 1509–1518. http://doi.org/10.1016/j.envsoft.2006.10.004

Cannon, A. J., Sobie, S. R., & Murdock, T. Q. (2015). Bias Correction of GCM Precipitation by Quantile Mapping: How Well Do Methods Preserve Changes in Quantiles and Extremes? *Journal of Climate*, *28*(17), 6938–6959. http://doi.org/10.1175/JCLI-D-14-00754.1

Carrier, C., Kalra, A., & Ahmad, S. (2013). Using paleo reconstructions to improve streamflow forecast lead time in the western United States. *JAWRA Journal of the American Water Resources Association*, *49*(6), 1351-1366. https://doi.org/ 10.1111/jawr.12088

Carrier, C., Kalra, A., & Ahmad, S. (2016). Histo rical tem mporal l variati ion in precipita p ation ov ver We stern Hima alayan Region :, *13*, 672–681. http://doi.org/10.1007/s11629

Carter, T.R., Parry, M.L., Harasawa, H., & Nishioka, S. (1994). IPCC technical guidelines for assessing climate change impacts and adaptations. Special Report toWorking Group II, Intergovernment Panel on Climate Change.

Chambers, J. C. (2008). Climate Change and the Great Basin. *Management and Research in the Great Basin—*, (Wagner 2003), 29–32. Retrieved from http://www.sagestep.org/educational_resources/bibliographies/articles/Chambersetal2008.pdf#page=35

Chase, K. J., Hay, L. E., & Markstrom, S. L. (2012). Watershed Scale Response to Climate Change--South Fork Flathead River Basin, Montana. U.S. Geologic Survey. Fact sheet 2011-3124.

Chen, C., Kalra, A., & Ahmad, S. (2015a). Exploring Water Management Strategies in an Inland Arid Area Using Dynamic Simulation Model. In *World Environmental and Water Resources Congress 2015* (pp. 1009-1018). https://doi.org/10.1061/9780784479162.098

Chen, C., Fenstermaker, L., Stephen, H., & Ahmad, S. (2015b). Distributed Hydrological Modeling for a Snow Dominant Watershed Using a Precipitation and Runoff Modeling System. In *World Environmental and Water Resources Congress 2015* (2527-2536). https://doi.org/10.1061/9780784479162.248

Chen, C., Ahmad, S., Mejia, J., & Kalra, A. (2016). Study of Lehman Creek Watershed's Hydrologic Response to Climate Change Using Downscaled CMIP5 Projections. In *World Environmental and Water Resources Congress 2016,* (508-517). https://doi.org/10.1061/9780784479872.052

Chen, C., Ahmad, S., Kalra, A., & Xu, Z. X. (2017a). A dynamic model for exploring water-resource management scenarios in an inland arid area: Shanshan County, Northwestern China. *Journal of Mountain Science*, *14*(6), 1039-1057. https://doi.org/10.1007/s11629-016-4210-1

Chen, C., Kalra, A., & Ahmad, S. (2017b). A Conceptualized Groundwater Flow Model Development for Integration with Surface Hydrology Model. In *World Environmental and Water Resources Congress 2017* (pp. 175-187). https://doi.org/10.1061/9780784480601.017

Chiew, F. H. S., & McMahon, T. A. (2002). Modelling the impacts of climate change on Australian streamflow. Hydrological Processes, 16 (6), 1235-1245. http://doi.org/10.1002/hyp.1059

Choubin, B., Khalighi-Sigaroodi, S., Malekian, A., Ahmad, S., & Attarod, P. (2014). Drought forecasting in a semi-arid watershed using climate signals: a neuro-fuzzy modeling approach. *Journal of Mountain Science*, *11*(6), 1593-1605. https://doi.org/10.1007/s11629-014-3020-6

Christiansen, D. E., Hay, L. E., & Markstrom, S. L. (2012). Watershed Scale Response to Climate Change--Clear Creek Basin, Iowa. U.S. Geologic Survey. Fact sheet 2011-3127.

Collins, M., Knutti, R., Arblaster, J., Dufresne, J.-L., Fichefet, T., Friedlingstein, P., … Wehner, M. (2013). Long-term Climate Change: Projections, Commitments and Irreversibility. *Climate Change 2013: The Physical Science Basis. Contribution of Working Group I to the Fifth Assessment Report of the Intergovernmental Panel on Climate Change*, 1029–1136. http://doi.org/10.1017/CBO9781107415324.024

Cooley, K.R. (1990). Effects of CO^2 -induced climatic changes on snowpack and streamflow. *Hydrological Sciences Journal*, 35, 511-522. http://dx.doi.org/10.1080/02626669009492455

Court, A. (1962). Measures of streamflow timing. *Journal of Geophysical Research*, *67*(11), 4335–4339. http://doi.org/10.1029/JZ067i011p04335

Cubashi, U., Meehl, G. A., & Boer, G. J. (2001). Projections of future climate change. Pages 525-582, In Houghton, J. T. et al. (Ed.). Climate Change 2001: The Scientific Basis. Contribution of the Working Group I to the Third Assessment Report of the Intergovern- mental Panel on Climate Change. Cambridge University Press.

Dai, A., Qian, T., Trenberth, K.E. & Milliman, J.D. (2009). Changes in continental freshwater discharge from 1948 to 2004. *Journal of Climate*, *22*(10), 2773-2792. http://dx.doi.org/10.1175/2008JCLI2592.1

Davis, P. R. (2001). ISGW - The Integrated Hydrologic Model Coupling HSPF and MODFLOW.

Integrated Surface and Ground Water Management, 100–109.

Dawadi, S., & Ahmad, S. (2012). Changing climatic conditions in the Colorado River Basin: implications for water resources management. *Journal of Hydrology, 430,* 127-141. https://doi.org/10.1016/j.jhydrol.2012.02.010.

Dawadi, S., & Ahmad, S. (2013). Evaluating the impact of demand-side management on water resources under changing climatic conditions and increasing population. *Journal of Environmental Management*, *114*, 261–275. http://doi.org/10.1016/j.jenvman.2012.10.015

Dettinger, M.D., Cayan, D.R., Meyer, M.K., & Jeton, A.E. (2004). Simulated hydrologic responses to climate variations and change in theMerced, Carson, and American river basins, Sierra Nevada, California, 1900–2099. *Climatic Change*, *62*, 283-317. http://doi.org/10.1023/B:CLIM.0000013683.13346.4f

Di Luzio, M., Johnson, G. L., Daly, C., Eischeid, J. K., & Arnold, J. G. (2008). Constructing retrospective gridded daily precipitation and temperature datasets for the conterminous United States. *Journal of Applied Meteorology and Climatology*, *47*(2), 475–497. http://doi.org/10.1175/2007JAMC1356.1

Digital Elevation Models (DEM). (2013). U.S. Geological Survey, National Elevation Dataset. Assessed by: http://nationalmap.gov/elevation.html

Dressler, K. a., Leavesley, G. H., Bales, R. C., & Fassnacht, S. R. (2006). Evaluation of gridded snow water equivalent and satellite snow cover products for mountain basins in a hydrologic model. *Hydrological Processes*, *20*(4), 673–688. http://doi.org/10.1002/hyp.6130

Dudley, R. W., Hay, L. E., Markstrom, S. L., & Hodgkins, G. A. (2012). Watershed Scale Response to Climate Change-Cathance Stream Basin, Maine.

Dullinger, S., Gattringer, A., Thuiller,W., Moser, D., Zimmermann, N.E., Guisan, A., Willner,W., Plutzar, C., Leitner, M., Mang, T., Caccianiga, M., Dirnbock,T., Ertl, S., ischer,A., Lenoir, J., Svenning, J.C., Psomas, A. D., Schmatz, R., Silc, U., Vittoz, P., & Hulber, K. (2012). Extinction

debt of high-mountain plants under twenty-firstcentury climate change. *Nature Climate Change*, 2(8), 619-622. http://10.1038/nclimate1514

Dunne, T., & Black, R. G. (1970). An experimental investigation of runoff production in permeable soils. *Water Reoucres Research*, *6*, 478–490.

Eckhardt, K., & Ulbrich, U. (2003). Potential impacts of climate change on groundwater recharge and streamflow in a central European low mountain range. *Journal of Hydrolology*, *284* (1-4), 244-252. http://dx.doi.org/10.1016/j.jhydrol.2003.08.005

Ehret, U., Zehe, E., Wulfmeyer, V., Warrach-Sagi, K., & Liebert,J. (2012). HESS opinions " Should we apply bias correction to global and regional climate model data?" *Hydrology and Earth System Sciences*, 16, 3391-3404. http://dx.doi.org/10.5194/hess-16-3391-2012

Elliott, P. E., Beck, D. a, & Prudic, D. E. (2006). Characterization of Surface-water Resources in the Great Basin National Park Area and Their Susceptibility to Ground-water Withdrawals in Adjacent Valleys, White Pine County, Nevada, 168.

Ely, D. M., & Kahle, S. C. (2012). Simulation of Groundwater and Surface-Water Resources and Evaluation of Water-Management Alternatives for the Chamokane Creek Basin, Stevens County , Washington.

Eslamian, S. (Eds.). (2014). Handbook of Engineering Hydrology: Modeling, Climate Change, and Variability. Bosa Roca, US: CRC Press, 2014.

Essaid, H., & Hill, B. R. (2014). Watershed-scalemodeling of streamflow change in incised montanemeadows. *Water Resource Research*, *50*, 2657–2678. http://doi.org/10.1002/2013WR014420.Received

Essaid, H., & Hill, B. R. (2014). Watershed-scalemodeling of streamflow change in incised montanemeadows. *Water Resource Research*, *50*, 2657–2678. http://doi.org/10.1002/2013WR014420.Received

Farag, A.A., Khalil, A.A., & Hassanein, M.K. (2010) Chilling requirement for deciduous fruit under climate change in Egypt. *Research Journal of Agriculture and Biological Sciences*, *6*, 815-822. http://dx.doi.org/10.1007/s00484-013-0714-3

Fatichi, S., Vivoni, E. R., Ogden, F. L., Ivanov, V. Y., Mirus, B., Gochis, D., … Tarboton, D. (2016). An overview of current applications, challenges, and future trends in distributed process-based models in hydrology. *Journal of Hydrology*, *537*, 45–60. http://doi.org/10.1016/j.jhydrol.2016.03.026

Fischer, T., Gemmer, M., Liu,L., & Su,B. (2011) Temperature and precipitation trends and dryness/wetness pattern in the Zhujiang River basin, south China, 1961- 2007. *Quaternary International*, *244*(2), 138-148. http://dx.doi.org/10.1016/j.quaint.2010.08.010

Fischer, T., Menz, C., Su, B., & Scholten, T. (2013) Simulated and projected climate extremes in the Zhujiang River basin, south China, using the regional climate model COSMO-CLM. *International Journal of Climatology*, *33*, 2988-3001. http://dx.doi.org/10.1002/joc.3643

Ford, D., Pingel, N., & DeVries, J. J. (2008). *Hydrologic Modeling System Applications Guide*.

Forsee, W. J., & Ahmad, S. (2011). Evaluating urban storm-water infrastructure design in response to projected climate change. *Journal of Hydrologic Engineering*, *16*(11), 865-873. https://doi.org/10.1061/(ASCE)HE.1943-5584.0000383.

Franke, O. L., Reilly, T. E., & Bennett, G. D. (1987). *Definition of boundary and initial conditions in the analysis of saturated ground-water flow systems: an introduction*. US Government Printing Office.

Fulton, J. W., Risser, D. W., Regan, R. S., Walker, J. F., Hunt, R. J., Niswonger, R. G., Hoffman, S. A., & Markstrom, S. L. (2015). Water-Budget and Recharge-Area Simulations for Spring Creek and Nittany Creek Basins and Parts of the Spruce Creek Basin, Centre and Huntingdon Counties, Pennsylvania, Water Years 2000-06. Scientific Investigation Report 2015-5073.

Furman, A. (2008). Modeling Coupled Surface-Subsurface Flow Processes: A Review. *Vadose Zone J*, *7*(2), 741–756. http://doi.org/10.2136/vzj2007.0065

Gamvroudis, C., Dokou, Z., Nikolaidis, N. P., & Karatzas, G. P. (2017). Impacts of surface and

groundwater variability response to future climate change scenarios in a large Mediterranean watershed. *Environmental Earth Sciences*, *76*(11). http://doi.org/10.1007/s12665-017-6721-7

Gao, H., Tang, Q., Shi, X., Zhu, C., & Bohn, T. (2010). Water budget record from Variable Infiltration Capacity (VIC) model. *Algorithm Theoretical Basis Document for Terrestrial Water Cycle Data Records*, (Vic), 120–173. Retrieved from http://scholar.google.com/scholar?hl=en&btnG=Search&q=intitle:Water+Budget+Record+from+Variable+Infiltration+Capacity+(+VIC+)+Model#2

Gemmer, M., Fischer,T., Jiang,T., Su, B. & Liu, L.L. (2011) Trends in precipitation extremes in the Zhujiang River basin, South China. *Journal of Climate*, *24*(3), 750-761. http://dx.doi.org/10.1175/2010JCLI3717.1

Gentine, P., Trot, T.j., Lintner, B.R., & Findell, K.L. (2012). Scaling in Surface Hydrology: Progress and Challenges. *Journal of Contemporary Water Research & Education*, *147*(1), 28-40. http://dx.doi.org/10.1111/j.1936-704X.2012.03105.x.

Ghasemizade, M., & Schirmer, M. (2013). Subsurface flow contribution in the hydrological cycle: Lessons learned and challenges ahead-a review. *Environmental Earth Sciences*, *69*(2), 707-718. http://doi.org/10.1007/s12665-013-2329-8

Giertz, S., Diekkruger, B., Jaeger, A., & Schopp, M. (2006). An interdisciplinary scenario analysis to assess the water availability and water consumption in the upper oueme catchment in Benin. *Advances in Geosciences*, *9*, 3-13. http://doi.org/10.5194/adgeo-9-3-2006

Gilbert, J. M., & Maxwell, R. M. (2017). Examining regional groundwater-surface water dynamics using an integrated hydrologic model of the San Joaquin River basin. *Hydrology and Earth System Sciences*, *21*(2), 923–947. http://doi.org/10.5194/hess-21-923-2017

Giorgi, F., & Mearns,L.O. (1991) Approaches to the simulation of regional climate change: a review. *Reviews of Geophysics*, 29, 191-216. http://doi.org/10.1029/90RG02636

Glassley, W. E., Nitao, J. J., Grant, C. W., Johnson, J. W., Steefel, C. I., & Kercher, J. R. (2003). The impact of climate change on vadose zone pore waters and its implication for long-term monitoring. *Computers and Geosciences*, *29*(3), 399–411. http://doi.org/10.1016/S0098-3004(03)00014-1

Gleick, P.H. (1986). Methods for evaluating the regional hydrologic impacts of global climatic changes. *Journal of Hydrology*, *88*:97-116. http://doi.org/10.1016/0022-1694(86)90199-X

Gleick, P.H. (1987). The development and testing of a water balance model for climate impact assessment: Modelling the Sacramento basin. *Water Resources Research*, 23, 1049-1061. http://doi.org/10.1029/WR023i006p01049

Goddard, L., Mason, S.J., Zebiak, S.E., Ropelewski, C.F., Basher, R., & Cane, M.A. (2001). Current approaches to seasonal to interannual climate predictions. *International Journal of Climatology*, 21, 1111-1152. http://doi.org/10.1002/joc.636

Goderniaux, P., Brouyère, S., Fowler, H. J., Blenkinsop, S., Therrien, R., Orban, P., & Dassargues, A. (2009). Large scale surface–subsurface hydrological model to assess climate change impacts on groundwater reserves. *Journal of Hydrology*, *373*(1), 122–138. http://doi.org/10.1016/j.jhydrol.2009.04.017

Govindaraju, R. S., & Kavvas, M. L. (1991). Dynamics of Moving Boundary Overland Flows Over Infiltrating Surfaces at Hillslopes. *Water Resources Research*, *27*(8), 1885–1898. http://doi.org/10.1029/91WR00689

Green, T. R., Taniguchi, M., Kooi, H., Gurdak, J. J., Allen, D. M., Hiscock, K. M., … Aureli, A. (2011). Beneath the surface of global change: Impacts of climate change on groundwater. *Journal of Hydrology*, *405*(3–4), 532–560. http://doi.org/10.1016/j.jhydrol.2011.05.002

GSFLOW Input Instructions (2015).: A Supplement to Appendix 1 of the GSFLOW manual (USGS TM 6-D1) Information Related to GSFLOW Input Tables, (August), 134–139.

Gudmundsson, L., Bremnes, J. B., Haugen, J. E., & Engen-Skaugen, T. (2012). Technical Note: Downscaling RCM precipitation to the station scale using statistical transformations – A

comparison of methods. *Hydrology and Earth System Sciences, 16*(9), 3383–3390. http://doi.org/10.5194/hess-16-3383-2012

Guo, Y. X., Yang, Z. Y., Qin, D. Y., Chen, G. F., Gao, X. R., & Chen, C. (2012). Development and application of a distributed hydrological model for discharge predictions in un-gauged basins: case study in malian river basin. *HKIE Transactions, 19*(3), 25-32.

Gupta, H.V., Sorooshian, S., & Yapo, P.O. (1999). Status of automatic calibration for hydrologic models: comparison with multilevel expert calibration. *Journal of Hydrologic Engineering, 4* (2), 135-143. http://dx.doi.org/10.1061/(ASCE)1084-0699(1999)4:2(135)

Guzha, A. C. (2008). Integrating Surface and Sub Surface Flow Models of Different Spatial and Temporal Scales Using Potential Coupling Interfaces Integrating Surface and Sub Surface Flow Models of Different Spatial and Temporal Scales Using Potential Coupling Interfaces.

Haerter, J. O., Hagemann, S., Moseley, C., & Piani, C. (2011) Climate model bias correction and the role of timescales. *Hydrology and Earth System Sciences*, 15, 1065-1079. http://doi.org/10.5194/hess-15-1065- 2011.

Hagemann, S., Chen, C., Haerter, J. O., Heinke, J., Gerten, D., & Piani, C. (2011). Impact of a Statistical Bias Correction on the Projected Hydrological Changes Obtained from Three GCMs and Two Hydrology Models. *Journal of Hydrometeorology*, *12*(4), 556–578. http://doi.org/10.1175/2011JHM1336.1

Haitjema, H. M., & Mitchell-Bruker, S. (2005). Are water tables a subdued replica of the topography? *Ground Water*, *43*(6), 781–786. http://doi.org/10.1111/j.1745-6584.2005.00090.x

Hall, F. R. (1968). Base‐Flow Recessions—A Review. *Water Resources Research*, *4*(5), 973–983. http://doi.org/10.1029/WR004i005p00973

Halladay, O. J., & Peacock, V. L. (1972). The Lehman Caves Story. Baker, Nevada: Lehman Caves Natural History Association.

Hamel, P., Daly, E., & Fletcher, T. D. (2013). Source-control stormwater management for mitigating the

impacts of urbanisation on baseflow: A review. *Journal of Hydrology*, *485*, 201–211. http://doi.org/10.1016/j.jhydrol.2013.01.001

Hamon, W.R. (1961). Estimating potential evapotranspiration: Proceedings of the American Society of Civil Engineers. *Journal of the Hydraulic Division*, 87(3), 107-120.

Harbaugh, B. A. W., Norton, G. a, & Survey, U. S. G. (2005). MODFLOW-2005 , The U . S . Geological Survey Modular Ground-Water Model - the Ground-Water Flow Process.

Hargreaves, G.H., & Samani, Z.A. (1985). Reference crop evapotranspiration from temperature. *Applied Engineering in Agriculture*, *1*(2), 96-99. http://doi.org/10.13031/2013.26773

Harrill, J.R., & Prudic, D.E. (1998), Aquifer systems in the Great Basin region of Nevada, Utah, and adjacent states— Summary report: U.S. Geological Survey Professional Paper 1409-A.

Hashmi, M.Z., Shamseldin, A.Y., & Melville, B.W. (2012). Statistically downscaled probabilistic multi-model ensemble projections of precipitation change in a watershed. *Hydrological Processes*, 27, 1021- 1032. http://doi.org/10.1002/hyp.8413

Hassan, S. M. T., Lubczynski, M. W., Niswonger, R. G., & Su, Z. (2014). Surface-groundwater interactions in hard rocks in Sardon Catchment of western Spain: An integrated modeling approach. *Journal of Hydrology*, *517*, 390–410. http://doi.org/10.1016/j.jhydrol.2014.05.026

Hay, L. E., & Clark, M. P. (2003). Use of statistically and dynamically downscaled atmospheric model output for hydrologic simulations in three mountainous basins in the western United States. *Journal of Hydrology*, *282*(1–4), 56–75. http://doi.org/10.1016/S0022-1694(03)00252-X

Hay, L. E., & Markstrom S. L. (2012). Watershed Scale Response to Climate Change--Flint River Basin, Georgia. U.S. Geological Survey. Fact sheet 2011-3116.

Hay, L. E., Battaglin, W. A., & Markstrom, S. L. (2012). Watershed Scale Response to Climate Change—Yampa River Basin, Colorado, (March).

Hay, L. E., Leavesley, G. H., Clark, M. P., Markstrom, S. L., Viger, R. J., & Umemoto, M. (2007). Step

Wise , Multiple Objective Calibration Of A Hydrologic Model For A Snowmelt Dominated Basin, *80225*, 877–890.

Hay, L. E., Leavesley, G. H., Clark, M. P., Markstrom, S. L., Viger, R. J., & Umemoto, M. (2007). Step wise , multiple objective calibration of a hydrologic model for a snowmelt dominated basin, *80225*, 877-890. http://doi.org/10.1111/j.1752-1688.2006.tb04501.x

Hay, L.E. & Umemoto, M. (2006). Multiple-Objective Stepwise Cal- ibration Using Luca. USGS Open-File Report 2006-1323.

Hay, L.E., Clark, M.P., Wilby, R.L., Gutowski, W.J., Leavesley, G.G., Pan, Z., Arritt, R.W., & Takle, E.S. (2002). Use of regional climate model output for hydrologic simulations. *Journal of Hydrometeorology*, 3, 571-590. http://dx.doi.org/10.1175/1525-7541(2002)003<0571:UORCMO>2.0.CO;2

Hayhoe, K.,Wake, C., Anderson, B., Liang, X.-Z.,Maurer, E., Zhu, J., Bradbury, J., DeGaetano, A., Stoner, A., & Wuebbles, D. (2008). Regional climate change projections for the Northeast USA, Mit- igation and Adaptation Strategies for Global Change, 13, 425- 436, http://doi.org/10.1007/s11027-007-9133-2

Heilweil, V., & Brooks, L. (2011). Conceptual model of the Great Basin carbonate and alluvial aquifer system. *U.S. Geological Survey Scientific Investigations Report 2010-5193*, 191. Retrieved from http://pubs.usgs.gov/sir/2010/5193/

Hodgkins, G. A., & Dudley, R. W. (2006). Changes in the timing of winter-spring streamflows in eastern North America, 1913-2002. *Geophysical Research Letters*, *33*(6), 1–5. http://doi.org/10.1029/2005GL025593

Homer, C.G., Dewitz, J.A., Yang, L., Jin, S., Danielson, P., Xian, G., Coulston, J., Herold, N.D., Wickham, J.D., & Megown, K. (2015). Completion of the 2011 National Land Cover Database for the conterminous United States-Representing a decade of land cover change information.

Hood, J. W., & Rush, F. E. (1965). *Water-Rsources Appraisal of The Snake Valley Area, Utah and Nevada*.

Hose, R.K., & Blake, M.C., Jr. (1976) Geology and mineral resources of White Pine County, Nevada, Part I, Geology: Nevada Bureau of Mines and Geology Bulletin 85.

Houghton, J.G., Sakamoto, C.M., & Gifford, R.O. (1975) Nevada's weather and climate: Nevada Bureau of Mines and Geology Special Publication 2.

Hsiang, S.M. (2010). Temperatures and cyclones strongly associated with economic production in the Caribbean and Central America. *Proceedings of the National Academy of Sciences of the United States of America*, 107(35), 15367-15372. http://doi.org/10.1073/pnas.1009510107

Hunt, R. J., Walker, J. F., Selbig, W. R., Westenbroek, S. M., & Regan, R. S. (2013). Simulation of Climate - Change effects on streamflow, Lake water budgets, and stream temperature using GSFLOW and SNTEMP, Trout Lake Watershed, Wisconsin. *USGS Scientific Investigations Report.*, 2013–5159.

Hunt, R. J., Walker, J. F., Westenbroek, S. M., Hay, L. E., & Markstrom, S. L. (2012). Watershed Scale Response to Climate Change-Black Earth Creek Basin, Wisconsin. U.S. Geologic Survey. Fact sheet 2011-3129.

Huntington, J. L., & Niswonger, R. G. (2012). Role of surface-water and groundwater interactions on projected summertime streamflow in snow dominated regions: An integrated modeling approach. *Water Resources Research*, *48*(11), 1–20. http://doi.org/10.1029/2012WR012319

Hwang, H. T., Park, Y. J., Frey, S. K., Berg, S. J., & Sudicky, E. A. (2015). A simple iterative method for estimating evapotranspiration with integrated surface/subsurface flow models. *Journal of Hydrology*, *531*, 949–959. http://doi.org/10.1016/j.jhydrol.2015.10.003

Ines, A. V. M., & Hansen, J. W. (2006). Bias correction of daily GCM rainfall for crop simulation studies. *Agricultural and Forest Meteorology*, *138*(1-4), 44-53. http://doi.org/10.1016/j.agrformet.2006.03.009

IPCC, (2014). *Climate Change 2014: Synthesis Report*. Contribution of Working Groups I, II and III to the Fifth Assessment Report of the Intergovernmental Panel on Climate Change.

IPCC. (2007). *Climate change 2007. Mitigation of climate change.* Contribution of Working Groups III to the Forth Assessment Report of the Intergovernmental Panel on Climate Change. http://dx.doi.org/10.1017/CBO9780511546013

Jakob Themeßl, M., Gobiet, A., & Leuprecht, A. (2011). Empirical-statistical downscaling and error correction of daily precipitation from regional climate models. *International Journal of Climatology*, *31*(10), 1530–1544. http://doi.org/10.1002/joc.2168

Jeelani, G. (2008). Aquifer response to regional climate variability in a part of Kashmir Himalaya in India. *Hydrogeology Journal*, *16*(8), 1625-1633. http://doi.org/10.1007/s10040-008-0335-9

Jensen, M.E., & Haise, H.R. (1963). Estimating evapotrans- piration from solar radiation: Proceedings of the American Society of Civil Engineers. *Journal of Irrigation and Drainage*, 89, 15-41. http://dx.doi.org/10.1061/(ASCE)0733-9437(2000)126:4(265)

Jensen, M.E., Rob, D.C.N., & Franzoy, C.E. (1969). Scheduling irrigations using climate-crop-soil data, Proceedings: New Orleans, La., National Conference on Water Resources Engineering of the American Society of Civil Engineers, 20.

Jeton, A. E. (1999). Precipitation-Runoff Simulations for the lake Tahoe Basin, California and Nevada. U.S. Dept. of the Interior, U.S. Geological Survey: 99-4110

Jeton, A. E. (2000). Precipitation-Runoff Simulations for the Upper Part of the Truckee River Basin, California and Nevada. U.S. Dept. of the Interior, U.S. Geological Survey: 99-4282

Jiménez Cisneros, T. Oki, B.E., Arnell, N.W., Benito, G., Cogley, J.G., Döll, P., Jiang, T., & Mwakalila, S.S. (2014): Freshwater resources. In: Climate Change 2014: Impacts,Adaptation, and Vulnerability. Part A: Global and Sectoral Aspects. Contribution of Working Group II to the Fifth Assessment Report of the Intergovernmental Panel on Climate Change [Field, C.B., V.R. Barros, D.J. Dokken,

K.J. Mach, M.D. Mastrandrea, T.E. Bilir, M. Chatterjee, K.L. Ebi, Y.O. Estrada, R.C. Genova, B. Girma, E.S. Kissel, A.N. Levy, S. MacCracken, P.R. Mastrandrea, and L.L.White (eds.)]. Cambridge University Press, Cambridge, United Kingdom and New York, NY, USA, pp. 229-269.

Kalra, A., & Ahmad, S. (2012). Estimating annual precipitation for the Colorado River Basin using oceanic-atmospheric oscillations. *Water Resources Research*, *48*(6). http://doi.org/10.1029/2011WR010667

Kalra, A., Li, L., Li, X., & Ahmad, S. (2013a). Improving Streamflow Forecast Lead Time Using Oceanic-Atmospheric Oscillations for Kaidu River Basin, Xinjiang, China. *Journal of Hydrologic Engineering*, *18*(8), 1031–1040. http://doi.org/10.1061/(ASCE)HE.1943-5584.0000707

Kalra, A., Miller, W. P., Lamb, K. W., Ahmad, S., & Piechota, T. (2013b). Using large-scale climatic patterns for improving long lead time streamflow forecasts for Gunnison and San Juan River Basins. *Hydrological Processes*, *27*, 1543–1559. https://doi.org/10.1002/Hyp.9236

Kalra, A., Ahmad, S., & Nayak, A. (2013c). Increasing streamflow forecast lead time for snowmelt-driven catchment based on large-scale climate patterns. *Advances in Water Resources*, *53*, 150-162. https://doi.org/10.1016/j.advwatres.2012.11.003

Kalra, A., Piechota, T.C., Davies, R., & Tootle, G.A. (2008). Changes in US streamflow and western US snowpack. *Journal of Hydrologic Engineering*, *13*(3), 156-163. http://dx.doi.org/10.1061/(ASCE)1084-0699(2008)13:3(156)

Kalra, A., & Ahmad, S. (2009). Using oceanic‐atmospheric oscillations for long lead time streamflow forecasting. *Water Resources Research*, *45*(3). http://dx.doi.org/10.1029/2008WR006855

Kalra, A., & Ahmad, S. (2011). Evaluating changes and estimating seasonal precipitation for the Colorado River Basin using a stochastic nonparametric disaggregation technique. *Water Resources Research*, *47*(5). http://dx.doi.org/10.1029/2010WR009118

Kalra, A., Sagarika, S., Pathak, P., & Ahmad, S. (2017). Hydro-climatological changes in the Colorado River Basin over a century. *Hydrological Sciences Journal*, (1-17).

http://dx.doi.org/10.1080/02626667.2017.1372855

Kampf, S. K., & Burges, S. J. (2007). A framework for classifying and comparing distributed hillslope and catchment hydrologic models. *Water Resources Research*, *43*(5). http://doi.org/10.1029/2006WR005370

Kenney, J. F. (2013). *Mathematics of statistics*. D. Van Nostrand Company Inc; Toronto; Princeton; New Jersey; London; New York,; Affiliated East-West Press Pvt-Ltd; New Delhi.

Kim, N. W., Chung, I. M., Won, Y. S., & Arnold, J. G. (2008). Development and application of the integrated SWAT-MODFLOW model. *Journal of Hydrology*, *356*(1–2), 1–16. http://doi.org/10.1016/j.jhydrol.2008.02.024

Koczot, B. K. M., Jeton, A. E., Mcgurk, B. J., & Dettinger, M. D. (2005). Precipitation-Runoff Processes in the Feather River Basin , Northeastern California , with Prospects for Streamflow Predictability , Water Years 1971 – 97, (February 2016), 82.

Kollet, S. J., & Maxwell, R. M. (2006). Integrated surface-groundwater flow modeling: A free-surface overland flow boundary condition in a parallel groundwater flow model. *Advances in Water Resources*, *29*(7), 945–958. http://doi.org/10.1016/j.advwatres.2005.08.006

Kuzara, S. (2011). *Groundwater surface-water interaction in the alluvial aquifer of the Middle Stillwater River Valley, Absarokee, Montana* (Doctoral dissertation, Montana Tech of The University of Montana).

Lafontaine, J. H., Hay, L. E., Viger, R. J., Regan, R. S., & Markstrom, S. L. (2015). Effects of Climate and Land Cover on Hydrology in the Southeastern U.S.: Potential Impacts on Watershed Planning. *Journal of the American Water Resources Association*, *51*(5), 1235–1261. http://doi.org/10.1111/1752-1688.12304

Lajos, B. (2008) Soil Science. http://www.tankonyvtar.hu/en/tartalom/tamop425/0032_talajtan/ch07s05.html

Lambert, S.J., & Boer, G.J. (2001). CMIP1 evaluation and intercomparison of coupled climate models. *Climate Dynamics*, 17(2), 83-106. http://dx.doi.org/10.1007/PL00013736

Lawrence, D.M., & Slater, A.G. (2010). The contribution of snow condition trends to future ground Climate. *Climate Dynamics*, 34, 969-981. http://dx.doi.org/10.1007/s00382-009-0537-4

Leavesley, G. H., Lichty, R. W., Troutman, B. M., & Saindon, L. G. (1983). Precipitaion-Runoff Modeling System:User's manual. Water-Resources Investigations Report 83-4238

Leavesley, G. H., Markstrom, S. L., Viger, R. J., & Hay, L. E. (1996). The Modular Modeling System (MMS): A Toolbox for Water- and Environmental-Resources Management. Proceedings of the 2005 Watershed Management Conference - Managing Watersheds for Human and Natural Impacts: Engineering, Ecological, and Economic Challenges.

Legates, D.R., McCabe Jr., G.J., 1999. Evaluating the use of ''goodness- of-fit'' measures in hydrologic and hydroclimatologic model validation. *Water Resources Research*, 35, 233-241. http://dx.doi.org/10.1029/1998WR900018

Leibowitz, S. G., Wigington, P. J., Comeleo, R. L., & Ebersole, J. L. (2012). A temperature-precipitation-based model of thirty-year mean snowpack accumulation and melt in Oregon, USA. *Hydrological Processes*, *26*(5), 741–759.

Lettenmaier, D.P., & Gan, T.Y. (1990). Hydrologic sensitivity of the Sacramento-San Joaquin River Basin, California, to global warming. *Water Resources Research*, 26, 69- 86. http://dx.doi.org/10.1029/WR026i001p00069

Liu, H., Xu, Z., Chen, C., & Liu, Z. (2011). Study on Eutrophication of Guanting Reservoir. *Water Resources and Power*, *1*, 005.

Maraun, D. (2013). Bias Correction, Quantile Mapping, and Downscaling: Revisiting the Inflation Issue. *Journal of Climate*, *26*(6), 2137–2143. http://doi.org/10.1175/JCLI-D-12-00821.1

Maraun, D.,Wetterhall, F., Ireson, A. M., Chandler, R. E., Kendon, E. J., Widmann, M., … Thiele-Eich, I. (2010) Precipita- tion downscaling under climate change: Recent developments to bridge the gap between dynamical models and the end user, Reviews of Geophysics, 48, RG3003. http://dx.doi.org/10.1029/2009RG000314

Markstrom, S. L., Hay, L. E., Ward-Garrison, C. D., Risley, J. C., Battaglin, W. A., Bjerklie, D. M., … Walker, J. F. (2011). Integrated Watershed-Scale Response to Climate Change for Selected Basins Across the United *States*.Scientific Investigations Report 2011-5077. U.S. Department of the Interior, U.S. Geological Survey.

Markstrom, S. L., Niswonger, R. G., Regan, R. S., Prudic, D. E., & Barlow, P. M. (2005). GSFLOW - Coupled Ground-Water and Surface-Water Flow Model Based on the Integration of the Precipitation-Runoff Modeling System (PRMS) and the Modular Ground-Water Flow Model (MODFLOW-2005). U.S. Geological Survey.

Markstrom, S. L., Regan, S., Hay, L. E., Viger, R. J., Webb, R. M. T., Payn, R. A., & LaFontaine, J. H. (2015). PRMS-IV , the Precipitation-Runoff Modeling System , Version 4. *U.S. Geological Survey Techniques and Methods, Book 6, Chap. B7*, 158. http://doi.org/http://dx.doi.org/10.3133/tm6B7

Masbruch, M. D., & Gardner, P. M. (2014). Potential Effects of Existing and Proposed Groundwater Withdraws on Water Level and Natural Groundwater Discharge in Snake Valley, Juab and Millard Counties, Utah, White Pine County, Nevada and surrounding Area in Utah and Nevada.

Masbruch, M. D., Gardner, P. M., & Brooks, L. E. (2014). Hydrology and Numerical Simulation of Groundwater Movement and Heat Transport in Snake Valley and Surrounding Areas, Juab, Millard, and Beaver Counties, Utah, and White Pine and Lincoln Counties, Nevada.

Mastin, M. C., Hay, L. E., & Markstrom, S. L. (2012). Watershed Scale Response to Climate Change--Naches River Basin, Washington. U.S. Geological Survey. Fact sheet 2011-3123.

Maurer, E. P., & Duffy, P. B. (2005) Uncertainty in projections of stream- flow changes due to climate change in California. *Geophysical Research Letters*, 32, L03704, http://dx.doi.org/10.1029/2004GL021462, 2005.

Maxey, G. B. (1964). Hydrostratigraphic units. *Journal of Hydrology*, *2*(2), 124–129. http://doi.org/10.1016/0022-1694(64)90023-X

Maxwell, R. M., F. K. Chow, and S. J. Kollet. 2007. The groundwater-land-surface-atmosphere connection: Soil moisture effects on the atmspheric boundary layer in fully-coupled simulations. *Advances in Water Resources*, 30: 2447-2466. http://dx.doi.org/10.1016/j.advwatres.2007.05.018

McDoanld, M. G., & Harbaugh, A. W. (1988). Techniques of water-resources investigations of the United States Geological Survey. *Journal of Hydrology*. http://doi.org/10.1016/0022-1694(70)90079-X

McDonald, M.G., & Harbaugh, A.W., 1984, A modular three-dimensional finite-difference ground-water flow model: U.S. Geological Survey Open-File Report 83-875.

McGrew, A.J., Miller, E.L., & Brown, J.L., compiler. (1995) Geologic map of Kious Spring and Garrison 7.5' quadrangles, White Pine County, Nevada and Millard County, Utah: U.S. Geological Survey Open-File Report 95-10, scale 1:24,000.

Mearns, L.O., Giorgi, F., McDaniel, L., Shields, C., 1995. Analysis of daily variability of precipitation in a nested regional climate model: comparison with observations and doubled CO_2 results. *Global and Planetary Change*, 10, 55-78. http://dx.doi.org/ 10.1016/0921-8181(94)00020-E

Mearns, L.O., Schneider, S.H., Thompson, S.L., & McDaniel, L.R. (1990). Analysis of climate variability in general circulation models: comparison with observations and changes in variability in 2 x CO_2 experiments. Journal of Geophysical Research, D95, 20469-20490. http://dx.doi.org/10.1029/JD095iD12p20469

Mehrotra, A., & Sharma, A. (2006). Conditional resampling of hydrologic time series using multiple predictor variables: a K-nearest neighbour approach. *Advances in Water Resources*, *29*, 987-999. http://dx.doi.org/10.1016/j.advwatres.2005.08.007

Mejia, J. F., Huntington, J., Hatchett, B., Koracin, D., & Niswonger, R. G. (2012). Linking Global Climate Models to an Integrated Hydrologic Model: Using an Individual Station Downscaling Approach. *Journal of Contemporary Water Research & Education*, *147*(1), 17-27. http://doi.org/10.1111/j.1936-704X.2012.03100.x

Melesse, A. M., Ahmad, S., McClain, M. E., Wang, X., & Lim, Y. H. (2011). Suspended sediment load prediction of river systems: An artificial neural network approach. *Agricultural Water Management*, *98*(5), 855-866. https://doi.org/10.1016/j.agwat.2010.12.012

Miller, A.W., Reynolds, A.C., Sobrino, C., & Riedel, G.F. (2009). Shellfish face uncertain future in high CO_2 world: influence of acidification on oyster larvae calcification and growth in estuaries. *PLoS ONE*, *4*(5), e5661. http://dx.doi.org/10.1371/journal.pone.0005661

Miller, E.L., Gans, P.B., Grier, S.P., & Brown, J.L., compilers. (1995) Geologic map of Windy Peak 7.5' quadrangle, White Pine County, Nevada: U.S. Geological Survey Open-File Report 94-687, scale 1:24,000.

Miller, N., Kim, J. H. R. K., & Farrara, J. (1999). Downscaled Climate and Streamflow Study of the Southwestern United States. *Journal of The American Water Reources Association*. 35, 1525-1538. http://doi.org/10.1111/j.1752-1688.1999.tb04235.x

Mimikou, M., Kouvopoulos, Y., Cavadias, G., & Vayianos, N. (1991). Regional hydrological effects of climate change. *Journal of Hydrology*, *123*,119-146. http://doi.org/10.1186/s40677-015-0013-x

Mirchi, A., Madani, K., Watkins, D., & Ahmad, S. (2012). Synthesis of system dynamics tools for holistic conceptualization of water resources problems. *Water resources management*, *26*(9), 2421-2442. DOI: 10.1007/s11269-012-0024-2.

Misch, P., & Hazzard, J.C. (1962) Stratigraphy and metamorphism of the Late Precambrian rocks in central northeastern Nevada and adjacent Utah. *Bulletin of the American Association of Petroleum Geologists*. 46, 3, 289-343.

Mishra, B. K., & Herath, S. (2015). Assessment of future floods in the Bagmati River Basin of Nepal using bias-corrected daily GCM precipitation data. *Journal of Hydrologic Engineering*, *20*(8), 1–11. http://doi.org/10.1061/(ASCE) HE.1943-5584.0001090

MODFLOW and Related Programs. U.S. Geologic Survey: http://water.usgs.gov/ogw/modflow/. Accesse by Oct.2, 2016.

Mohammed, I. N., Bomblies, A., & Wemple, B. C. (2015). The use of CMIP5 data to simulate climate change impacts on flow regime within the Lake Champlain Basin. *Journal of Hydrology: Regional Studies*, *3*, 160–186. http://doi.org/10.1016/j.ejrh.2015.01.002

Monteith, J.L. (1965). Evaporation and environment, in the state and movement of water in living organisms. Symposia for the *Society of Experimental Biology*, 19, 205-234.

Moriasi, D. N., Arnold, J. G., Van Liew, M. W., Binger, R. L., Harmel, R. D., & Veith, T. L. (2007). Model evaluation guidelines for systematic quantification of accuracy in watershed simulations. *Transactions of the ASABE*, *50*(3), 885–900. http://doi.org/10.13031/2013.23153

Moriasi, D. N., Gitau, M. W., Pai, N., & Daggupati, P. (2015). Hydrologic and Water Quality Models: Performance Measures and Evaluation Criteria. *Transactions of the ASABE*, *58*(6), 1763–1785. http://doi.org/10.13031/trans.58.10715

Moron, V., Robertson, A.W., Ward, M.N., & Ndiaye, O. (2008). Weather types and rainfall over Senegal. Part II: downscaling of GCM simulations. *Journal of Climate*, *21*, 288-307. http://dx.doi.org/10.1175/2007JCLI1601.1

Morris, M. D. (1991). Factorial Sampling Plans for Preliminary Computational Experiments. *Technometrics*, *33*(2), 161. http://doi.org/10.2307/1269043

Mosquera-Machado, S., & Ahmad, S. (2007). Flood hazard assessment of Atrato River in Colombia. *Water resources management*, *21*(3), 591-609. https://doi.org/10.1007/s11269-006-9032-4

Mote, P. W., Hamlet, A. F., Clark, M. P., & Lettenmaier, D. P. (2005). Declining mountain snowpack in western North America. *Bulletin of the American Meteorological Society, 86*, 39-49. http://dx.doi.org/10.1175/BAMS-86-1-39

Moussa, R., Voltz, M., & Andrieux, P. (2002). Effects of the spatial organization of agricultural management on the hydrological behaviour of a farmed catchment during flood events. *Hydrological Processes*, *16*(2), 393–412. http://doi.org/10.1002/hyp.333

Najafi, M. R., Moradkhani, H., & Jung, I. W. (2011). Assessing the uncertainties of hydrologic model selection in climate change impact studies. *Hydrological Processes*, *25*(18), 2814–2826. http://doi.org/10.1002/hyp.8043

Nash, J. E., & Sutcliffe, J. V. (1970). River Flow Forecast Through Conceptual Models Part 1- A Discussion of Principles. *Journal of Hydrology*, *10*(3), 282–290. http://doi.org/10.1016/0022-1694(70)90255-6

Nash, L., & Gleick, P. (1991). Sensitivity of streamflow in the Colorado basin to climatic changes. *Journal of Hydrology, 125*, 119-146. http://dx.doi.org/10.1016/0022-1694(91)90030-L

Nijssen, B., O'Donnell, G.M., Hamlet, A.F., & Lettenmaier, D.P. (2008). Hydrologic sensitivity of global rivers to climate change. *Mountain Research and Development*, *28*(1), 4-7. http://dx.doi.org/10.1023/A:1010616428763

Niswonger, R. G., Allander, K. K., & Jeton, A. E. (2014). Collaborative modelling and integrated decision support system analysis of a developed terminal lake basin. *Journal of Hydrology*, *517*, 521–537. http://doi.org/10.1016/j.jhydrol.2014.05.043

Niswonger, R. G., Panday, S., & Ibaraki, M. (2011). *MODFLOW-NWT , A Newton Formulation for MODFLOW-2005*. *U.S. Geological Survey*. Retrieved from https://pubs.usgs.gov/tm/tm6a37/pdf/tm6a37.pdf

Niswonger, R. G., Prudic, D. E., & Regan, S. R. (2006). Documentation of the Unsaturated-Zone Flow (UZF1) Package for Modeling Unsaturated Flow Between the Land Surface and the Water Table with MODFLOW-2005. *Book 6, Modeliing Techniques, Section A, Ground Water*, 71. Retrieved from https://pubs.usgs.gov/tm/2006/tm6a19/pdf/tm6a19.pdf

O'Connell, P.E. (1991). A historical perspective. In Bowles D.S. and O'Connell P.E. (Eds.). Recent Advances in the Modeling of Hydrologic Systems. Kluwer, Dordrecht.

Online Guide to MODFLOW-NWT. (n.d.). Retrieved December 1, 2016, from https://water.usgs.gov/ogw/modflow-nwt/MODFLOW-NWT-Guide

Orndorff, R.L., Wieder, R.W., & Filkorn, H.F., 2001, Geology underfoot in central Nevada: Missoula, Mountain Press Publishing.

Osman, Y. Z., & Bruen, M. P. (2002). Modelling stream - Aquifer seepage in an alluvial aquifer: An improved loosing-stream package for MODFLOW. *Journal of Hydrology*, *264*(1–4), 69–86. http://doi.org/10.1016/S0022-1694(02)00067-7

Panday, S., & Huyakorn, P. S. (2004). A fully coupled physically-based spatially-distributed model for evaluating surface/subsurface flow. *Advances in Water Resources*, *27*(4), 361–382. http://doi.org/10.1016/j.advwatres.2004.02.016

Panofsky, H.W., & Brier, G.W. (1968). Some Applications of Statistics to Meteorology. The Pennsylvania State University Press: Philadelphia.

Pathak, P., Kalra, A., Ahmad, S., & Bernardez, M. (2016a). Wavelet-Aided Analysis to Estimate Seasonal Variability and Dominant Periodicities in Temperature, Precipitation, and Streamflow in the Midwestern United States. *Water Resources Management*, *30*(13), 868–874. http://doi.org/10.1007/s10745-006-9094-1

Pathak, P., Kalra, A., & Ahmad, S. (2016b). Temperature and precipitation changes in the Midwestern United States: implications for water management. *International Journal of Water Resources Development*, 1-17. http://dx.doi.org/10.1080/07900627.2016.1238343

Penman, H.L. (1948). Natural evaporation from open water, bare soil and grass: Proceedings of the Royal Society of London, England, series A, 193, 120-145. http://dx.doi.org/10.1098/rspa.1948.0037

Phillips, F.M. (1994). Environmental tracers for water in desert soils of the American Southwest. *Soil Science Society of America Journal*, *58*, 15-24. http://dx.doi.org/10.2136/sssaj1994.03615995005800010003x

Piao, S., Ciais, P., Huang, Y., Shen, Z., Peng, S., Li, J., Zhou, L., Liu, H., Ma, Y., Ding, Y., Friedlingstein, P., Liu, C., Tan, K., Yu, Y., Zhang, T., & Fang, J. (2010). The impacts of climate change on water resources and agriculture in China. *Nature*, *467*(7311), 43-51. http://dx.doi.org/10.1038/nature09364.

Pinder, G. F., & Sauer, S. P. (1971). Numerical Simulation of Flood Wave Modification Due to Bank Storage Effects. *Water Resources Research*, *7*(1), 63–70. http://doi.org/10.1029/WR007i001p00063

Ponce, V. M., Pandey, R. P., & Kumar, S. (1999). Groundwater recharge by channel infiltration in El Barbon basin, Baja California, Mexico. *Journal of Hydrology*, *214*(1–4), 1–7. http://doi.org/10.1016/S0022-1694(98)00220-0

Porter, J. R., Xie, L., Challinor, A. J., Cochrane, K., Howden, S. M., Iqbal, M. M., … Travasso, M. I. (2014). Food security and food production systems. *Climate Change 2014: Impacts, Adaptation, and Vulnerability. Part A: Global and Sectoral Aspects. Contribution of Working Group II to the Fifth Assessment Report of the Intergovernmental Panel on Climate Change*, 485–533. http://doi.org/10.1111/j.1728-4457.2009.00312.x

Porter, J.R., Xie, L., Challinor, A.J., Cochrane, K., Howden, S.M., Iqbal, M.M., Lobell, D.B., & Travasso, M.I. (2014): Food security and food production systems. In: Climate Change 2014: Impacts, Adaptation, and Vulnerability. Part A: Global and Sectoral Aspects. Contribution of Working Group II to the Fifth Assessment Report of the Intergovernmental Panel on Climate Change [Field, C.B., V.R. Barros, D.J. Dokken, K.J. Mach, M.D. Mastrandrea, T.E. Bilir, M. Chatterjee, K.L. Ebi, Y.O. Estrada, R.C. Genova, B. Girma, E.S. Kissel, A.N. Levy, S. MacCracken, P.R.

Mastrandrea, and L.L.White (eds.)]. Cambridge University Press, Cambridge, United Kingdom and New York, NY, USA, pp. 485-533.

Pratchett, M.S., Munday, P.L., Graham, N.A.J., Kronen, M., Pinca, S., Friedman, K., Brewer, T.D., Bell, J.D., Wilson, S.K., Cinner, J.E., Kinch, J.P., Lawton, R.J., Williams, A.J., Chapman, L., Magron, F. & Webb, A. (2011). Vulnerability of coastal fisheries in the tropical Pacific to climate change. In: Vulnerability of Tropical Pacific Fisheries and Aquaculture to Climate Change [Bell, J.D., J.E. Johnson, and A.J. Hobday (Eds.)]. Secretariat of the Pacific Community, Noumea, New Caledonia, 493-573.

Prickett, T. A., & Lonnquist, C. G. (1971). Selected Digital Computer Techniques for Groundwater Resource Evaluation, Illinois State Water Survey, Bulletin.

Prickett, T.A. (1975). Modeling Techniques for Groundwater Evaluation. In Advances In Hydroscience, Vol.10. New York: Academic Press.

Priestley, C.H.B., & Taylor, R.J. (1972). On the assessment of the surface heat flux and evaporation using large-scale parameters. *Monthly Weather Review*, *100*(2), 81-92. http://dx.doi.org/10.1175/1520-0493(1972)100<0081:OTAOSH>2.3.CO;2

PRISM Climate Group, Oregon State University, http://prism.oregonstate.edu, created 4 Feb 2004.

Prism, T., Group, C., Ppt, A., Tmin, T., Tdmean, T., Type, V., & Daily, D. (2013). Descriptions of PRISM Spatial Climate Datasets for the Conterminous United States Long-Term Average (“ Normals ”) Datasets, (August), 1–14.

PRISM. (2016) Description of PRISM Spatial Climate Datasets for the Conterminous United Sates. Available online at : http://prism.oregonstate.edu/documents/PRISM_datasets.pdf

PRISM. 30-year Normals for the period of 1981-2010. Available online at : http://prism.oregonstate.edu/normals/

Prudic, D. E. (1989). *Documentation of a computer program to simulate stream-aquifer relations using a*

modular, finite-difference, ground-water flow model. Retrieved from https://pubs.usgs.gov/of/1988/0729/report.pdf

Prudic, D. E. (2012). Report on the Drilling of Monitoring Wells near Lehman Caves, Great Basin National Park, White Pine County, Nevada, May—June 2012, (June), 1–38.

Prudic, D. E., & Glancy, P. A. (2009). Geochemical Investigation of Source Water to Cave Springs, Great Basin National Park, White Pine County, Nevada, (U.S. Geological Survey Scientific Investigations Report 2009–5073), 28.

Prudic, D. E., & Sweetkind, D. S. (2011). Evaluating Connection of Aquifers to Springs and Streams , Eastern Part of Great Basin National Park and Vicinity , Nevada.

Prudic, D. E., Konikow, L. F., & Banta, E. R. (2004). A New Streamflow-Routing (SFR1) Packate to Simulate Stream-Aquifer Interaction with MODFLOW-2000. *U.S. Geological Survey*, (Open-File Report 2004-1042), 104. Retrieved from http://pubs.er.usgs.gov/publication/ofr20041042

Prudic, D. E., Sweetkind, D. S., Jackson, T. L., Dotson, K. E., Plume, R. W., Hatch, C. E., & Halford, K. J. (2015). Evaluating Connection of Aquifers to Springs and Streams , Eastern Part of Great Basin National Park and Vicinity , Nevada.

Puri, S., Stephen, H., & Ahmad, S. (2011a). Relating TRMM precipitation radar land surface backscatter response to soil moisture in the southern United States. *Journal of Hydrology*, *402*(1), 115-125. https://doi.org/10.1016/j.jhydrol.2011.03.012

Puri, S., Stephen, H., & Ahmad, S. (2011b). Relating TRMM precipitation radar backscatter to water stage in wetlands. *Journal of Hydrology*, *401*(3), 240-249. https://doi.org/10.1016/j.jhydrol.2011.02.026

Qaiser, K., Ahmad, S., Johnson, W., & Batista, J. (2011). Evaluating the impact of water conservation on fate of outdoor water use: a study in an arid region. *Journal of environmental management*, *92*(8), 2061-2068. https://doi.org/10.1016/j.jenvman.2011.03.031

Qaiser, K., Ahmad, S., Johnson, W., & Batista, J. R. (2013). Evaluating water conservation and reuse policies using a dynamic water balance model. *Environmental management*, *51*(2), 449-458. https://doi.org/10.1007/s00267-012-9965-8

Räisänen, J., & Räty, O. (2013). Projections of daily mean temperature variability in the future: Cross-validation tests with ENSEMBLES regional climate simulations. *Climate Dynamics*, *41*(5-6), 1553-1568. http://doi.org/10.1007/s00382-012-1515-9

Rankl, J. G. (1987). Analysis Of Sediment Production From Two Small Semiarid Basins In Wyoming. (No. 85-4314). US Geological Survey.

Refsgaard, J. C., & Storm, B. (1995). Mike she. *Computer Models of Watershed Hydrology*, *1*, 809–846.

Regan, R. S., Niswonger, R. G., Markstrom, S. L., Maples, S. R., & Barlow, P. M. (2016). GSFLOW version 1.2.1: Coupled Groundwater and Surface-water FLOW model: U.S. Geological Survey Software Release. http://doi.org/10.5066/F7WW7FS0

Ren-Jun, Z. (1992). The Xinanjiang model applied in China. *Journal of Hydrology*, *135*(1–4), 371–381. http://doi.org/10.1016/0022-1694(92)90096-E

Revelle, R.R., & Waggoner, P.E. (1983). Effect of carbon dioxide-induced climatic change on water supplies in the western United States, in: Changing Climate, National Academy of Sciences, National Academy Press, Washington, DC.

Risley, J., Hay, L. E., & Markstrom, S. L. (2012). Watershed Scale Response to Climate Change--Sprague River Basin, Oregon. U.S. Geological Survey. Fact sheet 2011-3120.

Rosenberg, N.J., Epstein, D.J., Wang, D., Vail, L., Srinivasan, R., & Arnold, J.G. (1999). Possible impacts of global warming on the hydrology of the Ogallala Aquifer region. *Climate Change*, *42* (4), 677-692. http://doi.org/10.1023/A:1005424003553

Running, S. W., & Nemani, R. R. (1991). Regional hydrologic carbon balance responses of forests resulting from potential climate change. *Climatic Change*, 19, 349-368. http://doi.org/10.1007/BF00151173

Rushton, K.R., & Redshaw, S.C., 1979, Seepage and groundwater flow: Numerical analysis by analogue and digital methods: New York, John Wiley and Sons.

Rusuli, Y., Li, L., Ahmad, S., & Zhao, X. (2015). Dynamics model to simulate water and salt balance of Bosten Lake in Xinjiang, China. *Environmental Earth Sciences*, *74*(3), 2499-2510. https://doi.org/10.1007/s12665-015-4257-2

Sagarika, S., Kalra, A., & Ahmad, S. (2014). Evaluating the effect of persistence on long-term trends and analyzing step changes in streamflows of the continental United States. *Journal of Hydrology*, *517*, 36–53. http://doi.org/10.1016/j.jhydrol.2014.05.002

Sagarika, S., Kalra, A., & Ahmad, S. (2015). Interconnections between oceanic–atmospheric indices and variability in the U.S. streamflow. *Journal of Hydrology*, *525*, 724–736. http://doi.org/10.1016/j.jhydrol.2015.04.020

Sagarika, S., Kalra, A., & Ahmad, S. (2016). Pacific Ocean SST and Z_{500} climate variability and western U.S. seasonal streamflow. *International Journal of Climatology*, 36(3), 1515-1553. http://doi.org/10.1002/joc.4442

Santhi, C., Arnold, J.G., Williams, J.R., Dugas, W.A., Srinivasn, R., & Hauck, L.M. (2001). Validation of the SWAT model on a large river basin with point and nonpoint sources. *Journal of the American Water Resources Association*, *37*(5):1169-1188. http://doi.org/10.1111/j.1752-1688.2001.tb03630.x

Scanlon, B. R., Healy, R. W., & Cook, P. G. (2002). Choosing appropriate techniques for quantifying groundwater recharge. *Hydrogeology Journal*, *10*, 18–39. http://doi.org/10.1007/s10040-001-0176-2

Schaake, J.C. (1990). From climate to flow, in: Climatic Change and U.S. Water Resources, P.E. Waggoner (Ed.). John Wiley & Sons, New York.

Schmidli, J., Frei, C., & Vidale, P.L. (2006). Downscaling from GCM precipitation: a benchmark for dynamical and statistical downscaling methods. *International Journal of Climatology*, *26*, 679-689. http://doi.org/10.1002/joc.1287

Scott, D. W. (1992) Multivariate Density Estimation. Theory, Practice and Visualization. New York: Wiley.

Seaber, P. R. (1988). Hydrostratigraphic units. In *The Geology of North America*. Retrieved from http://www.clemson.edu/ces/hydro/murdoch/Courses/Aquifer Systems/documents/Heath and Back books/Chapter 2.pdf

Seneviratne, S. I., Corti, T., Davin, E. L., Hirschi, M., Jaeger, E. B., Lehner, I., Orlowsky, B., & Teuling, A. J. (2010). Investigating soil moisture–climate interactions in a changing climate: a review. *Earth-Science Reviews, 99* (3-4), 125-161. http://dx.doi.org/10.1016/j.earscirev.2010.02.004

Settele, J., Scholes, R. J., Betts, R. A., Bunn, S., Leadley, P., Nepstad, D., Overpeck, J.T., & Toboada, M. A. (2014). Terrestrial and inland water systems. *Climate Change 2014: Impacts, Adaptation, and Vulnerability. Part A: Global and Sectoral Aspects. Contribution of Working Group II to the Fifth Assessment Report of the Intergovernmental Panel on Climate Change*, 271-359.

Shi, P., Hou, Y., Xie, Y., Chen, C., Chen, X., Li, Q., ... & Srinivasan, R. (2013). Application of a SWAT model for hydrological modeling in the Xixian Watershed, China. *Journal of Hydrologic Engineering*, *18*(11), 1522-1529. http://ascelibrary.org/doi/abs/10.1061/(ASCE)HE.1943-5584.0000578

Shi, P., Chen, C., Srinivasan, R., Zhang, X., Cai, T., Fang, X., ... & Li, Q. (2011). Evaluating the SWAT model for hydrological modeling in the Xixian watershed and a comparison with the XAJ model. *Water resources management*, *25*(10), 2595-2612. https://doi.org/10.1007/s11269-011-9828-8

Sheather, S. J., & Jones M. C. (1991). A reliable data-based bandwidth selection method for kernel density estimation. *Journal of the Royal Statistical Society*, 683-690.

Shrestha, E., Ahmad, S., Johnson, W., Shrestha, P., & Batista, J. R. (2011). Carbon footprint of water conveyance versus desalination as alternatives to expand water supply. *Desalination*, *280*(1), 33-43. https://doi.org/10.1016/j.desal.2011.06.062

Shrestha, E., Ahmad, S., Johnson, W., & Batista, J. R. (2012). The carbon footprint of water management policy options. *Energy Policy*, *42*, 201-212. https://doi.org/10.1016/j.enpol.2011.11.074.

Silverman, B. W. (1986) Density Estimation. London: Chapman and Hall.

Singh, V.P. (1995). Computer Models of Watershed Hydrology. Water Resource Publications, Highlands Ranch, CO.

Sippel, S., Otto, F. E. L., Forkel, M., Allen, M. R., Guillod, B. P., Heimann, M., … Mahecha, M. D. (2015). A novel bias correction methodology for climate impact simulations. *Earth System Dynamics Discussions*, *6*(2), 1999–2042. http://doi.org/10.5194/esdd-6-1999-2015

Skaugen, T., Stranden, H.B. & Saloranta,T. (2012) Trends in snow water equivalent in Norway (1931-2009). *Hydrology Research*, *43*(4), 489-499. http://dx.doi.org/10.2166/nh.2012.109

Smakhtin, V. U. (2001). Low flow hydrology: A review. *Journal of Hydrology*, *240*(3–4), 147–186. http://doi.org/10.1016/S0022-1694(00)00340-1

Smith, P. C., Heinrich, G., Suklitsch, M., Gobiet, A., Stoffel, M., & Fuhrer, J. (2014). Station-scale bias correction and uncertainty analysis for the estimation of irrigation water requirements in the Swiss Rhone catchment under climate change. *Climatic Change*, *127*(3-4), 521-534. http://doi.org/10.1007/s10584-014-1263-4

Smith, R.E., & Hebbert, R.H.B. (1983) Mathematical simulation of interdependent surface and subsurface hydrologic processes. *Water Resources Research*, *19*, 4, 987-1001. http://doi.org/10.1029/WR019i004p00987

SNWA. (2012). Southern Nevada Water Authority Clark, Lincoln, and White Pine Counties Groundwater Development Project Draft Conceptual Plan of Development. *Prepared for US Bureau of Land*

Management, 153. Retrieved from https://www.snwa.com/assets/pdf/ws_gdp_copd.pdf

Soil Survey Staff, Natural Resources Conservation Service, United States Department of Agriculture. Web Soil Survey. Available online at http://websoilsurvey.nrcs.usda.gov/.

Song, X., Zhang, J., Zhan, C., Xuan, Y., Ye, M., & Xu, C. (2015). Global sensitivity analysis in hydrological modeling: Review of concepts, methods, theoretical framework, and applications. *Journal of Hydrology*, *523*(225), 739–757. http://doi.org/10.1016/j.jhydrol.2015.02.013

Sophocleous, M. (2002). Interactions between groundwater and surface water: the state of the science. *Hydrogeology Journal*, *10*(1), 52–67. http://doi.org/10.1007/s10040-001-0170-8

Stephen, H., Ahmad, S., & Piechota, T. C. (2010a). Land surface brightness temperature modeling using solar insolation. *IEEE Transactions on Geoscience and Remote Sensing*, *48*(1), 491-498. https://doi.org/10.1109/TGRS.2009.2026893

Stephen, H., Ahmad, S., Piechota, T. C., & Tang, C. (2010b). Relating surface backscatter response from TRMM precipitation radar to soil moisture: results over a semi-arid region. *Hydrology and Earth System Sciences*, *14*(2), 193.

Sterman, J. D. (2000). Business dynamics: systems thinking and modeling for a complex world (No. HD30. 2 S7835 2000).

Sulis, M., Paniconi, C., Rivard, C., Harvey, R., & Chaumont, D. (2011). Assessment of climate change impacts at the catchment scale with a detailed hydrological model of surface-subsurface interactions and comparison with a land surface model. *Water Resources Research*, *47*(1), 1–22. http://doi.org/10.1029/2010WR009167

Swain, E. D., & Wexler, E. j. (1996). *Techniques of Water-Resources Investigations Survey of the United States Geological Chapter* A Coupled Surface-Water And Ground- Water Flow Model (Modbranch) Simulation Of Stream-Aquifer. *USGS report*. Retrieved from https://pubs.usgs.gov/twri/twri6a6/pdf/TWRI_6-A6.pdf

Tague, C., Grant, G., Farrell, M., Choate, J., &Jefferson, A. (2008). Deep groundwater mediates streamflow response to climate warming in the Oregon Cascades. *Climate Change*, 86 (1-2), 189-210. http://doi.org/10.1007/s10584-007-9294-8

Takala, M., Pulliainen, J., Metsamaki, S. J., & Koskinen, J.T. (2009). Detection of snowmelt using spaceborne microwave radiometer data in Eurasia from 1979 to 2007. *IEEE Transactions on Geoscience and Remote Sensing*, 47(9), 2996-3007. http://doi.org/10.1109/TGRS.2009.2018442

Takle, E.S., Gutowski, W.J. Jr., Arritt, R.W., Pan, Z., Anderson, C.J., Silva, R., Caya, D., Chen, S.-C., Christensen, J.H., Hong, S.-Y., Juang, H.-M.H., Katzfey, J.J., Lapenta, W.M., Laprise, R., Lopez, P., McGregor, J., & Roads, J.O. (1999). Project to intercompare regional climate simulations (PIRCS): description and initial results. *Journal of Geophysical Research*, *104*, 19443-19461. http://doi.org/10.1029/1999JD900352

Tamaddun, K. A., Kalra, A., & Ahmad, S. (2015). Spectral Analysis of Streamflow for Continental USA. *World Environmental & Water Resources Congress 2015*, 1135-1144. Austin, TX, May 17-21.

Tamaddun, K., Kalra, A., & Ahmad, S. (2016a). Identification of Streamflow Changes across the Continental United States Using Variable Record Lengths. *Hydrology*, *3*(2), 24. http://doi.org/10.3390/hydrology3020024

Tamaddun, K., Kalra, A., & Ahmad, S. (2016b). Patterns and periodicities of continental U.S. streamflow change. *World Environmental & Water Resources Congress 2016*, 658-667.West Palm Beach, FL, May 22-26.

Tamaddun, K. A., Kalra, A., & Ahmad, S. (2017a). Wavelet analyses of western us streamflow with ENSO and PDO. *Journal of Water and Climate Change*, *8*(1), 26–39. http://doi.org/10.2166/wcc.2016.162

Tamaddun, K. A., Kalra, A., Bernardez, M., & Ahmad, S. (2017b). Multi-Scale Correlation between the Western U.S. Snow Water Equivalent and ENSO/PDO Using Wavelet Analyses. *Water Resources Management*, *31*(9), 2745–2759. http://doi.org/10.1007/s11269-017-1659-9

Tamaddun, K. A., Kalra, A., & Ahmad, S. (2017c). Multi-Scale Correlation Analyses between California Streamflow and ENSO/PDO. *World Environmental & Water Resources Congress 2017*, 93-103. Sacramento, California, May 21-25.

Tang, Y, Xu, Q., & Min, Y. (2014). A Coupled Model for Evaluating Surface and Subsurface Flow-MODHMS. *Advanced Materials Research, 1073–1076*, 1716–1719. DOI: 10.4028/www.scientific.net/AMR.1073-1076.1716

Taylor, K. E., Stouffer, R. J., & Meehl, G. A. (2011). An overview of CMIP5 and the experiment design. *Bulletin of the American Meteorological Society*, *93*(4), 485–498. http://doi.org/10.1175/BAMS-D-11-00094.1

Themeßl, M. J., Gobiet, A., & Leuprecht, A. (2011). Empirical-statistical downscaling and error correction of daily precipitation from regional climate models. *International Journal of Climatology*, *31*(10), 1530-1544. doi:10.1002/joc.2168.

Thomsen, R. (1990). Effect of climate variability and change in groundwater in Europe. *Hydrology Research*, *21*,185-194.

Thornbury, W.D. (1969) Principles of geomorphology: New York, John Wiley & Sons.

Thrasher, B., Maurer, E. P., McKellar, C., & Duffy, P. B. (2012). Technical Note: Bias correcting climate model simulated daily temperature extremes with quantile mapping. *Hydrology and Earth System Sciences*, *16*(9), 3309–3314. http://doi.org/10.5194/hess-16-3309-2012

Todini, E. (1996). The ARNO rainfall—runoff model. *Journal of Hydrology*, *175*(1–4), 339–382. http://doi.org/10.1016/S0022-1694(96)80016-3

Townley, L.R. (1990). AQUIFEM-N: a multiple-layers finite element aquifer flow model, user's manual and description, CSIRO Division of Water Resources, Perth, Western Australia.

Townley, L.R., & Wilson, J.L. (1980). Description of and user's manual for a finite element aquifer flow model AQUIFEM-1, MIT Ralph M. Parsons Laboratory for Water Resources and Hydrodynamics, Technology Adaptation Program Report No.79-3.

Trenberth, K.E., Jones, P.D., Ambenje, P., Bojariu, R., Easterling, D., Klein Tank, A., Parker, D., Rahimzadeh, F., Renwick, J.A., Rusticucci, M., Soden B., & Zhai, P. (2007) Observations: Surface and Atmospheric Climate Change. In: Climate Change 2007: The Physical Science Basis. Contribution of Working Group I to the Fourth Assessment Report of the Intergovernmental Panel on Climate Change [Solomon, S., D. Qin, M. Manning, Z. Chen, M. Marquis, K.B. Averyt, M. Tignor and H.L. Miller (Eds.)]. Cambridge University Press, Cambridge, United Kingdom and New York, NY, USA.

Unpublished Digital Geologic Map of Great Basin National Park and Vicinity, Nevada (NPS, GRD, GRI, GRBA, GRBA digital map) adapted from a Stanford University unpublished digital map by Miller and others (2007). NPS Geologic Resources Inventory Program. Lakewood, Colorado, 2014.

Urban,M.C., Tewksbury, J.J., & Sheldon, K.S. (2012). On a collision course: competition and dispersal differences create no-analogue communities and cause extinctions during climate change. *Proceedings of the Royal Society B, 279*(1735), 2072-2080. http://doi.org/10.1098/rspb.2011.2367.

Van Dijck, S. J. E., Laouina, A., Carvalho, A. V., Loos, S., Schipper, A. M., Van der Kwast, H., Nafaa, R., Antari, M., Rocha, A., Borrego, C., & Ritsema, C. J. (2006). Desertification in northern Morocco due to effects of climate change on groundwater recharge. In: Kepner, W.G., Rubio, J.L., Mouat, D.A., Pedrazzini, F. (Eds.). Desertification in the Mediterranean region: A Security Issue. Springer, Dordrecht, The Netherlands.

Venables, W. N. & Ripley, B. D. (2002) Modern Applied Statistics with S. Fourth Edition. Springer, New York.

Venkatesan, A. K., Ahmad, S., Johnson, W., & Batista, J. R. (2011a). Salinity reduction and energy conservation in direct and indirect potable water reuse. *Desalination, 272*(1), 120-127. https://doi.org/10.1016/j.desal.2011.01.007

Venkatesan, A. K., Ahmad, S., Johnson, W., & Batista, J. R. (2011b). Systems dynamic model to forecast salinity load to the Colorado River due to urbanization within the Las Vegas Valley. *Science of the Total Environment*, *409*(13), 2616-2625. https://doi.org/10.1016/j.scitotenv.2011.03.018

Vining, K. C., Hay, L. E., & Markstrom, S. L. (2012). Watershed Scale Response to Climate Change-Starkweather Coulee Basin, North Dakota. U.S. Geologic Survey, Fact sheet 2011-3118.

Volk, J. M. (2014). Potential Effects of a Warming Climate on Water Resources within the Lehman and Baker Creek Drainages , Great Basin National Park , Nevada © by John M . Volk 2014 All Rights Reserved.

von Storch, H., & Zwiers, F.W. (1999). Statistical Analysis in Climate Research. Cambridge University Press: Cambridge.

Walker, J. F., Hunt, R. J., Hay, L. E., & Markstrom, S. L. (2012). Watershed Scale Response to Climate Change-Trout Lake Basin, Wisconsin. U.S. Geologic Survey, Fact sheet 2011-3119.

Walton, R., Wexler, E. J., & Chapman, R. S. (1999). An integrated groundwater-open channel flow model (MODNET). *Tech. Recport, West Consultants, Bellevue, Washington*.

Wang, H.F., & Anderson, M.P. (1982) Introduction to Groundwater Modeling: finite difference and finite element methods. San Diego, Academic Press.

Weigel, A. P., Chow, F. K., & Rotach, M. W. (2007). The effect of mountainous topography on moisture exchange between the 'surface' and the free atmosphere. *Boundary-Layer Meteorology* 125, 227-244. http://dx.doi.org/10.1007/978-0-387-74321-9_6

Weill, S., Mazzia, A., Putti, M., & Paniconi, C. (2011). Coupling water flow and solute transport into a physically-based surface-subsurface hydrological model. *Advances in Water Resources*, *34*(1):128-136. http://dx.doi.org/10.1016/j.advwatres.2010.10.001

Weill, S., Mouche, E., & Patin, J. (2009). A generalized Richards equation for surface/subsurface flow modelling. *Journal of Hydrology*, *366*(1–4), 9–20. http://doi.org/10.1016/j.jhydrol.2008.12.007

Welch, A. H., Bright, D. J., & Knochenmus, L. A. (2007). Water Resources of the Basin and Range Carbonate-Rock Aquifer System , White Pine County , Nevada , and Adjacent Areas in Nevada and Utah — Draft Report. *Open File Report, 1156*, 102.

Wheater, H.S., Jakeman, A.J., & Beven K.J. (1993). Progress and directions in rainfall-runoff modelling. In Jakeman A.J., Beck M.B. and McAleer M.J. (Eds.). Modeling Change in Environmental Systems. John Wiley, Chichester.

Whitebread, D.H. (1969) Geologic map of the Wheeler Peak and Garrison quadrangles, Nevada and Utah: U.S. Geological Survey Miscellaneous Geologic Investigations Map I-578, scale 1:48,000.

Whitfield, P.H., Wang, J. Y., & Cannon, A. J. (2003). Modeling future streamflow extremes-floods and low flows in Georgia Basin, British Columbia. *Canadian Water Resources Journal*, 28, 633-656. http://dx.doi.org/10.4296/cwrj2804633

Wilcke, R. A. I., Mendlik, T., & Gobiet, A. (2013). Multi-variable error correction of regional climate models. *Climatic Change*, *120*(4), 871-887. http://doi.org/10.1007/s10584-013-0845-x

Winter, T. C. (2007). The role of ground water in generating streamflow in headwater areas and in maintaining base flow. *Journal of the American Water Resources Association*, *43*(1), 15–25. http://doi.org/10.1111/j.1752-1688.2007.00003.x

Winter, T.C., Harvey, J.W., Lehn Franke, O., & Alley, W.M. (1998). Ground water and surface water-a single resource. U.S. Geological Survey Circular 1139.

Wood, A.W., Leung, L.R., Sridhar, V., & Lettenmaier, D.P. (2004). Hydrologic implications of dynamical and statistical approaches to downscale climate model outputs. *Climatic Change*, *62*, 189-216. http://doi.org/10.1023/B:CLIM.0000013685.99609.9e

Woolfenden, R., & Nishikawa, T. (2014). Simulation of Groundwater and Surface-Water Resources of the Santa Rosa Plain Watershed, Sonoma County, California. *U.S. Geological Survey Scientific Investigations Report*. http://doi.org/10.3133/sir20145052

Wu, G., Li, L., Ahmad, S., Chen, X., & Pan, X. (2013). A dynamic model for vulnerability assessment of regional water resources in arid areas: a case study of Bayingolin, China. *Water resources management*, *27*(8), 3085-3101. https://doi.org/10.1007/s11269-013-0334-z

Wu, R., Chen, C., Ahmad, S., Volk, J. M., Luca, C., Harris, F. C., & Dascalu, S. M. (2016). A Real-time Web-based Wildfire Simulation System. In *Industrial Electronics Society, IECON 2016-42nd Annual Conference of the IEEE* (pp. 4964-4969). IEEE. https://doi.org/10.1109/IECON.2016.7793478

Xu, C.Y., & Singh, V.P. (1998). A review on monthly water balance models for water resources investigations. *Water Resources Management*, 12, 31-50. http://dx.doi.org/10.1023/A:1007916816469

Xu, X., Huang, G., Zhan, H., Qu, Z., & Huang, Q. (2012). Integration of SWAP and MODFLOW-2000 for modeling groundwater dynamics in shallow water table areas. *Journal of Hydrology, 412–413*, 170–181. http://doi.org/10.1016/j.jhydrol.2011.07.002

Zhang, F. Y., Li, L. H., Ahmad, S., & Li, X. M. (2014). Using path analysis to identify the influence of climatic factors on spring peak flow dominated by snowmelt in an alpine watershed. *Journal of Mountain Science*, *11*(4), 990-1000. https://doi.org/10.1007/s11629-013-2789-z

Zhang, F., Ahmad, S., Zhang, H., Zhao, X., Feng, X., & Li, L. (2016). Simulating low and high streamflow driven by snowmelt in an insufficiently gauged alpine basin. *Stochastic environmental research and risk assessment*, *30*(1), 59-75. https://doi.org/10.1007/s00477-015-1028-2.

Zhang, T. (2005). Influence of the seasonal snow cover on the ground thermal regime: an overview. *Reviews of Geophysics*, *43*, 1-23. http://dx.doi.org/10.1029/2004RG000157

Zorita, E., & von Storch, H. (1999). The analog method as a simple statistical downscaling technique: comparison with more complicated methods. *Journal of Climate*, 12, 2474-2489. http://dx.doi.org/10.1175/1520-0442(1999)012<2474:TAMAAS>2.0.CO;2

Curriculum Vitae

Chao Chen
Chenc6@unlv.nevada.edu

Degrees:
Bachelor of Science, Water Conservancy and Hydropower Engineering, 2009
Zhejiang University of Technology, China

Master of Science, Hydrology and Water Resources, 2012
Hohai University, China

Publications:

Chao Chen, Sajjad Ahmad, Ajay Kalra. (2017) Hydrologic Responses to Climate Change Using Downscaled GCM Data on a Watershed Scale. Journal of Water and Climate Change. (Submitted)

Chao Chen, Sajjad Ahmad, Ajay Kalra. (2017) Coupling of a Groundwater-Flow Model with a Surface Hydrologic Model: Some Guidelines and Lessons Learned. Journal of Mountain Science. (Submitted)

Chao Chen, Ajay Kalra, Sajjad Ahmad (2017) A Conceptualized Groundwater Flow Model Development for Integration with Surface Hydrology Model. World Environmental and Water Resources Congress 2017: pp. 175-187. Doi: 10.1061/9780784480601.017.

Rui Wu, ***Chao Chen***, Sajjad Ahmad, John M. Volk, Cristina Luca, Frederick Harris, Sergiu Dascalu (2016) A Real-time Web-based Wildfire Simulation System. 42nd IEEE Industrial Electronics Conference (IEEE IECON2016) to be held in Firenze (Florence), Italy, October 24-27, 2016. DOI: 10.1109/IECON.2016.7793478

Chao Chen, Sajjad Ahmad, John Mejia, and Ajay Kalra (2016). Study of Regional Hydrologic Response to Climate Change Using CMIP5 data. World Environmental and Water Resources Congress 2016: pp. 508-517. doi: 10.1061/9780784479872.052.

Chao Chen, Ajay Kalra, Sajjad Ahmad (2015). *Exploring Water Management Strategies in an Inland Arid Area Using Dynamic Simulation Model.* World Environmental and Water Resources Congress 2015: pp. 1009-1018. doi: 10.1061/9780784479162.098.

Chao Chen, Lynn Fenstermaker, Haroon Stephen, Sajjad Ahmad (2015) *Distributed Hydrological Modeling for a Snow Dominant Watershed Using a Precipitation and Runoff Modeling System*. World Environmental and Water Resources Congress 2015: pp. 2527-2536. doi: 10.1061/9780784479162.248.

Dissertation Title: Understanding the Long-Term Changes in Hydrologic Processes on a Watershed Scale due to Climate Variability and Change

Dissertation Examination Committee:

Chairperson:	Sajjad Ahmad, Ph.D., P.E.
Committee Members:	Lynn Fenstermaker, Ph.D.
Committee Members:	Alexander Paz, Ph.D., P.E.
Committee Members:	Haroon Stephen, Ph.D.
Graduate Representative:	Ashok Singh, Ph.D.